UNIVERSITÀ DEGLI STUDI DI MILANO

SCUOLA DI DOTTORATO in Informatica

DIPARTIMENTO di Informatica

Scuola di Dottorato in Informatica XXIV Ciclo

Quantum Information Methods for Entanglement Computation: the case of the Helium Atom.

INF/01

DOTTORANDO

Stefano Siccardi

TUTOR

Prof.ssa Rita Pizzi

CO-TUTOR

Prof. Giuliano Strini

COORDINATORE DEL DOTTORATO

Prof. Ernesto Damiani

A.A. 2011-2012

To prof. Pizzi for her advice and

to prof. Strini for his teachings

Contents

List of Figures

List of Tables

Chapter 1

Abstract

The thesis aims to study the applicability of techniques of Quantum Information theory to complex systems, like molecules and biomolecules.

Recently, concepts of Quantum Information theory have been applied to the study of phenomena involving molecules, for instance the interaction light-biomolecules. In particular, the entanglement has been proposed to quantify the non-classicality of interactions.

The computation of molecular structures and interactions, on the other hand, has been studied for decades mainly to understand reactions' kinetic and energetic characteristics. It is not straightforward to apply these methods to the computation of quantum correlations.

We have therefore explored the computability of such effects using Quantum Information techniques. We started with the study of the electronic correlations in the Helium atom, that is the simplest non trivial case, in order to evaluate the computational problems and to develop approximate methods suitable to more complex systems.

We start recalling the definition and basic properties of entanglement, as it is considered in Quantum Information theory. We illustrate how it can be measured and the difficulties one encounters when identical particles are involved, then we concentrate on the case of Helium in particular.

In order to study the entanglement in Helium, we treat separately the singlet and the triplet configurations. The method we use consists in computing the reduced density matrix and then the entropy.

The possible choices of coordinates, basis functions and computation strategies are discussed, together with their impact on the algorithms.

The reduced, single-electron von Neumann and linear entropy for several low-energy eigenstates of Helium are computed by means of a simple configuration-interaction variational method.

This approach has several advantages.

First of all, we do not need to evaluate multidimensional integrals: the reduced density matrix is obtained by purely algebraic methods.

The reduced density matrix can then be easily diagonalized and therefore we can access not only the linear entropy but also the von Neumann entropy.

We report the main results of our computation, starting with the energy values, that are compared to high precision results from the literature to check our computations. Then we discuss our results for entanglement of fundamental and first excited states of Helium, with a special consideration for their sensitivity to the dimension of the spaces that are used.

In order to apply our method to more complex situations, as the Hydrogen molecule, we compare the above results, obtained using Slater Type Orbitals, with an approximation using gaussian expansions. After having adapted the computation algorithms, we compute the fundamental and first three excited levels of the Hydrogen molecule (S shell only).

Chapter 2

Introduction

2.1 General description of the present work

Quantum information and computation of atoms and molecules

Quantum information has been related from its very beginning to the problem of computing the structure of atoms and molecules. Feynman's proposal to use a quantum system for solving problems in quantum chemistry and many body physics (see e.g. (Feynman , 1982)) is most frequently quoted as the beginning of the quantum information field.

On the other hand, entanglement is a key factor for quantum computers. We quote for instance:

- quantum algorithms, such as the Shor's factoring algorithm and the Grover's search

- quantum teleportation

- some protocols used in quantum cryptography e.g. the E91 protocols

Moreover entanglement is necessary to build any 2 qubit gate, that in turn is mandatory in any quantum computer implementation. A typical case is the C-NOT gate, that flips the state of a qubit, depending on the state of a control qubit. It generates entangled states whenever it is applied to a superposition of states. All these examples are well-known and can be found in any text on quantum information, e.g. (Benenti, Casati et al.

, 2007).

It is necessary, therefore, to obtain a **measure** of entanglement in specific physical settings, to make sure that it is not a negligible effect, and that it can be used to process information in sight of the above described applications.

More specifically, it is important to measure entanglement in **natural atoms and molecules**, as they play a central role in several situations, as:

- classical computers where miniaturization is approaching the molecular dimensions. Here the quantum effects could interfere with the normal behaviour of the systems

- computers having molecules as their active elements. Already in the eighties, (Carter , 1987) proposed a (classical) molecular computer. It could be proposed a quantum molecular computer too.

- in Biology some authors proposed models of phenomena like the photosynthesis where the entanglement would be a critical factor to enhance the efficiency. It have also been proposed to use similar mechanisms to build devices to convert the light in electrochemical energy (Sarovar, Whaley , 2012).

- in Chemistry it has been proposed a method based on orbital entanglement to evaluate the relative importance of several components of the correlation energy, and to accordingly choose the best model for the case at hand (Boguslawski, Tecmer et al. , 2012).

The role of entanglement and quantum coherence has also been considered in laser-induced fragmentation experiments, see e.g. (Akoury, Kreidi et al. , 2007) (Becker, Langer, 2009).

We will review the main methods that can be found in the literature to compute eletronic structures and their entanglement in section 4. We here limit ourselves to some general considerations:

- models used to compute entanglement **for implementing quantum computers**, both with natural atoms, ions, molecules and artificial atoms, consider these systems in very special conditions, e.g. at ultra low temperature, trapped by electrical fields or in optical

lattices, etc. Moreover they focus only on the levels of interest for the experiments, or on the entanglement that can be generated between two systems. On the other hand we aim to compute entanglement in "natural" situations. See (Buluta, Ashab et al. , 2011), (Blatt, Wineland , 2008), (Bloch , 2008), (Saffman, Walker et al. , 2010), (Micheli, Brennen et al. , 2006).

- models used in **biology** e. g. (Renger, May , 1998), (Engel, Calhoun et al. , 2007), (Mohseni, Rebentrost et al. , 2008), (Pereverzev, Bittner et al. , 2009), (Adolphs, Müh et al. , 2010), (Sarovar, Ishizaki et al. , 2010), (Scholak, Mintert et al. , 2010), (Scholak, de Melo et al. , 2011), (Olbrich, Jansen et al. , 2011), (Scholak, Wellens et al. , 2011), (Christensson, Kauffmann , 2012), (Walschaers, Mulet et al. , 2012), (Zech, Mulet et al. , 2012), (Alicki, Miklaszewski , 2012). Unfortunately, in the biology the systems are so complex that authors are often forced to resort to models borrowed from the Quantum Computers. This means that phenomenological parameters are introduced, because an "ab initio" treatment is not feasible. The "active sites" are considered as two levels systems, without describing the underlying chemical structure. In this way just phenomenological descriptions can be obtained. Moreover, recently (Tiersch, Popescu et al. , 2012) pointed out that the presence of entanglement in photosynthesis could be illusory, and, even if present, its importance in the overall efficiency could be overestimated. Among their arguments, we recall that the light in these phenomena is classical, and that the models substitute the rich set of states of the involved molecules, with two states only. A simple model where two interacting molecules are represented by harmonic oscillators shows that no entanglement is present ((Tiersch, Popescu et al. , 2012)). Section 4.2 is devoted to a more detailed discussion of the quoted papers. In this situation it is hoped that more realistic models can be computed.

We now consider a more specific problem, i.e. the bipartite entanglement of two-particle systems as the Helium atom.

- the classical **Hartree-Fock method**, still used in computational chemistry, consists in approximating the state vector with a single Slater determinant

$$\psi(\mathbf{r}_1, \mathbf{r}_2) \;=\; \tfrac{1}{\sqrt{2}}(\phi_1(\mathbf{r}_1)\,\phi_2(\mathbf{r}_2) \;-\; \phi_1(\mathbf{r}_2)\,\phi_2(\mathbf{r}_1))$$

where the ϕ are single particle wave functions. It is a first approximation method; moreover, using a single Slater determinant it is not suitable for entanglement computation.

The **Interaction of Configuration** method, that we use in the present work, can be coinsidered an evolution of the Hartree-Fock method, considering a linear combination of Slater determinants or permanents for each atomic shell:

$$F_{n1,l1;n2,l2}(r1,r2)Y_{l1m1}(\Omega_1)Y_{l2m2}(\Omega_2)$$

where the Y are spherical harmonics, and the F are Slater determinants or permanents. In section 5.4 we will describe in depth our implementation of this method, the choice of coordinates, the orthonormalization issues, etc. in order to obtain the best simplification in the density matrix and reduced density matrix computations (section 5.3).

- other classical methods that were proposed for energy computation can be difficult to extend to entanglement computations. In section 4.4.2 we describe for instance the **Pekeris' method** that uses the Hylleras coordinates $u = \epsilon(r_2 + r_{12} - r_1)$, $v = \epsilon(r_1 + r_{12} - r_2)$, $w = \epsilon(r_1 + r_2 - r_{12})$ where ϵ is a parameter, r_1 e r_2 are the distances of the electrons from the nucleus, and r_{12} is the distance between the electrons. See (Barnett , 2003), (Barnett, Capitani et al. , 2004), (Koutschan, Zeilberger , 2010), (Pekeris , 1958), (Pekeris , 1959). This method was used by (Bürgers, Wintgen et al. , 1995) with a complex variational parameter to compute double excited states of Helium, see also (Wintgen, Delande , 1993), (Gremaud, Delande , 1997), and to compute molecular structures (e.g. (Hilico, Billy et al. , 2000)).

The state vectors are then expressed by a Laguerre polynomial expansions whose coefficients can be found solving recursive equations. In this way high precision values for energies can be computed.

However the computation of the density matrix, that is necessary for entanglement evaluation, is complex as it must be made integrating in these coordinates, that do not allow any simplifications.

- other approximate methods are used in computational Chemistry, one of the most im-

portant being the **Density Matrix Renormalization Group**, see (White , 1992). It has been applied to entanglement computations, e.g. (Barcza, Legeza et al. , 2011). One of the aims of the present work is to establish a simple example that can be computed with full accuracy, against which such approximate methods could be evaluated

Also **Quantum algorithms** for Physics and Chemistry have been proposed, and recently reviewed by (Yung, Whitfield et al. , 2012). The simulation of the time evolution of the quantum state of the system according to the Schrödinger equation on a "quantum computer" is one of the main application of quantum computation. Actually it is not granted that quantum computers, let alone their simulations on classical ones, could achieve better results than computational physicists have obtained so far.

These simulations could compute both typical physical quantities, like the energy, and information-related quantities, like non classical correlations, that is entanglement.

The Hamiltonian H of the system can be represented in first or second quantized form.

When represented in first quantized form, it is decomposed in the kinetic and potential energy terms, that are written considering the nuclei, the electrons and their interactions. The time evolution is then simulated approximating the time evolution e^{-iHt} with products of the quantum Fourier transform of kinetic and potential energy.

An approach of this kind has been used e.g. by (Benenti, Strini , 2008); we recall some results of a simulation of this kind, in which we studied the entanglement within the simulator, in section 3.2.1. We stress, however, that we quote these results here just for the sake of completeness, because we are listing the methods that have been proposed to study the problem of atomic structures. The main topic of the present work is not related to quantum algorithms.

Moreover, the actual advantages of using quantum algorithms, compared to classical ones, cannot be given for granted, as standard techniques employed to integrate the Schrödinger equation have produced many important results. We quote e.g. (Scrinzi, Piraux , 1997), (Scrinzi, Piraux , 1998) who computed the evolution of a two-electron atom exposed to a laser field by direct time integration of the Schrödinger equation without any approxima-

tions except for the dipole approximation of the laser field; (Bachau, Lambropoulos et al. , 1991), (Cornier, Lambropoulos , 1995) who studied ionization in two-electron systems; (Dundas, Taylor et a. , 1999) and (Nikolopoulos, Lambropoulos , 2001) who studied double-ionization in Helium; (Madronero, Piraux , 2010) who studied ionization of atoms exposed to low frequency fields; (Madronero, Schlagheck et al. , 2005) who studied the autoionization rates of characteristic configurations of the doubly excited helium atom, in one, two and three dimensions; etc.

When represented in second quantization form, the Hamiltonian is written in the form:

$$H = \sum_{pq} h_{pq} a_p^+ a_q + \frac{1}{2} \sum_{pqrs} h_{pqrs} a_p^+ a_q^+ a_r a_s \tag{2.1}$$

where the a_p^+ are the creation operators that create an electron in the p mode, and the a_p are the annihilation operators.

The h_{pq} are the single-electron integrals and the h_{pqrs} are the electron-electron coulombian interaction integrals. The method requires that they must be pre-computed with classical computers, and their values are then passed to the quantum algorithms to simulate time dynamics.

Although we did not focus on this kind of problems, some preliminary computations of the H_2 molecule, that we report in section 5.2.5, seem to show that the computation of the h is actually much heavier than the other parts of the computation. This could lead to reconsider the importance of these methods.

Besides these problems of a computational nature, the quantification of entanglement of identical particles in the most general case still remains vague.

There are excellent review papers (Horodecki, Horodecki et al. (2009), Amico, Fazio et al. (2008)), but even these do not treat all the possible cases. A more modern review, Tichy, Mintert et al. (2011), treates extensively the entanglement of identical particles and the main measures that have been used for such situations.

We studied the entanglement in the Helium case (pioneered by the Dehesa group (Manzano, Plastino et al. , 2011), (Dehesa, Koga et al. , 2012)), in order to explore such difficulties, exactly define the problems and contribute to solving some of them.

We discuss some methods used to solve this problem in section 4.3, we now just stress that in spite of the large literature about several aspects of the Helium atom, only a few papers studied its electronic entanglement, and anticipate that:

- some models use **simplified Hamiltonians**, in order to obtain equations that can be **analytically solved**, see (Amovilli, March , 2003), (Amovilli, March , 2004), (Nagy , 2006), (Moshinsky , 1968), (March, Cabo et al. , 2008), (Yanez, Plastino et al. , 2010). Although useful to get some insight of the problem, these models cannot be considered realistic description of Helium

- (Osenda, Serra , 2007), (Osenda, Serra , 2008) used a **more realistic, but still not exact**, model and obtained interesting results. We compare our results to these works in 9.7

- (Dehesa, Koga et al. , 2012) obtained an **evaluation of entanglement in the Helium atom** using wavefunctions in the Hylleraas coordinates, and computing the linear entropy. The present work can be considered an extension of those computations, as we obtained some more levels, and computed the von Neumann entropy too.

Having summarized the scenario, we now state our main goals:

- find an exact method of computation to extend the available results on Helium and other atoms or molecules entanglement. The method found is an algebraic one and has two approximations only: the Hilbert space dimension and the hypothesis of nuclei at a fixed distance for molecules

- the method should be easy to extend to the computation of the entanglement to other cases and more complex situations. We tested it for the isoelectronic Helium series (see sec. 9.6) and studied its extension to the Hydrogen molecule (chapter 7). Of course, we do not expect that our method will cover without efforts all the more difficult situations

that on can consider, like the doubly excited states of Helium that can exhibit considerable complexity - see e.g. (Püttner, Gremaud et al. , 2001).

- obtain exact results in a simple case, the Helium atom, that can be used to test approximated methods suited to more complex situations. We replicated the (Osenda, Serra , 2007) results as an example of this idea (sect. 9.7).

- evaluate the hardness of the entanglement computation compared to the energy computation problem. A large number of computations has been devoted to the study of this point, varying the Hilbert space dimension of the S, P and D shells: tables and plots are reported in appendix 9.5; section 6.6 is devoted to the problem of optimizing the dimension of the Hilbert space for P and D shells, fixed the dimension for lower shells.

The problem has been divided into two parts: the first consisting of the Helium wave function computation (in the non relativistic setting, see (Drake , 1999), (Koga , 1996), (Pekeris , 1959), (Kono, Hattori , 1985), (Kono, Hattori , 1986), (Kono, Hattori , 1988); the second consisting of the computation of the reduced density matrix and of the evaluation of the entanglement, based on the reduced density matrix eigenvalues.

In the present work, the main issue considered is the reduced density matrix computation, and entanglement has been evaluated using simplifying hypotheses.

Another important point is that the computation is performed using the usual coordinates of the Fock space, so that the same method can be applied to more complex cases. The generalization would have been more difficult if we had used Hylleraas coordinates.

Of course, it is well known that to obtain the maximum precision it is in practice mandatory to use Hylleraas coordinates, or others of a similar kind, but in the case of entanglement we believe that such a great precision is unnecessary.

Once having defined the Fock space for the two Helium electrons, we introduced some variational parameters and optimized them separately for the fundamental and several excited states of triplet and singlet states.

The algorithm is described in detail in chapter 5, and appendix 9.1 contains several sections of the fortran code. No parts of the algorithm are original in themselves, however it is the general composition of the computation steps and its application to the problem at hand.

Several computational sides of the problem have been dealt with:

- first of all, after some tests with Fortran double precision, we adopted quadruple precision routines for all the computations of this kind

- we have already quoted the convergence rate of entropies versus the Hilbert space dimension

- we also considered the number of shells that must be taken into account and found that S-P-D shells suffice for singlets and S-P for triplets

- as one of the hardest sections, in principle, is the eigenvectors computation, we considered several algorithms, as specificed in sect. 5.2.1. For all the computations performed up to now, the Jacobi method gave satisfactory results.

- for the search of the minima too, we tested several methods (see 5.2.2), starting with euristic scans of the parameter intervals. In our final computations, we gave up the multimensional minimization (see 6.1.1.2 for an example) and used unidimensional minimization one shell at a time.

- in sight of the extension to the H_2 molecule computation, gaussian expansions of the base functions have been considered, see 5.2.3 for some general observations, and all chapter 7 for evaluations of the quality of the approximation

- the execution time of the heaviest subroutines has been measured and compared varying the Hilbert space dimension and the number of shells considered (sect. 5.2.5). These data will be considered to plan program extensions, and to consider which points should be reimplemented with more efficient algorithms

Our main results for Helium entanglement are described in sect. 6.3. Sect. 6.4 reports the

approximation of our computations of energy, compared to high quality standard results: a good energy approximation is the most important measure of the soundness of our work, as some of the entropy values that we got were obtained for the first time.

Another interesting result, that can be achieved with our method, is the explicit computation of the reduced density matrix eigenvalues. In sect. 6.5 we list some typical cases.

Two extensions of the method have been considered:

- in appendix 9.6 we briefly describe some preliminary results for the Li^+ ion, that were obtained with the same software used for Helium, just changing some parameters. We plan to investigate the Helium isoelectronic series in a forthcoming work

- in chapter 7 we extended our computation to the Hydrogen molecule. This task implied all the steps needed to check a "true" extension, that is: 1) we started with the simple case of the H_2^+, using a single STO, approximated it with 1 to 6 gaussians and studied the errors (sect. 7.1.1). 2) Then we modified the algorithms to use 1 or more gaussians in the H_2 computations (sect. 7.2, 7.3). 3) At this point, we compared our results to standard energy values from the literature. Moreover, we compared the results of the new programs for Hydrogen, run with the internuclear distance set equal to zero, to our results for Helium (sect. 7.4.1) 4) At the end, we were able to describe our preliminary results for the H_2 molecule entanglement considering the S shell only (sect. 7.4.2). Also this work will be completed considering other shells.

S states.

To obtain a precision of the order of 1% in Entanglement (that we presently consider sufficient), it has been enough to take into account the shells S-P-D for singlet and triplet. Using only S shells, on the other hand, is not sufficient.

It is to be noted that, optimizing separately the variational parameters for each level, we limit the Fock space dimension at the minimum possible value, but we obtain non orthogonal eigenfunctions for the states.

During the computation using this technique we were required to digonalize matrices up to dimension 400x400.

It must be noted that we used a single variational parameter for each shell, that is three parameters for singlet and three for triplet states.

A last important point is that we used othonormal base functions for the single particle spaces, so we avoided the generalized eigenvalue problem.

To diagonalize the biggest matrices at best we used the quadruple precision (fortran real*16). Fortunately the computation time took no more than a few hours even on a modern portable workstation.

Chapter 3

Entanglement

3.1 Entanglement in Quantum Information.

Entanglement is a key factor in Quantum Information: in this chapter we recall some basic definitions, examples and theoretical motivations.

3.1.1 Entanglement definition

A problem that one must face while developing Quantum Mechanics and Quantum Information theory is the study of composite systems. For instance, the Hydrogen atom is composed of a proton and an electron. Any system composed of two or more qubits is another example. The description of the dynamics can be developed, like in the classical case, starting from the dynamics of the components and adding their interactions. On the other hand, the description of the state space of such systems generates non classical effects.

The Hilbert space $\mathcal{H}$ associated with a composite system is the tensor product of the Hilbert spaces $\mathcal{H}_i$ associated with the subsystems.

For the sake of simplicity, we consider the case of just two subsystems, both of dimension 2, that is two qubits. Denoting $\{\,|0\rangle_1, |1\rangle_1\,\}$ and $\{\,|0\rangle_2, |1\rangle_2\,\}$ their bases, a base of the complete system is: $\{|0\rangle_1 \otimes |0\rangle_2, |0\rangle_1 \otimes |1\rangle_2, |1\rangle_1 \otimes |0\rangle_2, |1\rangle_1 \otimes |1\rangle_2, \}$ that can be written

$$\{|0\,0\rangle,\ |0\,1\rangle,\ |1\,0\rangle,\ |1\,1\rangle\} \tag{3.1}$$

The general state in the space $\mathcal{H}$ is a superposition of states of $\mathcal{H}_1$ and $\mathcal{H}_2$, and can be written:

$$|\,\psi\rangle\ =\ \sum_{i,j} c_{ij}\,|\,ij\rangle \tag{3.2}$$

where i refers to states in $\mathcal{H}_1$ and j to states in $\mathcal{H}_2$.

The state $|\,\psi\rangle$ is defined **entangled** if it cannot be expressed as the tensor product of a state in $\mathcal{H}_1$ and one in $\mathcal{H}_2$. On the contrary, if a relation like

$$|\,\psi\rangle\ =\ |\,\alpha\rangle_1\ \otimes\ |\,\beta\rangle_2 \tag{3.3}$$

holds, with $|\,\alpha\rangle_1$ in $\mathcal{H}_1$ and $|\,\beta\rangle_2$ in $\mathcal{H}_2$ the state is called **separable**.

Entanglement is a typical quantum mechanical effect, a key ingredient in quantum information science. There is wide consensus that it is one of the most fundamental characteristics of quantum physics, and its study has attracted intense efforts in recent years.

When two systems are entangled, it is not possible to assign them individual state vectors $|\,\alpha\rangle_1$ and $|\,\beta\rangle_2$. It is also well known that entangled states possess intriguing non-classical properties; those have been illustrated for the first times by Einstein, Podolsky and Rosen in 1935, with their celebrated paradox and by the also famous Schrödinger cat paradox.

We stress that entanglement is a resource. This resource is essential to quantum-information science in order to perform computation and communication tasks far beyond the classical

capabilities. In later sections we will briefly recall some topics of quantum-information science in which entanglement shows its importance.

3.1.2 Schrödinger's cat

Schrödinger described the following situation in order to enlighten the strange consequences of the superposition of states.

In a box there is a cat and a radioactive source, constituted of an atom, that can be in the excited state $|\,1\rangle$ and in the corresponding ground state $|\,0\rangle$. The atom is connected to a device that, if the atom decays, breaks a glass contanining some poisons, that will kill the cat. Call τ the hemilife time of the atom, $|\,\hat{1}\rangle$ the state of the alive cat, and $|\,\hat{0}\rangle$ the state of the dead cat, $|\,R_{en}\rangle$ the state of the environment.

At time $t = 0$ the box is closed; the total wave function of the system is:

$$|\,\psi\rangle \;=\; |\,1\rangle \,\otimes\, |\,\hat{1}\rangle \otimes |\,R_{en1}\rangle \tag{3.4}$$

As the evolution equation is linear, after the time τ, the state will be (we intend to present a qualitative argument, not an exact model):

$$|\,\psi\rangle \;=\; \frac{1}{\sqrt{2}}(|\,1\rangle \,\otimes\, |\,\hat{1}\rangle \otimes |\,R_{en1}\rangle \,+\, |\,0\rangle \,\otimes\, |\,\hat{0}\rangle \otimes |\,R_{en2}\rangle) \tag{3.5}$$

This means that the cat should be in a superposition state, having 50% probability of being alive and 50% of being dead. This superposition state, according to the Quantum Machanics postulates, ceases only when the system is observed. In that moment, the wave function "collapses" in one of the two states, with the quoted probabilities. This is the situation each time two systems interacts.

Two points must be stressed:

- the first is that quantum superposition does not have any analogous concepts in the classical setting, as it means that the system is in an undetermined state until it is measured and, after the measure it will be in one of the two states. On the contrary, in a classical setting "superposition" means that the system is in specific state, obtained summing in a suitable way two or more states, e.g. two waves. In the next paragraph we will see that also entanglement does not have any classical counterpart.

- the second is the problem related with the measuring act. The effect of the measure is that the system must choose one of two different states, and that cannot be described by the Schrödinger equation, that is linear. This means that the evolution of quantum systems must be described by two different kinds of processes: the Schrödinger equation and the state collapse during the measure.

3.1.3 The EPR paradox

The paradox described by Einstein, Podolsky and Rosen forms the basis for a class of interesting problems and situations in Quantum Mechanics. It is also the conceptual paradigm of many quantum information and quantum communication protocols based on entangled systems. We will follow a very simple version of the paradox, due to Bohm. We have a source, emitting two particles with spin 1/2 in a singlet state (that is two qubits, in quantum information terms). Call $|\,0\rangle$ the state with spin parallel to the z axis, and $|\,1\rangle$ the state with antiparallel spin. The total state is:

$$|\,\psi\rangle \;=\; \frac{1}{\sqrt{2}}\,(|\,01\rangle \;-\; |\,10\rangle) \tag{3.6}$$

One of the particles travels towards Alice, the other towards Bob. From (3.6) it is obvious that if Alice measures the spin along the z axis and obtain the value 0, then if Bob too measures the spin along the z axis, he will find the value 1. Analogously, if Alice obtain 1, Bob will obtain 0. This has nothing extraordinary, and would be the same even using

classical objects.

Now suppose that Alice and Bob will measure the spin along the x axis. This means that they will use another instrument, that can be represented by the operator

$$\sigma_x = \begin{bmatrix} 0 & 1 \\ 1 & 0 \end{bmatrix} \tag{3.7}$$

This operator has eigenstates

$$|+\rangle = \frac{1}{\sqrt{2}}(|0\rangle + |1\rangle); \quad |-\rangle = \frac{1}{\sqrt{2}}(|0\rangle - |1\rangle) \tag{3.8}$$

The effect of this measure on the state (3.6) is obtained rewriting it in the new basis. The result is

$$|\psi\rangle = \frac{1}{\sqrt{2}}(|-+\rangle - |+-\rangle) \tag{3.9}$$

This means that if Alice measures the spin along this basis and finds the value -, then Bob will find the value +, and vice versa, that is the measures are still anticorrelated. The critical point is that the two measures are incompatible: if the spin is measured along the z axis, nothing can be said about its component about the x axis, because the corresponding operators do not commute. But Alice can decide without constraints the axis along which to perform the measure, and can forecast without any action on the other particle, which result will obtain Bob if he uses the same axis.

Alice's choice can be made when the particles have travelled far away from each other, and cannot interact anymore.

So their wave function must contain an "element of reality" pertaining the measures along the axes x and z (and any other). It is important to stress that the point is not the perfect anticorrelation of the measure, but the fact that it is not dependent on the choice of the Hilbert space basis.

3.2 Difficulties in the entanglement definition

A very important point, that is usually insufficiently covered by the literature, is that the Entanglement of a register in a pure state is defined as the entropy of the reduced density matrix obtained partitioning it. But the possibilities of such partitioning grow exponentially with the number of qubits, and a complete quantization of entanglement should take this fact into account.

It is still an open problem how such situations should be treated in general (see however (Mintert, Carvalho et al. , 2005) and (Facchi, Florio et al. , 2006) for discussions of multipartite entanglement measures and of the problem of the growth of the number of partitions).

3.2.1 Entanglement in the simulation of a quantum computer

It is important to have a method to measure the entanglement of a system. Here we introduce the problem with an example.

First of all, we recall that the entropy of a pure state is zero. If, for instance, a pure state of n qubits is decomposable into the product of two pure states of $\frac{n}{2}$ qubits, then the entropy of these states is zero too.

Computing the entropy of the reduced matrices of these two subsystems one can determine if their state is a pure one.

As an example, we consider the simulator of a quantum computer obtained solving the Schrödinger equation for a harmonic oscillator on a classical computer. The simulator

used 6 qubits.

The interval of the spatial coordinate x has been divided into 2^6 intervals, that have been represented by a 6 qubit register.

The Schrödinger equation has been solved propagating the initial wave function

$$\psi(x; t + \epsilon) \; = \; e^{-i/\hbar(H_0+V(x))\epsilon} \cdot \psi(x; t) \tag{3.10}$$

where $H_0 = -\frac{\hbar^2}{2m}\frac{d^2}{dx^2}$ and $V(x)$ is the potential energy. In a small interval of time ϵ one can approximate

$$e^{-i/\hbar(H_0+V(x))\epsilon} \approx e^{-i/\hbar H_0 \epsilon} \cdot e^{-i/\hbar V(x)\epsilon} \tag{3.11}$$

then a quantum Fourier transform is used to obtain the solution.

The method is illustrated in fig. 3.2, 3.3 and 3.4. In figure 3.2 left, the x axis represents the time evolution, in 40 steps. The y axis represents the spatial interval at each instant; it has been divided in $2^6 = 64$ subintervals. So the (monodimensional) wavefunction is moving from left to right. Figure 3.2 right shows the wavefunction, as a function of the spatial coordinate x only, at a fixed instant of time. Figures 3.3 and 3.4 show the same data, for different runs, with a three dimensional representation of the wavefunction, that again is to be understood as moving from time=0 to time=40.

Being a (simulation of) a quantum system, the quantum simulator has a density matrix, whose entropy can be computed to check that if it is in a pure state. Moreover, being made of 6 qubits, several reduced density matrix can be computed to check if there is entanglement between the qubits.

In all the plots of entropy, the abscissa represents time and the ordinate the von Neumann

entropy.

In fig. 3.1 the total entropy is plotted as expected it is very near to zero: the small values are due to numerical errors.

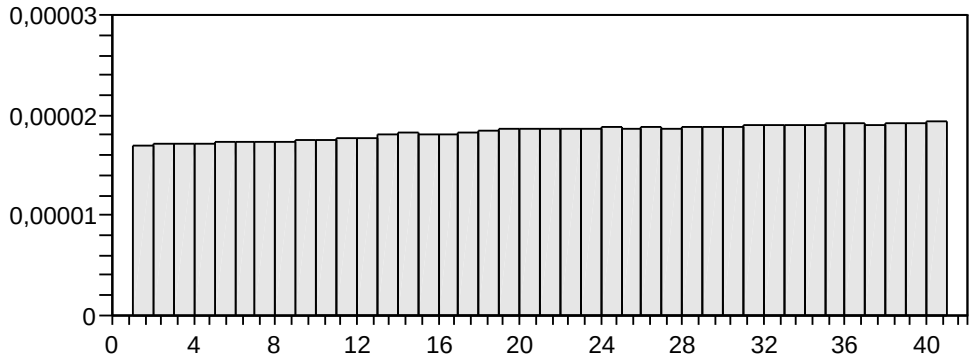

Figure 3.1 – Simulator - total entropy is zero, apart from small numerical errors.

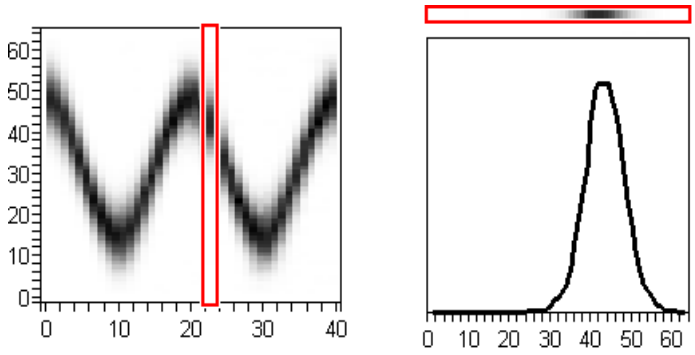

Figure 3.2 – Method to read the plots computed by the simulations

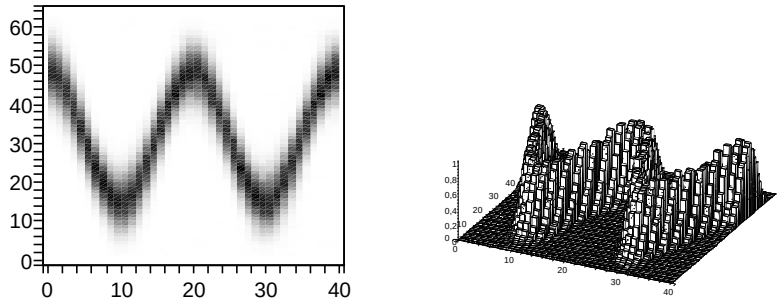

Figure 3.3 – Schrödinger's equation solutions with no errors

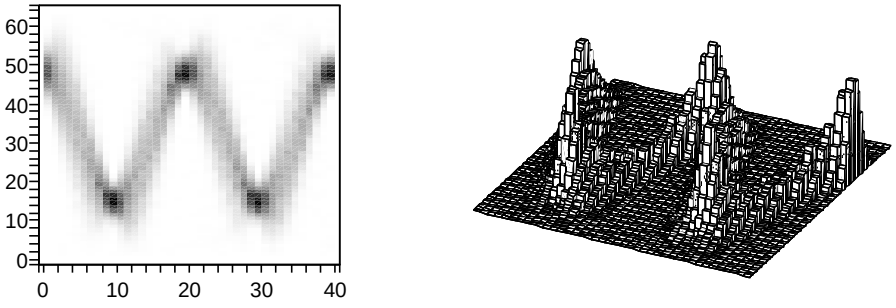

Figure 3.4 – Schrödinger's equation solutions with no errors with spreading of the Gaussian packet

To evaluate the entanglement, we have plotted the entropies of each single qubit, from qubit 0 to qubit 5 see fig. 3.5 - 3.8. In the first and last figures, also the values of the entropy of the other qubits have been plotted. The entropies are the same, as expected for a pure state.

Fig. 3.9 and 3.10 represent entropies of the systems of qubits 45 and 0123 and of qubits 012 and 345.

The results show a strong entanglement within the simulator.

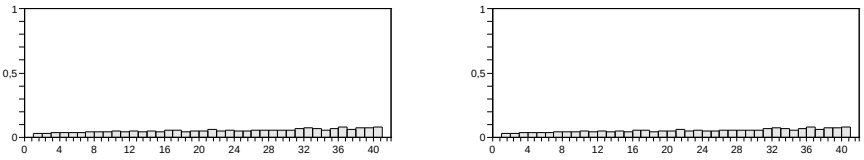

Figure 3.5 – Entropy on qubit 0 (LSB) and on qubits 12345

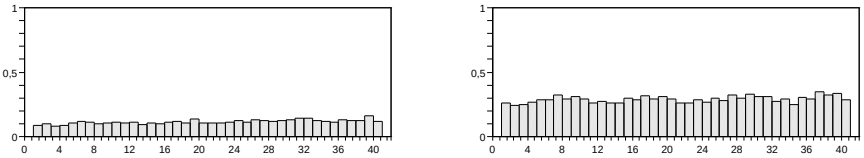

Figure 3.6 – Entropy on qubit 1 and on qubit 2

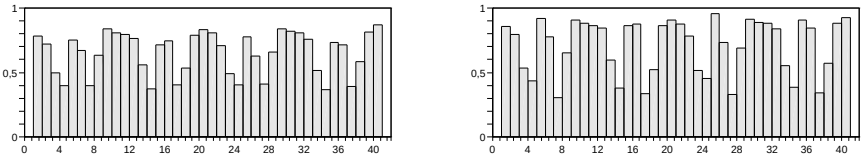

Figure 3.7 – Entropy on qubit 3 and on qubit 4

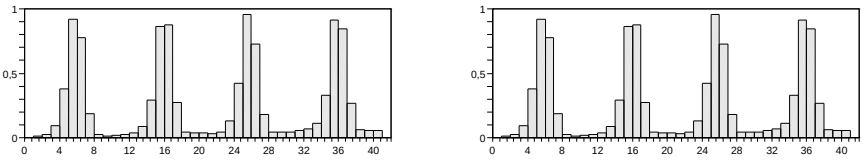

Figure 3.8 – Entropy on qubit 5 and on qubits 01234

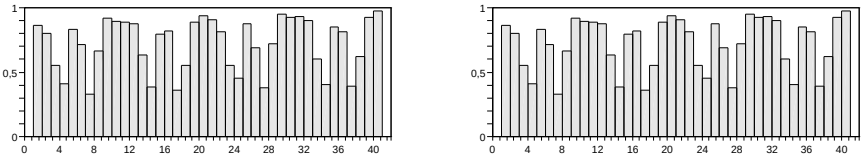

Figure 3.9 – Entropy on qubits 45 and on qubits 0123

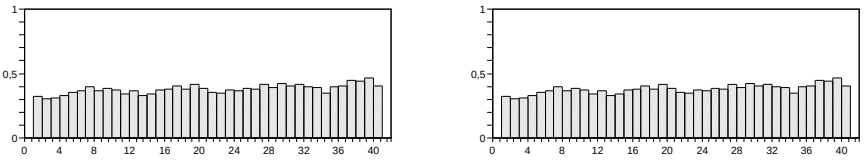

Figure 3.10 – Entropy on qubits 012 and on qubits 345

3.2.2 Entanglement in the Grover quantum search algorithm

As a second example of the simulator, in this section, we show the results of entropy computation in a simulation of the Grover algorithm. The case is analogous to the previous: the simulator used 6 qubits, and the entropies were computed as the von Neumann entropies of the reduced density matrices obtained tracing on one or more qubits. Of

course, the algorithm performed by the simulator was different and used the gate shown in fig. 3.11.

The plots have as usual time in abscissa and the von Neumann entropy in ordinate.

Entropies have been computed at every algorithm iteration. In the plots, q0 is the Least Significant Bit and q5 is the Most Significant Bit. Reduced entropies computed on more than 1 qubit are labelled with multiple indexes.

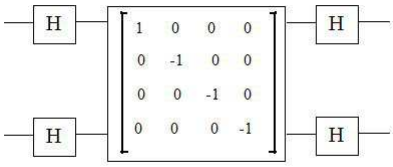

Figure 3.11 – Synthesis of Grover's D matrix by a generalized controlled phase gate

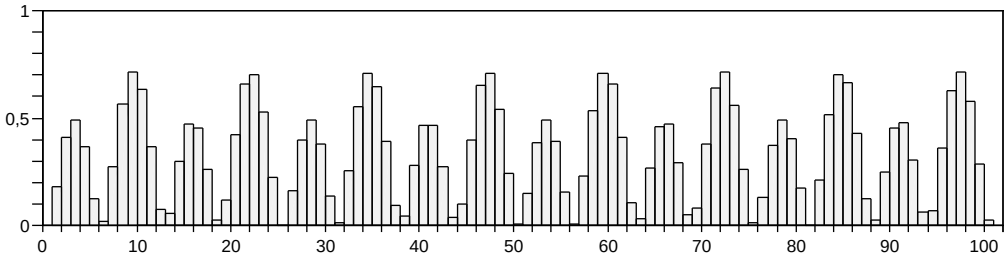

Figure 3.12 – q0 Entropy

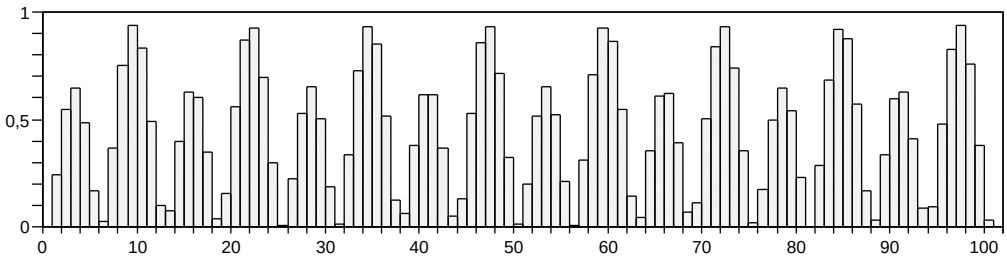

Figure 3.13 – q01 entropy

3.3 The problem of entanglement computation in Helium

The non-relativistic Hamiltonian of the helium atom reads, in atomic units,

$$H = \frac{1}{2}\,\mathbf{p}_1^2 + \frac{1}{2}\,\mathbf{p}_2^2 - \frac{Z}{r_1} - \frac{Z}{r_2} + \frac{1}{r_{12}}, \tag{3.12}$$

where $Z = 2$ denotes the nuclear charge, $\mathbf{p}_i$ the momentum of electron i ($i = 1, 2$), r_i its distance from the nucleus and r_{12} the inter-electronic separation.

Since we are neglecting the spin-orbit interaction, we can consider global wavefunctions Ξ factorized into the product of a coordinate wavefunction Ψ and a spin wavefunction χ:

$$\Xi_{\sigma_1,\sigma_2}(\mathbf{r}_1, \mathbf{r}_2) = \Psi(\mathbf{r}_1, \mathbf{r}_2)\chi_{\sigma_1\sigma_2}. \tag{3.13}$$

The overall state must be antisymmetric and therefore a measure (Schliemann, Cirac et al. , 2001), (Schliemann, Loss et al. , 2001) of the amount of entanglement $E(|\Xi\rangle)$ of the state Ξ has been proposed in terms of the von Neumann entropy of the reduced density operator $R_1 = \mathrm{Tr}_2(|\Xi\rangle\langle\Xi|)$ of one particle, say particle 1, obtained after tracing the overall, two-body density operator over the other particle (see also (Amico, Fazio et al. , 2008), (Ghirardi, Marinatto , 2004)):

$$E(|\Xi\rangle) = S(R_1) - 1, \tag{3.14}$$

with the von Neumann entropy

$$S(R_1) = -\sum_i \Lambda_i \log_2 \Lambda_i, \tag{3.15}$$

where $\{\Lambda_i\}$ are the eigenvalues of R_1. The term -1 is due to the fact that the entropy $S(R_1)$ of indistinguishable particles is bounded from below by unity instead than zero (See (Tichy, Mintert et al. , 2011)), as a state obtained by antisymmetrization of a product of two states has entropy=1, and is not entangled.

However, with such definition a first problem arises.

When considering the triplet subspace, spanned by the spin states $\chi_{\uparrow\uparrow}$, $\frac{1}{\sqrt{2}}(\chi_{\uparrow\downarrow}+\chi_{\downarrow\uparrow})$, and $\chi_{\downarrow\downarrow}$, it is clear that we should consider the case $\frac{1}{\sqrt{2}}(\chi_{\uparrow\downarrow}+\chi_{\downarrow\uparrow})$ separately from the cases $\chi_{\uparrow\uparrow}$ and $\chi_{\downarrow\downarrow}$.

Indeed, considering only the spin part, in the hypothesis of Spin-Orbit Independence, $\frac{1}{\sqrt{2}}(\chi_{\uparrow\downarrow}+\chi_{\downarrow\uparrow})$ is a maximally entangled Bell state of the two spins while $\chi_{\uparrow\uparrow}$ and $\chi_{\downarrow\downarrow}$ are separable states.

Therefore, the standard spectroscopic characterization in terms of triplet and singlet states is no longer useful for the purposes of computing entanglement and one should study separately the entanglement properties of the states composing the triplet.

In this context, we would like to point out that, neglecting spin-spin interaction, the choice of the basis states spanning the triplet state is completely arbitrary and that the above discussed $\{\chi_{\uparrow\uparrow}, \frac{1}{\sqrt{2}}(\chi_{\uparrow\downarrow}+\chi_{\downarrow\uparrow}), \chi_{\downarrow\downarrow}\}$ is only one in between the infinite possible choices.

In particular, in the Chemical literature, the spin degrees of freedom are referred to as $\{\alpha, \beta\}$ without any other specification, and are sometimes considered just as statistical weights.

In the present work, given the present uncertainty in entaglement definition for a group of fermions, we decided to use a more precise notation, namely the spectroscopic notation as it is used in spectroscopy of atoms and small molecules.

Obviously, in this way the entanglement characterization in complex molecules is completely omitted.

This is a major limit of the available knowledge in this field, while in the literature it is "popular" to affirm the key role of entanglement in important biological processes, such as light-harvesting in photosynthetic processes.

These processes are described quite schematically, modelling the excitons of the involved molecules as qubit systems, without more detailed descriptions.

Coming back to Helium, we have treated separatedly the orbital and spin degrees of freedom.

Another ambiguity that can be found in the literature is that sometimes a numerical factor is added to equation (3.14) for instance $\frac{1}{2}$ or 2, in order to normalize somehow the possible entanglement values. This must be taken into account when comparing the results reported herein with those of other works.

Another point, fortunately easy to detect, is that in the chemical literature natural logarithms are used in the von Neumann entropy definition, while in the informatical literature base 2 logarithms are almost always used. In the present work we will always use the second definition.

Another entropy definition that is sometimes used is the purity or linear entropy, defined by

$$Linear\,Entropy\ =\ 1\ -\ Tr\{\rho^2_{reduced}\} \tag{3.16}$$

For the sake of completeness, we will also report the linear entropy, together with the von Neumann entropy.

To avoid this ambiguity, we compute the entanglement for the orbital part Ψ only of the wavefunction.

Since the global wavefunction Ξ must be antisymmetric due to the Pauli principle, and in the triplet case the spin part is symmetric, the orbital part Ψ is antisymmetric and we can measure the amount of entanglement $E(|\Psi\rangle)$ of Ψ as follows:

$$E(|\Psi\rangle) = S(\rho_1) - 1, \tag{3.17}$$

where

$$S(\rho_1) = -\sum_i \lambda_i \log_2 \lambda_i \tag{3.18}$$

is the von Neumann entropy of the reduced density operator $\rho_1 = \mathrm{Tr}_2(|\Psi\rangle\langle\Psi|)$, and $\{\lambda_i\}$ are the eigenvalues of ρ_1.

When the spin part of the wavefunction is in the singlet state $\chi_S = \frac{1}{\sqrt{2}}(\chi_{\uparrow\downarrow} - \chi_{\downarrow\uparrow})$, the orbital part is necessarily symmetric and this causes an additional, open problem in the quantification of entanglement.

Indeed in this case the reduced von Neumann entropy alone is not sufficient to discriminate between entangled and separable states (Ghirardi, Marinatto , 2004).

The core of the problem is the fact that we can have separable states with either $S(\rho_1) = 0$ or $S(\rho_1) = 1$.

The first instance corresponds to basis states of the kind $\Psi_{ii}(\mathbf{r}_1, \mathbf{r}_2) = \phi_i(\mathbf{r_1})\phi_i(\mathbf{r}_2)$, the second to basis states like $\Psi_{ij}(\mathbf{r}_1, \mathbf{r}_2) = \frac{1}{\sqrt{2}}[\phi_i(\mathbf{r_1})\phi_j(\mathbf{r}_2) + \phi_j(\mathbf{r_1})\phi_i(\mathbf{r}_2)]$, with $i \neq j$.

On the other hand, even the quantification of entanglement of the global, antisymmetric wavefunction by means of Eq. (3.14) poses a problem.

Indeed, as the von Neummann entropy is additive for tensor products, for the state $\Xi = \Psi_{ii}\chi_S$ Eq. (3.14) gives $E(|\Xi\rangle) = 0$, while for the state $\Xi = \Psi_{ij}\chi_S$ $(i \neq j)$ we have $E(|\Xi\rangle) = 1$.

Even though measure (3.14) gives different results, the amount of entanglement in both cases is the same, since the orbital wavefunctions Ψ_{ii} and Ψ_{ij} are both separable: the reduced density matrices for these two states have different entropies only due to the symmetrization of the state Ψ_{ij}.

It is now worthwhile discussing separately the triplet and singlet cases, going into detail. We will first present the triplet case.

3.3.1 The triplet case

In this work, the Fock space of two particles is built from single particle orbitals, using Slater determinants. The antisymmetrical orbital states are therefore n(n-1)/2.

For the sake of clarity, we will make an explicit example, the simplest possible, for n=4 and a single shell.

For n=4 we have a basis of 6 Slater determinants, that can be denoted:

$$D_1 = |1,\,2\rangle = \frac{1}{\sqrt{2}}\{\phi_1(r_1)\phi_2(r_2) - \phi_2(r_1)\phi_1(r_2)\} \tag{3.19}$$

$$D_2 = |1,\,3\rangle = \frac{1}{\sqrt{2}}\{\phi_1(r_1)\phi_3(r_2) - \phi_3(r_1)\phi_1(r_2)\} \tag{3.20}$$

$$D_3 = |1,\,4\rangle = \frac{1}{\sqrt{2}}\{\phi_1(r_1)\phi_4(r_2) - \phi_4(r_1)\phi_1(r_2)\} \tag{3.21}$$

$$D_4 = |2,\,3\rangle = \frac{1}{\sqrt{2}}\{\phi_2(r_1)\phi_3(r_2) - \phi_3(r_1)\phi_2(r_2)\} \tag{3.22}$$

$$D_5 = |2,\,4\rangle = \frac{1}{\sqrt{2}}\{\phi_2(r_1)\phi_4(r_2) - \phi_4(r_1)\phi_2(r_2)\} \tag{3.23}$$

$$D_6 = |3,\,4\rangle = \frac{1}{\sqrt{2}}\{\phi_3(r_1)\phi_4(r_2) - \phi_4(r_1)\phi_3(r_2)\} \tag{3.24}$$

The wavefunction for the variational problem can therefore be written:

$$|\,\psi\rangle \;=\; \sum_{i=1}^{6} C_i D_i \tag{3.25}$$

Using this expression, one can compute the reduced entropy matrix and the von Neumann and linear entropies.

It is interesting to note that if the wavefunction is made of only one Slater determinant, (for instance only $C_1 \neq 0$) then the corresponding state is not entangled as the sum (3.25) is necessary to satisfy the Pauli exclusion principle.

Now we note that for $\{C_1 \neq 0, C_2 \neq 0\}$, the corresponding state can also be written as a single Slater determinant.

Indeed we have immediately:

$|\,\psi\rangle \;=\; C_1 D_1 \,+\, C_2 D_2 \;=$

$=\; C_1 \frac{1}{\sqrt{2}}\{\phi_1(r_1)\phi_2(r_2) \,-\, \phi_2(r_1)\phi_1(r_2)\} \,+\, C_2 \frac{1}{\sqrt{2}}\{\phi_1(r_1)\phi_3(r_2) \,-\, \phi_3(r_1)\phi_1(r_2)\} \;=$

$$=\; \frac{1}{\sqrt{2}}\{\phi_1(r_1)[C_1\phi_2(r_2) \,+\, C_2\phi_3(r_2)] - [C_1\phi_2(r_1) \,+\, C_2\phi_3(r_1)]\phi_1(r_2)\} \tag{3.26}$$

that obviously constitutes just one Slater determinant.

Analogously if only $\{C_1, C_2, C_3\}$ are different from zero.

We again have the same situation if only $\{C_4, C_5\}$ are different from zero. These observations have been very useful for interpreting our results.

We also note that we could describe in detail the entanglement origin, just because we used an orthonormal Fock basis. If we had used a non orthonormal basis, as in the Pekeris method, this detail would not have been possible, and the dubious cases would have been much more difficult to discuss (see the singlet discussion).

3.3.2 The singlet case

In this case the orbital eigenfunctions must be symmetrical, and Slater permanents must be used instead of determinants. The discussion parallels that of the triplet case, but we have a considerable extra complication. This is evident if one explicitly writes the Fock space for n=3 base orbitals. We have $3 \times 4/2 = 6$ states:

$$P_1 = |\,1,\,1\rangle = \phi_1(r_1)\phi_1(r_2) \tag{3.27}$$

$$P_2 = |\,1,\,2\rangle = \frac{1}{\sqrt{2}}\{\phi_1(r_1)\phi_2(r_2) + \phi_2(r_1)\phi_1(r_2)\} \tag{3.28}$$

$$P_3 = |\,1,\,3\rangle = \frac{1}{\sqrt{2}}\{\phi_1(r_1)\phi_3(r_2) + \phi_3(r_1)\phi_1(r_2)\} \tag{3.29}$$

$$P_4 = |\,2,\,2\rangle = \phi_2(r_1)\phi_2(r_2) \tag{3.30}$$

$$P_5 = |\,2,\,3\rangle = \frac{1}{\sqrt{2}}\{\phi_2(r_1)\phi_3(r_2) + \phi_3(r_1)\phi_2(r_2)\} \tag{3.31}$$

$$P_6 \;=\; |\,3,\,3\rangle \;=\; \phi_3(r_1)\phi_3(r_2) \tag{3.32}$$

The new problem is given by the states P_1, P_4 and P_6, that are clearly separable. There is therefore a great uncertainty about how to consider for instance the entanglement in the state

$$|\,\psi\rangle \;=\; C_1P_1 \,+\, C_2P_2 \tag{3.33}$$

This problem has to be added to the others already faced in the triplet case.

Anyway, we can assert that, in the present case, using a single particle orthonormal basis, we can state the problem in a very precise way. As already noted in the triplet case, using an unorthonormal basis, as in the Pekeris method, would completely obscure the situation.

We will not address here the unsolved problem of quantification of entanglement for a generic state Ψ.

On the other hand, since from our calculations it turns out that for each low-energy helium eigenstate the reduced density operator for the orbital part is rather weakly perturbed with respect to one of the two above non-entangled cases, we expect that an approximate quantification of entanglement is provided by the distance between the von Neumann entropy $S(\rho_1)$ of ρ_1 and the von Neumann entropy $S(\rho_1^{(0)})$ ($S(\rho_1^{(0)}) = 0$ or $S(\rho_1^{(0)}) = 1$) of the reduced density operator $\rho_1^{(0)}$ for the corresponding non-interacting, non-entangled state:

$$E(|\Psi\rangle) = |S(\rho_1) - S(\rho_1^{(0)})|. \tag{3.34}$$

We expect such quantification to be in general meaningful only in the regime of weak

interactions, such that $|S(\rho_1) - S(\rho_1^{(0)})| \ll 1$. Note, however, that for antisymmetric orbital wave functions this definition reduces to (3.17) and therefore could be applied in this case also for strong interactions.

First of all, it is necessary to develop some intuition about the physical nature of the eigenfunctions of the states listed in the tables that follow. We will limit our investigation to the ground state and singly excited eigenstates of helium.

With regards to the computation of energies, those states can be described with an optimal approximation using a single Slater determinant or permanent for the orbital part.

The spin part is not important, as in the adopted approximation the spin motion is separable.

This means that in a first approximation the orbital part of singlets in 3.2 is given by a Slater permanent, and that of triplets in 3.3 by a Slater determinant.

These two descriptions basically differ for the Fermi Heap of the singlet case and the Fermi Hole in the triplet case.

It must be taken into account that when one considers more excited cases, that is when n of states 1s,ns is increased, the difference between the orbital parts of states 1S and 3S is more and more attenuated, as it is confirmed considering the energies of the "exact" states, that become more similar. In table 3.1 we report the energies and their differences for some values of n, with data from (Kono, Hattori , 1986); see also (Kono, Hattori , 1985) and (Drake , 1999)

This suggests that in these Helium states, when the energy increases, one obtains the situation in which one electron is in the 1s state and the other is in the ns state.

This is confirmed by the von Neumann entropy values, as reported in tables 3.2 and 3.3, that are taken from the result section 6.3 and copied here to facilitate the discussion.

The von Neumann and linear entropies have been computed first finding the minimum value of the energy of each state, then computing the eigenvalues of the reduced density

n	singlet energy abs. value in a.u.	triplet energy abs. value in a.u	difference
1	2.903 724	—	—
2	2.145 974	2.175 229	0.029 255
3	2.061 272	2.068 689	0.007 417
4	2.033 587	2.036 512	0.002 925
5	2.021 177	2.022 619	0.001 442
6	2.014 563	2.015 377	0.000 814
7	2.010 626	2.011 130	0.000 504
8	2.008 094	2.008 427	0.000 333

Table 3.1 – Energy of singlet and triplet eigenstates from (Kono, Hattori , 1986)

State	$S(\rho_1)$	$S_L(\rho_1)$
$\|(1s)^2;{}^1S\rangle$	0.0785	0.01606
$\|1s,2s;{}^1S\rangle$	0.991099	0.48871
$\|1s,3s;{}^1S\rangle$	0.998513	0.49724
$\|1s,4s;{}^1S\rangle$	0.999577	0.49892
$\|1s,5s;{}^1S\rangle$	0.999838	0.499465
$\|1s,6s;{}^1S\rangle$	0.999923	0.499665
$\|1s,7s;{}^1S\rangle$	0.999961	0.499777

Table 3.2 – Reduced von Neumann and linear entropies for the lowest energy singlet eigenstates of helium.

State	$S(\rho_1)$	$S_L(\rho_1)$
$\|1s,2s;{}^3S\rangle$	1.00494	0.500378
$\|1s,3s;{}^3S\rangle$	1.00114	0.5000736
$\|1s,4s;{}^3S\rangle$	1.000453	0.5000267
$\|1s,5s;{}^3S\rangle$	1.000229	0.5000127
$\|1s,6s;{}^3S\rangle$	1.000133	0.5000070
$\|1s,7s;{}^3S\rangle$	1.000091	0.5000047

Table 3.3 – Same as in Table 3.2, but for the lowest energy triplet eigenstates of helium.

matrices built with the corresponding eigenvectors.

We remark that the von Neumann entropy, that has been computed in bits, that is using base 2 logarithms, approaches the value 1 for increasing energy.

This is in agreement with the fact that the approximation gets better using a single Slater permanent or determinant, with the exception of the case $1s^2$ that is separable.

But the value 1 must be subtracted from entanglement as it is due only to the wave function simmetry that must be imposed to fulfill the Pauli exclusion principle.

This subtraction must not be performed for the fundamental state $1s^2$ as this state is separable.

So the physical meaning of the figures in tables 3.2 and 3.3 is that the fundamental state has entropy near to zero, as it is separable. Higher states have some difference entropy from the other separable state, with entropy = 1 due to antisymmetrization only. Increasing the energy, however, their entropy approaches 1, that is they tend to a separable state.

Another point that must be noted in 3.2, corresponding to the Slater permanents, with the exception of the fundamental state, the entropy is constantly **increasing** and approaches 1 increasing n.

This suggests to take as a measure of entanglement the modulus of the difference between the entropy and the value 1 due to the symmetrization only. We do not intend to propose an entanglement measure in a rigorous sense; that is not one satisfying all the requirements listed e.g. in (Vedral, Plenio et al. , 1997), (Plenio, Virmani , 2007); in particular we are not going to show that it is not increasing under Local General Measurements and Classical Communication. Our aim is just to have some provisional heuristics that could put some order in the data.

In the analogous case of table 3.3, the von Neumann entropy value is always greater than 1, and approaches 1 increasing the energy. The same reasoning holds as before, but now the value 1 must be subtracted from the von Neumann entropy.

The fact that, with the exception of the fundamental state, the entropy is slightly less than 1 for table 3.2 and slightly greater than 1 for table 3.3 can be quite simply explained observing the reduced density eigenvalues, that in the case of table 3.3 are pairwise identical.

In this ways it is justified the expression (3.34) assumed for the entanglement of the

considered Helium states.

Chapter 4

Entanglement computation: state of the art

In order to highlight the specificities of our method and the importance of the points that we deal with, we now illustrate the main results from the literature.

As outlined in the introduction, we will consider studies from the quantum computers implementation area and from Biology, that apply to several systems, and other works that are specific for the Helium atom.

4.1 Studies related to implementations of quantum computers

Miniaturization provides us with an intuitive way of understanding why, in the near future, quantum mechanics will become important for computation, even for classical computers.

Smaller size circuits boost computer power because the communication between components is faster, smaller active components are faster and at the same time their density increases.

The progress in miniaturization may be quantified empirically in Moores law (Moore , 1965). This law is the result of a remarkable observation made by Gordon Moore in 1965: the number of transistors on a single integrated-circuit chip doubles approximately

every 18 - 24 months. This exponential growth has not yet saturated and Moores law is still valid. Presently integrated circuits feature minimum size is about 25 nm. In 8 years we can expect that it will decrease by another order of magnitude. As the size of the smallest molecule, H_2, is $\approx$ 0.1 nm at that point, quantum effects will become unavoidably dominant.

They will have a disturbance effect on classical computing devices, or will be used to build quantum computers. For both reasons it is important to study quantum effects in atoms and molecules, from the point of view of computing machines engineering.

Many studies have dealt with many physical systems that might be good candidates for the implementation of quantum computers, and very interesting few-qubit experiments have been performed both with natural and artificial atoms and molecules, see e.g. (Benenti, Strini , 2007), (Buluta, Ashab et al. , 2011).

However even when studying natural systems, pratically all the authors use some specific setting, that is well suited only to the experimental situation in which they are interested.

For instance (Blatt, Wineland , 2008) reviewed the research about entangled states of trapped atomic ions. Ions can be confined for long durations while experiencing only small perturbations from the environment, and can be coherently manipulated.

To study entanglement, a group of atomic ions is confined in a particular arrangement of electric and/or magnetic fields. In this way one gets a collection of quantum systems that can be individually manipulated, their states entangled, and their coherences maintained for long durations, while suppressing the effects of couplings to the environment.

Two specific internal states of each ion are selected, and entanglment between pairs of ions is studied.

(Bloch , 2008) considered neutral atoms in optical lattices. In these experiments, neutral atoms are trapped in microscopic potentials engineered by laser light and their interactions are controlled with increasing precision.

Ultracold atoms are loaded into three-dimensional arrays of microscopic trapping potentials, known as optical lattices, in such a way that every lattice site is occupied by a single atom. After initialization, the interactions and the states of the atoms are controlled to coax them into the correct entangled state.

Rydberg atoms, that is atoms with an external electron in a highly excited state, have been extensively used in quantum information experiments, as reviewed in (Saffman, Walker et al. , 2010). Also in this cases, in general, two specific levels are selected, and the experiments involve the interactions and entanglement of Rydberg atoms and photons or of couples of Rydberg atoms. The approach can be based on trapped atoms, or on cavity quantum electrodynamics.

Also polar molecules have been considered to realize qubits, see e.g. (Micheli, Brennen et al. , 2006). The basic building block is a system of two polar molecules strongly trapped at given sites of an optical lattice, where the qubit is represented by a single electron outside a closed shell of a molecule formed by more than one element in its rotational ground state.

All the above cases share the fact that 1) only a few states of the systems are selected, often just the two levels that are necessary to engineer a qubit, and the experimental setting tends to exclude all the other states; 2) the systems are artificially kept in the experimental environment. So, however intersting, they do not study entanglement in natural conditions.

On the other hand, studying natural atoms and molecules in their natural conditions, as we do in the present work, has two important advantages as it can shed light on:

1) the difficulties that one will meet when the dimensions of classical computer will become of the order of magnitude of molecules and atoms, and natural quantum effects in the materials will interfere with the computer operations

2) the possibility of using natural molecules, or polymers, to hold active elements (gates, etc.) instead of artificially trapping them. In this way one could achieve the maximal miniaturization, probably the same of biological systems.

4.2 Methods used in Biochemistry and Biology

We consider a family of models used to model active sites, see for instance (Sarovar, Ishizaki et al. , 2010) and (Whaley, Sarovar et al. , 2010). The physical elements that are relevant for the phenomenon of interest, e.g. the "chromophores" in photosyntesis, are described as two level systems, that can be grouped in higher level structures. A hamiltonian function is then derived for these structures, using measures of site energies and coupling strengths. In general, a term is added to take into account the interplay between internal coherent dynamics and decoherence effects due to enviromental interactions.

So the total Hamiltonian has the form:

$$H = H_{int} + H_{int-env} + H_{env} \tag{4.1}$$

where H_{int} is the term describing the dynamics of the N active elements considered as closed systems, and can be written in the form:

$$H_{int} = \sum_{i=1}^{N} E_i |\, i\rangle \langle i\,| + \sum_{i=1}^{N} \sum_{j>i}^{N} J_{ij}(|\, i\rangle \langle j\,| + |\, j\rangle \langle i\,|) \tag{4.2}$$

here $|\, i\rangle$ represents the state in which only the ith element is excited, E_i are the on-site energies and J_{ij} are the coupling strengths, both measured experimentally.

For the term expressing the interaction with the environment it is used a form like the following:

$H_{int-env} = \sum_{i=1}^{N} |\, i\rangle \langle i\,| \sum_{\xi} g_{\xi}^{i} Q_{\xi}^{i}$

where Q_{ξ}^{i} is a phonon mode indexed by ξ, coupled to the chromophore i with strength g_{ξ}^{i}. With some realistic hypotheses on the enviromental properties, one can obtain a practical expression of the above Hamiltonian, suitable for numerical calculations.

At this point, numerical values for the relevant quantities are derived from the experiments and used in simulations to evaluate the entanglement.

(Adolphs, Müh et al. , 2010) study the crystal structure of the photosystem I (PSI) core complex from the thermophilic cyanobacterium Thermosynechococcus (T.) elongatus. This pigment-protein complex (PPC) binds both RC pigments and light harvesting antenna pigments inseparably on the same protein. To model their optical spectra, they take into account the pigment-pigment (excitonic) as well as the pigment-protein (exciton-vibrational) coupling. Their approach is based on a standard Hamiltonian for PPCs that models the pigments as coupled two-level systems interacting with vibrational degrees of freedom of the protein. The method combines quantum chemical calculations on the pigments in vacuum with electrostatic Poisson-Boltzmann type calculations on the whole PPC in atomic detail. They calculate the site energies of the 96 Chlorophyll a molecules composing the PSI. These site energies are used together with the excitonic couplings to simulate optical spectra. The calculated spectra match the experimental data semiquantitatively and allow for a detailed analysis of structure-function relationships.

(Olbrich, Jansen et al. , 2011) give a parameter-free calculation of the excited-state dynamics and the linear and two-dimensional spectra for Fenna-Matthews-Olson (FMO) Light Harvesting system. Their method is based on a combination of classical molecular dynamics (to describe the systems) and electronic structure calculations (to model their optical properties and the excitation transfer). The computations are based on the Hartree Fock framework but two-center electron interaction integrals are neglected. They present simulations of the linear absorption, population transfer, and two-dimensional spectra of the FMO complex. From the simulations they find that even though little coherent population transfer between sites is observed in the FMO complex at room temperature the overall excitation transfer is very efficient with transfer times across the complex of only 100 fs.

(Christensson, Kauffmann , 2012) use a vibronic exciton model to explain the long-lived oscillatory features in the two-dimensional electronic spectra of the FMO complex. Using experimentally determined parameters and uncorrelated site energy fluctuations, the model predicts oscillations with dephasing times in a good agreement with the experi-

mental results. The long-lived oscillations are found to reflect coherent superpositions of vibronic exciton states with dominant contributions from vibrational excitations on the same pigment. Such "intrapigment" coherences experience weak homogeneous and inhomogeneous dephasing due to the inherent correlation of transition frequency fluctuations of the involved states.

(Alicki, Miklaszewski , 2012) propose a model based on a resonant, coherent energy exchange between the donor site and the acceptor one accompanied by an irreversible energy transfer to the sink. They consider an optical cavity which consists of two parabolic mirrors with a common symmetry axis and two identical two-level atoms placed in the focuses of the mirrors with transition dipoles parallel to the axis. When one of the atoms is excited the emitted photon will be bouncing between atoms. If additionally the first atom (donor) is excited by a light source and the second (acceptor) is coupled to an energy sink, a mechanism of energy transfer from a source to a sink is obtained. A standard tight-binding model of energy transport in quantum networks in the single-exciton approximation is used. This approximation is valid when the exciton lifetime is much longer than any other relevant time scale. To describe irreversible energy transfer phenomena they take into account the coupling to vibrational degrees of freedom.

(Pereverzev, Bittner et al. , 2009) consider the problem of partitioning a system with both discrete and continuous degrees of freedom into interacting subspaces such that the motions that are most strongly coupled are given explicit treatment while the remainder serve as auxiliary degrees of freedom, quantum or classical, as a thermal bath, or are ignored completely. Their methods can be applied to charge transfer in a model donor/acceptor system to reduce dramatically the number of explicit phonon modes needed to compute accurate correlation functions.

(Walschaers, Mulet et al. , 2012) describe a general mechanism to achieve fast quantum energy transport in disordered systems, that could be at the core of the light harvesting. The two main ingredients are: the centro-symmetry of the Hamiltonian H of the system and the existence of a dominant doublet coupling the input and output states. Centro-symmetry, with respect to the input and output sites' states, means that defining $J_{ij} = \delta_{i,N-j+1}$ the exchange matrix, $JH = HJ$ and $|\,in\rangle = J|\,out\rangle$. This property has been

shown to be strongly correlated to transfer efficiency by (Zech, Mulet et al. , 2012). These authors found that, starting from a random network of intermediate sites and using a genetic algorithm to maximize the efficiency, one moves towards higher degrees of centro-symmetry.

The role of quantum interference on the transport effciency has been studied by (Scholak, Mintert et al. , 2010). As the Hamiltonian of the whole system in many cases is not known, they introduced disorder into the model, treating the matrix elements of the Hamiltonian as stochastic variables. In some conditions (localization in 1 or 2 dimensions and short range interactions), the quantum interference suppresses the classical transport, and the input remains localized near the initial site. There are however some realization of the disorder for which the transfer may be enhanced by quantum interference. Moreover, it is shown that exceptional multisite entanglement properties characterize those configurations that show particularly good transport properties. In particular, entanglement must ensure that the excitation is distributed on several sites of the chain from the input to the target (e.g. at least four out in a chain of seven). Moreover entanglement must vanish when the excitation reaches the output site.

(Scholak, Wellens et al. , 2011) used a statistical ensemble of Hamiltonians of the form 4.2 to evaluate the importance of coherence on the energy transport efficiency and the effect of noise. They considered a chain of N molecules, with the first one acting as the "input" site, that is receiving energy from outside, and the last acting as the "output" of the transport. Two quantitative measures of efficiency are defined: the first is the probability $\mathcal{P}$ that the excitation reaches the output site in a short time; the second is the transfer time $\mathcal{T}$ to a "sink", that is a reservoir that absorbs energy. A numerical optimization method is used to find the configurations that maximize $\mathcal{P}$ or minimize $\mathcal{T}$, both in absence and in presence of noise. The authors point out that the two efficiency measures lead to different optimal configurations. Moreover, the fastest excitation transfer is realized without noise. Most configurations of the statistical ensemble are not very efficient, as the quantum interference is destructive: in these cases, adding noise accelerates the transfer of energy. However, there are some very efficient coherent configurations that benefit of constructive interference and that are slowed down by noise.

(Scholak, Wellens et al. , 2011) conclude that molecular Hamiltonian should be characterized as precisely as possible, since their statistical studies indicate that the transport properties sensitively depend on the particular configuration. The same need for more detailed models is stressed by (Tiersch, Popescu et al. , 2012), who describe a counter-example showing that the arguments presented so far are not sufficient to prove neihter the presence of entanglement in the excitation transport nor its importance, even if present.

For our purposes, it is important to stress that, however detailed, these models do not start from the basic chemical structures of the proteins involved, they are not "ab-initio" computations, but phenomenological models that provide entaglement estimates, once they are feeded with experimental data.

The approach that we will follow in the present work is, on the contrary, to start from the bottom level of intra atomic entanglement, with the goal of eventually arrive at the level of the phenomenological description.

In this way, models like those described above will be completely justified.

4.3 Computations for Helium and other atoms

4.3.1 Analytical methods

Some authors, see e.g. (Amovilli, March , 2003), (Amovilli, March , 2004), (Nagy , 2006), (Moshinsky , 1968), (March, Cabo et al. , 2008), (Yanez, Plastino et al. , 2010), used analytical models to compute the entanglement in atoms. Some of these will be described more extensively in section 4.4.1.

Although these papers highlight some interesting aspects of the problem, it must be stressed that all of them use some simplifications in the hamiltonian, so that the problem can be treated analytically.

We used the hamiltonian of the system, that has the form:

$$H = -\frac{1}{2}\nabla_1^2 - \frac{1}{2}\nabla_2^2 - \frac{z}{r_1} - \frac{z}{r_2} + \frac{1}{r_{12}} \tag{4.3}$$

on the contrary, these models use hamiltonians like the following:

$$H = -\frac{1}{2}(\nabla_1^2 + \nabla_2^2) + \frac{1}{2}\omega^2(r_1^2 + r_2^2) + P(r_{12}) \tag{4.4}$$

where $P(r_{12})$ is the interaction potential, and is $\propto r_{12}^2$ in the Moshinsky, $\propto \frac{1}{r_{12}^2}$ in the Crandall and $\propto \frac{1}{r_{12}}$ in the Hooke model.

As a consequence, none of those models can be considered an high precision description of a real atom.

The main enhancement of our method is that we decided to use the hamiltonian without any simplifications, in order to represent the actual behaviour of the Helium and other atoms or molecules. We used standard high precision results about energies to check that our model did not substantially differ from an accurate description of the atom, as it will be extensively shown in the result sections.

4.3.2 The Osenda Serra results

In a set of papers, (Osenda, Serra , 2007) (Osenda, Serra , 2008) (Ferron, Osenda et al. , 2009), the authors computed the von Neumann entropy of a two electron system, a heliumlike atom, near the ionization threshold.

Their model considers again a simplified hamiltonian, namely one of the form:

$$H = -\frac{1}{2}\nabla_1^2 - \frac{1}{2}\nabla_2^2 - \frac{z}{r_1} - \frac{z}{r_2} + \lambda\frac{1}{r_>} \tag{4.5}$$

where $r_> = max(r_1, r_2)$. This means that the models uses a spherical average of the repulsion between electrons.

We note that, on the contrary, we considered both the interactions for $r_>$ and for $r_<$, see section 5.11 about the Coulson and Sharma integrals.

Results: in (Osenda, Serra , 2007) the von Neumann entropy of the ground state only of Helium is computed. The focus of the paper is on its dependence on the "coupling" parameter λ. When $\lambda \to 0$ the two electrons become independent, and a critical value λ_c is found such that for $\lambda > \lambda_c$ the system consists of one electron bounded to the nucleus and a free electron.

In (Osenda, Serra , 2008) a similar model is used to compute the dependence on λ of the von Neumann entropy of the lowest energy triplet state.

In (Ferron, Osenda et al. , 2009) a differend model is used, namely a quantum dot system is considered, in which the two electrons are confined by a potential of radius R. The hamiltonian has the form:

$$H = -\frac{1}{2}(\nabla_1^2 + \nabla_2^2) + V(r_1) + V(r_2) + \frac{1}{|r_{12}|} \tag{4.6}$$

with

$$V(r) = V_0,\ r < R;\ \ V(r) = 0,\ r \geq R \tag{4.7}$$

This model is actually quite different from the Helium atom that we are considering.

4.3.3 A computation for the Helium atom

In (Dehesa, Koga et al. , 2012) the entanglement of a full model of the Helium atom is computed.

State	present work	(Dehesa, Koga et al. , 2012)
$\vert\,(1s)^2;\,^1S\rangle$	0.01606	0.015914 ± 0.000044
$\vert\,1s,2s;\,^1S\rangle$	0.48871	0.48866 ± 0.00030
$\vert\,1s,3s;\,^1S\rangle$	0.49724	0.49857 ± 0.00097
$\vert\,1s,4s;\,^1S\rangle$	0.49892	0.49892 ± 0.00052
$\vert\,1s,5s;\,^1S\rangle$	0.499465	0.4993 ± 0.0019
$\vert\,1s,6s;\,^1S\rangle$	0.499665	-
$\vert\,1s,7s;\,^1S\rangle$	0.499777	-

Table 4.1 – Comparison of Linear Entropy values for singlet

The model employes wavefunctions in Hylleraas coordinates, described in section 4.4.2, eq. (4.23) and (4.24).

The entanglement is evaluated computing the linear entropy, that implies to evaluate:

$$Tr[(\rho_1^{(coord)})^2] = \int_{R^6} |\,\rho_1^{(coord)}(\mathbf{r'_1},\,\mathbf{r_1})\,|^2\,d\mathbf{r_1}\,d\mathbf{r'_1} = \int_{R^6} |\int_{R^3}\psi(\mathbf{r'_1},\,\mathbf{r_2})\psi^*(\mathbf{r_1},\,\mathbf{r_2})\,d\mathbf{r_2}\,|^2\,d\mathbf{r_1}\,d\mathbf{r'_1} =$$

$$= \int_{R^{12}}\psi(\mathbf{r'_1},\,\mathbf{r_2})\psi^*(\mathbf{r_1},\,\mathbf{r_2})\psi(\mathbf{r'_1},\,\mathbf{r'_2})\psi(\mathbf{r_1},\,\mathbf{r'_2})\,d\mathbf{r'_1}\,d\mathbf{r_1}\,d\mathbf{r'_2}\,d\mathbf{r_2} \tag{4.8}$$

that is a 12-dimensional integral, that was computed using Monte Carlo multidimensional numerical integration.

The authors computed the linear entropy for several levels of the singlet and triplet; in tables (4.1) and (4.2) we report their results and a comparison with ours when applicable.

Actually, our work can be considered an extension of (Dehesa, Koga et al. , 2012), as we computed some more levels, and we were able to evaluate also the von Neumann entropy, because our method computes the eigenvalues of the density matrix.

Another difference is that the Monte Carlo integration implies some numerical errors, as reported in the tables. On the contrary, in our method, once one has attained a requested precisions in the energy, the entropies are computed using only algebraic operations, so no other approximations or errors are involved.

State	present work	(Dehesa, Koga et al. , 2012)
$\mid 1s, 2s;\ ^3S\rangle$	0.500378	0.47778 ± 0.00027
$\mid 1s, 3s;\ ^3S\rangle$	0.5000736	0.49342 ± 0.00045
$\mid 1s, 4s;\ ^3S\rangle$	0.5000267	0.49746 ± 0.00055
$\mid 1s, 5s;\ ^3S\rangle$	0.5000127	0.499 55 ± 0.00098
$\mid 1s, 6s;\ ^3S\rangle$	0.5000070	-
$\mid 1s, 7s;\ ^3S\rangle$	0.5000047	-

Table 4.2 – Comparison of Linear Entropy values for triplet

As (Dehesa, Koga et al. , 2012) aims are very similar to ours, we will spend some words to describe their computation, the main differences with our results, and their physical meaning.

Considering a pure state $\mid \Phi\rangle$ of N identical fermions, the autors consider the single particle reduced density matrix $\rho_1^{spin+coord} = Tr_{2,3,\ldots,N}(\mid \Phi\rangle\langle\Phi \mid)$, that includes both the spin and orbital contributions to entanglement, and propose as a measure for the amount of entanglement:

$$\xi(\mid \Phi\rangle) \;=\; N[S_L(\rho_1^{spin+coord}) \;-\; \frac{N-1}{N}\,] \tag{4.9}$$

where $S_L(\rho) = 1 - Tr(\rho^2)$ is the linear entropy and the factor $\frac{N-1}{N}$ takes into account the fact that even for separable states the linear entropy of the single particle density matrix does not vanish. In the Helium case N=2 and we get:

$$\xi(\mid \Phi\rangle) \;=\; 2\,S_L(\rho_1^{spin+coord}) \;-\; 1 \tag{4.10}$$

Then the authors, as we ourselves will do, consider wavefunctions factorized in a coordinate and a spin factor, obtaining for the density matrix:

$$\rho \;=\; \rho^{coord} \otimes \rho^{spin} \tag{4.11}$$

and substituting in 4.10:

$$\xi(|\,\Phi\rangle) \;=\; 1 \;-\; 2\,Tr[(\rho_1^{spin})^2]\,Tr[(\rho_1^{coord})^2] \tag{4.12}$$

At this point the authors discuss separately the case of parallel and anti-parallel spins. In case of parallel spins, that is in two out of the three possibilities for triplets, $Tr[(\rho_1^{spin})^2] = 1$, and the entanglement measure becomes:

$$\xi(|\,\Phi\rangle) \;=\; 1 \;-\; 2\,Tr[(\rho_1^{coord})^2] \tag{4.13}$$

The anti-parallel case can happen for the third triplet possibility, with an antisymmetric coordinate wavefunction, and for the singlet states, with a symmetric coordinate wavefunction. In both cases $Tr[(\rho_1^{spin})^2] = 1/2$ and we get for the entanglement measure:

$$\xi(|\,\Phi\rangle) \;=\; 1 \;-\; Tr[(\rho_1^{coord})^2] \tag{4.14}$$

that is the Linear Entropy of the reduced density matrix of the coordinate part.

Table 4.1 shows that there is a good agreement between our and (Dehesa, Koga et al. , 2012) values for the entanglement of the singlet states, (that coincides with the Linear Entropy of ρ_1^{coord}) and that it is increasing with the energy of the states.

Table 4.2 compares our results for the Linear Entropy of ρ_1^{coord} of the triplet states and (Dehesa, Koga et al. , 2012) values for the entanglement of the anti-parallel spin triplets, that is computed with the same formula (4.14). It can be seen that in this case we do not

State	present work	(Dehesa, Koga et al. , 2012)+err	-err
$\|1s, 2s;\ ^3S\rangle$	0.000756	-0.0439	-0.04498
$\|1s, 3s;\ ^3S\rangle$	0.000147	-0.01226	-0.01406
$\|1s, 4s;\ ^3S\rangle$	0.000053	-0.00398	-0.00618
$\|1s, 5s;\ ^3S\rangle$	0.000025	0.00106	-0.00286
$\|1s, 6s;\ ^3S\rangle$	0.000014	-	-
$\|1s, 7s;\ ^3S\rangle$	0.000009	-	-

Table 4.3 – Comparison of Entanglement values for triplet, parallel spin

have a good agreement, specifically we get values greater that 1/2, while (Dehesa, Koga et al. , 2012) are lower than 1/2.

Of course, it is possible to compute also the entanglement for the parallel spin triplets, using the data in table 4.2 and formulas (4.14), (4.13). This computation is shown in table 4.3 both for our and (Dehesa, Koga et al. , 2012) data, adding and subtracting the errors; in this case it is seen that one gets negative values for the entanglement, something that should not happen.

4.4 Examples of computation methods

Many methods have been used for the study of energies, some of these could be modified for the study of entanglement.

4.4.1 The Moshinsky, Crandall and Hooke models

These models have been used to obtain estimates of energies and entanglement in two electrons atoms. As they are solvable analytically, the role of some aspects of atomic physics can be investigated through detailed computations. Entanglement has been one of the most studied properties of the models.

The Moshinsky model consists of a system of two particles, interacting harmonically and immersed in a common harmonic isotropic potential. The model has been used to investigate fundamental properties of atomic physics, and to test the applicability in this

field of quantum information concepts. (See (Amovilli, March , 2003), (Amovilli, March , 2004), (Nagy , 2006), (Moshinsky , 1968), (March, Cabo et al. , 2008), (Yanez, Plastino et al. , 2010)

In the monodimensional case, if x_1 and x_2 are the coordinates of the particles, λ is the frequency of their interaction and ω is the frequency of the external field, the system's hamiltonian is:

$$H = -\frac{1}{2}\frac{\partial^2}{\partial x_1^2} - \frac{1}{2}\frac{\partial^2}{\partial x_2^2} + \frac{1}{2}\omega^2 x_1^2 + \frac{1}{2}\omega^2 x_2^2 + \frac{1}{2}\lambda^2(x_1 - x_2)^2 \tag{4.15}$$

We have set the common mass of the particles = 1, and $\hbar = 1$, that is we are using atomic units.

In the Crandall model, the Hamiltonian is:

$$H = -\frac{1}{2}(\nabla_1^2 + \nabla_2^2) + \frac{1}{2}\omega^2 (r_1^2 + r_2^2) + \frac{\lambda}{r_{12}^2} \tag{4.16}$$

while in the Hooke's model (see (Atre, Mohapatra et al. , 2004), (Coe, Sudbery et al. , 2008), (Loos , 2010)) it is:

$$H = -\frac{1}{2}(\nabla_1^2 + \nabla_2^2) + \frac{1}{2}\omega^2 (r_1^2 + r_2^2) + \frac{1}{r_{12}} \tag{4.17}$$

where ω is the frequency of the confining potential.

Using the center of mass system of coordinates, that is defining:

$$R = \frac{1}{\sqrt{2}}(x_1 + x_2) \quad r = \frac{1}{\sqrt{2}}(x_1 - x_2) \tag{4.18}$$

in the monodimensional case and in the three dimensional:

$\mathbf{R} = \frac{1}{\sqrt{2}}(\mathbf{r}_1 + \mathbf{r}_2), \quad \mathbf{r} = \frac{1}{\sqrt{2}}(\mathbf{r}_1 - \mathbf{r}_2)$

the Hamiltonian splits in a term depending only on r (or $\mathbf{r}$) and one depending only on R (or $\mathbf{R}$), and it is possible to find analytical solutions of the form f(r)g(R).

In this way, (Yanez, Plastino et al. , 2010) have computed the linear entropy of the Moshinsky atom through the reduced density matrix

$$\tilde{\rho}(x_1', x_1) = \int_{-\infty}^{+\infty} \psi^*(x_1, x_2)\, \psi(x_1', x_2)\, dx_2 \tag{4.19}$$

computing the trace of its square:

$$Tr(\tilde{\rho}^2) = \int_{-\infty}^{+\infty} |\, \langle x' \,|\, \tilde{\rho} \,|\, x \rangle \,|^2\, dx\, dx' \tag{4.20}$$

Defining the parameter

$\tau = \frac{\lambda}{\omega}$

that represents the relative strength of the interactions between the two particles, compared with the external field, they have derived the following behaviour of the entanglement:

state	$lim_{\tau\to\infty}$	$lim_{\tau\to 0}$
$\|00\rangle$	1	0
$\|01\rangle$	1	0.5
$\|10\rangle$	1	0.5
$\|11\rangle$	1	0.5
$\|20\rangle$	1	5/8
$\|02\rangle$	1	5/8

The same authors report some interesting qualitative observations for this model:

- in general the entanglement increases with τ, the strength of the interaction

- the entanglement tends to increase also with the energy (that is considering more excited states)

- however, there are exceptions to this rule, for instance for high values of the interaction the state $|11\rangle$ with anti parallel spins has more entanglement than $|02\rangle$ also with anti parallel spins.

- for states sharing the same anti symmetric coordinate wave function states with parallel spins have less entanglement than those with anti parallel spins

- the entanglement of excited states with anti parallel spins does not go to zero for $\tau \to 0$. This entanglement is not due to the correlations arising from the antisymmetry of the global state.

Turning to the Hooke's atom, (Coe, Sudbery et al. , 2008) have computed both the linear and von Neumann entropies of the model in function of the parameter ω. The entanglement increases with decreasing confining potential, as this means that the relative strength of the electrons' interaction increases.

For large values of ω the entanglement is essentially zero. For intermediate values of ω, the entanglement increases sharply. When $\omega \leq 0.001$ Hartrees, the increase of entanglement diminishes significantly. The behaviour is qualitatively the same both for the linear and

the von Neumann entropies.

4.4.2 Helium in Hylleraas coordinates - the Pekeris model

This model is more realistic than the Moshinsky, Crandall and Hooke atoms, as it uses a physically sound potential.

Following Pekeris's approach (see (Barnett , 2003), (Barnett, Capitani et al. , 2004), (Koutschan, Zeilberger , 2010), (Pekeris , 1958), (Pekeris , 1959)), we used this model to perform some preliminary computations.

The Hamiltonian is:

$$H = -\frac{1}{2}\nabla_1^2 - \frac{1}{2}\nabla_2^2 - \frac{z}{r_1} - \frac{z}{r_2} + \frac{1}{r_{12}} \tag{4.21}$$

where z is the nucleus charge, r_1 and r_2 are the distances of the electrons from the nucleus and r_{12} is their mutual distance. One has:

$$\psi = \psi(r_1, r_2, r_{12}) \tag{4.22}$$

With

$$s = r_1 + r_2, \;\; t = r_2 - r_1, \;\; u = r_{12} \tag{4.23}$$

We look for a ψ of the form

$$\psi \;=\; N\, e^{-\frac{1}{2}ks} \sum c_{lmn} k^{l+m+n} s^l\, t^m\, u^n \tag{4.24}$$

The so-called perimetric coordinates u, v e w are defined in the following way:

$$u \;=\; \epsilon(r_2 \,+\, r_{12} \,-\, r_1) \tag{4.25}$$

$$v \;=\; \epsilon(r_1 \,+\, r_{12} \,-\, r_2) \tag{4.26}$$

$$w \;=\; 2\epsilon(r_1 \,+\, r_2 \,-\, r_{12}) \tag{4.27}$$

u, v and w are independent from each other and vary from 0 to ∞.

We set

$$\psi \;=\; e^{-\frac{1}{2}(u+v+w)} F(u,\, v,\, w) \tag{4.28}$$

We consider the series expansion

$$F \;=\; \sum_{l,m,n=0}^{\infty} A(l,\, m,\, n)\, L_l(u)\, L_m(v)\, L_n(w) \tag{4.29}$$

Where $L_n(w)$ is the Laguerre normalized plynomial of order n.

$$L_n(w) \;=\; \sum_{k=0}^{n} \tbinom{n}{k}\, \frac{(-w)^k}{k!}, \quad \int_0^{\infty} e^{-w}\, [\, L_n(w)\,]^2\, dw \;=\; 1 \tag{4.30}$$

Substituting the expressions (4.29) and (4.28) in the equation (4.21), and using the properties of the Laguerre polynomials, we obtain a (rather complex) recursion relation for the coefficients A(l,m,n), that is we obtain an equation in the A, that can be written in the more concise form

$$\sum_{\alpha,\beta,\gamma=-2}^{+2} C_{\alpha,\beta,\gamma}(l,\, m,\, n)\, A(l\, +\, \alpha,\, m\, +\, \beta,\, n\, +\, \gamma)\, =\, 0 \tag{4.31}$$

Then:

$$C_{-\alpha,-\beta,-\gamma}(l,\, m,\, n)\, =\, C_{\alpha,\beta,\gamma}(l - \alpha,\, m - \beta,\, n - \gamma) \tag{4.32}$$

If ψ is symmetric in the two electrons (singlet case) we have

$$A(l,\, m,\, n)\, =\, A(m,\, l,\, n) \tag{4.33}$$

while, if it is antisymmetric (triplet):

$$A(l,\, m,\, n)\, =\, -\, A(m,\, l,\, n) \tag{4.34}$$

The recursion equations represent a linear system for the A(l,m,n) coefficients. To manage this system, it is necessary to arrange the triple set of coefficients in a monodimensional array. This is done by first ordering the triples (l,m,n) and then assigning to each triple an index k in the following way:

$$A(l,\, m,\, n) \,=\, B_k \tag{4.35}$$

$k(l,\, m,\, n) \,=\, (\frac{1}{24})\omega\,(\omega \,+\, 2)\,(2\omega \,+\, 5) \,+\, \frac{1}{16}[\,1 \,-\, (-1)^{\omega}] +$

$$+\,\frac{1}{4}(l \,+\, m)^2 + \frac{1}{8}[1 \,-\, (-1)^{l+m}] \,+\, l \,+\, 1 \,+\, \frac{1}{2}(l+m) \tag{4.36}$$

where

$$\omega \,=\, l \,+\, m \,+\, n \tag{4.37}$$

The triples (l,m,n) are obtained with the schema of table 9.5 for the singlet and of table 9.6 for the triplet, (appendix 9.2), together with the a_{ik} and b_{ik} of order 13 for the singlet and triplet.

Substituting the triples (l,m,n) and the B_k in the equation (4.31), we obtain the equations:

$$\sum_k C_{ik}B_k \,=\, 0,\;\; C_{ik} \,=\, a_{ik} \,+\, \epsilon b_{ik} \tag{4.38}$$

The a_{ik} and b_{ik} are integers, and $C_{ik} \,=\, C_{ki}$

In order to evaluate the quality of the Pekeris equations, we solved the generalized eigenvalue problem for Z=2.

The results of 13 eigenvalues for states ^1S are reported in table 4.4.

In the first column there are the fundamental, 1st excited,... etc. states. In column A

		A		B		C
F		2.90357		2.903724366		53
1		2.07015		2.145974044		35333
2		1.53793		2.061271989		253893
3		0.884622		2.033586716		564994
4		0.787611		2.021176851		610321
5		0.721997		2.014563098		641611
6		0.618008		2.010625776		692629
7		0.510235		2.008093621		745911
8		0.453354				
9		0.292778				
10		0.219117				
11		0.123265				
12		0.00681448				

Table 4.4 – Pekeris energies ^1S z=2

we have reported the energies computed with the present method. In column B we have reported the standard energies (Kono, Hattori , 1985) and in column C the differencies in parts per million.

It must be noted that the Pekeris method does not have any variational parameters. Even if it was originally thought only for the computation of the fundamental state, one can see from the table that it gives good results also for some excited states.

It must also be noted that we used a matrix of dimension 13x13 only.

In table 4.5, we report the analogous computations for the triplet, Z=2.

Unfortunately, although we had these encouraging results, we did not pursue this kind of computation, because of the difficulty of the reduced density matrix computation.

Heavy numerical integration would be necessary in this case, that uses a unorthonormal basis.

In the next chapter we will describe the method that we employed, using an orthonormal basis.

	A	B	C
1	2.16715	2.175229378	3714
2	1.84795	2.068689067	106705
3	1.27713	2.036512083	372884
4	0.762199	2.0226189	623162
5	0.585709	2.015377452	709380
6	0.577895	2.011129919	712652
7	0.519663	2.008427122	741259
8	0.406628		
9	0.400415		
10	0.227294		
11	0.197454		
12	0.116188		
13	0.000405704		

Table 4.5 – Pekeris energies ^3S z=2

Chapter 5

Method used for the computations

5.1 Aims of the chapter

The present work basically consists of the computation of entanglement in Helium.

We aim at solving a standard problem, as simple as possible but not trivial, to test several computation methods and different approximations.

For this reason it is very useful to decribe in detail the method we employed, so that possible changes can be easily made. This will be necessary, as the numerical computation showed to be not trivial, and it must be checked which points can be simplified, to obtain a method that can be suitable even for more complex and interesting cases.

An important point is that we use a variational method to find the optimal values of the parameters. We use a well-known theorem, stating that the optimal values of the parameters can be found looking for the minimum energy, both for the fundamental and for the excited states.

We stress that we optimize the parameters looking for the minimum energy, but the goal of the computation is the evaluation of entanglement.

One of the goals of the present work is the evaluation of the sensitivity of the entanglement value on the parameters. Fortunately, we found that the entanglement computation is

not more critical than the energy, and the von Neumann entropy is slightly more difficult to compute than the linear entropy. By "difficulty" we mean the dimension of the Hilbert space that one must use to obtain a given precision.

In the following pages we report many details about the Hilbert and Fock spaces we employeded, so that when different bases are used in other chapters, a simple change of symbols will suffice.

5.2 Sketch of the algorithm

The computation is composed by the following steps:

Step 1: computation of the energy of a specific state of the system. The computation is done solving the stationary Schrödinger equation:

$$H\psi = \lambda\psi \tag{5.1}$$

where H is the system's hamiltonian, and finding the minimum of the eigenvalue corresponding to the selected state. The minimum is found varying a suitable parameter of the Hilbert space.

We have 3 substeps:

Step 1.1: computation of the Hamiltonian H of the system

Step 1.2: computation of eigenvalues and eigenvectors of H

Step 1.3: computation of the minimum of the eigenvalues

Step 2: computation of entanglement, with the substeps

Step 2.1: computation of the density matrix and reduced density matrix using the eigen-

vectors computed in step 1

Step 2.2: computation of the eigenvalues of the reduced density matrix, then computation of the entropies using eqs. (3.16), (3.18) and of the entanglement using eq. (3.34).

Step 1.1 will be extensively discussed in sections 5.4 and the following for Helium and in section 7.3 for the H_2 molecule.

Step 2.1 will be discussed in depth in section 5.3.

We now describe the other main substeps from a computational point of view.

5.2.1 Step 1.2: computation of eigenvalues and eigenvectors of the hamiltonian H

The computation of eigenvalues and eigenvectors of a matrix is a well-studied topic, see e.g. (Saad , 2011) where the calculation of electronic structure is quoted as a classical eigenvalue problem.

We considered several algorithms, trying to find the best mix of simplicity, speed, and accuracy. It is to be noted that the H matrix is symmetric.

The Jacobi algorithm consists of a sequence of plane rotations, designed to annihilate one of the off-diagonal elements. Even if successive transformations undo previously set zeroes, it is possible to make off-diagonal elements smaller and smaller.

The product of the transformations gives the matrix of eigenvectors, and the elements of the final diagonal matrix are the eigenvalues.

The method is slower than other, more sophisticated, but is quite simple, and it was our first choice.

A Jacobi rotation is a matrix of the form:

$$\mathbf{P}(pq) = \begin{bmatrix} 1 & 0 & ... & .. & 0 \\ 0 & 1 & 0.. & .. & 0 \\ 0 & ... & C.. & S & ..0 \\ 0 & ... & ...1 & .. & ..0 \\ 0 & ... & -S.. & C & ..0 \\ 0 & ... & ... & ... & ..0 \\ 0 & 0 & ... & .. & 1 \end{bmatrix} \tag{5.2}$$

that is, it is a unit matrix, except for the elements P_{pp}, P_{pq}, P_{qp} and P_{qq}, that are chosen to be:

$$S = sin\phi, \;\; C = cos\phi \tag{5.3}$$

with an angle ϕ that has to be determined. Given the H matrix, rotations are applied in order to obtain:

$$\mathbf{H}' = \mathbf{P}^T(pq)\,\mathbf{HP}(pq) \tag{5.4}$$

Only elements in the columns and rows p and q of H are changed, and one can compute explicitly the transformed element:

$$h'_{pq} = (C^2 - S^2)h_{pq} + SC\,(h_{pp} - h_{qq}) \tag{5.5}$$

Setting $h'_{pq} = 0$ one can find ϕ. Defining

$$\Sigma = \sum_{r \neq s} |\, h_{rs} \,|^2 \tag{5.6}$$

it can be shown that at each stage

$$\Sigma' = \Sigma - 2 \mid h_{pq} \mid^2 \tag{5.7}$$

so the sequence converges monotonically to a diagonal matrix $\mathbf{D}$. The elements of this matrix are the eigenvalues of H and the columns of the matrix

$$\mathbf{V} = \mathbf{P}(pq)\,\mathbf{P}'(p'q')\,... \tag{5.8}$$

are the eigenvectors, since $\mathbf{H}\,\mathbf{V} = \mathbf{V}\,\mathbf{D}$.

The divide and conqueror algorithm

We considered some improvements of the algorithm just described. We adopted as a starting point the Lapack library, and its divide and conquer driver (DSYEVD routine).

The first step of such algorithms is to reduce the input symmetric matrix to tridiagonal form. This is performed, in the Lapack library, by the routine DSYTRD, finding a decomposition

$$\mathbf{H} = \mathbf{Q}\,\mathbf{T}\,\mathbf{Q}^T \tag{5.9}$$

with $\mathbf{Q}$ orthogonal and $\mathbf{T}$ tridiagonal.

The second step is to compute the eigenvalues and eigenvectors of $\mathbf{T}$, that is equivalent to factorizing

$$\mathbf{T} = \mathbf{S}\,\mathbf{\Lambda}\,\mathbf{S}^T \tag{5.10}$$

Then the diagonal entries of Λ are the eigenvalues and coincide with the eigenvalues of the input matrix $\mathbf{H}$. The columns of $\mathbf{S}$ are the eigenvectors of $\mathbf{T}$, and the eigenvectors of $\mathbf{H}$ are the columns of $\mathbf{Q}\,\mathbf{S}$.

The idea of the divide and conqueror algorithm is the following. Consider:

$$\mathbf{T} = \left[\begin{array}{cccc|cccc} a_1 & b_1 & & & & & & \\ b_1 & b_2 & . & & & & & \\ & . & . & b_{m-1} & & & & \\ & & b_{m-1} & a_m & b_m & & & \\ -- & -- & -- & -- & -- & -- & -- & -- \\ & & & b_m & a_{m+1} & b_{m+1} & & \\ & & & & b_{m+1} & a_{m+2} & . & \\ & & & & & . & . & b_{n-1} \\ & & & & & & b_{n-1} & a_n \end{array}\right] =$$

$$= \left[\begin{array}{cccc|cccc} a_1 & b_1 & & & & & & \\ b_1 & b_2 & . & & & & & \\ & . & . & b_{m-1} & & & & \\ & & b_{m-1} & a_m \mp b_m & & & & \\ -- & -- & -- & -- & -- & -- & -- & -- \\ & & & & a_{m+1} \mp b_m & b_{m+1} & & \\ & & & & b_{m+1} & a_{m+2} & . & \\ & & & & & . & . & b_{n-1} \\ & & & & & & b_{n-1} & a_n \end{array}\right] +$$

$$+ \left[\begin{array}{ccc|ccc} & & & & & \\ & & & & & \\ & & & & & \\ & & \pm b_m & b_m & & \\ - & - & -- \quad - & -- & -- \quad - & - \\ & & b_m & \pm b_m & & \\ & & & & & \\ & & & & & \\ & & & & & \end{array}\right] =$$

$$= \begin{bmatrix} T_1 & | & \\ -- & | & -- \\ & | & T_2 \end{bmatrix} + \rho \mathbf{u}\mathbf{u}^T, \;\; \rho = \pm b_m \tag{5.11}$$

Then one solves the smaller eigenvalue problems (i=1,2):

$$\mathbf{T}_i = \mathbf{Q}_i \mathbf{\Lambda}_i \mathbf{Q}_i^T, \quad with\, \mathbf{Q}_i^T \mathbf{Q}_i = \mathbf{I} \tag{5.12}$$

These decompositions can be computed by any algorithm, and can also be further split by the same divide and conqueror algorithm. In this way one obtains a sequence of small problems, that can also be made suitable for parallel solving.

Then, sobstituting in (5.11), we arrive at the problem:

$$(\mathbf{D} + \rho \mathbf{v}\mathbf{v}^T)\mathbf{x} = \lambda \mathbf{x} \tag{5.13}$$

where $\mathbf{D}$ is the diagonal matrix of the eigenvalues of $\mathbf{Q}_1$ and $\mathbf{Q}_2$ and

$$\mathbf{v} = \begin{bmatrix} \mathbf{Q}_1^T & | & \\ & | & \mathbf{Q}_2^T \end{bmatrix} \mathbf{u} \tag{5.14}$$

Finding this spectral decomposition is the hearth of the algorithm. If

$$\mathbf{D} + \rho \mathbf{v}\mathbf{v}^T = \mathbf{Q}\mathbf{\Lambda}\mathbf{Q}^T \tag{5.15}$$

then we have for the original tridiagonal matrix:

$$\mathbf{T} = \begin{bmatrix} \mathbf{Q}_1 & | & \\ & | & \mathbf{Q}_2 \end{bmatrix} \mathbf{Q}\mathbf{\Lambda}\mathbf{Q}^T \begin{bmatrix} \mathbf{Q}_1^T & | & \\ & | & \mathbf{Q}_2^T \end{bmatrix} \tag{5.16}$$

Parallel algorithms

Although we did not face the problem of using very fast algorithms in the actual computations that we performed, we considered the possibility that, further increasing the dimension of the spaces, some major improvement could be necessary.

For this reason we considered the possibility of parallelization of the algorithms.

As already mentioned, one way could be to parallelize the divide and conqueror algorithm, see e.g. (Tisseur, Dongarra , 1999), who used the Lapack divide and conqueror routines as building blocks.

Other authors have adapted approximation methods, e.g (Dashti, Siahpirani et al. , 2010) have started with the classical Matrix Power Method. As it is well known, the main idea is to repeatedly apply the matrix to a suitably chosen start vector $\mathbf{x}$. Eventually the trasformed vectors will align in the direction of the eigenvector associated with the largest (in absolute value) eigenvalue.

Very sophisticated refinements of this algorithm have been proposed for parallel computation, but we did not study in deep the topic, as it is not presently needed for our goals.

5.2.2 Step 1.3: computation of the minimum of the eigenvalues

In what follows we consider the function

$$\lambda = f(\xi) \tag{5.17}$$

where λ is the eigenvalue of the level in which we are interested, and f is the hamiltonian

considered as a funciton of the variational parameter of the Hilbert space; we will now discuss algorithms to find local minima of f.

Golden search algorithm

The algorithm (Press, Teukolsky et al. , 2001) starts with a "bracketed" minimum of the function f, that is three points, say $a < b < c$ such that $f(b) < f(a)$ and $f(b) < f(c)$.

Then a new point d is chosen, either between a and b, if $b - a > c - b$ or between b and c in the opposite case. Suppose for instance that d is chosen between b and c. Then if $f(b) < f(d)$ the new bracketing triple is (a,b,d), on the contrary if $f(b) > f(d)$ the new triplet is (b,d,c).

The bracketing process is continued until the desired tolerance is reached, at each step:

- the middle point of the new triplet is the abscissa of the best minimum obtained

- the new point is choosen in the bigger of the two segments, at a distance of 0.38197 from one end and 0.61803 from the other (the golden section).

The initial bracketing was done either by a first coarse scanning or starting with any two points a,b and using a routine that computes f in a point external to (a,b) until a bracketing triplet is found.

Multidimensional minimum - Powell's method

In some tests we used bidimensional minimization, to evaluate the advantages one gets either using two parameters for a single shell or seeking the minima of the (single) parameters of two shells. Our tests showed that these advantages do not compensate for the higher complexity of those methods, and we accordingly minimized one shell at a time in our final computations. Nevertheless, we report the algorithm used, as it could be useful in some other system configurations.

The algorithm supposes that a linear minimization routine is available that, given as input the function f to be minimized, and vectors $\mathbf{P}$ (the initial point) and $\mathbf{n}$ (the initial

direction), finds the scalar λ that minimizes $f(\mathbf{P} + \lambda\mathbf{n})$. Then the initial point is replaced by $\mathbf{P} + \lambda\mathbf{n}$ and the initial direction by $\lambda\mathbf{n}$.

This linear minimization routine is basically a monodimansional minimization routine, like the one already described, applied to the function of one variable which is the value of f along the line from the initial point in the initial direction.

The structure of Powell's algorithm in N dimensional space is:

1) start with the directions $\mathbf{u}_i = \mathbf{e}_i$, the basis vectors, for $i = 1, ..., N$.

2) call the initial point $\mathbf{P}_0$.

3) for $i = 1, ..., N$ start from $\mathbf{P}_{i-1}$ and find the minimum along $\mathbf{u}_i$ and call this point $\mathbf{P}_i$

4) for $i = 1, ..., N$ set $\mathbf{u}_i = \mathbf{u}_{i+1}$ (that is: discard direction $\mathbf{u}_1$)

5) set $\mathbf{u}_N = \mathbf{P}_N - \mathbf{P}_0$

6) start from $\mathbf{P}_N$ and find the minimum along $\mathbf{u}_N$ and call this point $\mathbf{P}_0$

As pointed out in (Brent , 2002), the procedure of throwing away, at each step, $\mathbf{u}_1$ in favor of $\mathbf{P}_N - \mathbf{P}_0$ can result in a set of directions that become linearly dependent. When this happens, the procedures finds a minimum over a subspace of the full N dimensional space.

There are several ways of overcoming this problem, we used the simplest, consisting of throwing away, instead of $\mathbf{u}_1$, the old direction along which the function f made the largest decrease.

Before doing this, however, f is evaluated in a point further away in the direction $\mathbf{P}_N - \mathbf{P}_0$. If this value is greater of $f(\mathbf{P}_0)$ the old set of directions is kept.

5.2.3 Gaussian approximation

As it will be discussed in the chapter about the H_2 molecule computation, in order to calculate the hamiltonian when two or more centers are involved, it is convenient to approximate the functions of the Hilbert space basis with gaussians.

The great advantage of the gaussian representation, based on the linear combination of gaussian functions, is that an integral over a product of two gaussians of the form $ke^{-\alpha r_1^2}$, $he^{-\beta r_2^2}$ centered about two positions reduces to a single integral over a third gaussian centered in an intermediate point. Even more complicated integrals can be deduced from this basic result.

In our exploratory computations we used standard values computed in (Stewart , 1969), however we considered also the algorithm used by this author to compute gaussian expansions, so that, if necessary, we could compute other terms of the expansion.

The algorithm used in (Stewart , 1969) consists in minimizing the error

$$\epsilon = \int \mid \phi - \chi \mid^2 d\tau + \lambda(1 - \int \chi^* \chi \, d\tau) \tag{5.18}$$

where ϕ is the orbital to approximate, χ is the linear combination of N gaussian functions, λ is a Lagrange multiplier, and the integration is performed in the three dimensional space. As both the ϕ and χ have the same angular components, the integration is actually carried on the volume element $r^2 dr$.

To have a minimum with respect to the gaussian parameters P_i, a necessary condition is

$$\epsilon_i' = \frac{\partial \epsilon}{\partial P_i} = 0, \;\; P_i = 1, ..., 2N \tag{5.19}$$

Expanding in Taylor series about an approximate starting set of parameters P_i^0, one gets:

$$\epsilon'_i = \epsilon'_i(P^0) + \sum_k (\partial\epsilon'_i/\partial P_k)_{P^0} (P_k - P^0_k) \tag{5.20}$$

for i=1,...,2N. Hence:

$$\left(\frac{\partial\epsilon}{\partial P_i}\right)_{P_0} = - \sum_{k=1}^{2N+1} \left(\frac{\partial^2\epsilon}{\partial P_i \partial P_k}\right)_{P_0} (P_k - P^0_k) \tag{5.21}$$

In the above equation the Lagrange multiplier has been considered as one of the parameters P_i.

We have thus a system of linear equations in the 2N+1 unknown parameters P_i, that can be solved iteratively until $P_k - P^0_k \approx 0$.

5.2.4 Complexity considerations and quantum algorithms proposals

Some authors, e.g. (Whitfield, Loved et al. , 2012) considered the problem of evaluating the computational complexity of the algorithms used to compute the electronic structure. One of the purposes of these considerations is to investigate if and when quantum computers would be useful.

The main focus of the quoted paper is about time complexity, that is how the running time required by the computation increases with the problem size.

Among the computational problems considered there is the **electronic structure** problem, that basically corresponds to our Step 1. It can be formalized as follows: given the number of electrons N, the number of orbitals M, a configuration of nuclei, a trial energy E an error tolerance δ and the hamiltonian

$$H = T + V_{ee} + V_{eN} \tag{5.22}$$

where the operators are: T the kinetic energy, V_{ee} the electron-electron interaction end V_{eN} the electron-nuclear interaction. The problem consists in deciding if the ground energy is less than $E - \delta$ or greater than $E + \delta$, promised that it is not between those values.

It can be shown that methods for getting approximate solutions to this problem have complexities ranging from NP-complete to QMA-complete. We recall that QMA, Quantum Merlin Arthur, contains problems that are hard to solve even by quantum computers, but that, once a solution is found, it can be efficently checked by a quantum computer.

In particular, the quoted paper and (Schuch, Verstraete , 2010) show that the Hartree-Fock method is NP-complete. The Hartree-Fock method consists in minimizing the energy of N electrons given n basis functions that must be optimized, starting from the antisymmetrized product of single particle wave functions.

It is also known that this method scales as somewhere between $O(n^2)$ and $O(n^3)$.

We did not try to rigorously evaluate the computational complexity of our algorithms. We performed, however, some test to get some estimates of the scaling of the complexity increasing the basis dimension.

5.2.5 Execution time

During the computations, we measured the time needed to perform the main subroutines.

Tables 5.1, 5.2 and 5.4 report summaries that were obtained:

- taking the system time before and after the routine calls

- summing all the calls in a program run (e. g. 30 loops to find the minimum of energy)

- taking the average of several runs with different parameters

The entries = 0 mean that the time was too short for the fortran cpu_time instruction.

Table 5.1 refers to computation of the S states of Helium for the singlet. We have taken as unit of measure the total duration of the run for n=3. The columns correspond to the main subroutines. Here eig1 is the computation of eigenvalues of the reduced density matrix, while eig2 is the computation of eigenvalues of the hamiltonian for energy computation. The subroutine ulm computes the single particle matrix elements, the other subroutines compute some auxiliary matrices.

It can be seen that we have the following approximate scaling with n:

- eig1 $\approx$ linear: the dimension of the reduced density matrix is n, that is < 20 in our tests, a value that is not critical at all, to low to show the actual scaling of the algorithm.

- eig2 $\approx n^{5.8}$. Note that the actual dimension of the matrix to diagonalize is $m = n(n+1)/2$, so the scaling in function of the matrix dimension is $\approx m^{2.9}$, that is reasonable for this kind of problems

- calcx $\approx$ linear and cikkr $\approx$ constant

- ulm, the single particle matrix elements computation, $\approx n^{4.6}$

- ampp $\approx n^{3.5}$

- for the total runtime, neglecting the cases $n < 9$, we have a scaling $\approx n^{3.8}$

The plot 5.1 shows the scaling of the subroutines, relative to the highest time of each of them. Table 5.2 and plot 5.2 refer to the scaling of routines for S-P computations. Here twoq computes the interactions between electron in different shells. The scaling of this routine is $n^{3.5}$. ortho orthogonalizes the STO functions, and scales linearly. All the others are similar to the case of shell S only.

We compared also the total run times for runs considering only the S, the S-P and the S-P-D shells. Mean times in seconds are shown in table 5.3. For these runs we used a 1.66 Ghz, 1 Gb Ram, 32 bit Windows system. The ratio between the S and S-P runs scales approximately as $n^{1.5}$, and the ratio between S and S-P-D runs as $n^{2.6}$.

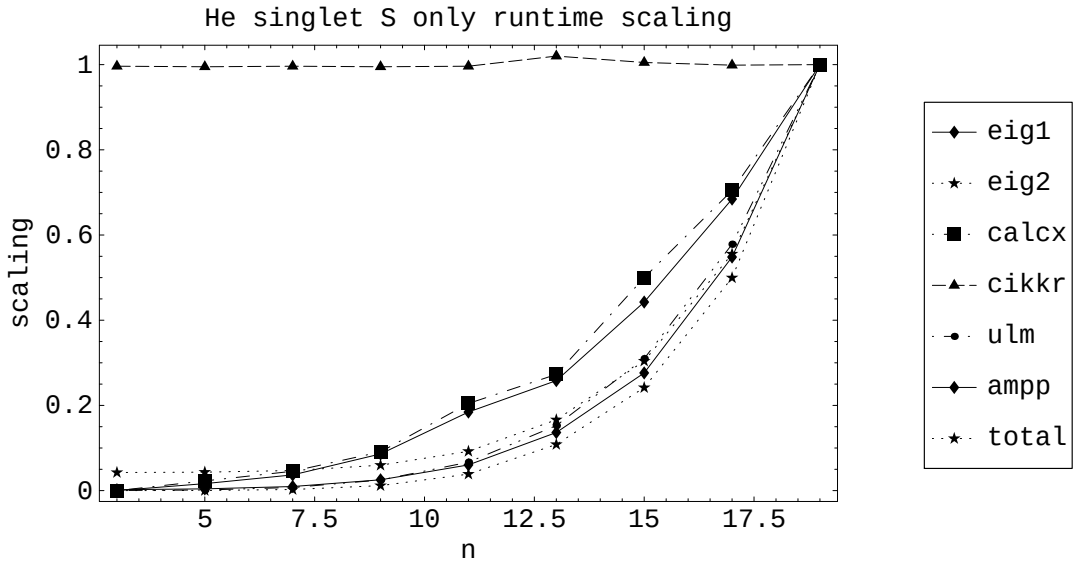

Figure 5.1 – Scaling of the main subroutines with n; He singlet S states

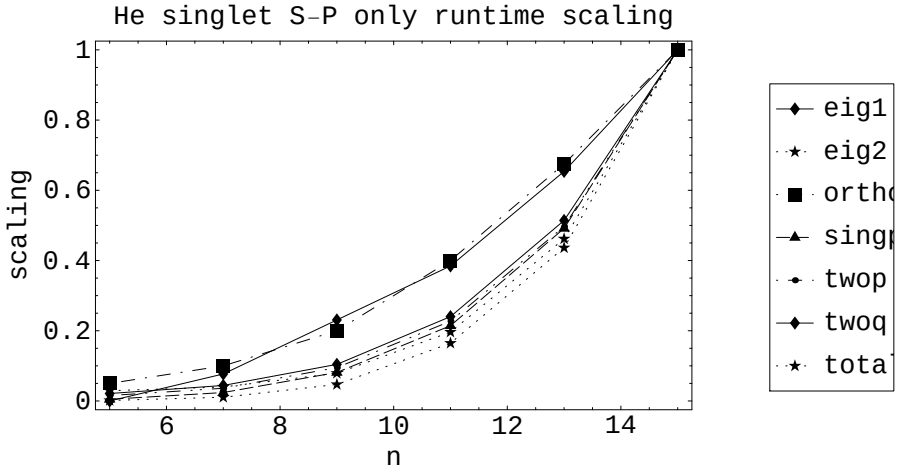

Figure 5.2 – Scaling of the main subroutines with n; He singlet S-P states

For the H_2 computation we have considered the scaling with the number of basis functions and with the number of gaussian functions used in the expansions. In table 5.4, S, the number of STO of the basis, corresponds to n in table 5.1, and G is of course the number of gaussians. The table shows that, notwithstanding some fluctuations, increasing the values of S and G, the time needed to compute the 2 bodies interactions (twdir, twsc) is far longer than the duration of all the other subroutines. Times are relative to the total run time for n=3, G=1.

n	eig1	eig2	calcx	cikkr	ulm	ampp	total
3	0.0000	0.0003	0.0000	0.2659	0.0023	0.0010	1.0000
5	0.0013	0.0043	0.0003	0.2655	0.0144	0.0020	1.0187
7	0.0030	0.0314	0.0007	0.2659	0.0725	0.0047	1.1089
9	0.0070	0.1416	0.0013	0.2655	0.2438	0.0124	1.4021
11	0.0150	0.4693	0.0030	0.2659	0.6536	0.0294	2.1690
13	0.0210	1.3133	0.0040	0.2722	1.4957	0.0665	3.9092
15	0.0361	2.9312	0.0073	0.2682	3.0361	0.1346	7.1523
17	0.0558	6.0564	0.0104	0.2665	5.6673	0.2672	13.0631
19	0.0815	12.1232	0.0147	0.2669	9.7993	0.4873	23.5164

Table 5.1 – Execution time - He S

n	eig1	eig2	Ortho	singp	twop	twoq	total
5	0.000	0.040	0.001	0.027	0.005	0,004	1.000
7	0.001	0.288	0.001	0.136	0.011	0.008	1.361
9	0.002	1.277	0.002	0.459	0.028	0.018	2.701
11	0.003	4.471	0.005	1.210	0.068	0.042	6.701
13	0.005	11.85	0.008	2.775	0.149	0.090	15.80
15	0.008	27.16	0.012	5.645	0.299	0.175	34.22

Table 5.2 – Execution time - He S-P

n	S	S-P	S-P-D	S-P / S	S-P-D / S
5	47.6	50.6	56.8	1.06	1.19
7	51.8	68.8	115.3	1.33	2.23
9	65.5	136.5	350.3	2.08	5.35
11	101.3	339.4	1032.5	3.35	10.19
13	182.6	798.4	2598.6	4.37	14.23
15	334.1	1728.9	6525.2	5.18	18.72

Table 5.3 – Execution time - He S, S-P, S-P-D shells

This point should be considered in more depth, as it is sometimes proposed to use quantum algorithms to compute the electronic structure (e.g. yung2012, seeley2012), but these algorithms need that the single electron and electron-electron integrals are classically computed before applying the algorithm.

n	G	eig1	eig2	ortho	twop
3	1	0.0000	0.0294	0.0009	0.0069
3	3	0.0000	0.0025	0.0057	0.3173
3	6	0.0000	0.0018	0.0261	4.4026
5	3	0.0003	2.0691	0.0186	2.8533
5	6	0.0006	0.1536	0.0742	40.6721

Table 5.4 – Relative execution time - H_2 S

5.3 Computation of the reduced density matrix and entropy evaluation

We will treat separtely the main cases for triplet and singlet.

5.3.1 Case I: one configuration, triplet

We have for the state vector:

$$\Psi = \sum_{i=1}^{n-1} \sum_{j=i+1}^{n} C_{i,j} Det[i,j] \tag{5.23}$$

and for the density matrix:

$$\rho \equiv |\Psi\rangle\langle\Psi| \equiv \sum_{i=1}^{n-1} \sum_{j=i+1}^{n} \sum_{k=1}^{n-1} \sum_{l=k+1}^{n} C_{ij} \cdot C_{kl} \cdot Det[i,j]\, Det[k,l] \tag{5.24}$$

that is:

$\rho \equiv \sum_{i=1}^{n-1} \sum_{j=i+1}^{n} \sum_{k=1}^{n-1} \sum_{l=k+1}^{n} C_{ij} \cdot C_{kl} \frac{1}{2} \cdot$

$$\cdot[\phi_i(\mathbf{r}_1) \cdot \phi_j(\mathbf{r}_2) - \phi_j(\mathbf{r}_1) \cdot \phi_i(\mathbf{r}_2)] \cdot [\phi_k^*(\mathbf{r'}_1) \cdot \phi_l^*(\mathbf{r'}_2) - \phi_l^*(\mathbf{r'}_1) \cdot \phi_k^*(\mathbf{r'}_2)] \tag{5.25}$$

To obtain the reduced density matrix, we set $\mathbf{r}_2 = \mathbf{r'}_2$ and integrate in $\mathbf{r}_2$:

$\rho^I \equiv \sum_{i=1}^{n-1} \sum_{j=i+1}^{n} \sum_{k=1}^{n-1} \sum_{l=k+1}^{n} \frac{1}{2} \cdot C_{ij} \cdot C_{kl} \cdot$

$\cdot[\phi_i(\mathbf{r}_1) \cdot \phi_k^*(\mathbf{r'}_1)\delta(j,l) + \phi_j(\mathbf{r}_1) \cdot \phi_l^*(\mathbf{r'}_1)\delta(i,k) -$

$$-\phi_i(\mathbf{r}_1) \cdot \phi_l^*(\mathbf{r'}_1)\delta(j,k) - \phi_j(\mathbf{r}_1) \cdot \phi_k^*(\mathbf{r'}_1)\delta(i,l)] \tag{5.26}$$

The δs consent to drop a sum.

This is a n x n matrix in the single particle space. We now break it into four pieces, rewriting the indexes.

$\rho^I_{(1)} \equiv \sum_{i=1}^{n-1} \sum_{j=i+1}^{n} \sum_{k=1}^{n-1} \sum_{l=k+1}^{n} \frac{1}{2} \cdot C_{ij} \cdot C_{kl} \cdot \phi_i(\mathbf{r}_1) \cdot \phi_k^*(\mathbf{r'}_1)\, \delta(j,l) =$

$$= \sum_{i=1}^{n-1} \sum_{k=1}^{n-1} \left\{ \frac{1}{2} \sum_{l=k+1}^{n} C_{il}\, C_{kl} \right\} |i\rangle\langle k| \tag{5.27}$$

$\rho^I_{(2)} \equiv \sum_{i=1}^{n-1} \sum_{j=i+1}^{n} \sum_{k=1}^{n-1} \sum_{l=k+1}^{n} \frac{1}{2} \cdot C_{ij} \cdot C_{kl}\, |j\rangle\langle l|\, \delta(i,k) =$

$$= \sum_{k=1}^{n-1} \sum_{j=k+1}^{n} \sum_{l=k+1}^{n} \frac{1}{2} C_{kj}\, C_{kl}\, |j\rangle\langle l| \tag{5.28}$$

$\rho^I_{(3)} \equiv \sum_{i=1}^{n-1} \sum_{j=i+1}^{n} \sum_{k=1}^{n-1} \sum_{l=k+1}^{n} -\frac{1}{2} \cdot C_{ij} \cdot C_{kl}\, |i\rangle\langle l|\, \delta(j,k) =$

$$= \sum_{i=1}^{n-1} \sum_{l=k+1}^{n} \sum_{k=1}^{n-1} -\frac{1}{2}\, C_{ik}\, C_{kl}\, |i\rangle\langle l| \tag{5.29}$$

$\rho^I_{(4)} \equiv \sum_{i=1}^{n-1} \sum_{j=i+1}^{n} \sum_{k=1}^{n-1} \sum_{l=k+1}^{n} -\frac{1}{2} \cdot C_{ij} \cdot C_{kl} \, |j\rangle\langle k| \, \delta(i,l) =$

$$= \sum_{i=1}^{n-1} \sum_{j=i+1}^{n} \sum_{k=1}^{n-1} -\frac{1}{2} C_{ij} \, C_{ki} \, |j\rangle\langle k| \tag{5.30}$$

So we obtain:

$\rho^I = \rho^I_{(1)} + \rho^I_{(2)} + \rho^I_{(3)} + \rho^I_{(4)} =$

$= \sum_{i=1}^{n-1} \sum_{k=1}^{n-1} \left\{ \frac{1}{2} \sum_{l=k+1}^{n} C_{il} \, C_{kl} \right\} |i\rangle\langle k| + \sum_{k=1}^{n-1} \sum_{j=k+1}^{n} \sum_{l=k+1}^{n} \frac{1}{2} C_{kj} \, C_{kl} \, |j\rangle\langle l| -$

$$- \sum_{i=1}^{n-1} \sum_{l=k+1}^{n} \sum_{k=1}^{n-1} \frac{1}{2} C_{ik} \, C_{kl} \, |i\rangle\langle l| - \sum_{i=1}^{n-1} \sum_{j=i+1}^{n} \sum_{k=1}^{n-1} \frac{1}{2} C_{ij} \, C_{ki} \, |j\rangle\langle k| \tag{5.31}$$

It is useful to expand the C_{ij} matrix with zeroes in order to get indexes varying always in the set $\{1, ..., n\}$

With this convention, we get:

$\rho^I = \sum_{ij} \left\{ \frac{1}{2} \sum_l C_{il} \, C_{jl} \right\} |i\rangle\langle j| + \sum_{ij} \left\{ \frac{1}{2} \sum_k C_{ki} \, C_{kj} \right\} |i\rangle\langle j| -$

$- \sum_{ij} \left\{ \frac{1}{2} \sum_k C_{ik} \, C_{kj} \right\} |i\rangle\langle j| - \sum_{ij} \left\{ \frac{1}{2} \sum_k C_{ki} \, C_{jk} \right\} |i\rangle\langle j| \; =$

$$= \sum_{ij} |i\rangle\langle j| \cdot \left\{ \frac{1}{2} \sum_k [C_{ik} \, C_{jk} + C_{ki} \, C_{kj} - C_{ik} \, C_{kj} - C_{ki} \, C_{jk}] \right\} \tag{5.32}$$

This is the expression used in our fortran programs for the triplet case.

In the case of interacting configurations, it is easy to verify that the total reduced density matrix is block-diagonal, and that each block refers to a single shell.

For instance, for S and P we have:

$$|\,\psi\rangle \;=\; |\,\psi\rangle^{(S)} \;+\; |\,\psi\rangle^{(P)} \tag{5.33}$$

and for the density matrix:

$$\rho \;=\; \rho^{SS} \;+ \rho^{PP} \tag{5.34}$$

We haven't written terms ρ^{SP} and ρ^{PS} because of the angular integrations.

For the reduced density matrix we have the situation:

$$\rho^{I} \;=\; \begin{bmatrix} X & X & X & & \\ X & X & X & & \\ X & X & X & & \\ & & & X & X \\ & & & X & X \end{bmatrix} \begin{matrix} \\ \\ ndds \\ \\ nddp \end{matrix} \tag{5.35}$$

where ndds is the dimension of the S states, and nddp that of the P states.

An explicit example: triplet, n=3

We consider the simplest case, with the dimension of the Hilbert space of single particle n=3. Then also the dimension of the Fock space is $n(n-1)/2 \;=\; 3$.

Supposing for the sake of simplicity that the components a, b, c of the state vector are real, we write:

$$|\psi\rangle = \begin{bmatrix} a \\ b \\ c \end{bmatrix}; \quad cc = \begin{bmatrix} 0 & a & b \\ 0 & 0 & c \\ 0 & 0 & 0 \end{bmatrix} \tag{5.36}$$

that is we build the matrix cc disposing the state vector components from left to right above the principal diagonal. This is the same operation of expanding the state vector with zeroes that conducted to eq. (5.32).

The total density matrix is:

$$\rho = \begin{bmatrix} a \\ b \\ c \end{bmatrix} [\, a\, b\, c\,] = \begin{bmatrix} a^2 & a \cdot b & a \cdot c \\ b \cdot a & b^2 & b \cdot c \\ c \cdot a & c \cdot b & c^2 \end{bmatrix} \tag{5.37}$$

The partial reduced density matrices $\rho^I_{(1)}$, $\rho^I_{(2)}$ $\rho^I_{(3)}$ $\rho^I_{(4)}$ can be written applying eq. (5.32):

$$\rho^I_1 = \frac{1}{2} \begin{bmatrix} a^2 + b^2 & b \cdot c & 0 \\ c \cdot b & c^2 & 0 \\ 0 & 0 & 0 \end{bmatrix}; \quad \rho^I_2 = \frac{1}{2} \begin{bmatrix} 0 & 0 & 0 \\ 0 & a^2 & a \cdot b \\ 0 & b \cdot a & b^2 + c^2 \end{bmatrix} \tag{5.38}$$

$$-\rho^I_3 = \frac{1}{2} \begin{bmatrix} 0 & 0 & a \cdot c \\ 0 & 0 & 0 \\ 0 & 0 & 0 \end{bmatrix}; \quad -\rho^I_4 = \frac{1}{2} \begin{bmatrix} 0 & 0 & 0 \\ 0 & 0 & 0 \\ c \cdot a & 0 & 0 \end{bmatrix} \tag{5.39}$$

and the total reduced density matrix is then:

$$\rho^I = \frac{1}{2}\begin{bmatrix} a^2 + b^2 & b \cdot c & -a \cdot c \\ c \cdot b & a^2 + c^2 & a \cdot b \\ -c \cdot a & b \cdot a & b^2 + c^2 \end{bmatrix} \tag{5.40}$$

Note that this matrix has trace = 1, as expected.

To link this computation of the reduced density matrix to the methods used in the Theory of Quantum Information, we embed the density matrix (5.37) in the Fock space of **distinguishable** particles, obtaining a 9x9 matrix.

Starting from this 9x9 matrix, one can obtain the partial density matrix ρ^I summing the elements in the principal diagonals of the nine 3x3 matrices in the way indicated in fig. 5.3 left (only 2 elements have been explicitly drawn):

The matrix ρ^{II} can be obtained summing as in figure 5.3 right. The method is illustrated in the following pages. The disposition of fig. 5.4 is obtained multiplying $[0,a,b,0,0,c,0,0,0]^T \cdot [0,a,b,0,0,c,0,0,0]$, 5.5 multiplying $[0,0,0,a,0,0,b,c,0]^T \cdot [0,0,0,a,0,0,b,c,0]$, that is exchanging rows with columns of the matrix cc of formula (5.36), 5.6 multiplying $[0,a,b,0,0,c,0,0,0]^T \cdot [0,0,0,a,0,0,b,c,0]$, and 5.7 multiplying $[0,0,0,a,0,0,b,c,0]^T \cdot [0,a,b,0,0,c,0,0,0]$.

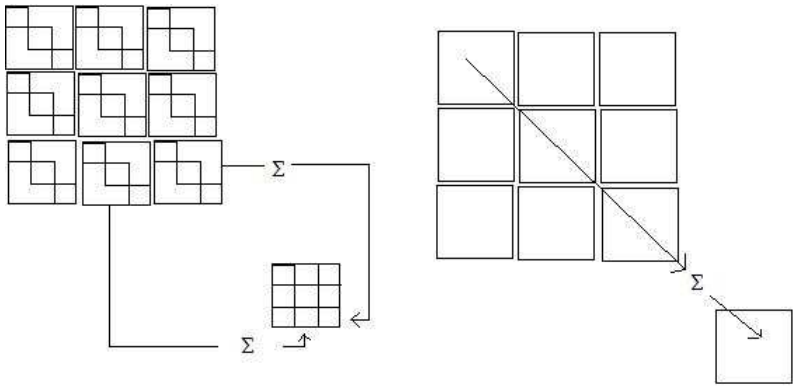

Figure 5.3 – Summing elements to obtain ρ^I and ρ^{II}

Computing ρ_1^I

$$\rho_1^I = \frac{1}{2}\begin{bmatrix} a^2 + b^2 & b \cdot c & 0 \\ c \cdot b & c^2 & 0 \\ 0 & 0 & 0 \end{bmatrix}; \tag{5.41}$$

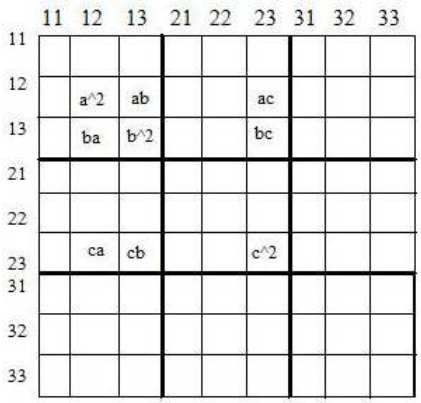

Figure 5.4 – Computation of ρ_1^I

Computing ρ_2^I

$$\rho_2^I = \frac{1}{2}\begin{bmatrix} 0 & 0 & 0 \\ 0 & a^2 & a \cdot b \\ 0 & b \cdot a & b^2 + c^2 \end{bmatrix} \tag{5.42}$$

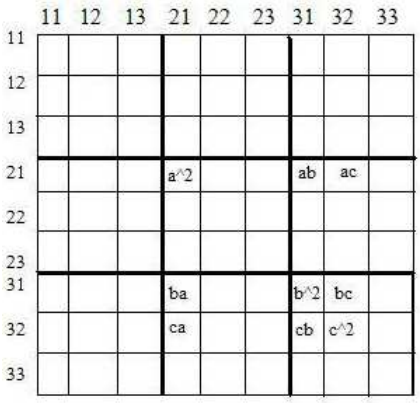

Figure 5.5 – Computation of ρ_2^I

Computing ρ_3^I

$$\rho_3^I = \frac{1}{2}\begin{bmatrix} 0 & 0 & a\cdot c \\ 0 & 0 & 0 \\ 0 & 0 & 0 \end{bmatrix}; \tag{5.43}$$

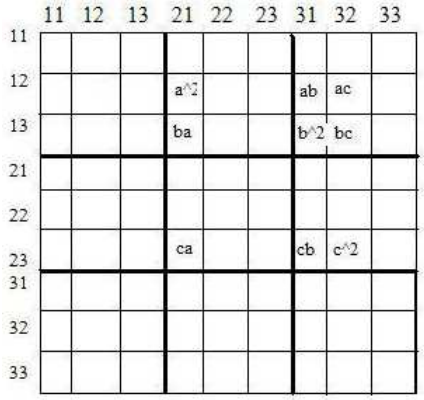

Figure 5.6 – Computation of ρ_3^I

Computing ρ_4^I

$$\rho_4^I = \frac{1}{2}\begin{bmatrix} 0 & 0 & 0 \\ 0 & 0 & 0 \\ c\cdot a & 0 & 0 \end{bmatrix} \tag{5.44}$$

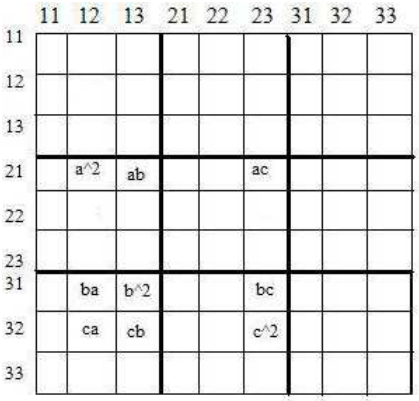

Figure 5.7 – Computation of ρ_4^I

At the end we find the (5.40):

$$\rho^I = \frac{1}{2}\begin{bmatrix} a^2 + b^2 & b \cdot c & -a \cdot c \\ c \cdot b & a^2 + c^2 & a \cdot b \\ -c \cdot a & b \cdot a & b^2 + c^2 \end{bmatrix} \tag{5.45}$$

In the same way, we obtain:

$$\rho^{II} = \frac{1}{2}\begin{bmatrix} a^2 + b^2 & b \cdot c & -a \cdot c \\ c \cdot b & a^2 + c^2 & a \cdot b \\ -c \cdot a & b \cdot a & b^2 + c^2 \end{bmatrix} \tag{5.46}$$

That is $\rho^I \equiv \rho^{II}$ as it must be. It is easy to extend those computations to the general case.

5.3.2 Case II: one configuration, singlet

In this case, we have permanents instead of determinants, and instead of $\frac{1}{\sqrt{2}}$ as a normalizing factor, we have:

$$N_{ij} = \frac{1}{2} \; for\, i = j \tag{5.47}$$

$$N_{ij} = \frac{1}{\sqrt{2}} \; for\, i < j \; e \; i > j \tag{5.48}$$

$$\langle \mathbf{r}_1 \, \mathbf{r}_2 \, | \, \psi \rangle = \sum_{i \leq j} C_{ij} \cdot N_{ij} \cdot [\phi_i(\mathbf{r}_1) \cdot \phi_j(\mathbf{r}_2) + \phi_j(\mathbf{r}_1) \cdot \phi_i(\mathbf{r}_2)] \tag{5.49}$$

For the reduced density matrix of the simmetrical case (singlet), we have:

$$\rho^I \equiv \int d\mathbf{r} \, \rho(\mathbf{r}_1, \mathbf{r}; \mathbf{r'}_1, \mathbf{r}) =$$

$$= \int d\mathbf{r} \, \textstyle\sum_{i \leq j} \sum_{k \leq l} C_{ij} \, C^*_{kl} \, N_{ij} \, N_{kl} \cdot$$

$$\cdot [\phi_i(\mathbf{r}_1) \cdot \phi_j(\mathbf{r}) + \phi_j(\mathbf{r}_1) \cdot \phi_i(\mathbf{r})] \cdot [\phi^*_k(\mathbf{r'}_1) \cdot \phi^*_l(\mathbf{r}) + \phi^*_l(\mathbf{r'}_1) \cdot \phi^*_k(\mathbf{r})] =$$

$$= \textstyle\sum_{i \leq j} \sum_{k \leq l} C_{ij} \, C^*_{kl} \, N_{ij} \, N_{kl} \cdot$$

$$\cdot \{\phi_i(\mathbf{r}_1) \cdot \phi^*_k(\mathbf{r'}_1) \cdot \delta(j,l) + \phi_j(\mathbf{r}_1) \cdot \phi^*_l(\mathbf{r'}_1) \cdot \delta(i,k) +$$

$$+ \phi_i(\mathbf{r}_1) \cdot \phi^*_l(\mathbf{r'}_1) \cdot \delta(j,k) + \phi_j(\mathbf{r}_1) \cdot \phi^*_k(\mathbf{r'}_1) \cdot \delta(i,l)\} \tag{5.50}$$

Defining $C_{ij} = 0$ for $i > j$ we obtain

$$\rho^I = \rho_1^I + \rho_2^I + \rho_3^I + \rho_4^I \tag{5.51}$$

$$(\rho_1^I)_{ij} = \sum_m C_{im}\, C^*_{jm}\, N_{im}\, N_{jm} \tag{5.52}$$

$$(\rho_2^I)_{ij} = \sum_m C_{mi}\, C^*_{mj}\, N_{mi}\, N_{mj} \tag{5.53}$$

$$(\rho_3^I)_{ij} = \sum_m C_{im}\, C^*_{mj}\, N_{im}\, N_{mj} \tag{5.54}$$

$$(\rho_4^I)_{ij} = \sum_m C_{mi}\, C^*_{jm}\, N_{mi}\, N_{jm} \tag{5.55}$$

An explicit example: singlet, n=3

Taking again n=3 as the dimension of the Hilbert space of a particle, we have that the Fock space dimension now is $n(n+1)/2 = 6$.

Setting:

$$d2 = \frac{1}{\sqrt{2}}, \quad d8 = \frac{1}{\sqrt{8}} \tag{5.56}$$

$$N = \begin{bmatrix} 0.5 & d2 & d2 \\ d2 & 0.5 & d2 \\ d2 & d2 & 0.5 \end{bmatrix}; \quad |\psi\rangle = \begin{bmatrix} a \\ b \\ c \\ d \\ e \\ f \end{bmatrix} \tag{5.57}$$

$$cc = \begin{bmatrix} a & b & c \\ 0 & d & e \\ 0 & 0 & f \end{bmatrix} \tag{5.58}$$

we obtain:

$$\rho_1^I = \begin{bmatrix} 0.25a^2 + 0.5b^2 + 0.5c^2 & d8\,bd + 0.5ce & d8\,cf \\ d8\,bd + 0.5ce & 0.25d^2 + 0.5e^2 & d8\,ef \\ d8\,cf & d8\,ef & 0.25f^2 \end{bmatrix} \tag{5.59}$$

$$\rho_2^I = \begin{bmatrix} 0.25a^2 & d8\,ab & d8\,ac \\ d8\,ab & 0.5b^2 + 0.25d^2 & 0.5bc + d8\,de \\ d8\,ac & 0.5bc + d8\,de & 0.5c^2 + 0.5e^2 + 0.25f^2 \end{bmatrix} \tag{5.60}$$

$$\rho_3^I = \begin{bmatrix} 0.25a^2 & d8\,ab + d8\,bd & d8\,ac + 0.5be + d8\,cf \\ 0 & 0.25d^2 & d8\,de + d8\,ef \\ 0 & 0 & 0.25f^2 \end{bmatrix} \tag{5.61}$$

$$\rho_4^I = \begin{bmatrix} 0.25a^2 & 0 & 0 \\ d8\,ab + d8\,bd & 0.25d^2 & 0 \\ d8\,ac + 0.5be + d8\,cf & d8\,de + d8\,ef & 0.25f^2 \end{bmatrix} \tag{5.62}$$

In the following pages, we illustrate the computation. The figures are built embedding the density matrix in the space of distinguishable particles, in the same way as for the triplet. The vector cc of formula (5.58) is multiplied by itself to obtain the disposition for ρ_1^I in fig. 5.8. The other dispositions are obtained switching rows and columns of cc. In all the pictures, the vectors that have been multiplied are specified by the dots in the top row and leftmost column, outside of the squares. Each dot stands for a nonzero element of vectors and matrices.

Computing ρ_1^I

In order to simplify the figures, we indicated with a dot the nonzero elements.

$$\rho_1^I = \begin{bmatrix} 0.25a^2 + 0.5b^2 + 0.5c^2 & d8\,bd + 0.5ce & d8\,cf \\ d8\,bd + 0.5ce & 0.25d^2 + 0.5e^2 & d8\,ef \\ d8\,cf & d8\,ef & 0.25f^2 \end{bmatrix} \tag{5.63}$$

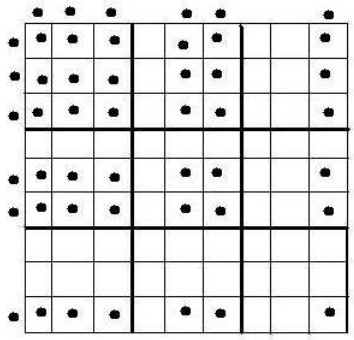

Figure 5.8 – Computing ρ_1^I

Computing ρ_2^I

$$\rho_2^I = \begin{bmatrix} 0.25a^2 & d8\,ab & d8\,ac \\ d8\,ab & 0.5b^2 + 0.25d^2 & 0.5bc + d8\,de \\ d8\,ac & 0.5bc + d8\,de & 0.5c^2 + 0.5e^2 + 0.25f^2 \end{bmatrix} \tag{5.64}$$

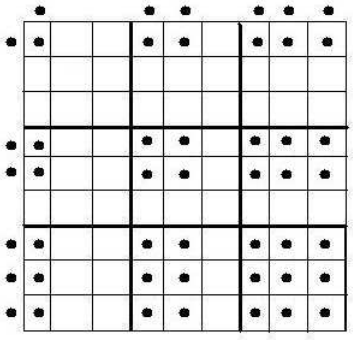

Figure 5.9 – Computing ρ_2^I

Computing ρ_3^I

$$\rho_3^I = \begin{bmatrix} 0.25a^2 & d8\,ab + d8\,bd & d8\,ac + 0.5be + d8\,cf \\ 0 & 0.25d^2 & d8\,de + d8\,ef \\ 0 & 0 & 0.25f^2 \end{bmatrix} \tag{5.65}$$

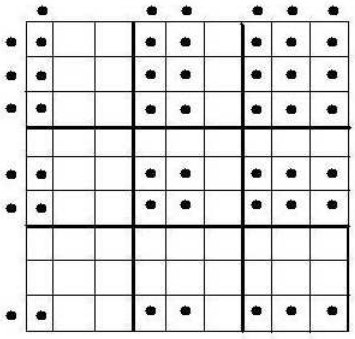

Figure 5.10 – Computing ρ_3^I

Computing ρ_4^I

$$\rho_4^I = \begin{bmatrix} 0.25a^2 & 0 & 0 \\ d8\,ab + d8\,bd & 0.25d^2 & 0 \\ d8\,ac + 0.5be + d8\,cf & d8\,de + d8\,ef & 0.25f^2 \end{bmatrix} \tag{5.66}$$

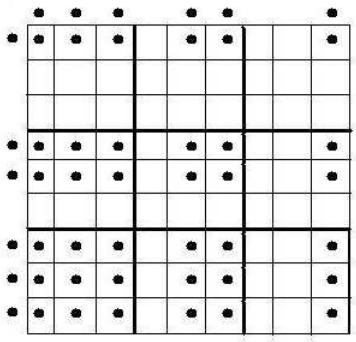

Figure 5.11 – Computing ρ_4^I

The reduced density matrix is:

$$\rho^I = \begin{bmatrix} a^2 + 0.5b^2 + 0.5c^2 & d2\,ab + d2\,bd + 0.5ce & d2\,ac + 0.5be + d2\,cf \\ d2\,ab + d2\,bd + 0.5ce & 0.5b^2 + d^2 + 0.5e^2 & 0.5bc + d2\,de + d2\,ef \\ d2\,ac + 0.5be + d2\,cf & 0.5bc + d2\,de + d2\,ef & 0.5c^2 + 0.5e^2 + f^2 \end{bmatrix} \tag{5.67}$$

whose trace is, as expected:

$$Tr(\rho^I) = a^2 + b^2 + c^2 + d^2 + e^2 + f^2 = 1 \tag{5.68}$$

5.4 The method in summary

We compute with high accuracy the lowest energy eigenstates of helium by means of a variational method, the configuration-interaction method. This method, in several variants, has been extensively used in atomic physics, see, for instance, (Fulde , 2002), (Hilico, Billy et al. , 2000), (Bürgers, Wintgen et al. , 1995), (Wintgen, Delande , 1993). Orthonormal basis functions are provided by

$$\begin{aligned} &\Phi_{n_1,l_1,m_1;n_2,l_2m_2}(\mathbf{r}_1,\mathbf{r}_2) \\ &= F_{n_1,l_1;n_2,l_2}(r_1,r_2)Y_{l_1m_1}(\Omega_1)Y_{l_2m_2}(\Omega_2), \end{aligned} \tag{5.69}$$

where $Y_{l_im_i}$ are spherical harmonics, with Ω_i solid angle for particle i and the radial functions $F_{n_1,l_1;n_2,l_2}(r_1,r_2)$ are obtained after orthonormalizing the Slater-type orbitals

$$R_{nl}(r) = r^{n+l-1}\exp(-\xi_{n,l}r), \tag{5.70}$$

with $\xi_{n,l}$ variational parameters, and properly symmetrizing the products of the obtained one-particle radial wafefunctions $f_{nl}(r)$. That is, if the spin wavefunction is symmetric, F must be antisymmetric,

$$F_{n_1,l_1;n_2,l_2}(r_1,r_2) = \frac{1}{\sqrt{2}}[f_{n_1l_1}(r_1)f_{n_2l_2}(r_2) - f_{n_2l_2}(r_1)f_{n_1l_1}(r_2)]; \tag{5.71}$$

if the spin wavefunction is antisymmetric, F must be symmetric:

$$F_{n_1,l_1;n_2,l_2}(r_1,r_2) = \frac{1}{\sqrt{2}}[f_{n_1l_1}(r_1)f_{n_2l_2}(r_2) + f_{n_2l_2}(r_1)f_{n_1l_1}(r_2)] \tag{5.72}$$

if $(n_1,l_1) \neq (n_2,l_2)$,

$$F_{n_1,l_1;n_1,l_1}(r_1,r_2) = f_{n_1l_1}(r_1)f_{n_1l_1}(r_2) \tag{5.73}$$

otherwise.

We then compute the reduced (single-electron) density matrix

$$\rho_1(\mathbf{r}_1,\mathbf{r}_1') = \int d\mathbf{r}_2 \Psi(\mathbf{r}_1,\mathbf{r}_2)\Psi^\star(\mathbf{r}_1',\mathbf{r}_2), \tag{5.74}$$

with

$$\Psi(\mathbf{r}_1,\mathbf{r}_2) = \sum_{I_1,I_2} c_{I_1,I_2}\Phi_{I_1,I_2}(\mathbf{r}_1,\mathbf{r}_2), \tag{5.75}$$

with the multi-indexes $I_1 \equiv (n_1,l_1,m_1)$ and $I_2 \equiv (n_2,l_2,m_2)$. Since the expansion is done over an orthonormal basis the reduced density matrix on that basis is simply given by a partial trace over the second particle of the overall density matrix: $(\rho_1)_{I_1,I_1'} = \sum_{I_2} \rho_{I_1,I_2;I_1',I_2}$, where $\rho_{I_1,I_2;I_1',I_2'} = c_{I_1I_2}c^\star_{I_1'I_2'}$. We point out a major advantage of the configuration-interaction method and the use of orthonormal orbitals: the reduced density matrix is obtained by purely algebraic methods, without numerical computation of the multi-dimensional integrals of Eq. (5.74). Of course this kind of methods and their advantages are well-known in the treatment of atomic problems; we chose them just be-

cause are particularly well suited for the entanglement computation. The reduced density matrix can then be easily diagonalized and in this paper we will study the entanglement properties of helium by means of the eigenvalues $\{\lambda_k\}$ of ρ_1.

5.5 About the choice between an orthonormal basis and a non orthonormal one

A critical point is the choice of the Hilbert space basis, in particular the choice between an orthonormal and an unorthonormal basis. Moreover, one has to choose the coordinate system.

As reported in the literature, "Hylleraas" or "Pekeris" coordinates are often used when one aims at an optimal precision, and excellent results have been obtained for two electrons.

This method, however, cannot easily be applied to cases with more than 2-3 electrons, therefore, after some initial tests with the Pekeris method, we decided to discard it. Another reason is that to compute the entropy we need the reduced density matrix and, using this method, to obtain it one has to perform numerical integrations on a large number of variables.

For this reason we decided to use the usual polar coordinates.

Given that, one has still to choose between orthonormal and unorthonormal basis functions.

Non orthonormal functions, like for instance simple STO (Slater Type Orbitals), have the great advantage that the radial wavefunctions are expressed by monomials, instead of polynomials as in the orthonormal case. This greatly simplifies the computation of the matrix elements.

Unfortunately, on the other hand, in this case one has to solve a generalized eigenvalue problem to compute the eigenvalues and eigenfunctions of the Hamiltonian, and the computation of the reduced density matrix is still a complex task.

After several tests, we decided to use orthonormal radial functions, as will be described in the following sections.

5.6 About the choice between Slater Type Orbitals and Gaussian functions

This is a very important choice, because using gaussians one obtains a great simplification, but it can be a too crude approximation if a great precision is needed.

As we aim at solving the Helium case as a standard against which to evaluate other approximate solutions, we decided to use STO at first, then switch to gaussians, and compare the results (see section 7.1).

We recall the form of the Gaussian Type Orbitals (GTO:

$$GTO(\alpha,\, r) \;=\; (2\alpha/\pi)^{3/4}\, exp(-\alpha r^2) \tag{5.76}$$

where α is a parameter that identifies the specific GTO; we will use the notation:

$$GTO(k,\, \xi_{n,l}) \;=\; (2\alpha_k/\pi)^{3/4}\, exp(-\alpha_k(\xi_{n,l} r)^2) \tag{5.77}$$

to highlight that we are using a set of k GTOs and that the variational parameter $\xi_{n,l}$ is used.

For convenience, we report here the radial part of the wave function:

$$\langle r \,|\, \psi_{n,l} \rangle \;=\; \sum_{i=1}^{n-l} uc[n,\, l,\, i] \cdot STO(i,\, \xi_{n,l}) \tag{5.78}$$

$n = l + 1,\, l + 2,\, ...$

Setting

$$STO(i,\, \xi_{n,l}) \;=\; \sum_{k=1}^{k_{max}} C[i,\, k] \cdot GTO(k,\, \xi_{n,l}) \tag{5.79}$$

we have

$$\langle r \,|\, \psi_{n,l} \rangle \;=\; \sum_{k=1}^{k_{max}} AG(n,\, l,\, k) \cdot GTO(k,\, \xi_{n,l}) \tag{5.80}$$

with

$$AG(n,\, l,\, k) \;=\; \sum_{i=1}^{n-l} uc[n,\, l,\, i] \cdot CG(i,\, k) \tag{5.81}$$

5.7 Details about the Slater Type Orbitals

Instead of a generic function of the coordinates, for the above exposed reasons, we use a specific basis to express the state vector: the "Slater Type Orbitals" (STO)

The STO, in polar coordinates, are by definition:

$$|i> = r^{i-1} exp(-\xi r) Y_l^m(\theta, \phi) \tag{5.82}$$

where the Y are the spherical harmonics, and depend on the considered atomic shell. ξ is a scalar parameter, that has to be optimized.

Each shell corresponds to a different ξ parameter. The dimension n of the basis is fixed in order to obtain the desired precision.

The $|\, i\rangle$ function are unorthogonal and unnormalized. For every shell l, we define the orthonormal functions $\|k\rangle\rangle_l$ as linear combinations of the $|\, i\rangle$.

The $\|k\rangle\rangle_l$ are the basis of the Hilbert space of a single particle.

For two particles, a basis of the so-called Fock space is defined using combinations of the functions that have just been defined

For instance, in the anti symmetric case:

$$\|k, k'\rangle\rangle \;=\; c \begin{bmatrix} \phi_k(r_1) & \phi_k(r_2) \\ \phi_{k'}(r_1) & \phi_{k'}(r_2) \end{bmatrix} \tag{5.83}$$

where c is a normalization coefficient, the ϕ functions are the orthonormalized STOs and the indexes k, k' are all the distinct combinations of numbers from 1 to the dimension n of the single particle Hilbert space.

In this way we obtain a basis of $n(n-1)/2$ elements for the Hilbert space of the 2 electrons.

Using this basis, we solve the Schrödinger equation, to find the energies of the stationary states.

Varying the ξ parameters, we find the minimum of the energy. It corresponds to the best approximation for the state considered.

With the optimum values of the parameters we compute the density matrix, the reduced matrix, its eigenvalues, and the von Neumann entropy, using only algebraic procedures.

In order to have a self-contained description, to avoid too many cross-references with the literature, and to explain the conventions we used, we report some details.

Notation l = quantum orbital number $ll \, = \, l + 1$

We assume the following definitions for the STO:

ORBITALS - Definition

1) $ll = Shell : \{ll = 1, \, 2, \, 3, \, ... = S, \, P, \, D, \, F, \, G, \, H, \, I, \, J, \, ... \}$

2) $n = STATE : \{ \, n \, = \, ll, \, ll + 1, \, ... \}$

3) $i = component$

Slater orbital: definition

Setting $ll \equiv l + 1$ we have

$$\langle r|n, ll, i\rangle \; = \; r^{i-1} \, exp[\, - \, \xi_{n,ll,i} \, * \, r] \tag{5.84}$$

In the simplest case, when one does not use the i degree of freedom, we get: $\xi(n, \, ll, \, i \,) \, = \, \xi(n, \, ll, \, ll \,)$

The angular moment is $l \, \equiv \, ll \, - \, 1$. The maximum of the (5.84) is achieved for

$$r_{max} \; = \; \frac{(i-1)}{\xi_{n,ll,i}} \tag{5.85}$$

The parameters $\xi_{n,ll,i}$ are the variational parameters.

5.7.1 Orthogonalization of the Slater Type Orbitals and of similar systems

Starting with a system that is not orhtonormal, it is always possible to build an orthonormal one.

In our programs it is done by the routine calcx(n,l) for the STOs and by clxnn for the generic case. In the following sections we give some details.

Case of the Slater Type Orbitals: routine calcx(n,l)

Starting with the unorthogonal basis functions, we numerically deduce an orthogonal set.

The orthogonalization is performed by the routine $calcx(n,\, l)$ and checked by the routine $arn(n\,, l)$

Starting from the first STO, and implying the indexes n, ll:

$$\| \, 1 \, \rangle\rangle \; = \; | \, 1 \, \rangle \tag{5.86}$$

The second orthonormal eigenfunction is obtained by the linear combination:

$$\| \, 2 \, \rangle\rangle \; = \; | \, 1 \, \rangle \; + \mathbf{A} \, | \, 2 \, \rangle \tag{5.87}$$

imposing $\langle\langle \, 2 \, \| \, 1 \, \rangle\rangle \; = \; 0$ that determines the coefficient $\mathbf{A}$

$$\langle 1 \,\|2\,\rangle\rangle = 0 = \langle 1\,|\,1\rangle + \mathbf{A}\,\langle 1\,|\,2\rangle \tag{5.88}$$

One goes on, solving linear systems of increasing dimensions. Finally, the states are normalized. The coefficients of the orbitals are given by the vector $uc(n,\, l+1,\, i)$

From the large number of tests run, we noted that optimizing the $\xi_{n,l,i}$ using for instance two parameters

$$\xi_{n,l,i} = A_{n,l} + B_{n,l} \cdot i \tag{5.89}$$

one gets a more rapid convergence to the optimal energy value, specially for low values of the maximum n used for the Hilbert space dimension.

On the contrary, if one seeks a great precision, using a high value of n, then the use of two variational parameters is not justified, that is optimizing $A_{n,l}$, $B_{n,l}$ instead of taking simply $\xi_{n,l,i} \equiv \xi_{n,l}$, one does not get major advantages (indipendence on i)

Anyway this possibility has been maintained in the development of the computation software.

Orthonormalization in the Fock space

In the general case of many particles, we start with a single particle space, then we build the Fock space.

For atoms, and specifically for the Helium atom, we found that a convenient basis was obtained orthonormalizing a STO basis.

For molecules, starting with a multicentric, **non** orthonormal STO basis of single particles, one has two possibilities.

The first consists of orthonormalizing the single particle space, and then build the Fock space, that automatically results in an orthonormal one.

The second, that we used for the H_2 molecule, consists of starting with single particle monocentric orthonormal functions, obtaining non orthonormal multicenter eigenfunctions, building the Fock space, and finally orthonormalizing its basis.

General case: clxnn routine

This general case will be used in chapter 7 to orthonormalize the Fock space basis to compute the H_2 molecule.

We call sovr(ki, kj) the superposition matrix of the function set that must be orthonormalized.

It is given for the symmetrical states by the following formula:

$$sovr(ki,\, kj) \;=\; \langle i, j \,|\, k, l \rangle \;=\; 2 \cdot \mathcal{N}_{ij} \cdot \mathcal{N}_{kl} \cdot \{\, \delta_{ik}\delta_{jl} \;+\; ss(i,\, l)\, ss(j,\, k) \,\} \tag{5.90}$$

where:

$$ss(i,\, j) \;=\; ssij(i,\, j) \tag{5.91}$$

$$\mathcal{N}_{ij} \;=\; \frac{1}{\sqrt{2\,(1 \,+\, ss(i,\, j)^2)}} \;=\; anij(i,\, j) \tag{5.92}$$

We recall that its dimension is given by:

nnzz = dimension of the single particle space = 1, ..., 5.

For the symmetrical two particles states we have:

ndim = nnzz (nnzz+1)/2 = 1; 3; 6; 10; 15

In appendix 9.3 we describe the program and the computational method used.

sovr(i, j) = initial superposition

axx(i, j) = unknown matrix to be recursively computed

The method is recursive on the index k

The unknown matrix must satisfy the condition:

axx(i, i) = 1

Define

$|\, h\rangle$ = non orthonormal vectors that must be orthonormalized.

$$sovr(i,\, j) \equiv \langle i \,|\, j \rangle \tag{5.93}$$

$\| h \rangle\rangle$ = orthonormal vectors that must be computed

Then define:

$$\| k \rangle\rangle \;=\; \sum_{j=1}^{k-1} axx(k,\, j) \,|\, j \rangle \;+\; |\, k \rangle \tag{5.94}$$

where the initial position has been written explicitly

$$axx(k,\, k) \;=\; 1 \tag{5.95}$$

The unknown is the axx(i, j) matrix. It will be computed recursively for h= 1, 2, ..., k-1.

Write

$$\| h \rangle\rangle \;=\; \sum_{i=1}^{h-1} axx(h,\, i) \,|\, i \rangle \;+\; |\, h \rangle \tag{5.96}$$

$$\| k \rangle\rangle \;=\; \sum_{j=1}^{k-1} axx(k,\, j) \,|\, j \rangle \;+\; |\, k \rangle \tag{5.97}$$

We have the k-1 equations

$$\langle\langle h \,\|\, k\rangle\rangle \;=\; 0 \;\; \{\, h \;=\; 1,\, 2,\, ...,\, k-1 \,\} \tag{5.98}$$

Writing explicitly, we have:

$$\{ \sum_{i=1}^{h-1} axx(h,\, i)\,|\, i\rangle \;+\; |\, h\rangle \,\} \cdot \{ \sum_{j=1}^{k-1} axx(k,\, j)\,|\, j\rangle \;+\; |\, k\rangle \,\} \;=\; 0 \tag{5.99}$$

Recalling that axx(h, h)=1, we have

$$\sum_{j=1}^{k-1} axx(k,\, j) \;\cdot\; \sum_{i=1}^{h} axx(h,\, i)\,\langle i\,|\, j\rangle \;=\; -\sum_{i=1}^{h} axx(h,\, i)\,\langle i\,|\, k\rangle \;\; \{\, h \;=\; 1,\, 2,\, ...,\, k-1 \,\} \tag{5.100}$$

The equations must be solved recursively, starting with k=1. For each other k, we get k-1 equation setting h = 1, 2, ..., k-1.

Fixed k, the unknown are:

$$axx(k,\, j) \;\; \{\, j \;=\; 1,\, 2,\, ...,\, k-1 \,\} \tag{5.101}$$

$$axx(k,\, k) \;=\; 1 \tag{5.102}$$

Writing the equations in matrix form, we have:

$$alf(h,\, j) \;=\; [\, axx(k,\, j)\,] \;=\; -\, vvk(h) \tag{5.103}$$

Then we can write the solution for the S shell as:

$$\|\, k\rangle\rangle \;=\; \sum_{ik=1}^{i} uf\,[i,\, 1,\, ik]\,|\,ik\rangle \tag{5.104}$$

analogously as for $uc\,[i,\, 1,\, ik]$ of the STOs.

Now we must normalize the vector $\|k\rangle\rangle$.

$$\|k\rangle\rangle \;=\; \sum_{l=1}^{k} axx(k,\, l)\,|\,l\rangle \;=\; \sum_{l=1}^{k} uf[k,\, 1,\, l]\,|\,l\rangle \tag{5.105}$$

$$\langle\langle k\,\|\,k\rangle\rangle \;=\; \sum_{l=1}^{k}\sum_{m=1}^{k} axx(k,\, l)\,\cdot\, axx(k,\, m)\,\cdot\, sovr(l,\, m) \tag{5.106}$$

5.8 Generalized Laguerre polynomials

In the special case when one takes $\xi_{n,ll,i} = \xi_{n,ll}$, that is one does not have any dependence on the index i, one obtains the generalized Laguerre polynomials for $\alpha = 2l + 2 = 2 * ll$

$$L_n^\alpha(x) = \sum_{m=0}^{n} (-1)^m \left[\begin{array}{c} n + \alpha \\ n - m \end{array} \right] \frac{1}{m!} * x^m; \;\; \{ n = 0, 1, ... \} \tag{5.107}$$

These polynomials are orthogonal, with the weighting function:

$$w(x) = x^\alpha \, exp\{-x\} \tag{5.108}$$

Moreover

$$\int_0^\infty w(x) \{ L_n^\alpha(x) \}^2 \, dx = \frac{(\alpha + n)!}{n!} \tag{5.109}$$

Then we get an orthonormal set if we define:

$$P_n(x) = \sqrt{\frac{n!}{(\alpha + n)!}} L_n^\alpha(x) \tag{5.110}$$

As we are interested in functions of the form

$$\psi(r) = \{ \, polynomial \, \} \cdot exp\{ -\xi \, r \, \} \tag{5.111}$$

we change the x variable accordingly to

$$x \,=\, 2\,\xi\,r \tag{5.112}$$

Important remark: in order to apply this method to molecules, which we will do later, we recall that for orbitals with $l \neq 0$, in atoms there are no problems defining the angular part of the wave functions using the usual spherical harmonics $Y_l^m(\theta,\,\phi)$.

In the case of molecules, however, e.g. the Hydrogen molecule, it is more convenient to combine the term r^l of the radial part with the angular part and develop

$$r^l\,Y_l^m(\theta,\,\phi) \,\rightarrow\, harmonics \tag{5.113}$$

of cartesian or cubic type.

Coming back to the spherical case, given the normalizations that we performed, we develop the uc[i, l+1, ik] in the following form, used in the calcnewx routine, in which the r dependent part is in STO form (note that the indexes start from 1 instead than from 0 as usual, for programming convenience):

$$uc[\,i,\,l+1,\,ik\,] \,=\, \mathcal{N}\,\sum_{ik=1}^{i}\,(-1)^{ik-1}\,\left[\begin{array}{c} i-1\,+\,2l\,+\,2 \\ i\,-\,ik \end{array}\right]\cdot\frac{(2\,\xi)^{ik-1}}{(ik,\,-1)!} \tag{5.114}$$

with

$$\mathcal{N} \,=\, \frac{(n\,-\,1)!}{(n-1\,+\,2l\,+\,2)!}\,(2\,\xi)^{2/3} \tag{5.115}$$

5.9 Useful expressions for Slater Type Orbitals

We report some expressions that will be useful in the following. From the:

$$\int_0^\infty dx[x^n * exp(-a * x)] \; = \; \frac{n!}{a^{n+1}} \tag{5.116}$$

we get:

1) Superposition integral fixed l $(lv = l - 1)$:

$$\langle n, l, i | m, l, j \rangle \; = \; \frac{(i + j + 2 * lv)!}{[\xi_{n,l,i} + \xi_{m,l,j}]^{[i+j+2*lv+1]}} \tag{5.117}$$

2) Matrix elements of r^k

$$\langle n, l, i | r^k | m, l, j \rangle \; = \; \frac{(i + j + 2 * lv + k)!}{[\xi_{n,l,i} + \xi_{m,l,j}]^{[i+j+2*lv+k+1]}} \tag{5.118}$$

3) Matrix elements of d^2/dr^2

$$\langle n, l, i | d^2/dr^2 | m, l, j \rangle \; =$$

$$= \; \frac{(j + lv - 1) * (j + lv - 2) * (i + j + 2 * lv - 2)!}{[\xi_{n,l,i} + \xi_{m,l,j}]^{[i+j+2*lv-1]}} -$$

$$-\frac{2*\xi_{m,l,j}*(j+lv-1)*(i+j+2*lv-1)!}{[\xi_{n,l,i}+\xi_{m,l,j}]^{[i+j+2*lv]}}+$$

$$+\frac{[\xi_{m,l,j}]^2*(i+j+2*lv)!}{[\xi_{n,l,i}+\xi_{m,l,j}]^{[i+j+2*lv+1]}}$$

4) Matrix elements of $(2/r)*d/dr$

$$\langle n,l,i|(2/r)*d/dr|m,l,j\rangle = \frac{2*(j+lv-1)*(i+j+2*lv-2)!}{[\xi_{n,l,i}+\xi_{m,l,j}]^{[i+j+2*lv-1]}}-$$

$$-\frac{2*\xi_{m,l,j}*(i+j+2*lv-1)!}{[\xi_{n,l,i}+\xi_{m,l,j}]^{[i+j+2*lv]}}$$

5) Sum of 3) + 4) = radial part of the Laplacian =

$$=\frac{(i+j+2*lv-2)!}{[\xi_{n,l,i}+\xi_{m,l,j}]^{[i+j+2*lv+1]}}*\{\xi^2_{n,l,i}*[(j+lv)*(j+lv-1)]+$$

$$+\xi^2_{m,l,j}*[(i+lv)*(i+lv-1)]-\xi_{n,l,i}*\xi_{m,l,j}*2*[(i+lv)*(j+lv)]\}$$

that is symmetrical, as expected.

6) Matrix elements of $exp[-\alpha*r]$

$$\langle n,l,i|exp[-\alpha*r]|m,l,j\rangle = \frac{(i+j+2*lv)!}{[\xi_{n,l,i}+\alpha+\xi_{m,l,j}]^{[i+j+2*lv+1]}}$$

It is useful to derive a second expression for the radial part of the Laplacian (here $l \equiv lv \equiv ltrue$)

$$\langle i \,|\, \frac{d^2}{dr^2} \,+\, \frac{2}{r}\frac{d}{dr} \,|\, j \rangle \,=$$

$$= \,(j{+}l)(j{+}l{-}1){\cdot}\frac{(i+j+2l-2)!}{[\xi_{n,i}+\xi_{m,j}]^{[i+j+2l-1]}} - \frac{2\xi_{m,j}(j+l)(i+j+2l-1)!}{[\xi_{n,i}+\xi_{m,j}]^{[i+j+2l]}} + \frac{\xi_{m,j}^2(i+j+2l)!}{[\xi_{n,i}+\xi_{m,j}]^{[i+j+2l+1]}}$$

To obtain the radial kinetik energy a -1/2 factor is still needed.

In the routine ancl

$an1 \,=\, -\frac{1}{2}n2(n2-1)$

$an2 \,=\, \xi_j \cdot n2$

$an3 \,=\, -\frac{1}{2}\xi_j^2$

$n1 \,=\, i+l; \;\; n2 \,=\, j+l$

$na1 \,=\, n1 \,+\, n2 \,-\, 1$

$na2 \,=\, n1 \,+\, n2$

$na3 \,=\, n1 \,+\, n2 \,+\, 1$

5.10 Routines for one and two particles operators

5.10.1 One particle operators

For the triplet (antisymmetric case) we have:

$\langle\phi_{ij}(r_1,r_2)[V(r_1)+V(r_2)]\phi_{kl}(r_1,r_2)\rangle =$

$= \langle\langle i\|V\|k\rangle\rangle \cdot \delta(j,l) + \langle\langle j\|V\|l\rangle\rangle \cdot \delta(i,k) -$

$$-\langle\langle i\|V\|l\rangle\rangle \cdot \delta(j,k) - \langle\langle j\|V\|k\rangle\rangle \cdot \delta(i,l) \tag{5.119}$$

For the singlet the different normalization of the Slater permanents must be taken into account. Defining the normalization of permanents according to:

$\mathcal{N}_{ij} = \frac{1}{2}$ for $i = j$

$\mathcal{N}_{ij} = \frac{1}{\sqrt{2}}$ for $i \neq j$

$\langle\phi_{ij}(r_1,r_2)[V(r_1)+V(r_2)]\phi_{kl}(r_1,r_2)\rangle =$

$= \mathcal{N}_{ij}\cdot\mathcal{N}_{kl}\cdot 2 \cdot \{\langle\langle i\|V\|k\rangle\rangle \cdot \delta(j,l) + \langle\langle j\|V\|l\rangle\rangle \cdot \delta(i,k) +$

$$+\langle\langle j\|V\|k\rangle\rangle \cdot \delta(i,l) + \langle\langle i\|V\|l\rangle\rangle \cdot \delta(j,k)\} \tag{5.120}$$

5.10.2 Two particles operators

The matrix elements of the two particles operators are computed by the routines: ampp(i) for the diagonal case in shells and amqq(i,j) for the out of diagonal case in shells.

Denoting $\langle i, j \,|\, V \,|\, k, l\rangle$ the matrix elements in the STO basis, in the orthonormal basis we have at once:

$\langle\langle n, m \| V \| n', m'\rangle\rangle \equiv$

$$\equiv \sum_{i=1}^{n} \sum_{j=1}^{m} \sum_{k=1}^{n'} \sum_{l=1}^{m'} uc(n,i) \cdot uc(m,j) \cdot uc(n',k) \cdot uc(m',l) \cdot \langle i, j | V | k, l\rangle \tag{5.121}$$

that holds, with obvious changes, both for the direct and the exchange integrals.

It is worthwhile recalling some details. The routines ampp and amqq call the subroutine

rrr(n, a, b, i, j, k)

where

n = vector of STO exponents

a = vector of the r exponents

b = output vector

The output vector contains the direct and exchange Coulson and Sharma integrals.

In turn the routine rrr calls the routines rmioz / u / d ... that compute the integrals

$$rmioz(m, n, a, b, output) \equiv \int_0^\infty \int_0^\infty \frac{r_<^k}{r_>^{k+1}} \cdot r_1^m \cdot r_2^n \cdot e^{-ar_1} \cdot e^{-br_2}\, dr_1\, dr_2 \tag{5.122}$$

5.11 The integrals of Coulson and Sharma

To use the STO, the following integrals are needed:

$$\int \int_0^\infty \frac{r_<^k}{r_>^{k+1}} r_1^m r_2^n \, e^{-a\,r_1} \, e^{-b\,r_2} \, dr_1 \, dr_2 \; =$$

$$= \sum_{i=0}^{n-k-1} \frac{(n\,-\,k\,-\,1)!}{(n\,-\,k\,-\,1\,-\,i)!} \frac{(m\,+\,n\,-\,1\,-\,i)!}{b^{i+1}\,(a\,+\,b)^{m+n-i}} +$$

$$+ \sum_{i=0}^{m-k-1} \frac{(m\,-\,k\,-\,1)!}{(m\,-\,k\,-\,1\,-\,i)!} \frac{(m\,+\,n\,-\,1\,-\,i)!}{a^{i+1}\,(a\,+\,b)^{m+n-i}} \tag{5.123}$$

m,n = positive integers, k = 0 or a positive integer $\leq$ *the least of* $\{(m-1),\,(n-1)\}$, $r_<$ = min(r1,r2), $r_>$ = max(r1,r2)

$$\int \int_0^\infty \frac{r_<^k}{r_>^{k+1}} r_1^m r_2^n \, e^{-a\,r_1} \, e^{-b\,r_2} \, dr_1 \, dr_2 \; =$$

$$= \frac{(m\,+\,n)!}{b^{k+n+1}} \sum_{i=0}^{k+n} \frac{(k\,+\,n)!}{i!\,(k\,+\,n\,-\,i)!} (-1)^i \, a^i \, \Gamma_{ikb}(a,m) +$$

$$+ \frac{(m\,+\,n)!}{a^{k+m+1}} \sum_{i=0}^{k+m} \frac{(k\,+\,m)!}{i!\,(k\,+\,m\,-\,i)!} (-1)^i \, b^i \, \Gamma_{ika}(b,n) \tag{5.124}$$

where

$$\Gamma_{ikd}(c,p) \; = \; \left[\frac{z^{k-p-i}}{k-p-i} \right]_c^{c+d} \quad if \; i \neq k-p$$

$$= ln\{(c\,+\,d)\,/\,c\} \;\; if \; i \,=\, k-p \tag{5.125}$$

that holds for k=0 and all positive values +[z="c+d"]; -[z="c"].

5.12 Singlet ^1S and triplet states ^3S in Configurations Interaction

5.12.1 Elements of two particles matrix

The interaction between the two electrons can be developed in the spherical coordinates of the two electrons:

$$\frac{e^2}{r_{12}} = 4\pi e^2 \sum_{k=0}^{\infty} \sum_{m=-k}^{k} \frac{1}{2k+1} \frac{r_<^k}{r_>^{k+1}} Y_{km}^*(\Omega_1)\, Y_{km}(\Omega_2) \tag{5.126}$$

Therefore the matrix element can be written:

$\langle a(1)\ b(2)|\frac{e^2}{r_{12}}|c(1)d(2)\rangle =$

$$= \langle \frac{1}{r_1} P_{n_l}^a(r_1)\ Y_{lm_l}^a(\Omega_1)\, \frac{1}{r_2} P_{n_l}^b(r_2)\ Y_{lm_l}^b(\Omega_2)| \frac{e^2}{r_{12}} | \frac{1}{r_1} P_{n_l}^c(r_1)\ Y_{lm_l}^c(\Omega_1)\, \frac{1}{r_2} P_{n_l}^d(r_2)\ Y_{lm_l}^d(\Omega_2)\rangle \tag{5.127}$$

We are interested in the S states, that can be written:

$$|c(1)d(2)\rangle \equiv \sum_{m=-l}^{l} (-1)^{l-m} \frac{1}{\sqrt{2l+1}} |\, Y_m^l(\Omega_1)\, Y_{-m}^l(\Omega_2)\,\rangle \tag{5.128}$$

$$|a(1)b(2)\rangle \equiv \sum_{m'=-l'}^{l'} (-1)^{l'-m'} \frac{1}{\sqrt{2l'+1}} |\, Y_{m'}^{l'}(\Omega_1)\, Y_{-m'}^{l'}(\Omega_2)\,\rangle \tag{5.129}$$

with $l_c \equiv l_d = l$; $\qquad l_a \equiv l_b = l'$

Therefore

$\langle a(1)\ b(2)|r_{12}|c(1)d(2)\rangle =$

$= \sum_{m=-l}^{l} \sum_{m'=-l'}^{l'} (-1)^{l-m}\,(-1)^{l'-m'}\,\frac{1}{\sqrt{2l+1}}\,\frac{1}{\sqrt{2l'+1}} \times$

$\times \sum_{k=0}^{\infty} \sum_{\tilde{m}=-k}^{k} \frac{4\pi}{2k+1} \cdot \left\{ R^k(abcd) \equiv\ e^2 \int_0^\infty \int_0^\infty \frac{r_<^k}{r_>^{k+1}}\, P_{nl}^a(r_1)\, P_{nl}^b(r_2)\, P_{nl}^c(r_1)\, P_{nl}^d(r_2)\, dr_1 dr_2 \right\} \times$

$$\times \left\langle\, Y_{l'm'}^a(\Omega_1) \right| Y_{k\tilde{m}}^*(\Omega_1) \left| Y_{lm}^c(\Omega_1) \,\right\rangle \left\langle\, Y_{l'm'}^b(\Omega_2) \right| Y_{k\tilde{m}}(\Omega_2) \left| Y_{lm}^d(\Omega_2) \,\right\rangle \tag{5.130}$$

The terms in the spherical harmonics can be written:

$$\langle l'm' \,|\, Y_{KM} \,|\, lm\rangle = (-1)^{m'} \sqrt{\frac{(2l'+1)(2K+1)(2l+1)}{4\pi}} \times$$

$$\times \begin{pmatrix} l' & K & l \\ -m' & M & m \end{pmatrix} \begin{pmatrix} l' & K & l \\ 0 & 0 & 0 \end{pmatrix} \tag{5.131}$$

It must be $-m' + M + m = 0$

$l' + K + l =$ EVEN; $\qquad \Delta(l'\, K\, l)$

It is usual to define the quantity $c^k(lm,\, l'm')$ as follows:

$$c^k(lm,\, l'm') = \sqrt{\frac{4\pi}{2k+1}}\, \langle Y_{lm} \,|\, Y_{k\, m-m'} \,|\, Y_{l'm'}\rangle = (-1)^{m-m'}\, c^k\,(l'm',\, lm) \tag{5.132}$$

5.12.2 Example for the S - S shell

$$|c(1)\,d(2)\rangle \equiv \frac{1}{4\pi}, \;\; |a(1)\,b(2)\rangle \equiv \frac{1}{4\pi} \tag{5.133}$$

Therefore

$\langle a(1)\; b(2)|\frac{1}{r_{12}}|c(1)d(2)\rangle =$

$= \sum_{k=0}^{\infty} \sum_{\tilde{m}=-k}^{k} \frac{4\pi}{2k+1} \cdot$

$\cdot \left\{ R^k(abcd) \equiv \; e^2 \int_0^\infty \int_0^\infty \frac{r_<^k}{r_>^{k+1}} P_{nl}^a(r_1)\, P_{nl}^b(r_2)\, P_{nl}^c(r_1)\, P_{nl}^d(r_2)\, dr_1 dr_2 \right\} \cdot$

$$\cdot \langle\, Y_{lm_l}^a(\Omega_1)|\, Y_{km}^*(\Omega_1)\, |Y_{lm_l}^c(\Omega_1)\,\rangle\, \langle\, Y_{lm_l}^b(\Omega_2)|\, Y_{km}(\Omega_2)\, |Y_{lm_l}^d(\Omega_2)\,\rangle \tag{5.134}$$

5.12.3 S states of two electrons

In sight of the more complex cases that we will consider later, it is useful to collect the expressions in the simplest case:

Case L=M=0

For the case $|\, l;\, L\, =\, 0;\, M\, =\, 0\rangle$, we have:

$\langle \Omega_1,\, \Omega_2\, |\, l;\, L = 0;\, M = 0\rangle\, =$

$= \sum_{m=-l}^{l} (-1)^{l-m}\, \frac{1}{\sqrt{2l+1}}\, \frac{2l+1}{4\pi}\, \frac{(l-|m|)!}{(l+|m|)!}\, P_l^{|m|}\,(cos\theta_1)\, P_l^{|m|}\,(cos\theta_2)\, e^{im(\phi_1-\phi 2)}\, =$

$$= \sum_{m=-l}^{l} (-1)^{l-m}\, \frac{1}{\sqrt{2l\, +\, 1}}\, Y_l^m(\Omega_1)\, Y_l^{-m}(\Omega_2) \tag{5.135}$$

From the definitions we have:

$$Y_{lm}(\theta,\, \phi)\, =\, \sqrt{(-1)^{m+|m|}}\, \sqrt{\frac{2l\, +\, 1}{4\pi}}\, \sqrt{\frac{(l\, -\, |m|)!}{(l\, +\, |m|)!}}\, P_l^{|m|}\,(cos\theta)\, e^{im\phi} \tag{5.136}$$

5.13 Partial trace in Ω

To compute the reduced density matrix we need the partial trace of the density matrix.

In sight of the applications to perturbative computations, that will follow, we will compute the partial trace of a more general expression: $\rho = |\,\phi_n\rangle\langle\phi_m\,|$

with

$$|\,\phi_n\rangle = \sum_l B^l\,\langle\Omega_1,\,\Omega_2\,|\,l;\,L=0,\,M=0\rangle \tag{5.137}$$

$$|\,\phi_m\rangle = \sum_{l'} C^{l'}\,\langle\Omega_1',\,\Omega_2'\,|\,l';\,L=0,\,M=0\rangle \tag{5.138}$$

We do not write explicitly the radial variables.

Now we are interested in the partial trace of the ρ in Ω for $\Omega_2 = \Omega_2' = \Omega$

Then we have:

$\rho^I(\Omega_1,\Omega_1') \equiv \int d\Omega\,|\,\phi_n\rangle\,\langle\phi_m\,| =$

$$= \sum_l\sum_{l'} B^l\cdot C^{l'*}\int d\Omega\langle\Omega_1,\,\Omega\,|\,l;\,0,\,0\rangle\cdot\langle l';\,0,\,0\,|\,\Omega_1',\,\Omega\rangle \tag{5.139}$$

The important point is to check if the double sum reduces to a single sum, and if so with which coefficients.

Explicitating the integral, we have:

$$I = \int d\Omega \langle \Omega_1, \Omega \,|\, l;\, 0,\, 0 \rangle \langle l';\, 0,\, 0 \,|\, \Omega'_1, \Omega \rangle =$$

$$= \int d\Omega \sum_{m_l=-l}^{l} (-1)^{l-m_l} \tfrac{1}{\sqrt{2l+1}} Y_l^{m_l}(\Omega_1)\, Y_l^{-m_l}(\Omega) \cdot$$

$$\cdot \sum_{m'_{l'}=-l'}^{l'} (-1)^{l'-m'_{l'}} \frac{1}{\sqrt{2l'+1}} Y_{l'}^{m'_{l'}*}(\Omega'_1)\, Y_{l'}^{-m'_{l'}*}(\Omega) \tag{5.140}$$

Then we need the integral

$$\int d\Omega\, Y_l^{-m_l}(\Omega)\, Y_{l'}^{-m'_{l'}*}(\Omega) \equiv \int d\Omega\, (-1)^{m_l}\, Y_l^{m_l *}(\Omega)\, (-1)^{m'_{l'}}\, Y_{l'}^{m'_{l'}}(\Omega) =$$

$$= (-1)^{m_l + m'_{l'}} \cdot \delta_{ll'} \cdot \delta_{m_l m'_{l'}} = \delta_{ll'} \cdot \delta_{m_l m'_{l'}} \tag{5.141}$$

We have:

$$I = \delta_{ll'} \sum_{m_l=-l}^{l} (-1)^{l-m_l} \tfrac{1}{\sqrt{2l+1}}\, (-1)^{l-m_l} \tfrac{1}{\sqrt{2l+1}}\, Y_l^{m_l}(\Omega_1)\, Y_l^{m_l *}(\Omega'_1) =$$

$$= \delta_{ll'} \sum_{m_l=-l}^{l} \frac{1}{(2l+1)}\, (-1)^{m_l}\, Y_l^{m_l}(\Omega_1)\, Y_l^{m_l}(\Omega'_1) \tag{5.142}$$

Then we obtain the final expression:

$$\rho^I(\Omega_1, \Omega'_1) = \sum_l B^l\, C^{l*}\, \frac{1}{(2l+1)} \sum_{m_l=-l}^{l} (-1)^{m_l}\, Y_l^{m_l}(\Omega_1)\, Y_l^{m_l}(\Omega'_1) \tag{5.143}$$

Chapter 6

Results

In this chapter we summarize our main results for the Helium atom.

After some general considerations about the general behaviour in function of the variational parameters, we report the von Neumann and linear values for several singlet and triplet states.

Plots of the error of energy, compared to standard high precision value, show the approximation level of our computations.

We report also details about the eigenvalues for some typical cases.

The final section discusses some optimization of the choice of the Hilbert space dimension for shells P and D.

6.1 Form of the eigenfunctions

It is very interesting to plot the radial single particle eigenfunctions that have been obtained optimizing different states, and compare them to the analogous eigenfunctions of Hydrogen.

The use of bound states of Hydrogen cannot suffice, as for a greater quantum number n

they correspond to more excited states, where consequently the electrons are at a greater distance from the nucleus.

On the contrary, to compute the electron-electron interaction one needs more "compact" functions, describing the short range effects.

For convenience we report the radial Hydrogen-like eigenfunctions for some values of the quantum numbers.

In the Helium case, and for instance considering the ^1S fundamental state, the single particle components are needed to describe the short range correlations due to the interactions between the two electrons.

We note that for such orbitals, increasing n the wavefunction concentrates near the origin, as it must be for short range correlations.

The situation is similar for other excited states and for the triplet.

6.1.1 Hydrogen-like eigenfunctions

The standard expression are:

$$u_{nlm}(r,\,\theta,\,\phi) \;=\; -\sqrt{\left(\frac{2Z}{na_0}\right)^3 \frac{(n-l-1)!}{2n[(n+l)!]^3}} \cdot e^{-\frac{Zr}{na_0}} \left(\frac{2Z}{na_0}r\right)^l L_{n+l}^{2l+1}\left(\frac{2Z}{na_0}r\right) Y_{lm}(\theta,\,\phi) \tag{6.1}$$

Ignoring the orbital part, we have:

$$u_{nl}(r) \;=\; C * e^{-(\xi r)} * (2\xi r)^l * L_{n+l}^{2l+1}(2\xi r) \tag{6.2}$$

with $\xi = \frac{Z}{na_0} \propto \frac{1}{n}$.

It must be observed that the indexes of the generalized Laguerre functions are defined following several conventions in the literature.

In our programs, we have (setting $\xi = \frac{1}{n}$):

```
az1 = (2/n)^3 * Factorial[n - l - 1],
az2 = 2*n*(Factorial[n + 1])^3,
axn = Sqrt[az1/az2],
a1 = Exp[- r/n]*(2*r/n)^l,
aa = axn*a1 * LaguerreL[n - l - 1, 2*l + 1, 2*r/n],
gg[[i]] = aa,
gp[[i]] = aa*aa*r*r
```

$\psi(r) = gg$, $|\psi(r)|^2 * r^2 = gp$.

The important point is that $\xi = 1/n$ and that it does not depend on l.

Level	aa1s=ξ	Tables in sect. 9.5
Fundamental	2.1553	9.7 $^1S/S$
I	1.0218	9.8 $^1S/I/S$
II	0.7861	9.9 $^1S/II/S$
III	0.6061	9.10 $^1S/III/S$
IV	0.4442	9.11 $^1S/III/S$

Table 6.1 – S Shell - ξ values

Shell S

Considering the data of the runs with mimimal dimension, we have table 6.1 for the shell S and the state ^1S.

This is in general agreement with the 1/n dependency of the Hydrogen eigenfunctions for Z=2.

Of course this must be intended in a qualitative sense.

If one now considers the variation of the ξ parameter when the basis dimension increases, it can be observed that, for the fundamental state the ξ varies greatly without a significant refinement of the energy value.

For the excited states, the ξ value resembles the Hydrogen value, but the variation is in general less pronunced when the Hilbert space dimension is increased.

This can be interpreted as a weaker radial correlation for more excited levels.

It is very important to note that the variational optimization was performed separately for each state. Therefore the energy values have been optimized separately, and the states that have been obtained are not necessarily orthogonal. We did not consider necessary to compute, in this preliminary study, the deviation from orthonormality, however, as it is not computationally heavy, it will be studied later.

Shell S-P

It is very interesting to compare those data to the optimization in Configurations Interaction for the shell S-P.

It is worthwhile noting that, in the case of shell S, only one has just one variational parameter, aa1s.

Now, considering also the P shell, we must optimize two parameters, one for the S shell and another for the P shell.

After several tests, we concluded that the search for a minimum in the aa1s/aa1p space, does not present a significant correlation, see fig. 6.1 and 6.2.

We then considered that it is sufficient to optimize one parameter at a time.

Moreover, several tests showed that it is sufficient to use the aa1s value that was obtained from the optimization of the S shell alone, in the optimization of the P shell for the case CI-S/P.

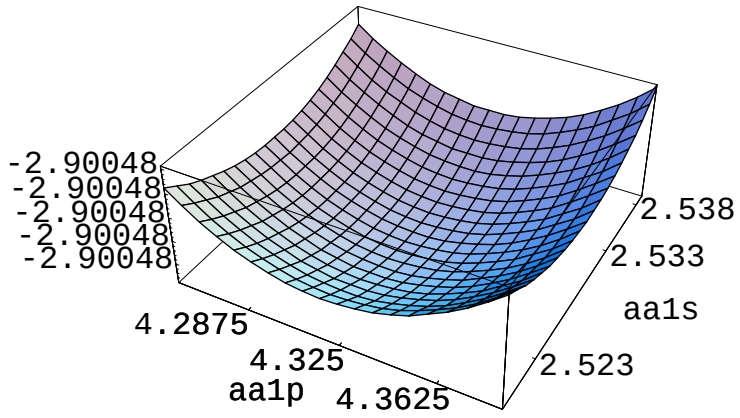

Figure 6.1 – Energy of shell S-P in 3D format. Fundamental levels

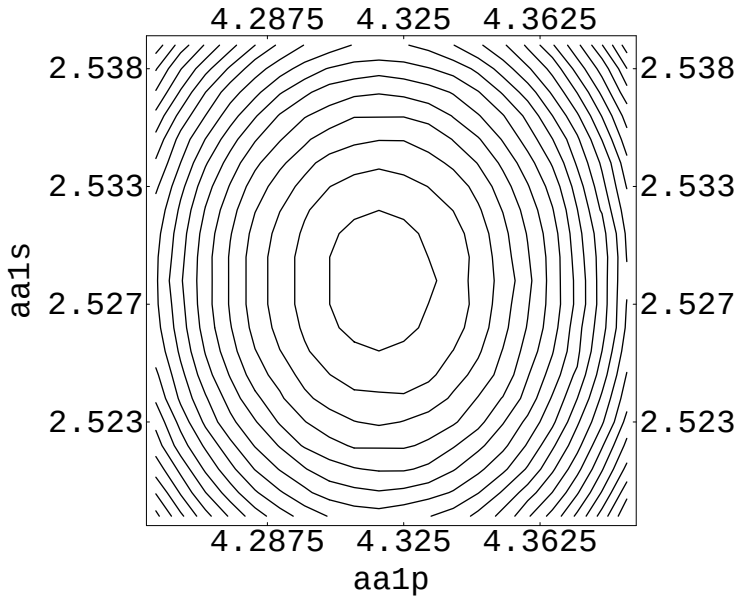

Figure 6.2 – Energy of shell S-P: level curves. Fundamental level.

Then the optimization task for the S-P shell reduces to the optimization of the single

Level	aa1p=ξ	Tables in sect. 9.5
Fundamental	4	9.14
I	2	9.15
II	2.4	9.16
III	1.7	9.17
IV	1.9	9.18

Table 6.2 – S-P Shell - ξ values

variational parameter of the P shell: aa1p.

Fundamental and excited states ^1S*: S-P shell*

It is sufficient to report the values of the aa1p parameters for the first excited states and for low n values (with ns = np). We have table 6.2.

From the plots and tables reported, is is evident that the aa1p parameter value is not critical.

A great qualitative difference can be noted between these variational parameters and those of the S shell.

We recall that, as we saw at the beginning of this discussion, the ξ parameters for the Hydrogen-like atoms are $\xi \propto 1/n$ independent on the quantic number l, and that for the S shell this dependence is qualitatively maintained.

Level	aa1d=ξ	Tables in sect. 9.5
Fundamental	4.4	9.21
I	3.4	9.22
II	3.8	9.23
III	3.9	9.24
IV	3.8	9.25

Table 6.3 – S-P-D Shell - ξ values

In the case of the P states for the P shell of the CI computation, the behaviour is quite different, and the result is not sensible to the aa1p parameter value, within a large interval.

One can easily interpret this difference in behaviour between S and P states for the computation of the ^1S levels. Indeed, we note that the S states must "compute" the "base" energy of the levels, plus the correlation corrections due to the electron-electron interactions; the P states, on the contrary, are only involved in the correlation computation.

Similar considerations can be made for the S-P-D shells, as shown by table 6.3.

6.2 Errors of energies of fundamental and excited states

In the following graph (fig. 6.3) we plot the error in ppm of the energy of the fundamental and first 7 excited levels of the states $|\, 1s,\, ns;\, {}^1S$. The abscissae are the maximum number of shells considered in the computation in Configurations Interaction.

The graph clearly shows that by increasing the number of shells considered the error quickly decreases . This implies the effect of the orbital correlation between the two electrons.

Moreover, we note that for the excited states the error decreases with increasing the excitation. This can be explained by the fact that the more excited the state, the less the electrons interact and as a consequence, the less perturbation we have.

It is reasonable to expect a smaller entanglement value for the excited states, as the interaction is weaker. This hypothesis will be discussed later.

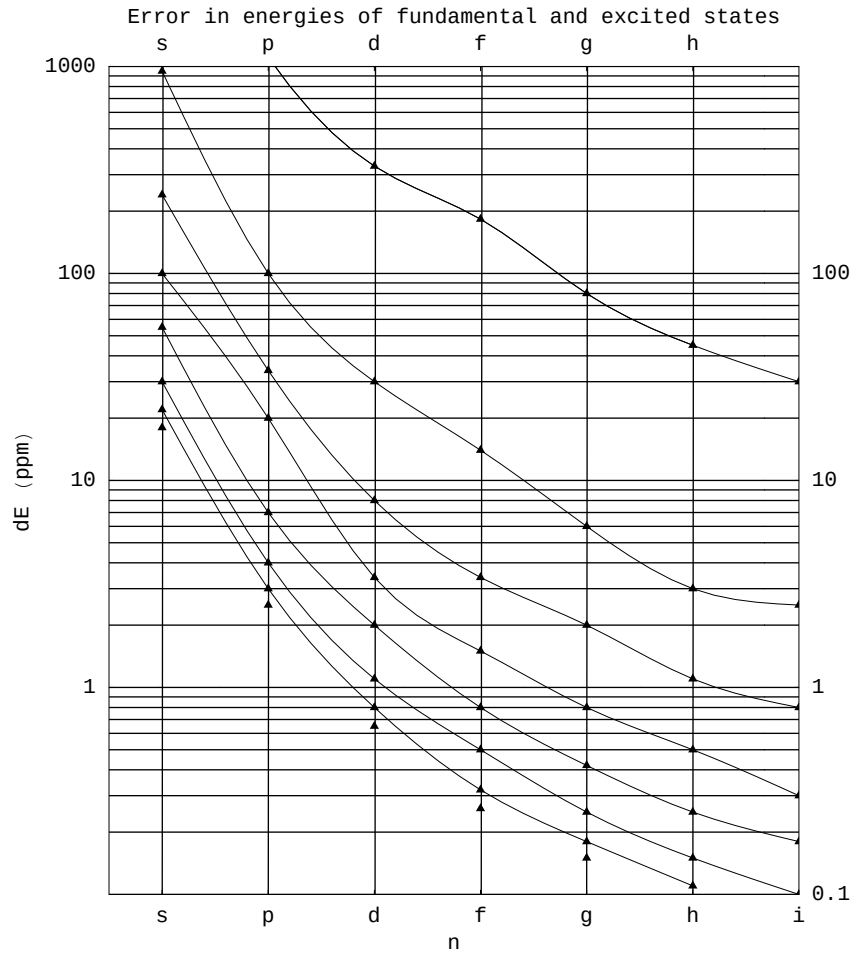

Figure 6.3 – Error of energies of fundamental (top line) and excited states I to VII, top to bottom.

In figure 6.4 we report the convergence of the energy of the fundamental state ^1S as a function of the single particle Hilbert space dimension. In abscissa the variational parameter ξ_l.

We note that increasing the dimension of the Hilbert space the sensitiveness on the variational parameter ξ_l decreases.

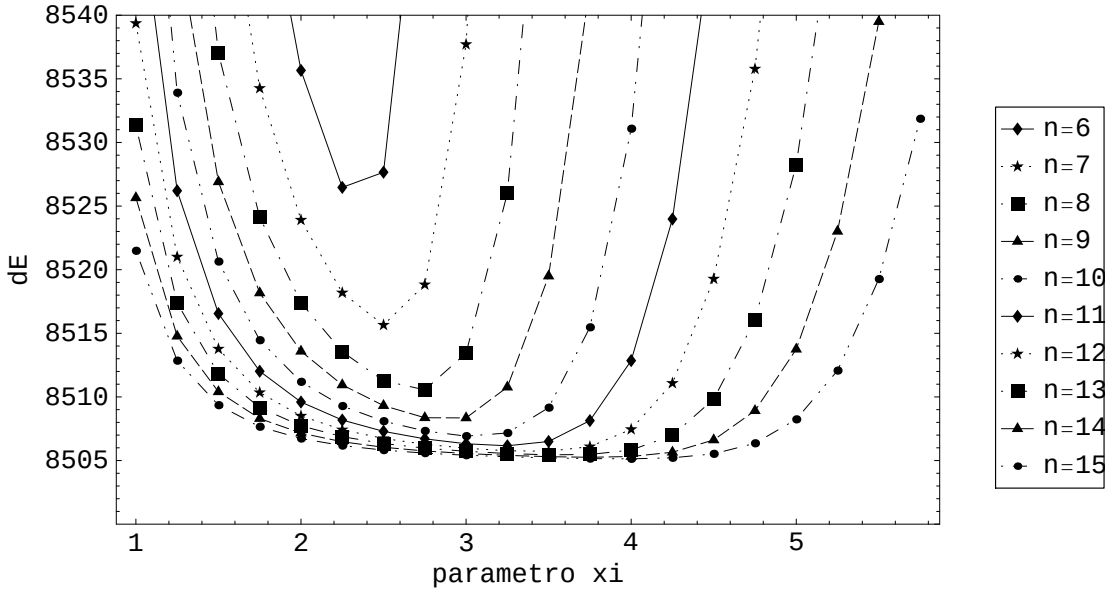

Figure 6.4 – Energy error for several Hilbert space dimensions

6.3 Entanglement in Helium: summary of results

In the following, we will present data only for total orbital momentum quantum number $L = 0$, thus implying $l_1 = l_2 \equiv l$ and $m_1 = -m_2$.

We first discuss convergence of our method, as a function of the number $n_{\max}(l)$ of radial wavefunctions for a given l and as a function of the cut-off $l_{\max}$ on l.

For the low-energy states discussed below, we found that $l_{\max} = 2$ (S, P, and D shells) and $n_{\max} \approx 10 - 20$ (from $n_{\max} = 10$ for the ground state up to $n_{\max} = 20$ for the highest excited states reported below) are sufficient to reproduce helium eigenergies with at least

	$l_{\max}=0$	$l_{\max}=1$	$l_{\max}=2$	$l_{\max}=3$
$n_{\max}=5$	0.04131	0.07772	0.07844	0.07833
$n_{\max}=6$	0.04133	0.07776	0.07848	0.07837
$n_{\max}=10$	0.04134	0.07777	0.07849	0.07839
$n_{\max}=11$	0.04134	0.07777	0.07849	0.07839

Table 6.4 – Reduced von Neumann entropy of the ground state of helium, computed with different cut-off values in the basis of Slater-type orbitals.

State	$S(\rho_1)$	$S_L(\rho_1)$
$\|(1s)^2;{}^1S\rangle$	0.0785	0.01606
$\|1s,2s;{}^1S\rangle$	0.991099	0.48871
$\|1s,3s;{}^1S\rangle$	0.998513	0.49724
$\|1s,4s;{}^1S\rangle$	0.999577	0.49892
$\|1s,5s;{}^1S\rangle$	0.999838	0.499465
$\|1s,6s;{}^1S\rangle$	0.999923	0.499665
$\|1s,7s;{}^1S\rangle$	0.999961	0.499777

Table 6.5 – Reduced von Neumann and linear entropies for the lowest energy singlet eigenstates of helium.

four significant digits (as deduced from comparison of our results with those of (Drake , 1999), (Koga , 1996), (Kono, Hattori , 1985), (Kono, Hattori , 1986) and reduced von Neumann entropy $S(\rho_1)$, estimating at least two-three significant digits.

To illustrate the convergence of our method, we provide in Table 6.4 the obtained values of $S(\rho_1)$ of the ground state of helium for different values of the cut-offs $l_{\max}$ and $n_{\max}$ (we take the same $n_{\max}$ for all values of l). It can be seen that increasing $n_{\max}$ the results are almost costant.

The reduced von Neumann entropy $S(\rho_1)$, as well as the linearized entropy $S_L(\rho_1) = 1-\mathrm{Tr}(\rho_1^2)$ often used in the literature, are shown in Table 6.5 and in Table 6.6 for several low-energy singlet and triplet eigenstates, respectively.

Since the obtained values of the von Neumann entropy are very close to those expected for Fock states, which are separable, the entanglement content is weak and can be estimated by means of Eq. (3.34).

The obtained results are shown in Fig. 6.5 as a function of the state number n, for both

State	$S(\rho_1)$	$S_L(\rho_1)$
$\|1s, 2s; {}^3S\rangle$	1.00494	0.500378
$\|1s, 3s; {}^3S\rangle$	1.00114	0.5000736
$\|1s, 4s; {}^3S\rangle$	1.000453	0.5000267
$\|1s, 5s; {}^3S\rangle$	1.000229	0.5000127
$\|1s, 6s; {}^3S\rangle$	1.000133	0.5000070
$\|1s, 7s; {}^3S\rangle$	1.000091	0.5000047

Table 6.6 – Same as in Table 6.5, but for the lowest energy triplet eigenstates of helium.

singlet states $|1s, ns; {}^1S\rangle$ and triplet states $|1s, ns; {}^3S\rangle$.

Note that data, with the exception of the ground state value of entanglement, are consistent with a power law decay of entanglement with n.

From a power-law fit we obtained $E(n) = 0.19\, n^{-4.41}$ for singlet states at $n \geq 2$ and $E(n) = 0.040\, n^{-3.19}$ for triplet states.

The same entanglement data are shown as a function of energy in Fig. 6.6.

It can be clearly seen that the entanglement content drops with energy.

This result is rather intuitive in that for states $|1s, ns; {}^1S\rangle$ and $|1s, ns; {}^3S\rangle$ the wave functions corresponding to the states $1s$ and ns are localized far apart for large n.

Therefore, electron-electron interactions become weaker (and entanglement smaller) when n increases.

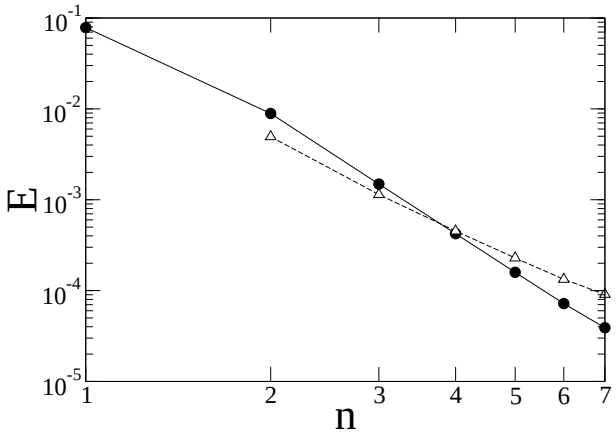

Figure 6.5 – Entanglement of the singlet states $|1s, ns; {}^1S\rangle$ (circles) and of the triplet states $|1s, ns; {}^3S\rangle$ (triangles).

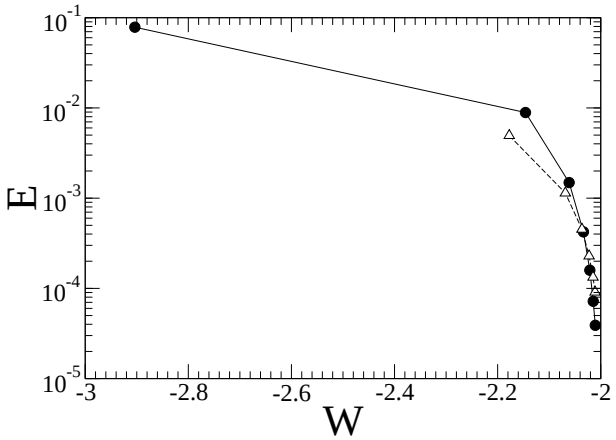

Figure 6.6 – Same as in Fig. 6.5, but with the entanglement of the helium eigenstates plotted as a function of their energy W (measured in hartrees).

	S	S-P	S-P-D
Fond.	8504.9	1105.7	332.8
I	828.1	97.4	31.4
II	232.1	29.8	14.7
III	95.7	13.6	15.0
IV	49.3	7.9	15.1
V	40.3	33.6	143.9
VI	125.3	201.2	348.0

Table 6.7 – ${}^1S$ ΔE (ppm) S shell

	n	S	S-P	S-P-D
I	2	443.0	26.7	3.3
II	3	96.3	6.9	1.8
III	4	36.3	2.8	2.2
IV	5	20.2	3.9	2.9
V	6	18.0	8.8	8.3
VI	7	84.5	78.4	78.0

Table 6.8 – ${}^3S$ ΔE (ppm) S shell

6.4 Results of energy computations in Configurations Interaction for shells S/S - P/S-P-D

In the following tables we report the final results of the energy computation for the first 6 levels of the ${}^1S$ and ${}^3S$ states as differences from the standard values (Kono, Hattori , 1985), (Kono, Hattori , 1986) in parts per million.

We immediately note an error reduction, comparing the results of the triplet with the correspondent singlet cases.

This is evidently due to the fact that, being the orbital eigenfunction antisimmetrical, it is necessarily zero for $\mathbf{r}_1 = \mathbf{r}_2$ and very little for $\mathbf{r}_1 \approx \mathbf{r}_2$.

This phenomenon is known as Fermi Hole. Then, because of this fact, the electrons have a weaker interaction and, if the other conditions are the same, we get smaller errors.

For the same reason, the error is in general bigger for the state $|\, 1s, 2s; {}^3S\rangle$, compared to

the states $|\,1s, ns; {}^3S\rangle$ for $n > 1$.

The bigger error for n=7 (VI level) is due to numerical errors.

Moreover, we remark that the error, with the exception of n=2, rapidly decreases passing from the shell S alone to the S-P shell. On the other hand, again with the only exception of n=2, we obtain a negligible improvement using the S-P-D shell.

For this reason we did not extend our computations to F-G-... shells, even if our programs allow these extensions.

In our computations we assume ndds=nddp=nddd to avoid useless parameters.

It is now interesting to compare the energy convergence versus the Hilbert space dimension.

In the graphs 6.7 6.8 6.9 6.10 6.11 6.12 we plotted the data for S/S - P/S-P-D shells for several levels; in abscissa the n=ndds=nddp=nddd values.

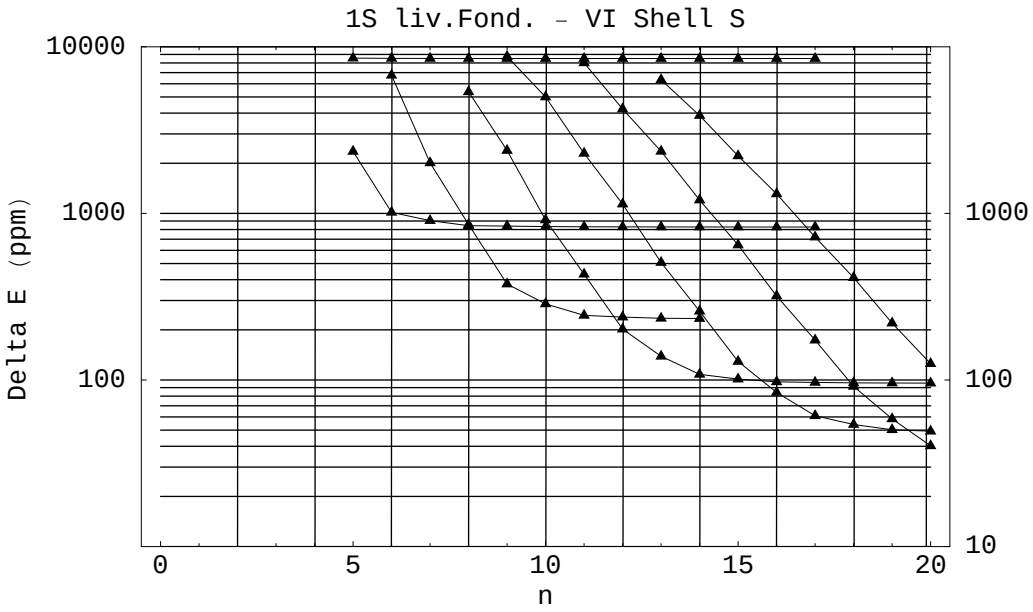

Figure 6.7 – ^1S Levels from Fund. to VI, S shell

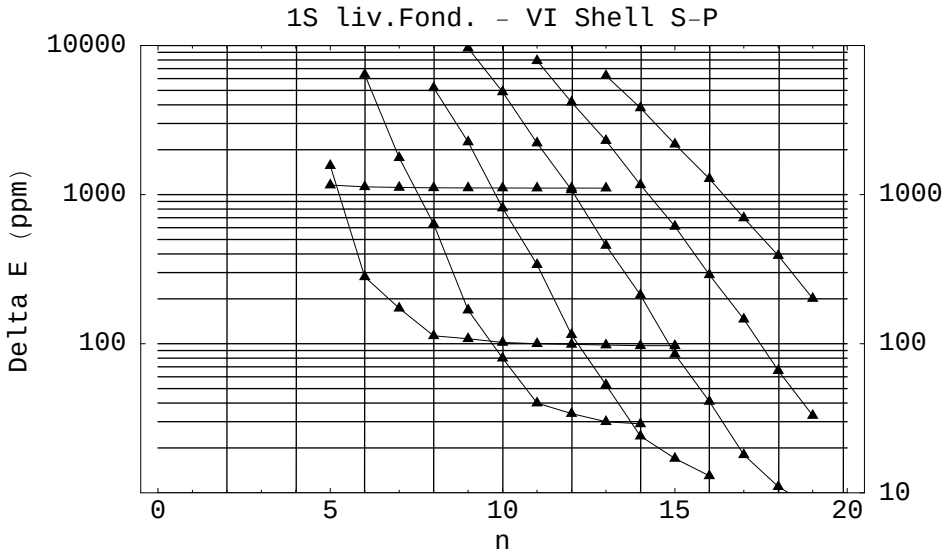

Figure 6.8 – ^1S Levels from Fund. to VI, S-P shell

In all these graphs we note that increasing n to n+2 the error initially decreases by about an order of magnitude. Then it stabilizes to an increase from n_c to $n_c + 3$, where n_c is the critical n value starting from which the dependence of the error on n ceases to be linear in a log-linear graph.

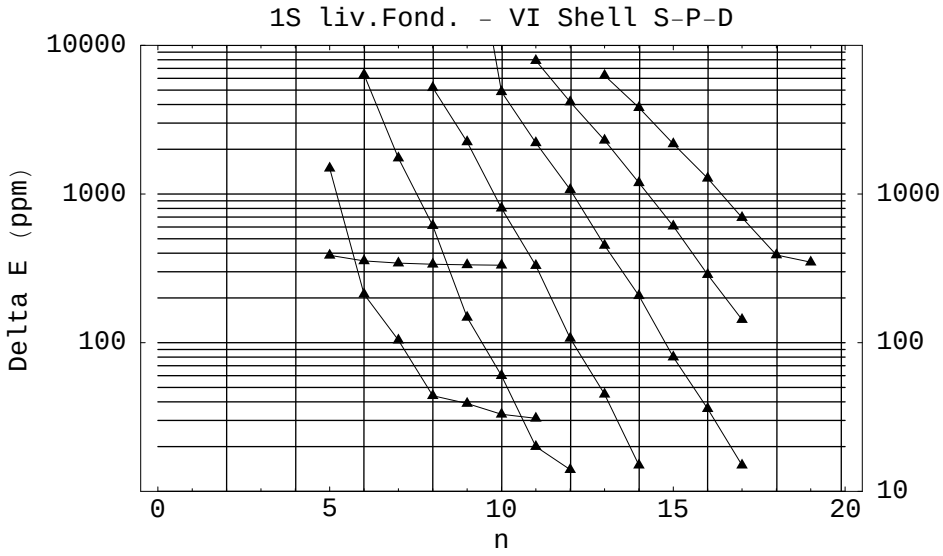

Figure 6.9 – ^1S Levels from Fundam. to VI, S-P-D shell

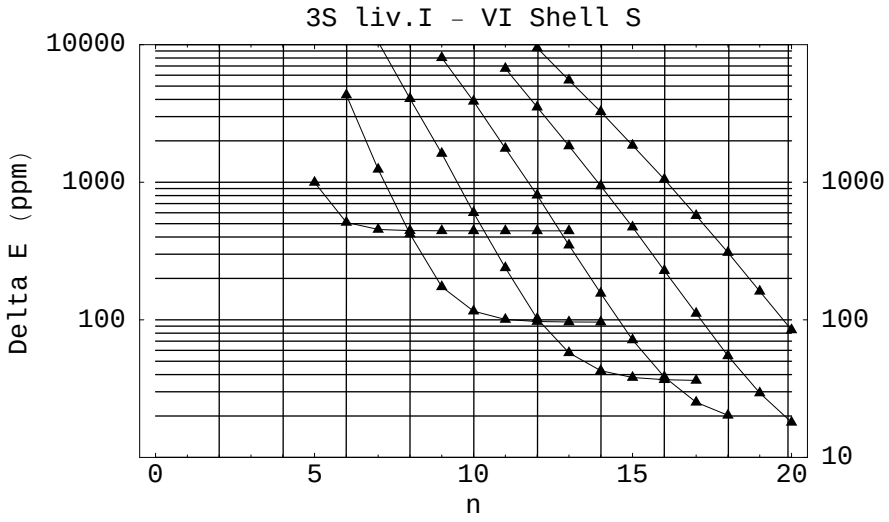

Figure 6.10 – ^3S Levels I to VI, S shell

A second evident feature is that the approximately linear part of the curve in the graphs 6.10 6.11 6.12 moves towards greater abscissae values for a value about $\Delta n = 2-3$ passing from a level to the next.

This implies that, increasing the excitation, one needs a Hilbert space of bigger dimension.

We recall that in the triplet case it is necessary to diagonalize matrices of n(n-1)/2 di-

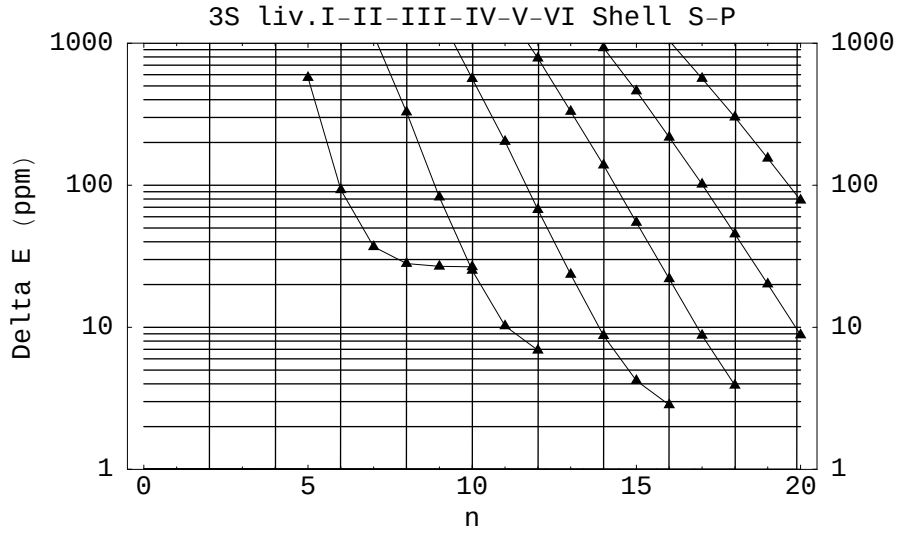

Figure 6.11 – ^3S Levels I-VI, S-P shell

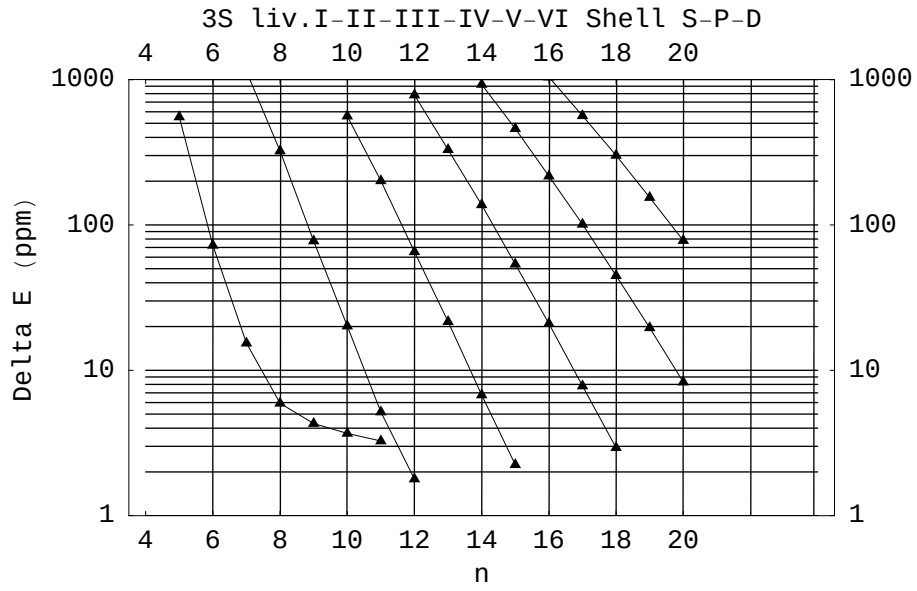

Figure 6.12 – ^3S Levels I-VI, S-P-D shell

mension.

This implies not only a longer computation time, but also the necessity of using quadruple precision (real*16) routines to compute high excitation levels.

In the plots 6.13 6.14 6.15 6.16 6.17 6.18 we report the minimum errors obtained in the present computations.

Comparing with the graphs 6.10 6.11 6.12, we remark that these are not the minimal asymptotic errors for highly excited levels, but just the numerical limits of the computation method used.

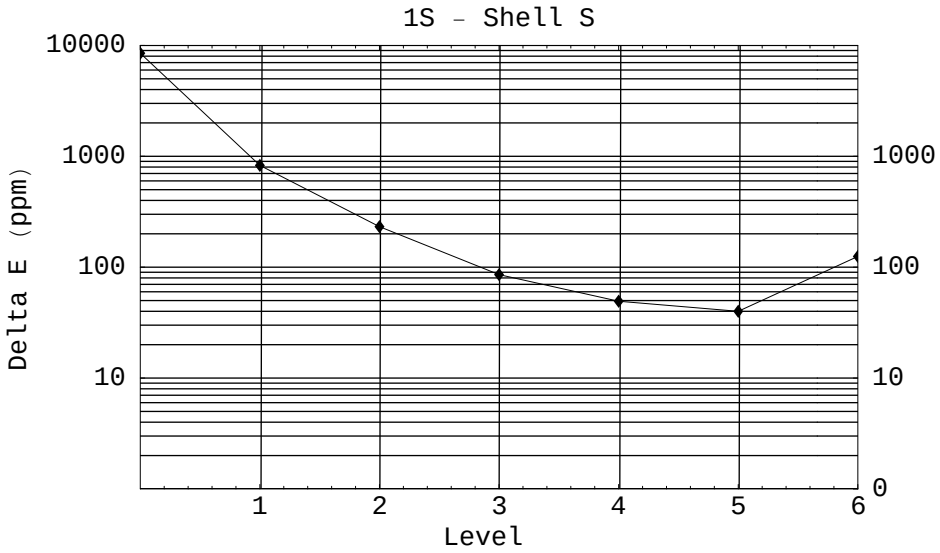

Figure 6.13 – ${}^1S$ ΔE vs. levels, S shell

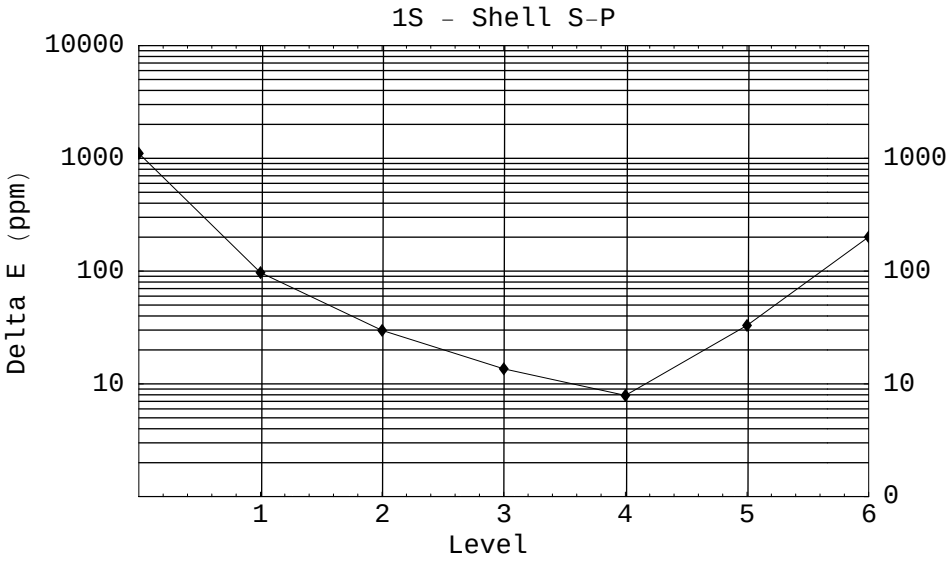

Figure 6.14 – ${}^1S$ ΔE vs. levels, S-P shell

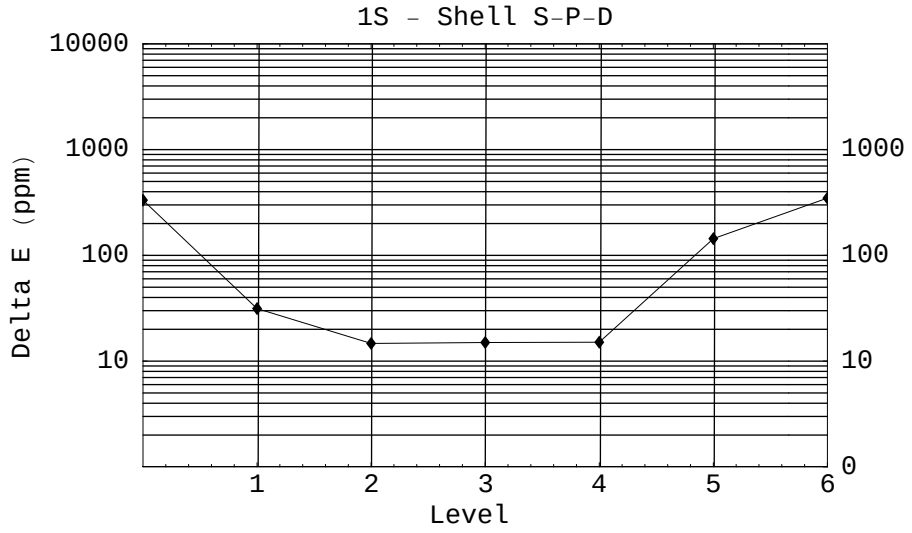

Figure 6.15 – ${}^1S$ ΔE vs. levels, S-P-D shell

It is also to be recalled that the aim of the present computation is the entropy not the energy evaluation. Energies have been reported just to evaluate the quality of the approximation that we obtained.

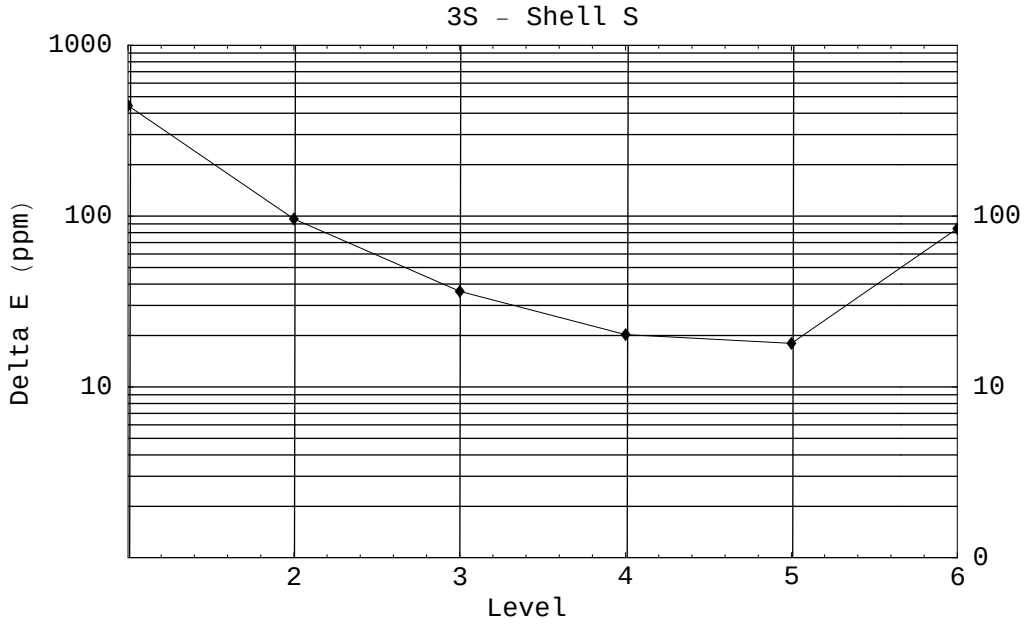

Figure 6.16 – ${}^3S$ ΔE vs. livels, shell S

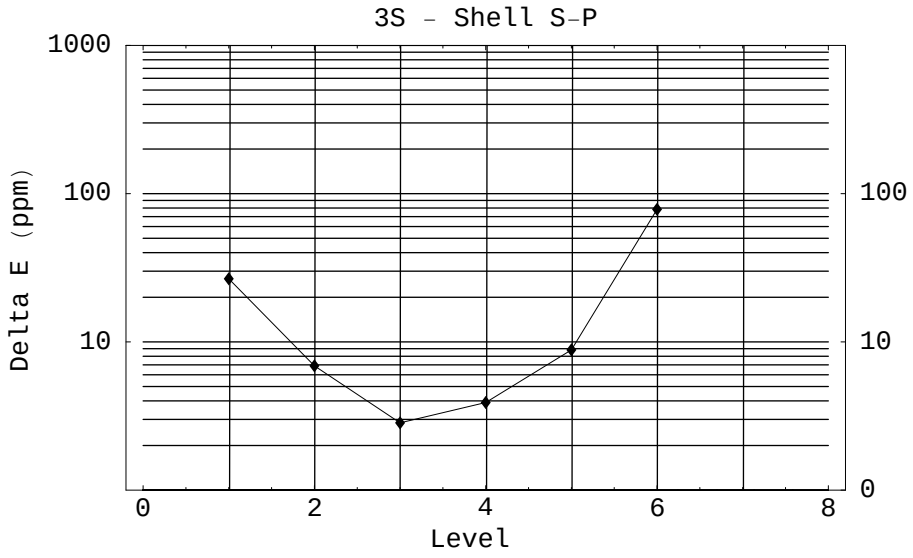

Figure 6.17 – ${}^3S$ ΔE vs. livels, shell S-P

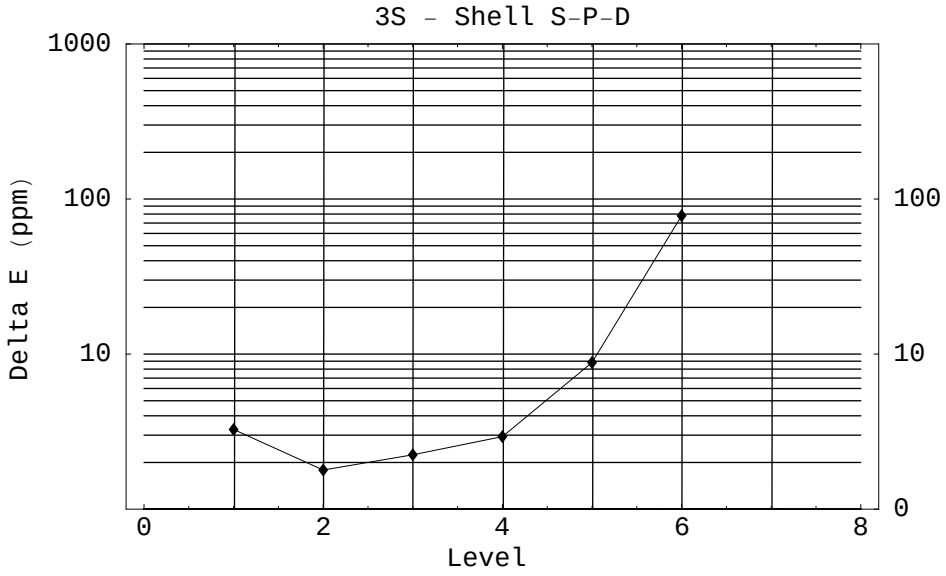

Figure 6.18 – ${}^3S$ ΔE vs. livels, shell S-P-D

6.5 Reduced density matrix eigenvalues

As the computation of the linear and von Neumann entropies depends on the eigenvalues of the reduced density matrix, it is very interesting to discuss their values, at least in some typical cases.

6.5.1 Fundamental and first excited states ^1S S-S Shell

The simplest case is the case of the S shell for states ^1S, both fundamental and excited.

In the tables 6.9, 6.10, 6.11, 6.12, and plots 6.19, 6.20, 6.21, 6.22 we report the data for the fundamental and first 3 excited states.

Table 6.9 shows that this state is very similar to a separable one, and the higher components reduce by 2 orders of magnitude at each step in n. This explains the quite low entropy of this state.

This entropy value can be considered the entanglement value in the approximation of the shell S alone.

In table 6.10, we report the data of the first excited state $|\,1s, 2s; {}^1S\rangle$. The first two eigenvalues are near to the 0.5 value that one gets with a single Slater permanent.

The other eignevalues are lower by at least 3 orders of magnitude. Using these values one immediatly computes the von Neumann entropy.

To evaluate the entanglement one must subtract "according to some convention" the part due to the simmetrization of the wave function, as discussed in sect. 3.2.

In tables 6.11 and 6.12, we report the analogous results for the II and III excited states.

Comparing tables 6.10, 6.11, 6.12 we note the remarkable feature that, increasing the excitation, the two bigger eigenvalues get nearer to the 0.5 value due to the symmetrization only, while the others are smaller by many orders of magnitude (up to 12), and decrease

N	value	$-\lambda_i log_2 \lambda_i$
1	0.9956101603245105	0.006319279
2	0.0043054470424728	0.033839183
3	0.0000779840413816	0.001064206
4	0.0000054942911793	9.60052E-05
5	0.0000007322303219	1.49237E-05
6	0.0000001470172639	3.33693E-06
7	0.0000000298761453	7.46797E-07
8	0.0000000037219788	1.0422E-07
9	0.0000000014124194	4.1524E-08
10	0.0000000000423267	1.45856E-09
Sum	1.0	0.041337828

Table 6.9 – Singlet, S shell, fundamental level eigenvalues

by increasing the energy. Thus the state approaches a separable symmetrized one.

In the presence of such a large range of orders of magnitude, it is worth recalling that all the computations have been done in quadruple precision (real*16).

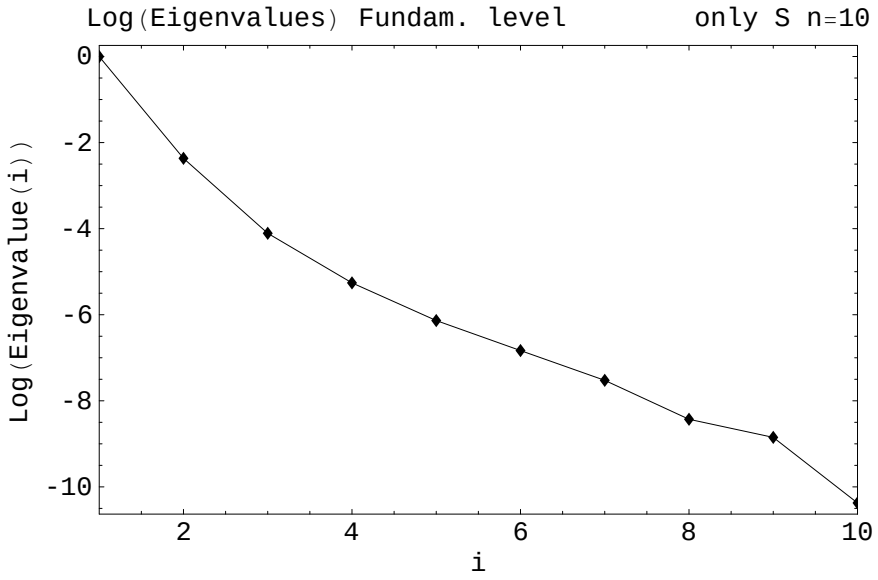

Figure 6.19 – Eigenvalues Singlet S only, fundamental, n=10, log scale

N	value	$-\lambda_i log_2 \lambda_i$
1	0.5793842200474583	0.456211598
2	0.4204485851413293	0.525560187
3	0.0001628527164212	0.002049362
4	0.0000040622321363	7.27517E-05
5	0.0000002630193014	5.74916E-06
6	0.0000000168342871	4.34729E-07
7	0.0000000000077432	2.85803E-10
8	0.0000000000012018	4.75888E-11
9	0.0000000000000821	3.56886E-12
10	0.0000000000000394	1.75443E-12
Sum	1.0	0.983900082

Table 6.10 – Singlet, S shell, level I eigenvalues

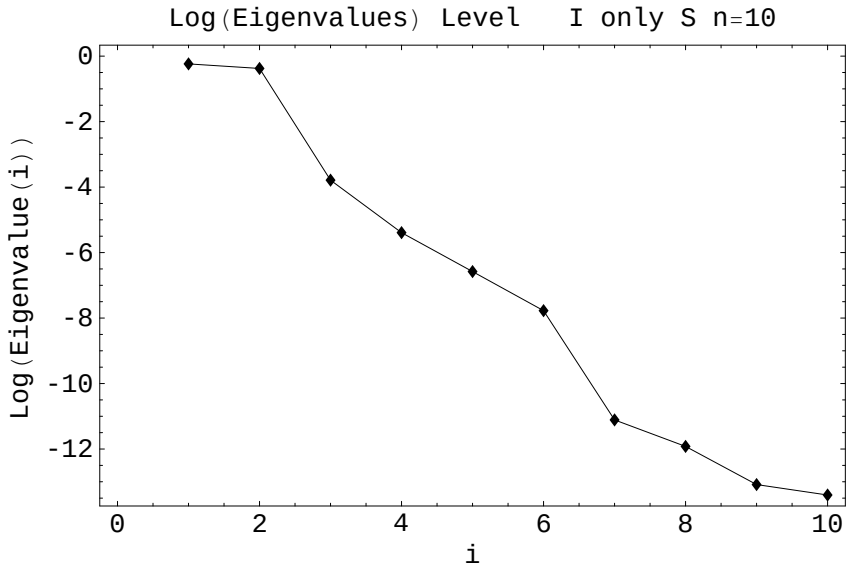

Figure 6.20 – Eigenvalues Singlet S only, level I, n=10, log scale

N	value	$-\lambda_i log_2 \lambda_i$
1	0.5396859946620111	0.480216833
2	0.4602574264847250	0.515252249
3	0.0000549866748567	0.000778092
4	0.0000015255975355	2.94779E-05
5	0.0000000660911895	1.57634E-06
6	0.0000000003650133	1.14437E-08
7	0.0000000000961249	3.19868E-09
8	0.0000000000247272	8.71266E-10
9	0.0000000000035127	1.3366E-10
10	0.0000000000003041	1.26446E-11
Sum	1.0	0.9962782

Table 6.11 – Singlet, S shell, level II eigenvalues

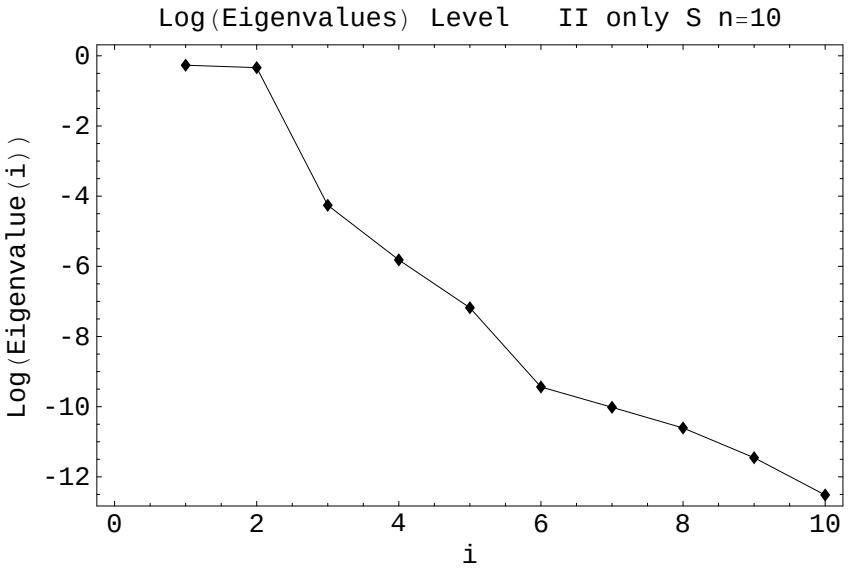

Figure 6.21 – Eigenvalues Singlet S only, level II, n=10, log scale

N	value	$-\lambda_i log_2 \lambda_i$
1	0.5271689590050625	0.486926289
2	0.4728015044789180	0.510953498
3	0.0000286227347072	0.000431988
4	0.0000009039700290	1.81492E-05
5	0.0000000065467414	1.77983E-07
6	0.0000000023847937	6.83088E-08
7	0.0000000007696116	2.33001E-08
8	0.0000000000975508	3.24406E-09
9	0.0000000000075941	2.80513E-10
10	0.0000000000049916	1.87403E-10
Sum	1.0	0.9983302

Table 6.12 – Singlet, S shell, level III eigenvalues

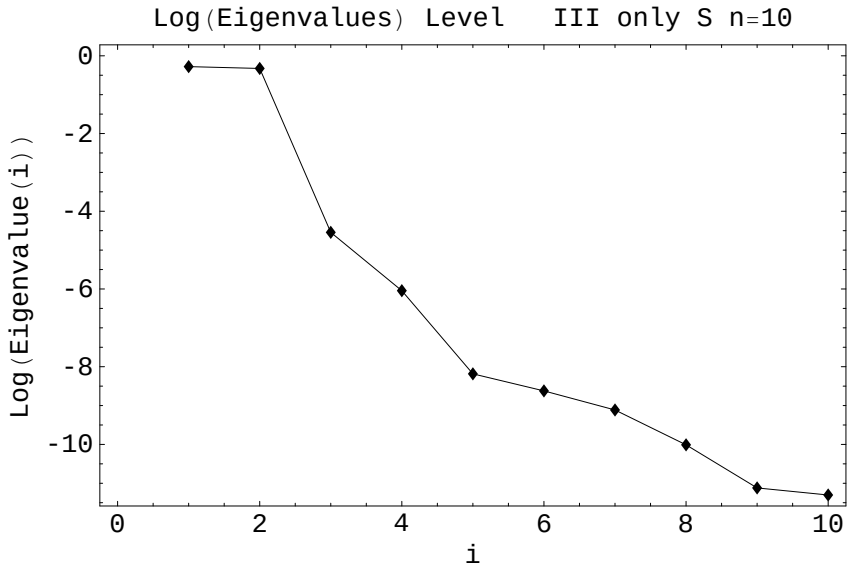

Figure 6.22 – Eigenvalues Singlet S only, level III, n=10, log scale

N	value	$-\lambda_i log_2 \lambda_i$
1	0.99186985949	0.011681503
2	0.003856134911	0.030920914
3	0.000064773376	0.000901272
4	0.000004253380	7.58929E-05
5	0.000000539815	1.12395E-05
6	0.000000107321	2.48465E-06
7	0.000000018895	4.84797E-07
8	0.000000003204	9.04088E-08
9	0.000000000771	2.33401E-08
10	0.0000000000223	7.89067E-10
Sum	0.995795691	0.04359

Table 6.13 – Singlet, S-P shells, fundamental level, part S eigenvalues

6.5.2 Fundamental and excited states ^1S. S-P Shell

No great qualitative differences from the case of S shell only can be noted. Obviously, we now have a contribution due to the P shell.

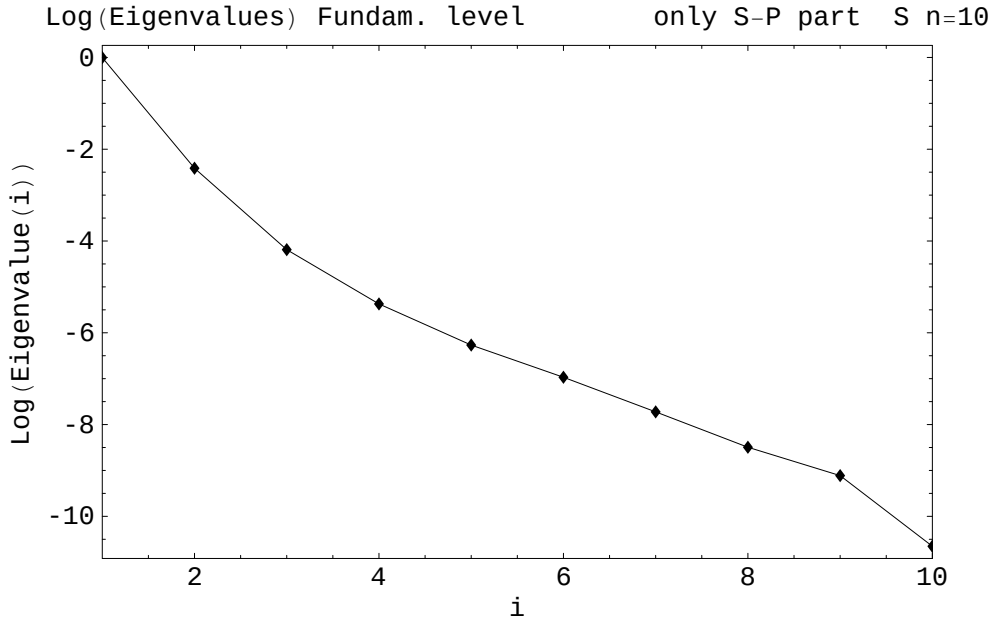

Figure 6.23 – Eigenvalues Singlet S-P only,S part, fund. level, n=10, log scale

N	value	$-\lambda_i log_2 \lambda_i$
1	0.004058167942	0.032241965
2	0.000133077867	0.001713436
3	0.000011035101	0.000181721
4	0.000001580425	3.04568E-05
5	0.000000325125	7.00726E-06
6	0.000000085452	2.00644E-06
7	0.000000025439	6.41785E-07
8	0.000000009040	2.41558E-07
9	0.000000001484	4.35225E-08
10	0.000000000923	2.7702E-08
Sum	0.004204309	0.03418
Sum S+P	1.0	0.07777

Table 6.14 – Singlet, S-P shells, fundamental level, part P eigenvalues

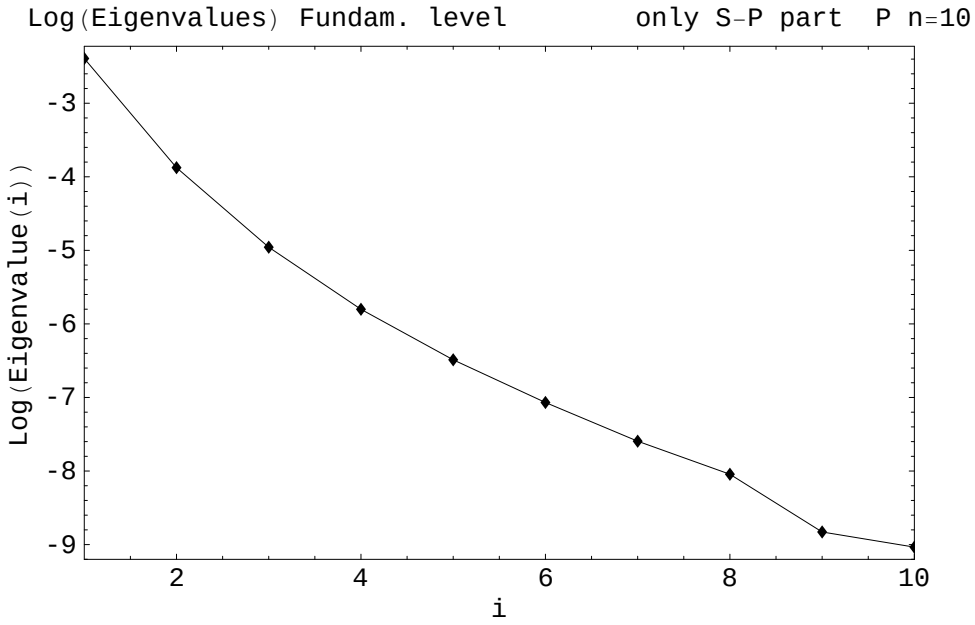

Figure 6.24 – Eigenvalues Singlet S-P only, P part, fund. llevel, n=10, log scale

N	value	$-\lambda_i log_2 \lambda_i$
1	0.5771793556581271	0.457650357
2	0.4221766345150768	0.525222082
3	0.0001723768839147	0.002155081
4	0.0000045108612084	8.01046E-05
5	0.0000002839657735	6.17563E-06
6	0.0000000257087672	6.48199E-07
7	0.0000000000594147	2.01834E-09
8	0.0000000000010217	4.06965E-11
9	0.0000000000003550	1.46818E-11
10	0.0000000000000024	1.16558E-13
Sum	0.999533188	0.98511

Table 6.15 – Singlet, S-P shells, level I, part S eigenvalues

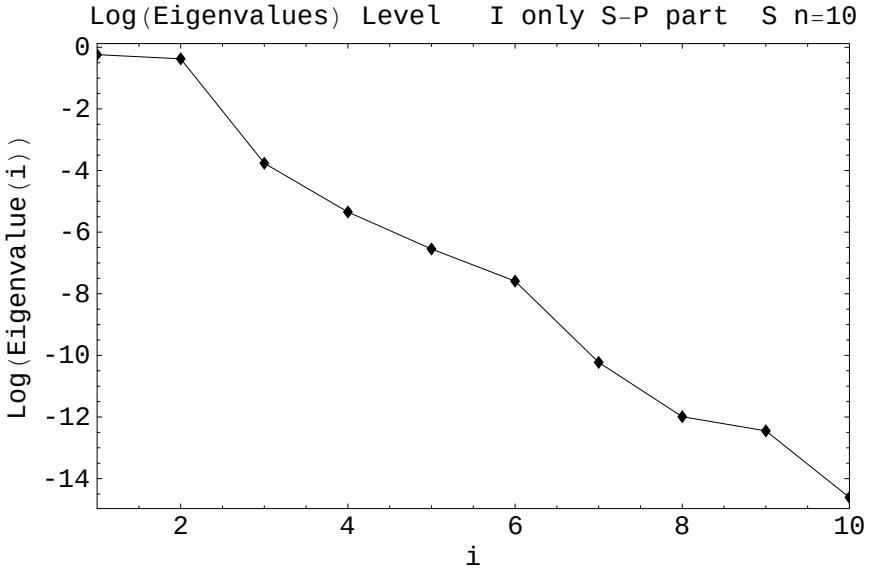

Figure 6.25 – Eigenvalues Singlet S-P only, S part, level I, n=10, log scale

N	value	$-\lambda_i log_2 \lambda_i$
1	0.00026353829987	0.003133391
2	0.00019510237361	0.00240434
3	0.00000741093141	0.000126296
4	0.00000066557989	1.3657E-05
5	0.00000008102990	1.90882E-06
6	0.00000001234285	3.24268E-07
7	0.00000000122588	3.62904E-08
8	0.00000000040001	1.2488E-08
9	0.00000000016170	5.25945E-09
10	0.00000000000116	4.59929E-11
Sum	0.000466812	0.005679972
Sum S+P	1.0	0.9907944

Table 6.16 – Singlet, S-P shells, level I, part P eigenvalues

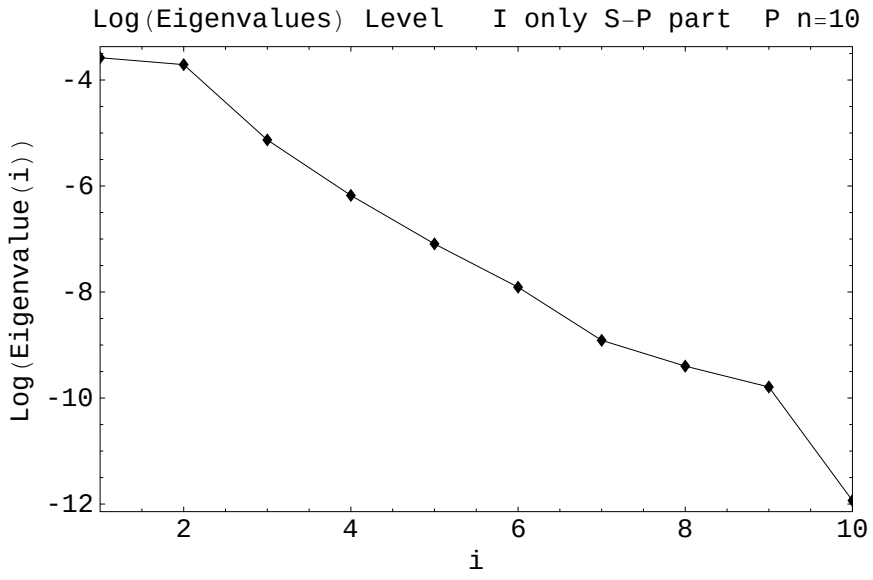

Figure 6.26 – Eigenvalues Singlet S-P only, P part, level I, n=10, log scale

N	value	$-\lambda_i log_2 \lambda_i$
1	0.53861317995912	0.480808439
2	0.46119916549997	0.514946483
3	0.00006051969241	0.000848016
4	0.00000177192525	3.38548E-05
5	0.00000009830323	2.28832E-06
6	0.00000000075634	2.29173E-08
7	0.00000000008071	2.70608E-09
8	0.00000000003176	1.1076E-09
9	0.00000000000341	1.29898E-10
10	0.00000000000012	5.15064E-12
Sum	0.999533188	0.996639

Table 6.17 – Singlet, S-P shells, level II, part S eigenvalues

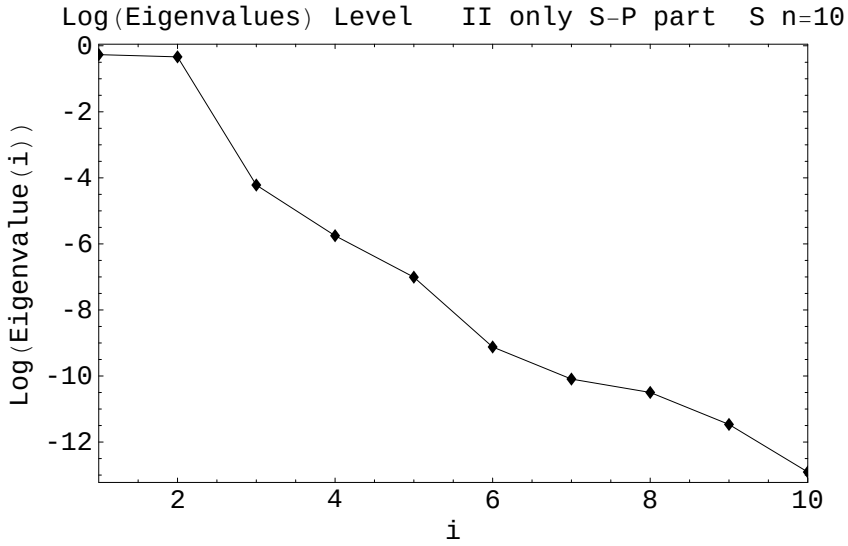

Figure 6.27 – Eigenvalues Singlet S-P only, S part, level II, n=10, log scale

N	value	$-\lambda_i log_2 \lambda_i$
1	0.00007538676917	0.001032447
2	0.00004808095928	0.000689682
3	0.00000164233203	3.15588E-05
4	0.00000013304918	3.03905E-06
5	0.00000001973873	5.05201E-07
6	0.00000000068913	2.09733E-08
7	0.00000000014130	4.62341E-09
8	0.00000000003520	1.22234E-09
9	0.00000000002795	9.79881E-10
10	0.00000000000563	2.10393E-10
Sum	0.000125264	0.001757259
Sum S+P	1.0	0.998396367

Table 6.18 – Singlet, S-P shells, level II, part P eigenvalues

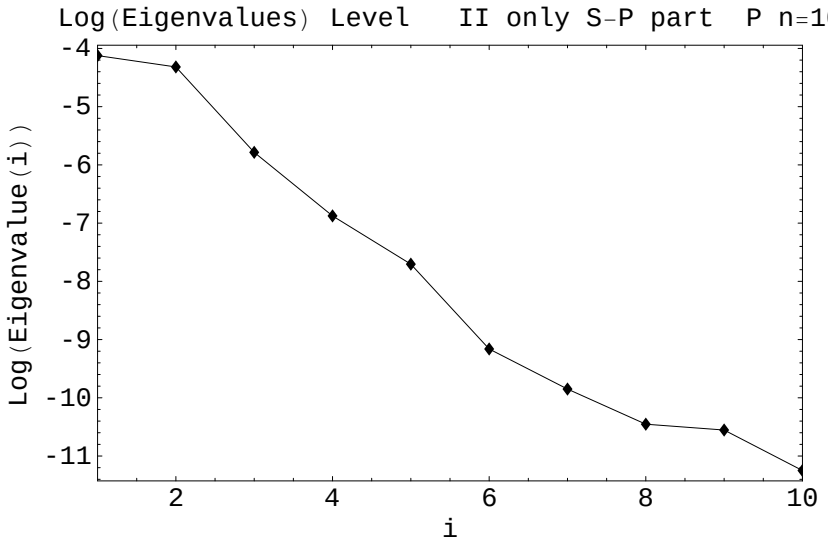

Figure 6.28 – Eigenvalues Singlet S-P only, P part, level II, n=10, log scale

N	value	$-\lambda_i log_2 \lambda_i$
1	0.52634345999714	0.487353817
2	0.47356285396475	0.510677004
3	0.00003154891359	0.000471721
4	0.00000105745533	2.09915E-05
5	0.00000001105074	2.92085E-07
6	0.00000000182748	5.30472E-08
7	0.00000000139155	4.09403E-08
8	0.00000000010593	3.51011E-09
9	0.00000000000465	1.75053E-10
10	0.00000000000021	8.84408E-12
Sum	0.999938935	0.998523923

Table 6.19 – Singlet, S-P shells, level III, part S eigenvalues

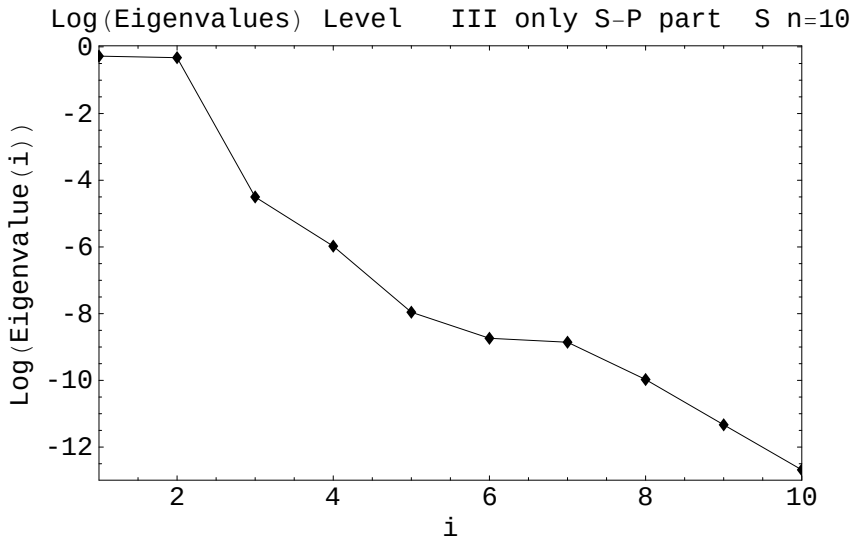

Figure 6.29 – Eigenvalues Singlet S-P only,S part, level III, n=10, log scale

N	value	$-\lambda_i log_2 \lambda_i$
1	0.00003777958387	0.000555059
2	0.00002247511010	0.000347045
3	0.00000073711972	1.50163E-05
4	0.00000006292539	1.50529E-06
5	0.00000000855280	2.29223E-07
6	0.00000000099196	2.96685E-08
7	0.00000000092249	2.76874E-08
8	0.00000000004546	1.56185E-09
9	0.00000000003043	1.06309E-09
10	0.00000000000633	2.35482E-10
Sum	6.10653E-05	0.000918915
Sum S+P	1.0	0.999442838

Table 6.20 – Singlet, S-P shells, level III, part P eigenvalues

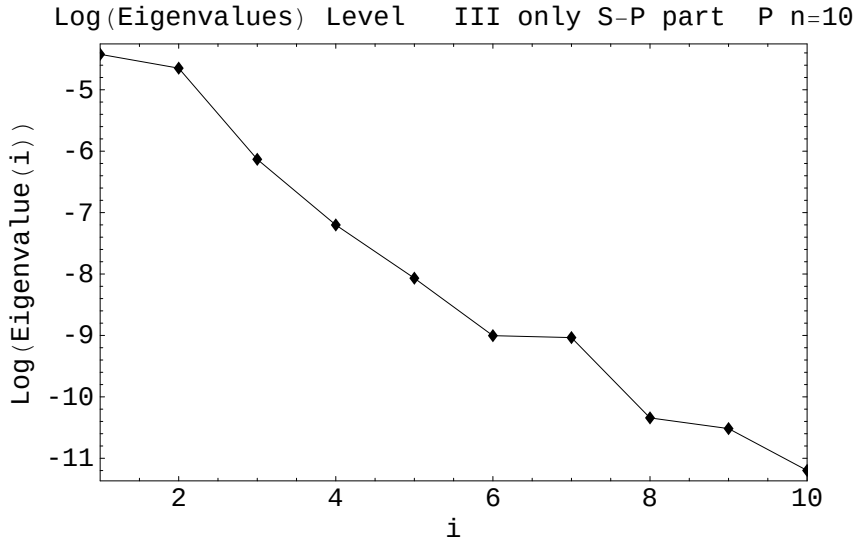

Figure 6.30 – Eigenvalues Singlet S-P only, P part, level III, n=10, log scale

N	value	$-\lambda_i log_2 \lambda_i$
1	0.991924498905	0.011603316486
2	0.003804264016	0.030579309135
3	0.000062939798	0.000878366916
4	0.000004047667	0.000072511835
5	0.000000503071	0.000010525629
6	0.000000098614	0.000002295099
7	0.000000016473	0.000000425920
8	0.000000003075	0.000000086955
9	0.000000000641	0.000000019579
10	0.000000000019	0.000000000684
Sum	0.995796372279	0.043146858239

Table 6.21 – Singlet, S-P-D shells, fundamental level, part S eigenvalues

6.5.3 Fundamental and excited states ^1S. S-P-D Shell

We limit ourselves to the fundamental and I excited level.

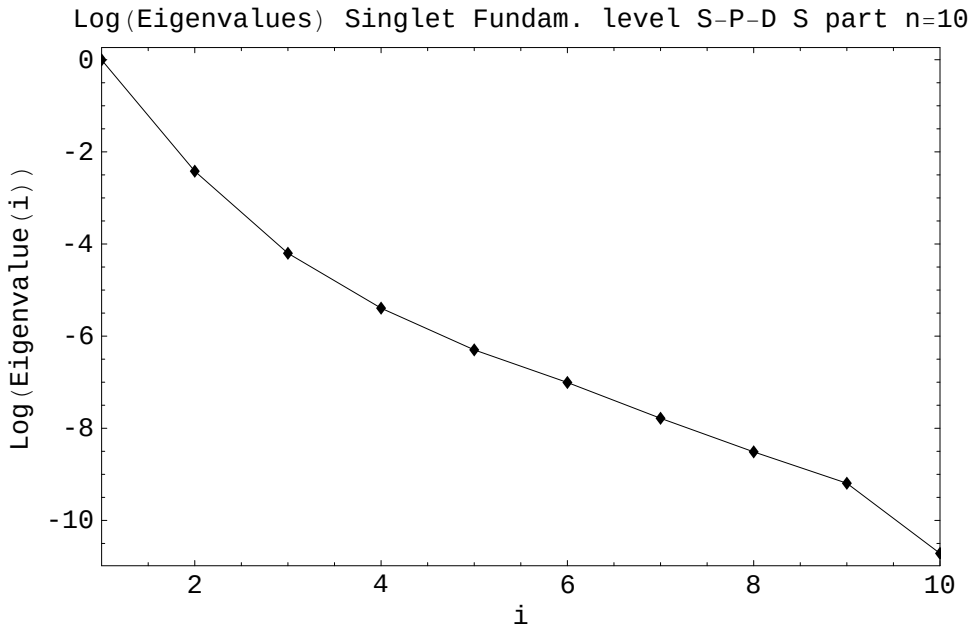

Figure 6.31 – Eigenvalues Singlet S-P-D, S part, fundamental level, n=10, log scale

N	value	$-\lambda_i log_2 \lambda_i$
1	0.003875223866	0.031046373945
2	0.000125262431	0.001623746650
3	0.000010190336	0.000168980630
4	0.000001434663	0.000027848040
5	0.000000291486	0.000006328173
6	0.000000075877	0.000001794615
7	0.000000022758	0.000000577798
8	0.000000007733	0.000000208382
9	0.000000001253	0.000000037040
10	0.000000000840	0.000000025316
Sum	0.004012511242	0.032875920589

Table 6.22 – Singlet, S-P-D shells, fundamental level, part P eigenvalues

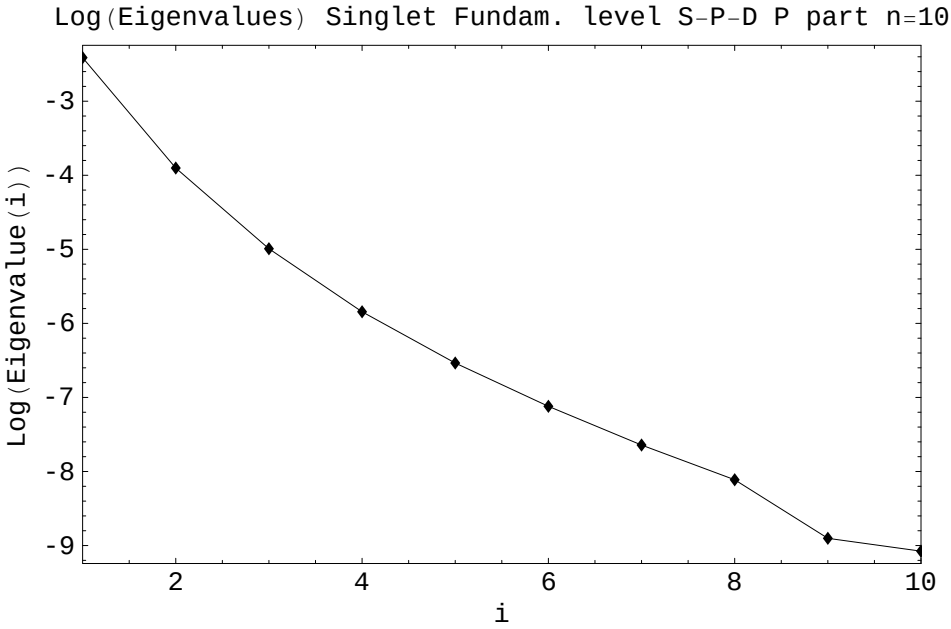

Figure 6.32 – Eigenvalues Singlet S-P-D, P part, fundamental level, n=10, log scale

N	value	$-\lambda_i log_2 \lambda_i$
1	0.000170798661	0.002137616249
2	0.000016943459	0.000268535398
3	0.000002610341	0.000048414860
4	0.000000548567	0.000011409000
5	0.000000144939	0.000003292736
6	0.000000045411	0.000001107678
7	0.000000015804	0.000000409564
8	0.000000006254	0.000000170439
9	0.000000002518	0.000000071913
10	0.000000000525	0.000000016178
Sum	0.000191116479	0.002471044015
Sum S+P+D	1.0	0.078493822844

Table 6.23 – Singlet, S-P-D shells, fundamental level, part D eigenvalues

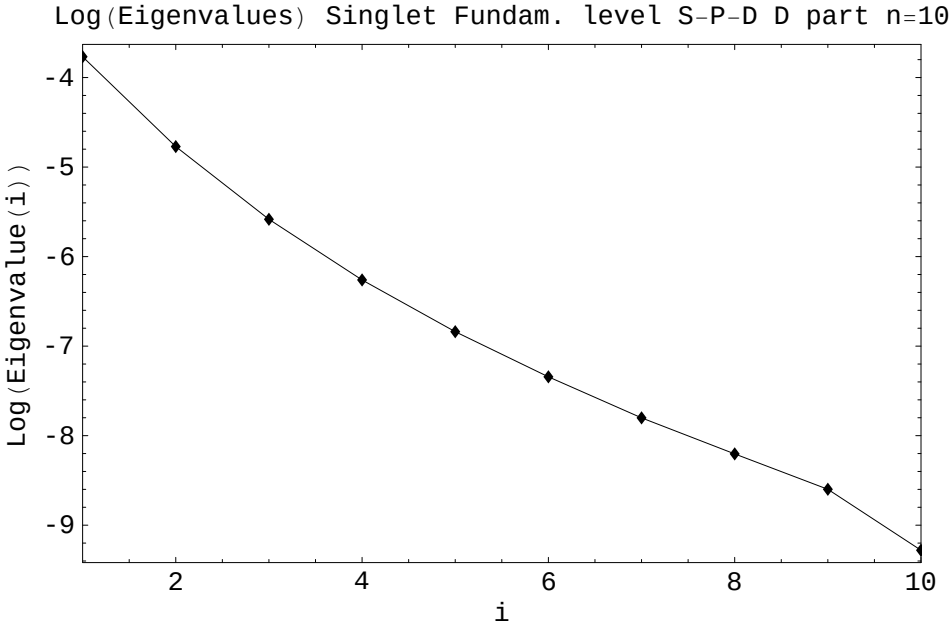

Figure 6.33 – Eigenvalues Singlet S-P-D, D part, fundamental level, n=10, log scale

N	value	$-\lambda_i log_2 \lambda_i$
1	0.576959454566	0.457793185408
2	0.422389174918	0.525179791175
3	0.000173911650	0.002172044819
4	0.000004607122	0.000081673687
5	0.000000290210	0.000006302314
6	0.000000028477	0.000000713801
7	0.000000000134	0.000000004382
8	0.000000000002	0.000000000072
9	0.000000000000	0.000000000004
10	0.000000000000	0.000000000000
Sum	0.999527467078	0.985233715661

Table 6.24 – Singlet, S-P-D shells, I level, part S eigenvalues

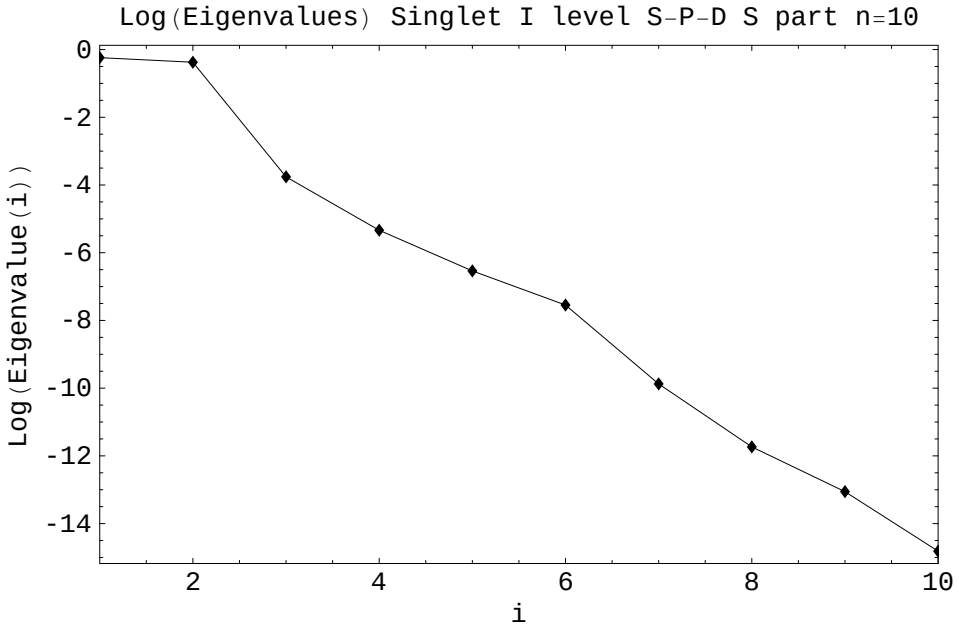

Figure 6.34 – Eigenvalues Singlet S-P-D, S part, I level, n=10, log scale

N	value	$-\lambda_i log_2 \lambda_i$
1	0.000254711264	0.003040959473
2	0.000189613397	0.002344503571
3	0.000007330251	0.000125037266
4	0.000000660714	0.000013564100
5	0.000000081492	0.000001919030
6	0.000000012569	0.000000329882
7	0.000000001679	0.000000048950
8	0.000000000187	0.000000006051
9	0.000000000065	0.000000002214
10	0.000000000004	0.000000000162
Sum	0.000452411622	0.005526370699

Table 6.25 – Singlet, S-P-D shells, I level, part P eigenvalues

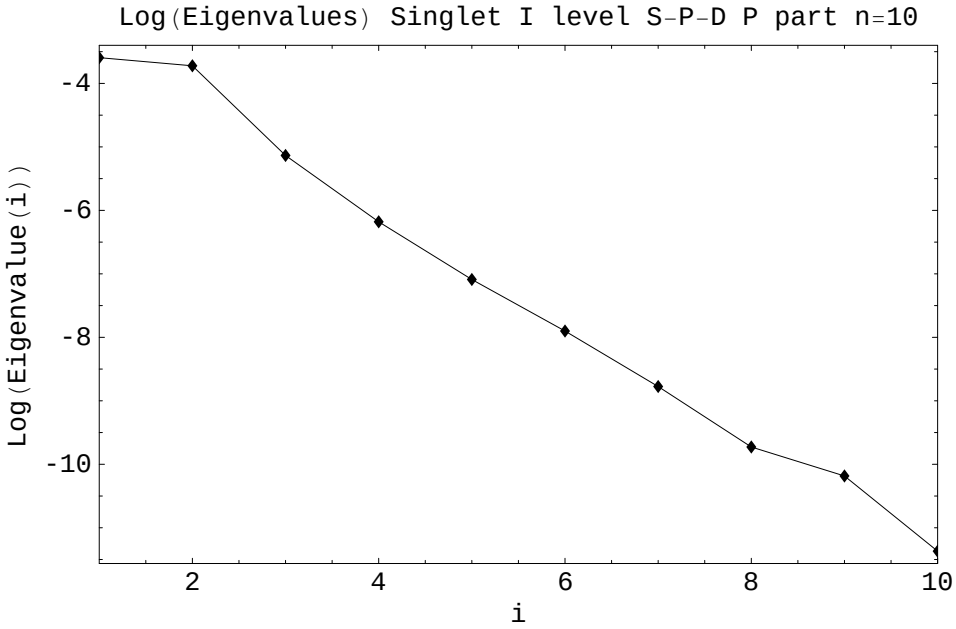

Figure 6.35 – Eigenvalues Singlet S-P-D, P part, I level, n=10, log scale

N	value	$-\lambda_i log_2 \lambda_i$
1	0.000013901230	0.000224288390
2	0.000005731921	0.000099807354
3	0.000000416728	0.000008832290
4	0.000000054984	0.000001326026
5	0.000000010777	0.000000285247
6	0.000000002528	0.000000072198
7	0.000000001576	0.000000046088
8	0.000000000846	0.000000025487
9	0.000000000704	0.000000021396
10	0.000000000006	0.000000000223
Sum	0.000020121299	0.000334704700
Sum S+P+D	1.0	0.991094791060

Table 6.26 – Singlet, S-P-D shells, I level, part D eigenvalues

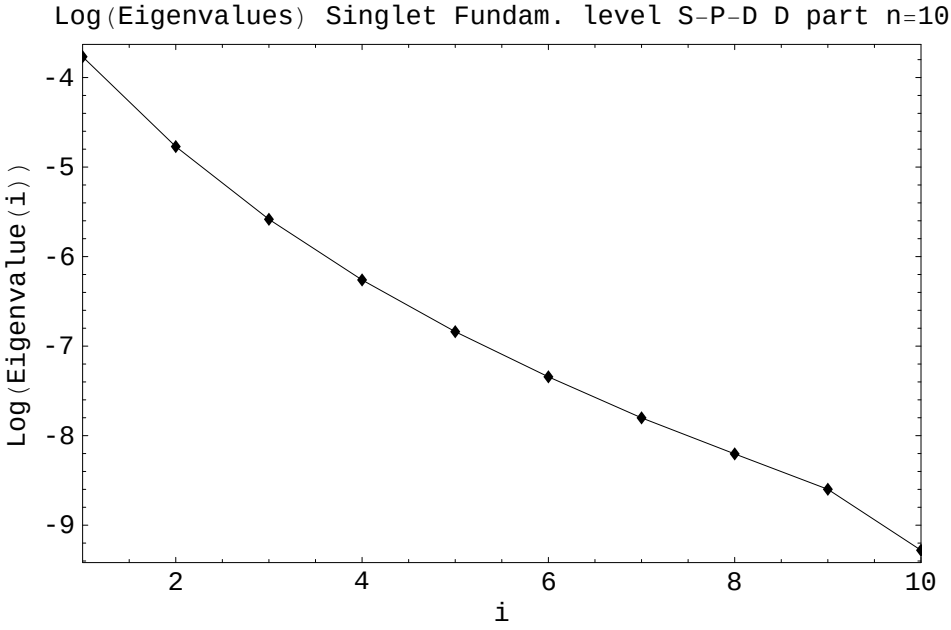

Figure 6.36 – Eigenvalues Singlet S-P-D, D part, I level, n=10, log scale

N	value	$-\lambda_i log_2 \lambda_i$
1	0.4999985023786676	0.500000663
2	0.4999985023786676	0.500000663
3	0.0000014897546265	2.88364E-05
4	0.0000014897546265	2.88364E-05
5	0.0000000078534824	2.11447E-07
6	0.0000000078534824	2.11447E-07
7	0.0000000000132234	4.77869E-10
8	0.0000000000132234	4.77869E-10
9	0.0000000000000000	
10	0.0000000000000000	
Sum	1	1.000059423

Table 6.27 – Triplet, S shell, level I eigenvalues

6.5.4 First excited states ^3S S-S Shell

In the tables 6.27, 6.28, 6.29, 6.32, we report the data for the first four ^3S states.

The tables show that the eigenvalues occur in pairs as expected. The first two eigenvalues are very near to 0.5, just $< 10^{-5}$ lower in all the cases that we considered.

The other eignevalues are lower by at least 6 orders of magnitude.

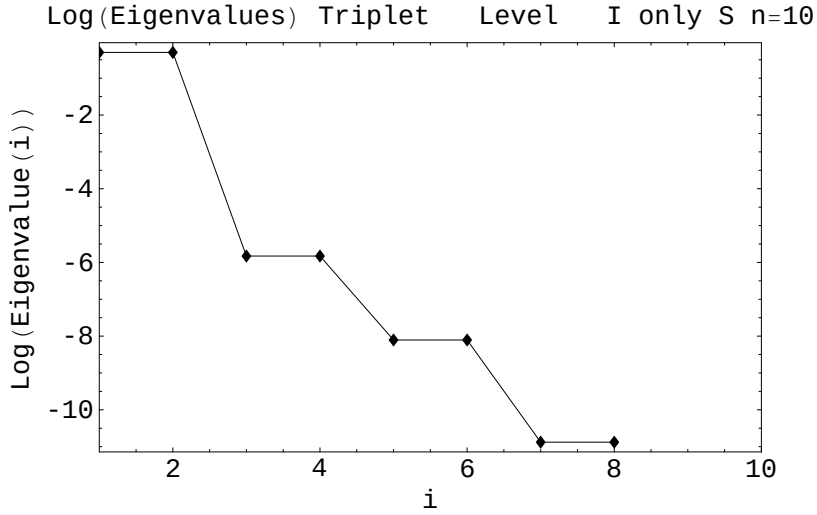

Figure 6.37 – Eigenvalues Triplet S only, level I, n=10, log scale

N	value	$-\lambda_i log_2 \lambda_i$
1	0.4999993605336170	0.500000283
2	0.4999993605336170	0.500000283
3	0.0000006371576348	1.31139E-05
4	0.0000006371576348	1.31139E-05
5	0.0000000022773766	6.53834E-08
6	0.0000000022773766	6.53834E-08
7	0.0000000000311200	1.08619E-09
8	0.0000000000311200	1.08619E-09
9	0.0000000000002516	1.05304E-11
10	0.0000000000002516	1.05304E-11
Sum	1	1.000026927

Table 6.28 – Triplet, S shell, level II eigenvalues

Table P Triplet S Shell, level II

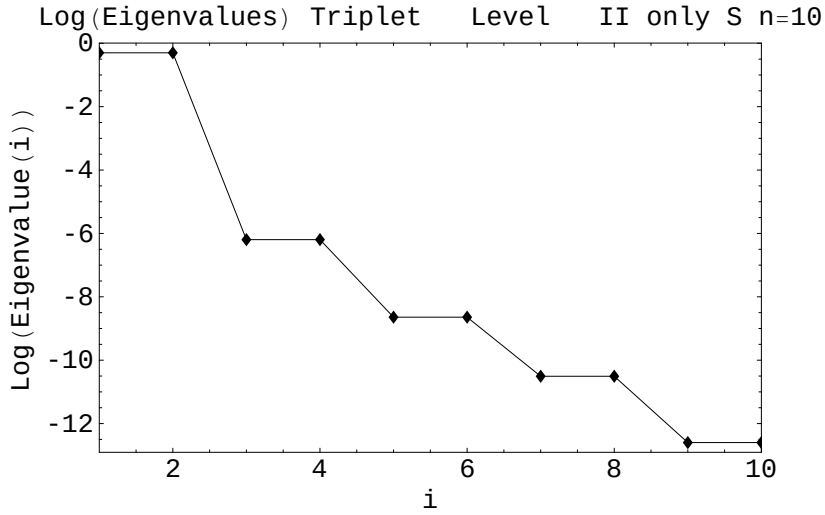

Figure 6.38 – Eigenvalues Triplet S only, level II, n=10, log scale

N	value	$-\lambda_i log_2 \lambda_i$
1	0.4999997147810680	0.500000126
2	0.4999997147810680	0.500000126
3	0.0000002813350571	6.12219E-06
4	0.0000002813350571	6.12219E-06
5	0.0000000036355178	1.01922E-07
6	0.0000000036355178	1.01922E-07
7	0.0000000002448654	7.81789E-09
8	0.0000000002448654	7.81789E-09
9	0.0000000000034916	1.32888E-10
10	0.0000000000034916	1.32888E-10
Sum	1	1.000012717

Table 6.29 – Triplet, S shell, level III eigenvalues

Table Q Triplet S Shell, level III

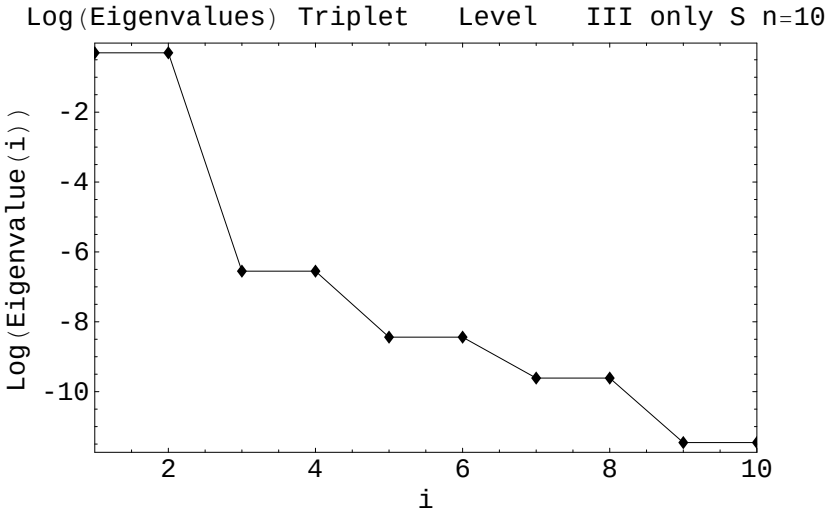

Figure 6.39 – Eigenvalues Triplet S only, level III, n=10, log scale

N	value	$-\lambda_i log_2 \lambda_i$
1	0.4999996506520183	0.500000155
2	0.4999996506520183	0.500000155
3	0.0000003390204608	7.28627E-06
4	0.0000003390204608	7.28627E-06
5	0.0000000101265390	2.68933E-07
6	0.0000000101265390	2.68933E-07
7	0.0000000001855780	5.99923E-09
8	0.0000000001855780	5.99923E-09
9	0.0000000000154039	5.53276E-10
10	0.0000000000154039	5.53276E-10
Sum	1	1.000015433

Table 6.30 – Triplet, S shell, level IV eigenvalues

Table R Triplet S Shell, level IV

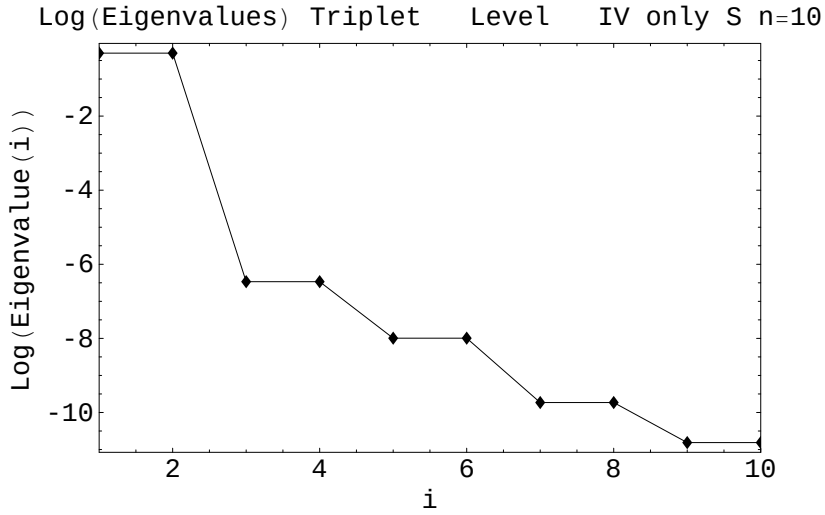

Figure 6.40 – Eigenvalues Triplet S only, level IV, n=10, log scale

N	value	$-\lambda_i log_2 \lambda_i$
1	0.499814480999730000	0.500082078681601
2	0.499814480999730000	0.500082078681601
3	0.000001020511748924	0.000020310506261
4	0.000001020511748924	0.000020310506261
5	0.000000004493259714	0.000000124596251
6	0.000000004493259714	0.000000124596251
7	0.000000000003420622	0.000000000130288
8	0.000000000003420622	0.000000000130288
9	0.000000000000000025	0.000000000000001
10	0.000000000000000025	0.000000000000001
Sum	0.9996310	1.0002050

Table 6.31 – Triplet, S-P shell, level I eigenvalues, S part

6.5.5 First excited state ^3S S-P Shell

We limit ourselves to the I excited level.

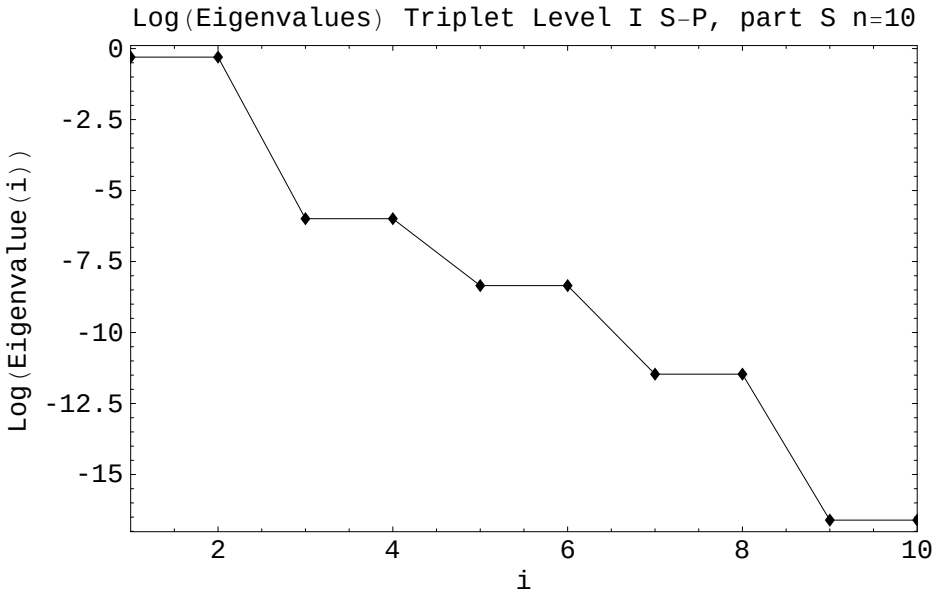

Figure 6.41 – Eigenvalues Triplet S-P only, S part, level I, n=10, log scale

N	value	$-\lambda_i log_2 \lambda_i$
1	0.000184216695698561	0.002285449168676
2	0.000184216695698561	0.002285449168676
3	0.000000271365762596	0.000005919371379
4	0.000000271365762596	0.000005919371379
5	0.000000005809870612	0.000000158951360
6	0.000000005809870612	0.000000158951360
7	0.000000000120017351	0.000000003955296
8	0.000000000120017351	0.000000003955296
9	0.000000000000491529	0.000000000020098
10	0.000000000000491529	0.000000000020098
Sum	0.0003690	0.0045831
Sum S+P	1	1.0047881

Table 6.32 – Triplet, S-P shell, P part, level I eigenvalues

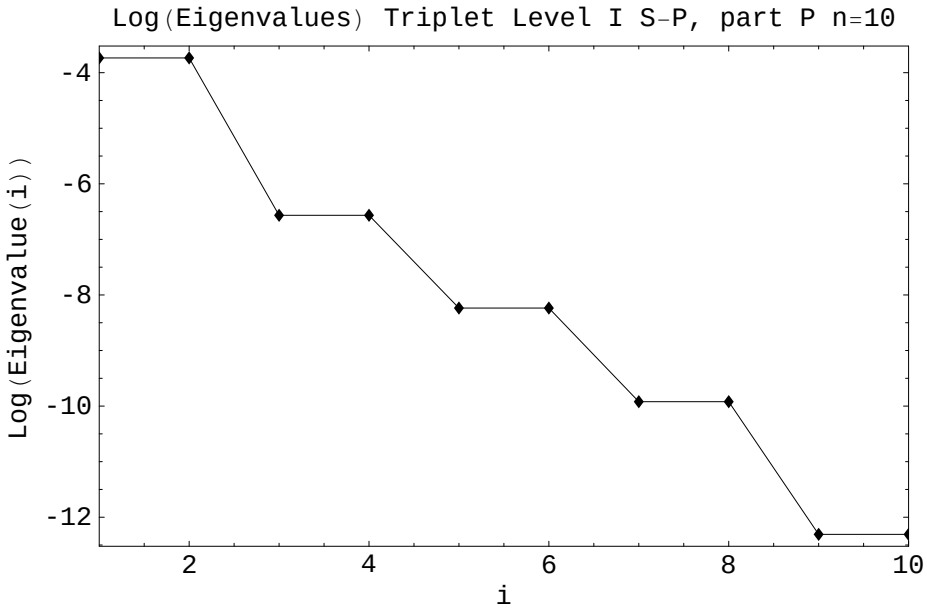

Figure 6.42 – Eigenvalues Triplet S-P only, P part level I, n=10, log scale

6.6 Sensitivity of the Configurations Interaction results to the Fock space dimension

6.6.1 ^1S states

For the singlet states ^1S, denoting n_s, n_p, n_d the single particle state dimensions, we have for the dimension of the matrices that must be diagonalized:

$n_{tot} = n_s(n_s+1)/2 \; + \; n_p(n_p+1)/2 \; + \; n_d(n_d+1)/2$

Taking $n_s = n_p = n_d$ it results that, especially for highly excited states (we studied up to the VI level) with $n_s = n_p = n_d = 20$ we have

$n_{tot} = 630$

Although it is possible to diagonalize matrices of this dimension, we investigated if it is possible to use smaller matrices for shells P and D, accelerating the computations.

We reconfirm that our aim is not the study of Helium itself, but the applicability of our method to more complex cases. Therefore it is mandatory to check if it is necessary to use high dimension matrices or not.

Singlet level III S-P

We studied in detail only some cases to estimate the general behaviour.

We chose two cases, $n_s = 10$ and $n_s = 15$ and studied the convergence vs. $n_p \leq n_s$ in both cases.

Singlet, level III $n_s = 10$

Energy: we note a slight improvement increasing n_p, but not enough to justify high values.

nddp	energy	von Neumann	linear
2	855	0.99875	0.49868
3	851	0.99871	0.49867
4	839	0.99883	0.49866
5	828	0.99905	0.49867
6	820	0.99923	0.49868
7	816	0.99934	0.49869
8	815	0.99939	0.49869
9	814	0.99941	0.49869
10	814	0.99942	0.49869

Table 6.33 – Singlet, level III S-P, dimension for S Shell=10

von Neumann entropy: it must be noted that the significant digits are those "beyond" the initial 9's.

Therefore we need at least $n_p = 8$

This, with respect to $n_p = n_s$, reduces the dimension from 110 to 91, with a small gain.

Linear entropy

From table A we note that linear entropy is pratically constant starting with $n_p = 2$.

Therefore, if one seeks only linear entropy, the matrix dimension can be reduced from 110 to 55+3=58.

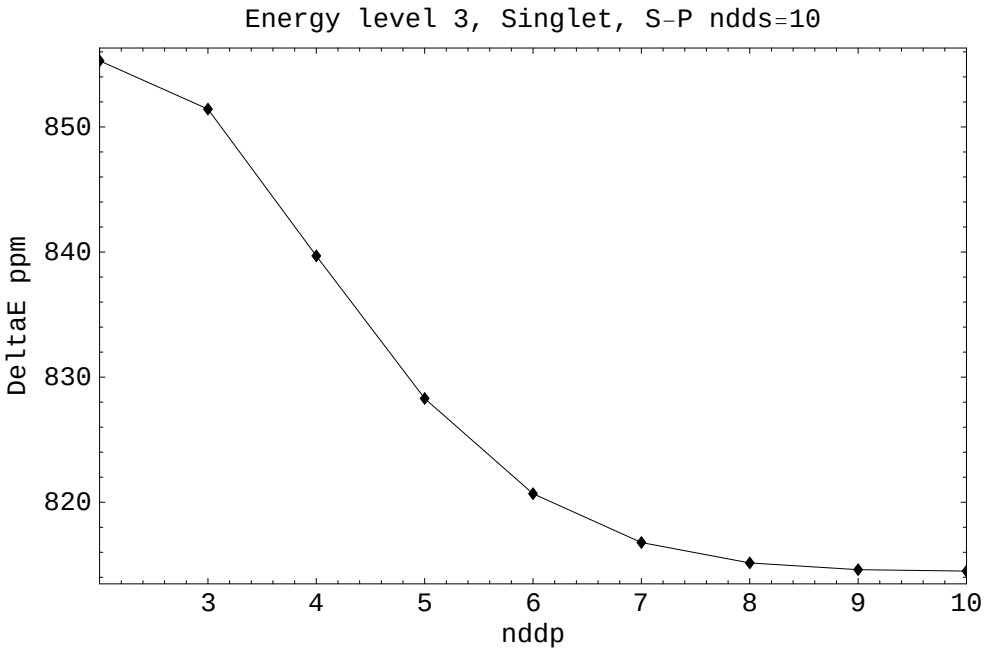

Figure 6.43 – Energy error, level 3, singlet, dimension for S Shell=10 and dimension for P Shell from 2 to 10

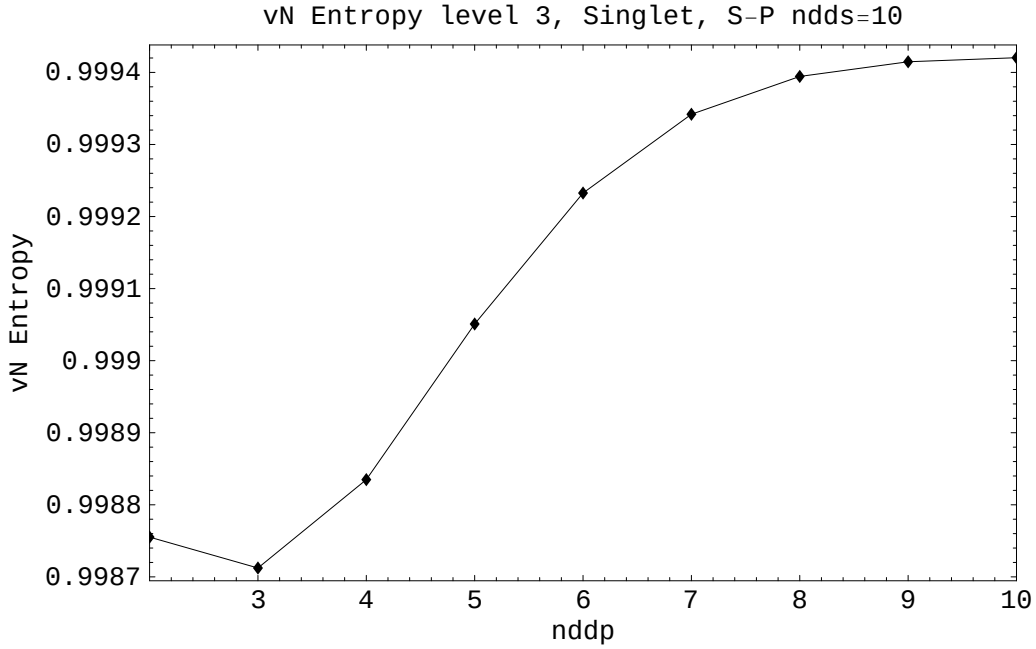

Figure 6.44 – von Neumann entropy, level 3, singlet, dimension for S Shell=10 and dimension for P Shell from 2 to 10

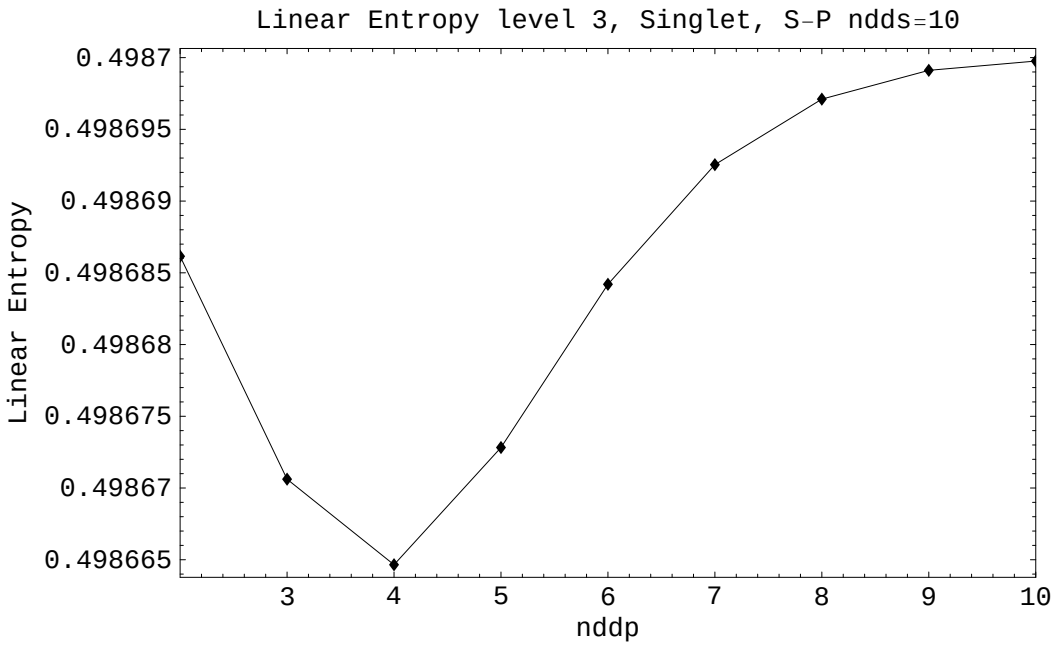

Figure 6.45 – Linear entropy, level 3, singlet, dimension for S Shell=10 and dimension for P Shell from 2 to 10

nddp	energy	von Neumann	linear
2	52.2	0.998969	0.498903
3	48.8	0.998932	0.498889
4	39.0	0.999037	0.498884
5	29.9	0.999214	0.498889
6	23.8	0.999361	0.498898
7	20.6	0.999453	0.498904
8	19.1	0.999498	0.498908
9	18.6	0.999517	0.498910
10	18.5	0.999522	0.498910
11	18.5	0.999522	0.498910
12	18.5	0.999522	0.498910
13	18.4	0.999522	0.498910
14	18.3	0.999524	0.498910
15	18.1	0.999526	0.498910

Table 6.34 – Singlet, level III S-P, dimension for S Shell=15

Singlet, level III $n_s = 15$

Energy: the improvement with n_p saturates starting from $n_p \approx 7$.

von Neumann entropy: with the same criterium as above, it suffices $n_p = 9$. Then we can decrease the dimension from 240 to 120-45=165, with a significan gain.

Linear entropy: with the same criterium as above, one can use $n_p \approx 4$ lowering the dimension from 240 to 120+6=126, significantly less.

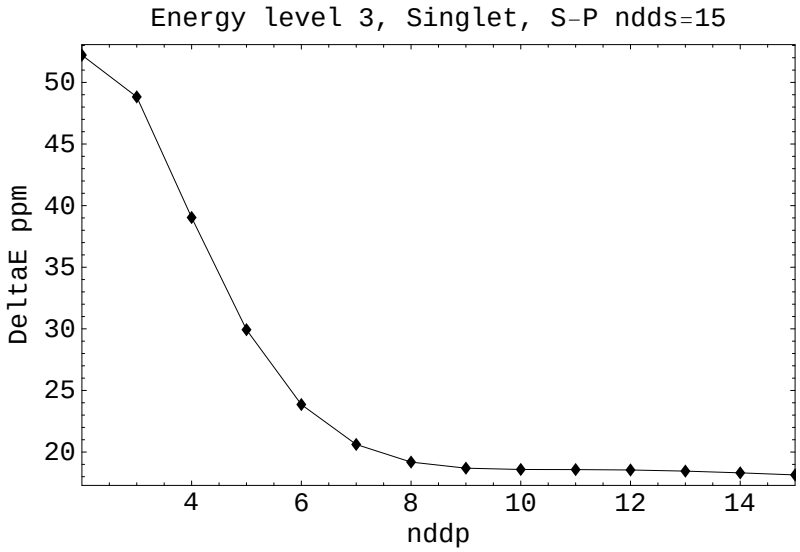

Figure 6.46 – Energy error, level 3, singlet, dimension for S Shell=15 and dimension for P Shell from 2 to 15

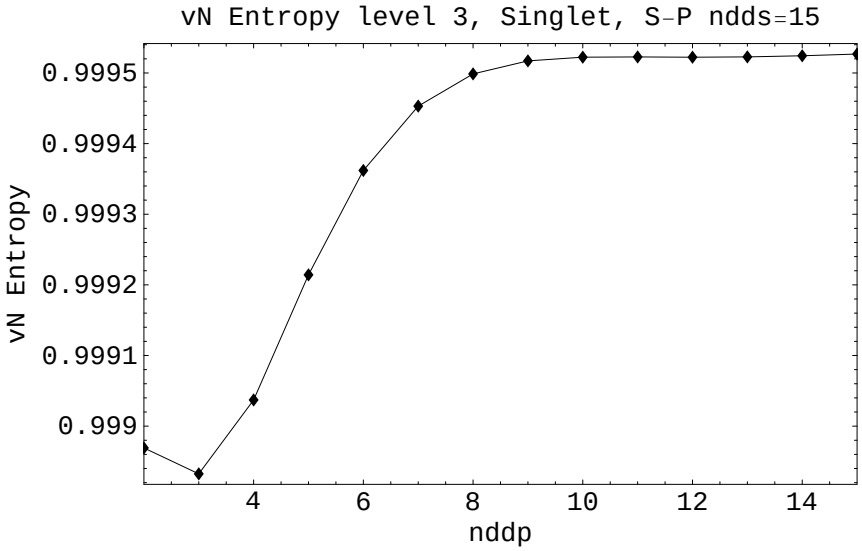

Figure 6.47 – von Neumann entropy, level 3, singlet, dimension for S Shell=15 and dimension for P Shell from 2 to 15

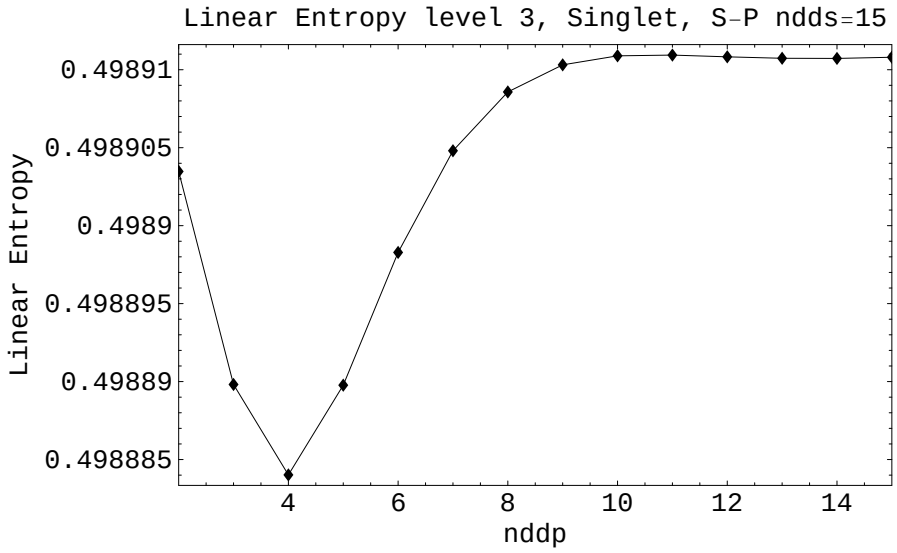

Figure 6.48 – Linear entropy, level 3, singlet, dimension for S Shell=15 and dimension for P Shell from 2 to 15

nddp	energy	von Neumann	linear
2	13980	0.998511	0.498339
3	13973	0.998465	0.498318
4	13957	0.998657	0.498316
5	13941	0.998960	0.498331
6	13930	0.999220	0.498349
7	13924	0.999382	0.498363
8	13922	0.999455	0.498370
9	13922	0.999476	0.498372
10	13922	0.999477	0.498372

Table 6.35 – Singlet, level V S-P, dimension for S Shell=10

Singlet level V S-P

Saturation n_p values: energy ≈ 7, von Neumann entropy ≈ 6, linear entropy ≈ 2.

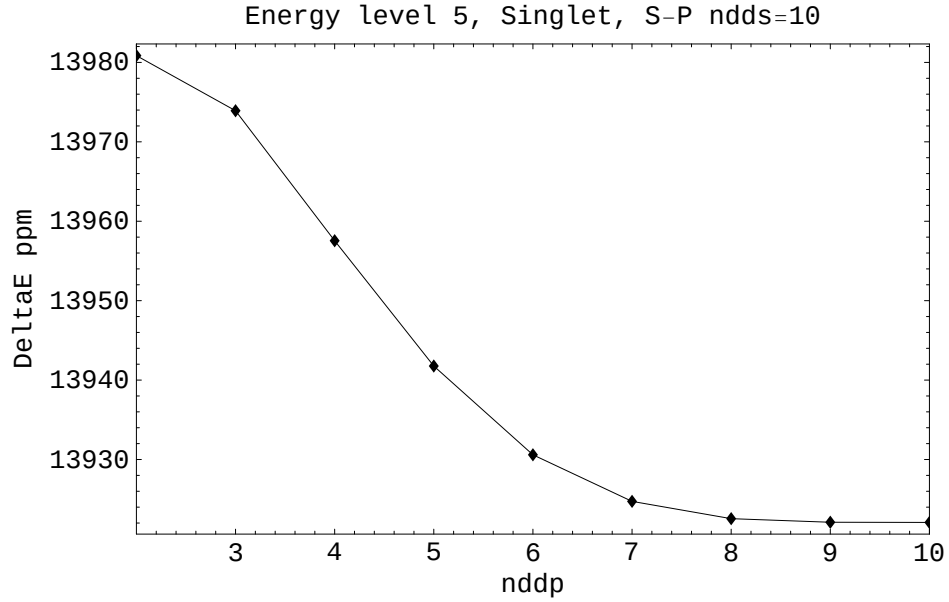

Figure 6.49 – Energy, level 5, singlet, dimension for S Shell=10 and dimension for P Shell from 2 to 10

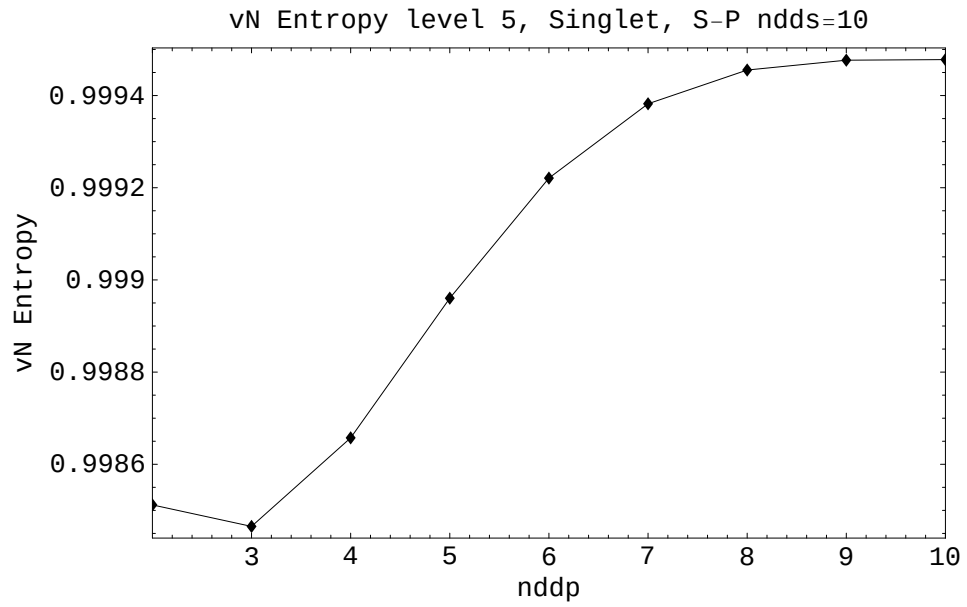

Figure 6.50 – von Neumann entropy, level 5, singlet, dimension for S Shell=10 and dimension for P Shell from 2 to 10

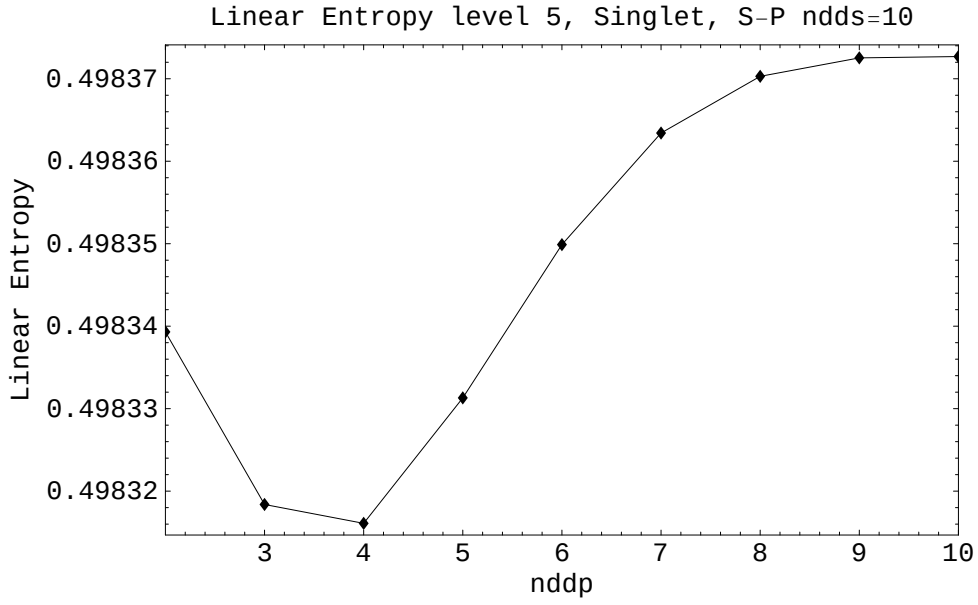

Figure 6.51 – Linear entropy, level 5, singlet, dimension for S Shell=10 and dimension for P Shell from 2 to 10

nddp	energy	von Neumann	linear
2	626.1	0.999623	0.499567
3	624.5	0.999607	0.499562
4	620.5	0.999657	0.499560
5	617.0	0.999734	0.499563
6	614.6	0.999798	0.499567
7	613.3	0.999837	0.499569
8	612.8	0.999856	0.499571
9	612.7	0.999863	0.499572
10	612.6	0.999864	0.499572
11	612.6	0.999864	0.499572
12	612.6	0.999864	0.499572
13	612.5	0.999865	0.499572
14	612.5	0.999866	0.499572
15	612.4	0.999867	0.499572

Table 6.36 – Singlet, level V S-P, dimension for S Shell=15

Singlet, level V dimension for S Shell = 15

Saturation n_p values: energy ≈ 7, von Neumann entropy ≈ 7, linear entropy ≈ 2.

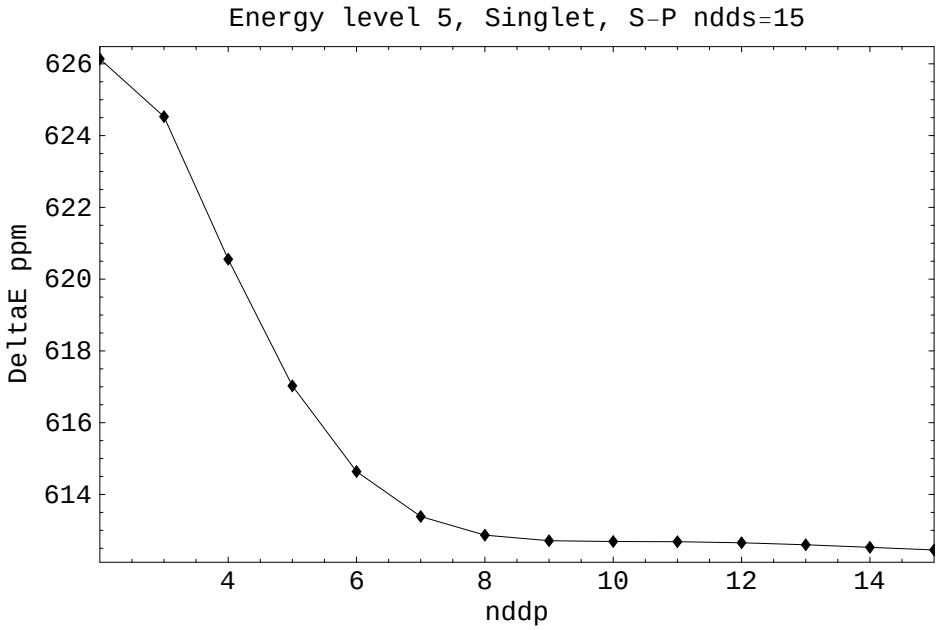

Figure 6.52 – Energy error, level 5, singlet, dimension for S Shell=15 and dimension for P Shell from 2 to 15

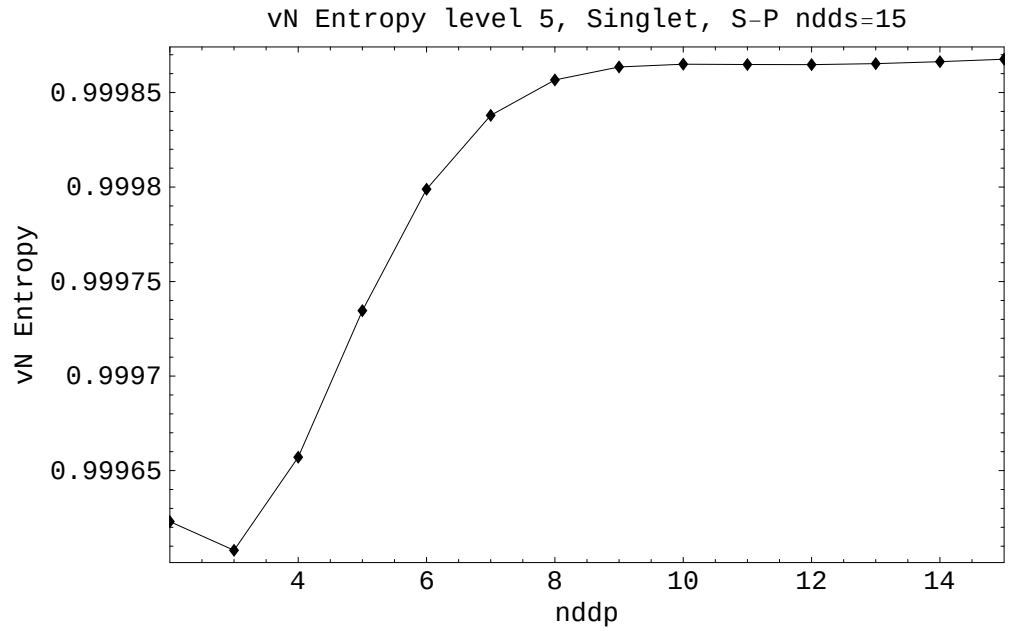

Figure 6.53 – von Neumann entropy, level 5, singlet, dimension for S Shell=15 and dimension for P Shell from 2 to 15

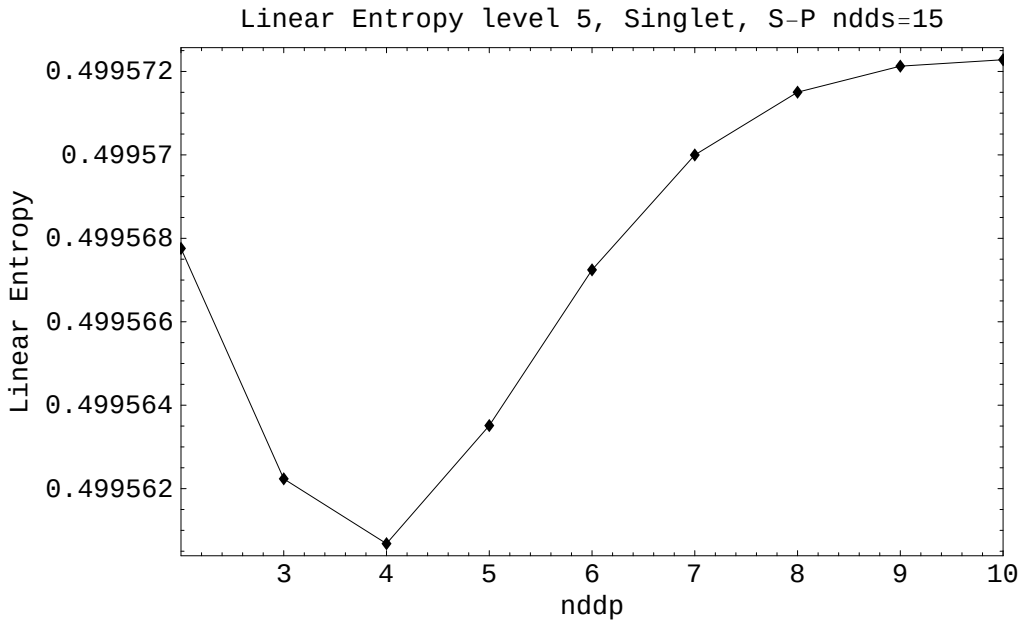

Figure 6.54 – Linear entropy, level 5, singlet, dimension for S Shell=15 and dimension for P Shell from 2 to 15

nddd	energy	von Neumann	linear
2	12.263927261	0.999556687	0.498919317
3	11.950255372	0.999560301	0.498920621
4	11.904629492	0.999559510	0.498920367
5	11.610134410	0.999558376	0.498919640
6	11.129510955	0.999559026	0.498919018
7	10.628428324	0.999561356	0.498918670
8	10.207898520	0.999564508	0.498918558
9	9.898319062	0.999567644	0.498918584
10	9.689921770	0.999570269	0.498918668

Table 6.37 – Singlet, level III S-P-D, dimension for S Shell=15, dimension for P Shell=10

Singlet level III S-P-D

dimension for S Shell = 15, dimension for P Shell = 10

Saturation n_d values: energy ≈ 9, von Neumann entropy ≈ 2, linear entropy ≈ 2.

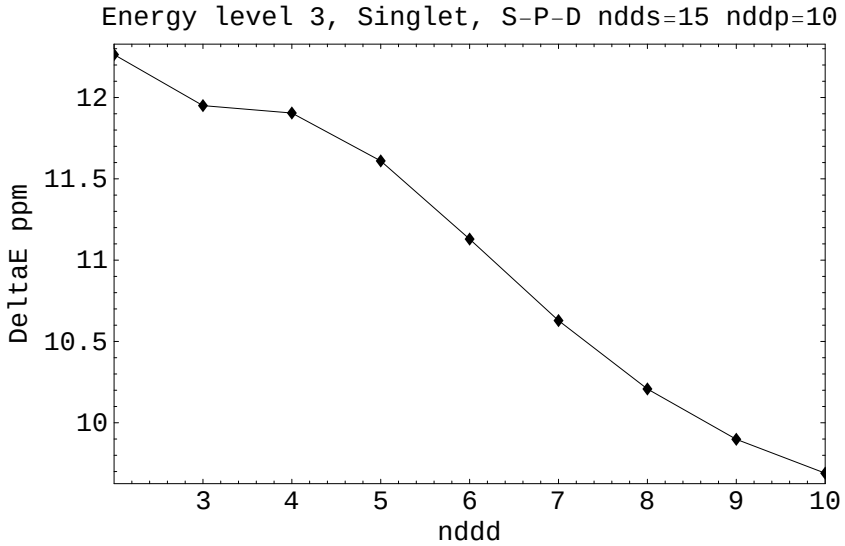

Figure 6.55 – Energy error, level 3, singlet, dimension for S Shell=15 dimension for P Shell=10 and dimension for D Shell from 2 to 10

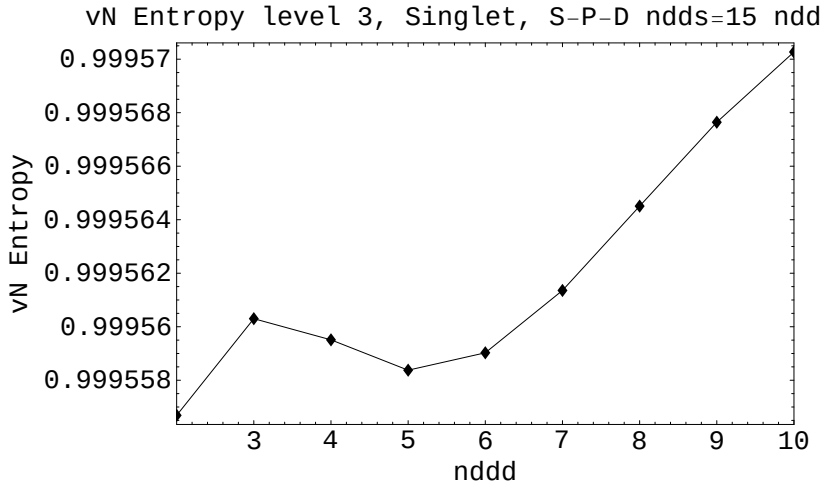

Figure 6.56 – von Neumann entropy, level 3, singlet, dimension for S Shell=15 dimension for P Shell=10 and dimension for D Shell from 2 to 10

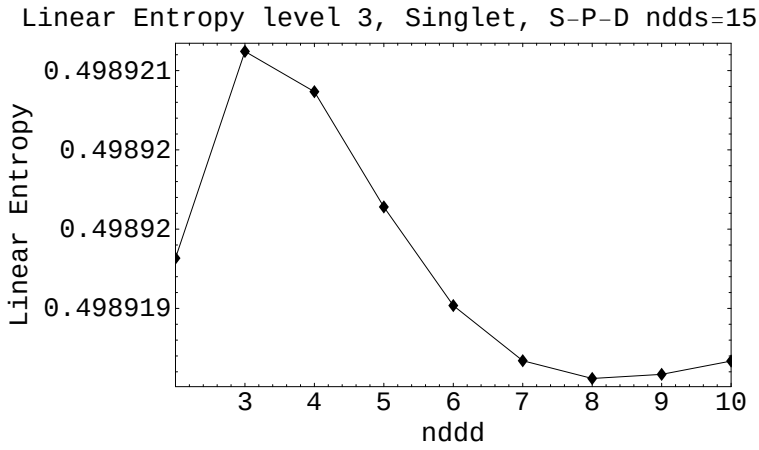

Figure 6.57 – Linear entropy, level 3, singlet, dimension for S Shell=15 dimension for P Shell=10 and dimension for D Shell from 2 to 10

nddd	energy	von Neumann	linear
2	13.0	0.999550	0.498918
3	12.7	0.999553	0.498919
4	12.7	0.999553	0.498919
5	12.4	0.999551	0.498918
6	11.9	0.999552	0.498918
7	11.4	0.999554	0.498917

Table 6.38 – Singlet, level III S-P-D, dimension for S Shell=15, dimension for P Shell=7

Singlet level III S-P-D, dimension for S Shell=15, dimension for P Shell=7

Saturation n_d values: energy > 7, von Neumann entropy ≈ 2, linear entropy ≈ 2.

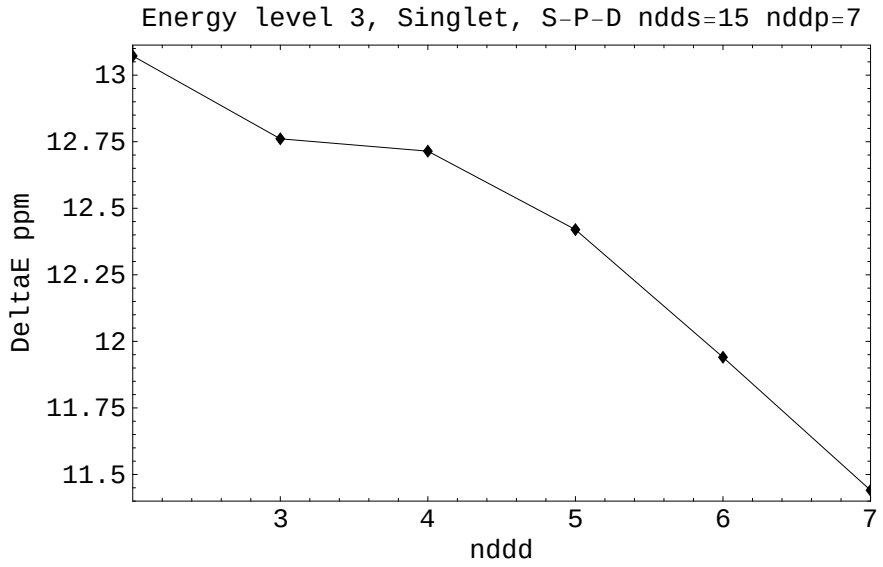

Figure 6.58 – Energy error, level 3, singlet, dimension for S Shell=15 dimension for P Shell=7 and dimension for D Shell from 2 to 7

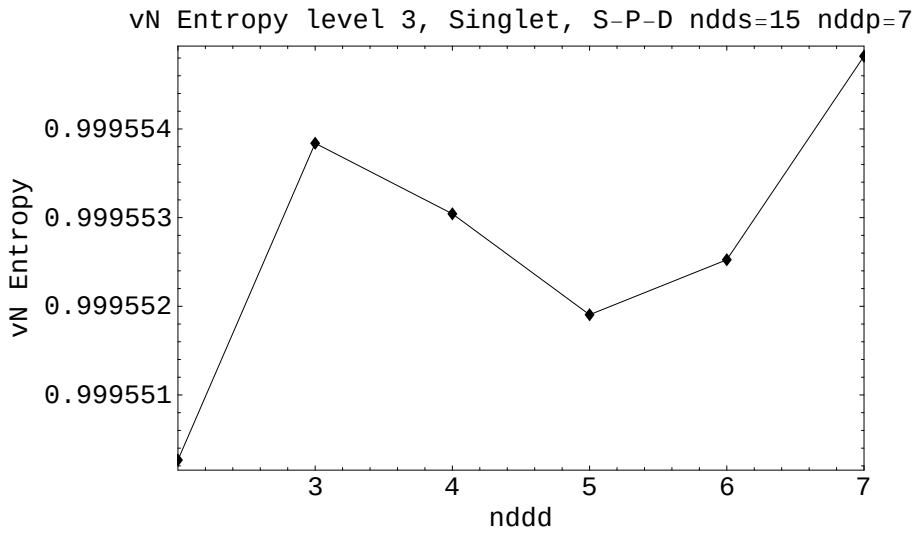

Figure 6.59 – von Neumann entropy, level 3, singlet, dimension for S Shell=15 dimension for P Shell=7 and dimension for D Shell from 2 to 7

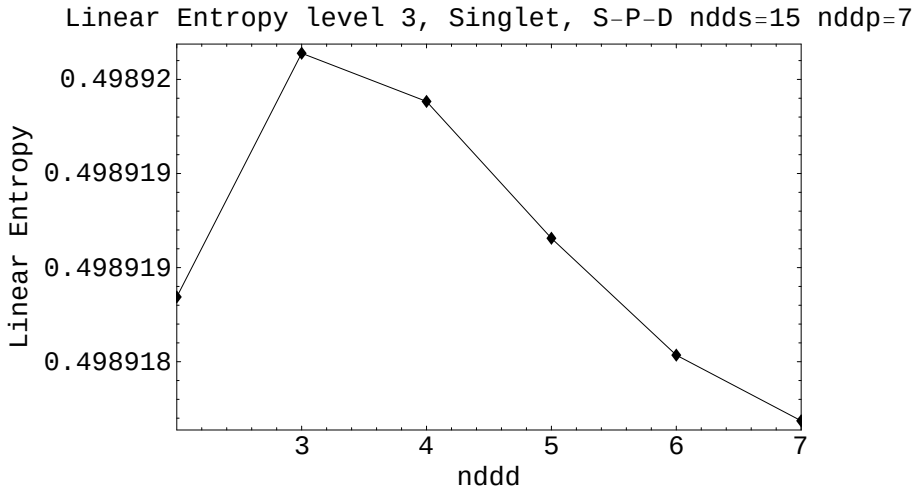

Figure 6.60 – Linear entropy, level 3, singlet, dimension for S Shell=15 dimension for P Shell=7 and dimension for D Shell from 2 to 7

nddd	energy	von Neumann	linear
2	612.6	0.999798	0.499570
3	612.5	0.999800	0.499570
4	612.4	0.999799	0.499570
5	612.3	0.999799	0.499570
6	612.1	0.999799	0.499569
7	611.9	0.999801	0.499569
8	611.7	0.999802	0.499569
9	611.6	0.999804	0.499569
10	611.5	0.999805	0.499570

Table 6.39 – Singlet, level V S-P-D, dimension for S Shell=15, dimension for P Shell=10

Singlet level V S-P-D

dimension for S Shell = 15, dimension for P Shell = 10

Saturation n_d values: energy ≈ 7, von Neumann entropy ≈ 2, linear entropy ≈ 2.

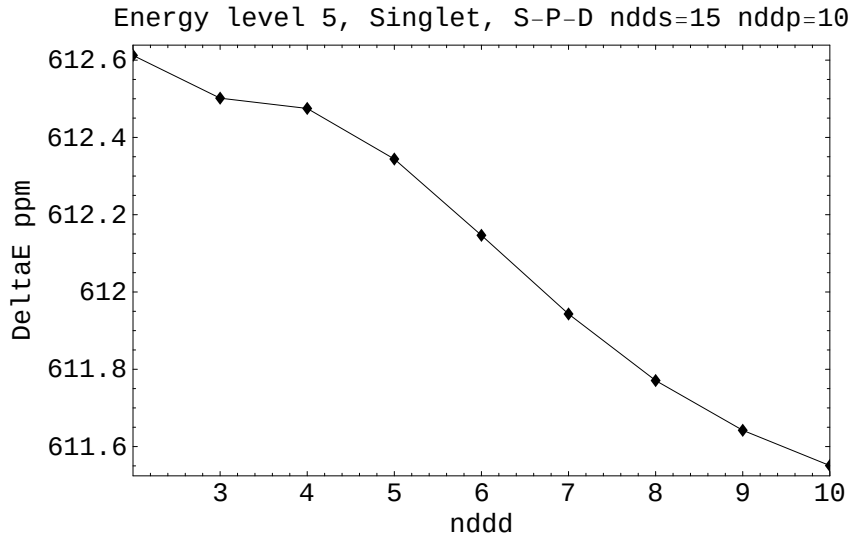

Figure 6.61 – Energy error, level 5, singlet, dimension for S Shell=15 dimension for P Shell=10 and dimension for D Shell from 2 to 10

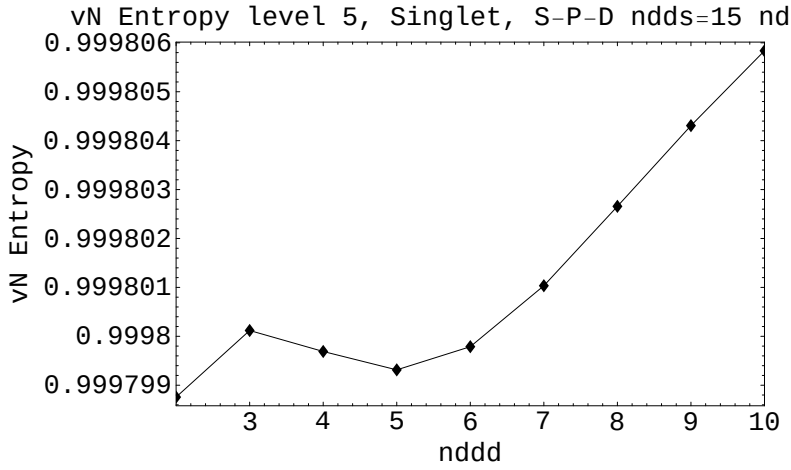

Figure 6.62 – von Neumann entropy, level 5, singlet,dimension for S Shell=15 dimension for P Shell=10 and dimension for D Shell from 2 to 10

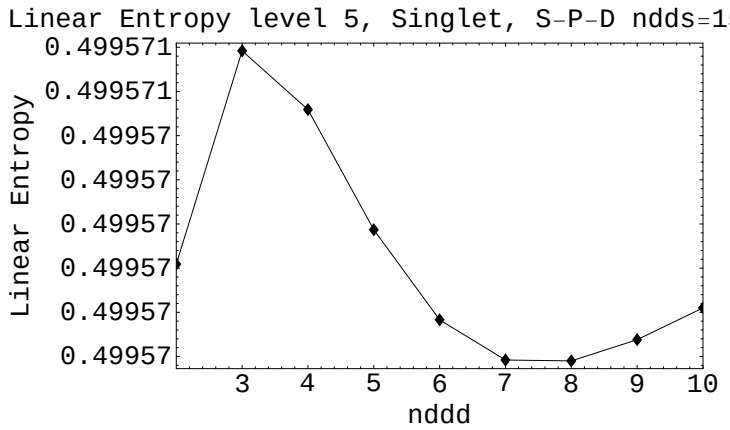

Figure 6.63 – Linear entropy, level 5, singlet, dimension for S Shell=15 dimension for P Shell=10 and dimension for D Shell from 2 to 10

nddd	energy	von Neumann	linear
2	610.4	0.999871	0.499575
3	610.3	0.999873	0.499575
4	610.3	0.999872	0.499575
5	610.1	0.999872	0.499575
6	609.9	0.999872	0.499575
7	609.8	0.999873	0.499574

Table 6.40 – Singlet, level V S-P-D, dimension for S Shell=15, dimension for P Shell=7

Singlet level V S-P-D, dimension for S Shell = 15, dimension for P Shell = 7

Saturation n_d values: energy ≈ 6, von Neumann entropy ≈ 2, linear entropy ≈ 2.

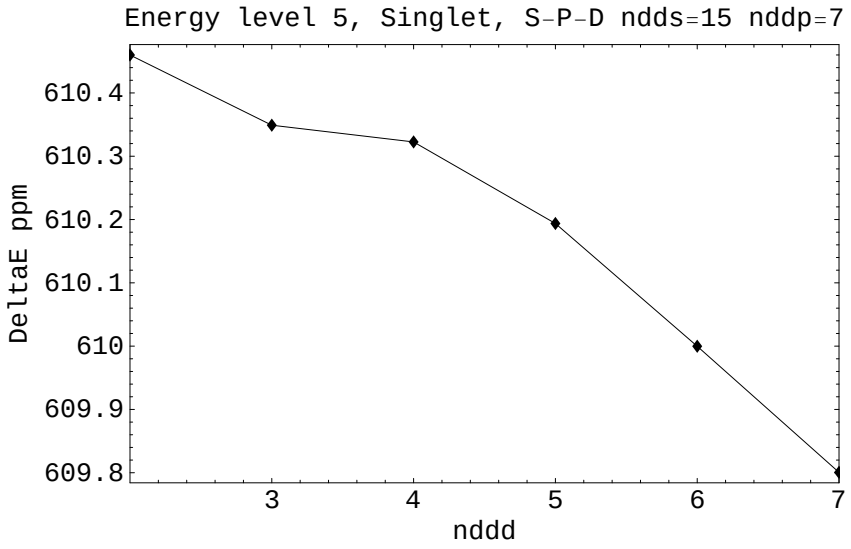

Figure 6.64 – Energy error, level 5, singlet, dimension for S Shell=15 dimension for P Shell=7 and dimension for D Shell from 2 to 7

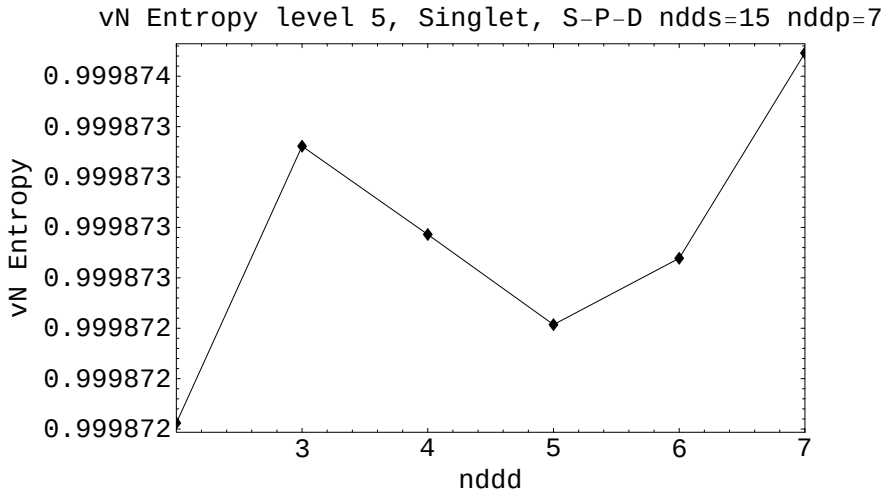

Figure 6.65 – von Neumann entropy, level 5, singlet, dimension for S Shell=15 dimension for P Shell=7 and dimension for D Shell from 2 to 7

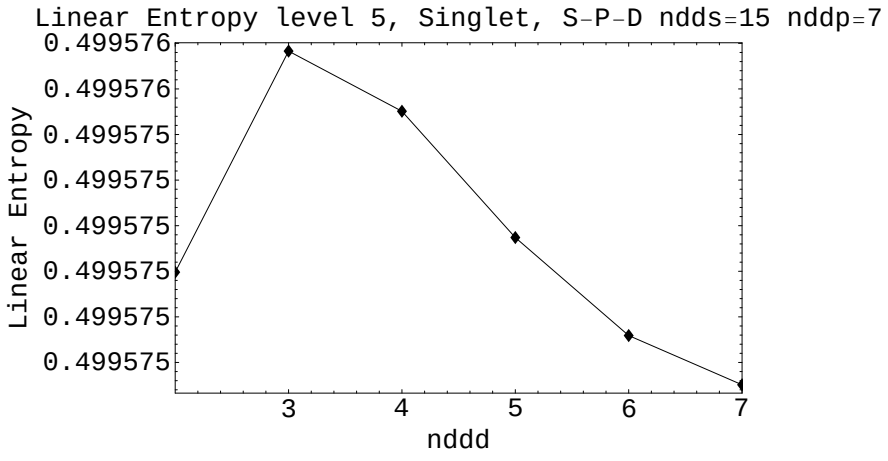

Figure 6.66 – Linear entropy, level 5, singlet, dimension for S Shell=15 dimension for P Shell=7 and dimension for D Shell from 2 to 7

nddp	energy	von Neumann	linear
2	568.572747101	1.007959855	0.500023220
3	564.328634484	1.000484467	0.500029153
4	563.914055196	1.000478124	0.500028734
5	563.496019459	1.000483267	0.500029052
6	562.968913882	1.000487109	0.500029301
7	562.926050640	1.000487660	0.500029334
8	562.882999140	1.000491090	0.500029563
9	562.644119204	1.000493406	0.500029714
10	562.615142611	1.000493940	0.500029748

Table 6.41 – Triplet, level III S-P, dimension for S Shell=10

6.6.2 States ^3S; shell S-P

Triplet level III S-P

dimension for S Shell = 10

Saturation n_p values: energy ≈ 6, von Neumann entropy ≈ 8, linear entropy ≈ 5.

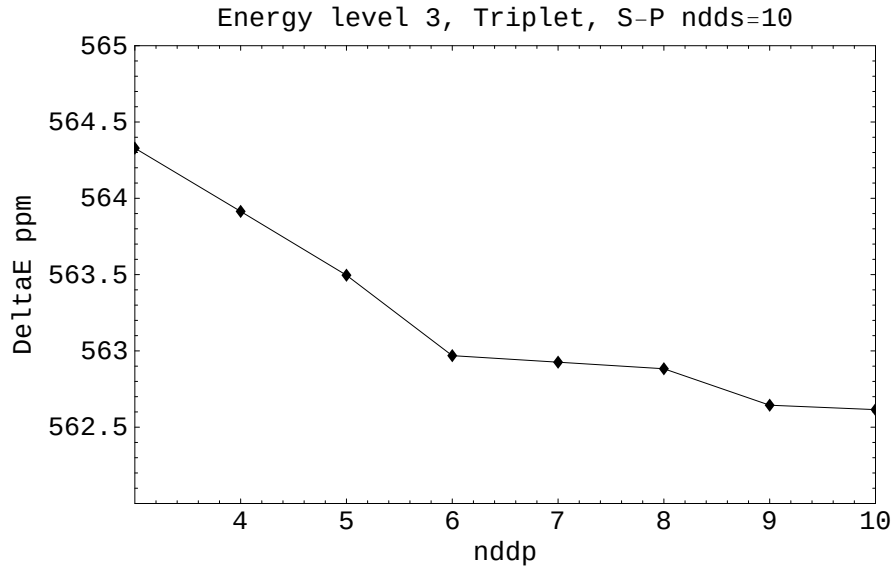

Figure 6.67 – Energy error, level 3, triplet, dimension for S Shell=10 and dimension for P Shell from 2 to 10

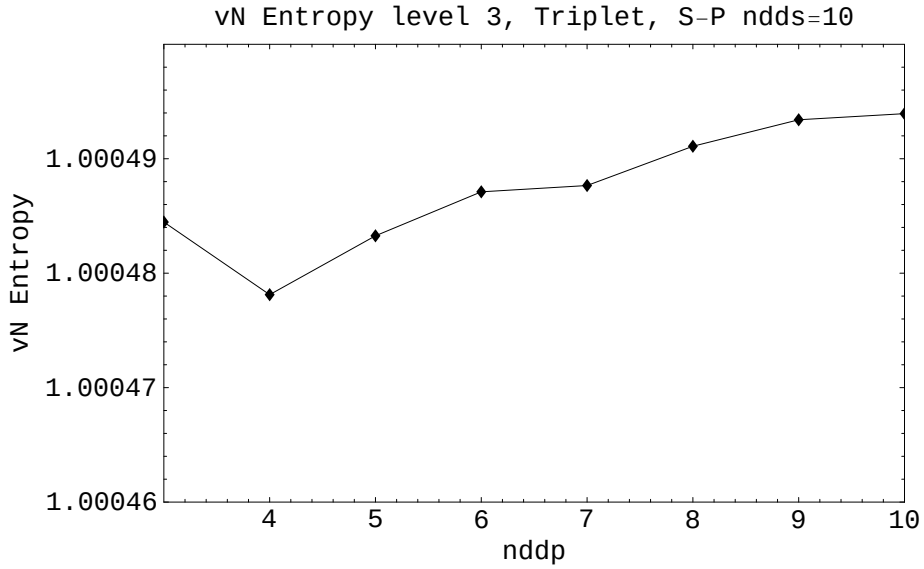

Figure 6.68 – von Neumann entropy, level 3, triplet, dimension for S Shell=10 and dimension for P Shell from 2 to 10

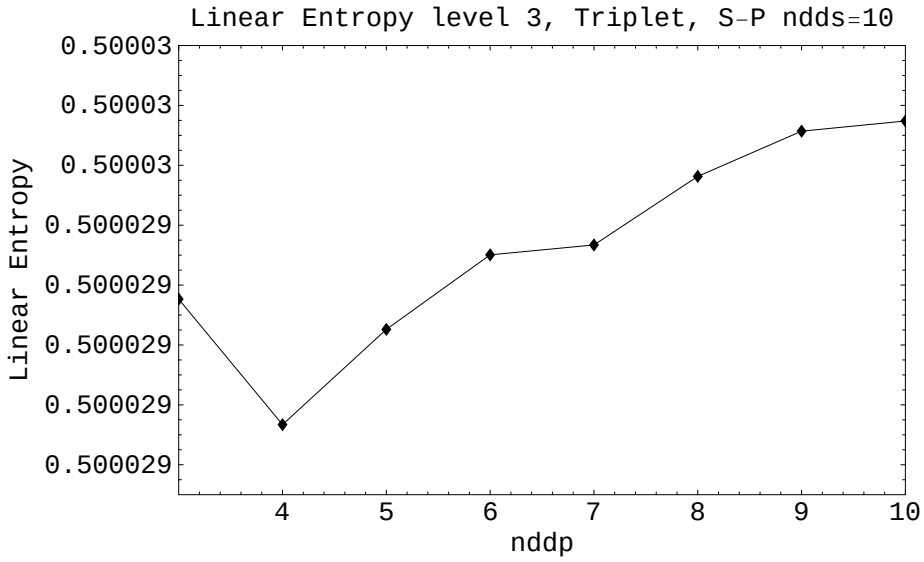

Figure 6.69 – Linear entropy, level 3, triplet, dimension for S Shell=10 and dimension for D Shellp from 2 to 10

nddp	energy	von Neumann	linear
2	9.563422923	1.007045879	0.500020554
3	5.903560481	1.000431918	0.500025697
4	5.523042986	1.000425600	0.500025286
5	5.108841265	1.000430572	0.500025590
6	4.639425836	1.000434100	0.500025816
7	4.599970850	1.000434439	0.500025836
8	4.562856613	1.000434711	0.500025851
9	4.354091466	1.000439601	0.500026174
10	4.330197861	1.000440033	0.500026201
11	4.261079719	1.000440619	0.500026238
12	4.245679793	1.000440853	0.500026253
13	4.227933033	1.000440977	0.500026260
14	4.219120360	1.000440950	0.500026258
15	4.213216506	1.000441020	0.500026262

Table 6.42 – Triplet, level III S-P, dimension for S Shell=15

Triplet level III, dimension for S Shell = 15

Saturation n_p values: energy ≈ 11, von Neumann entropy ≈ 10, linear entropy ≈ 9.

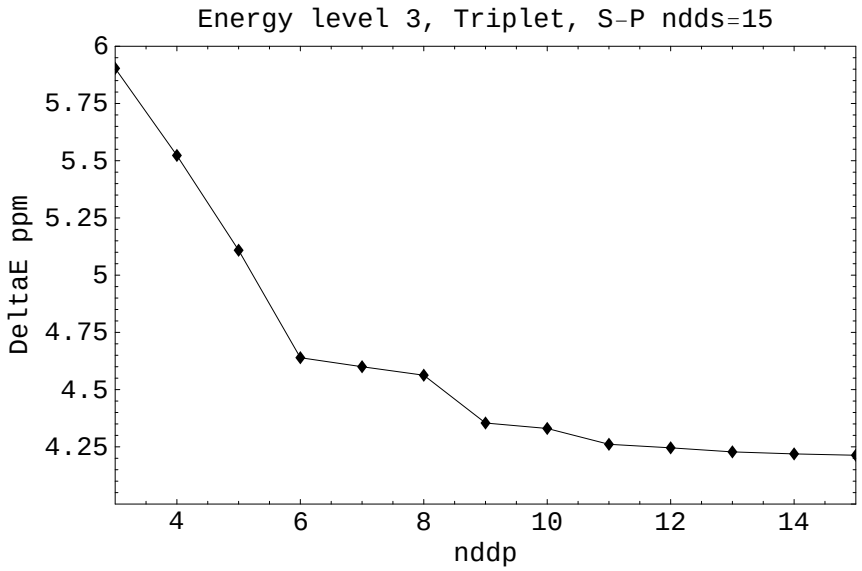

Figure 6.70 – Energy error, level 3, triplet, dimension for S Shell=15 and dimension for P Shell from 2 to 15

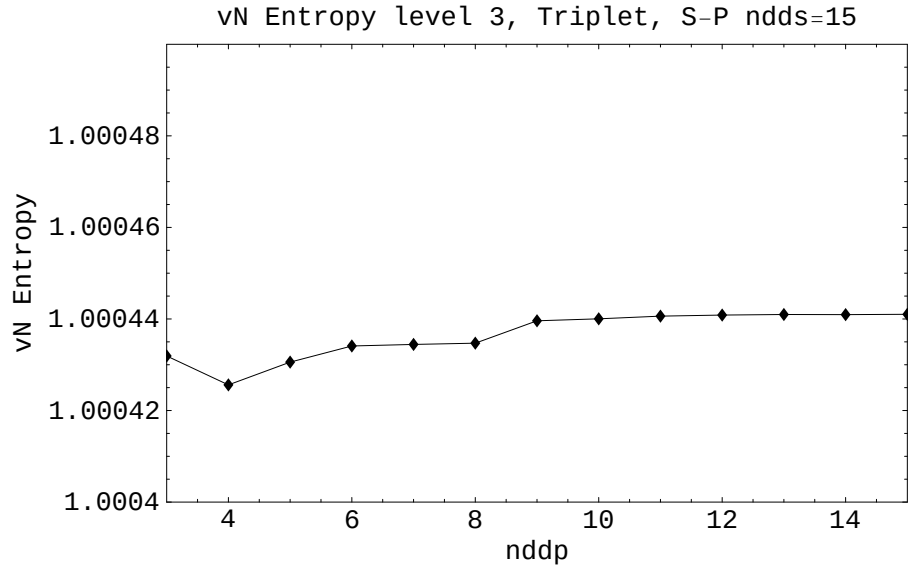

Figure 6.71 – von Neumann entropy, level 3, triplet, dimension for S Shell=15 and dimension for P Shell from 2 to 15

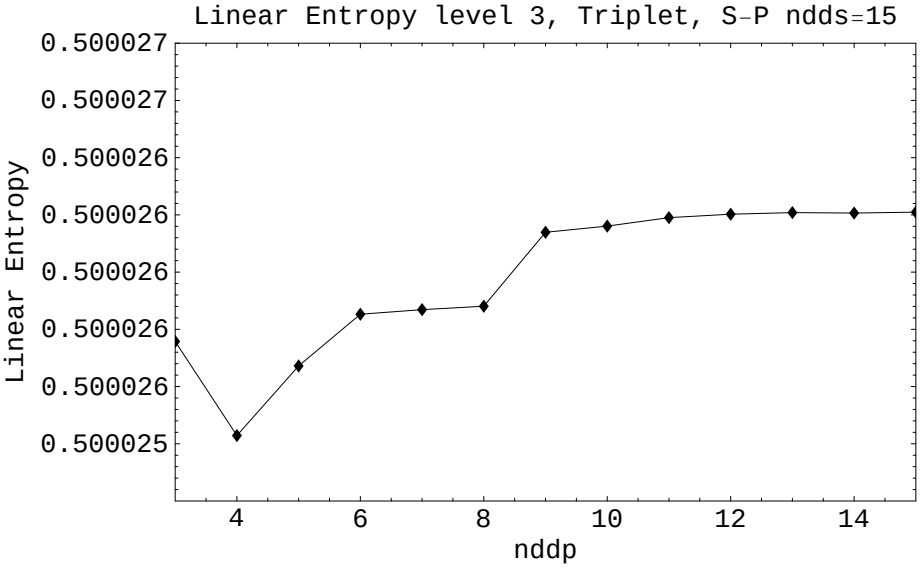

Figure 6.72 – Linear entropy, level 3, triplet, dimension for S Shell=15 and dimension for P Shell from 2 to 15

nddp	energy	von Neumann	linear
2	12139.707185585	1.034694508	0.500021087
3	12133.977101698	1.000583953	0.500035328
4	12133.187434831	1.000573945	0.500034651
5	12132.747465800	1.000573517	0.500034593
6	12132.367250557	1.000576948	0.500034814
7	12132.168511050	1.000582632	0.500035193
8	12132.068679865	1.000583266	0.500035230
9	12131.911622786	1.000584035	0.500035276
10	12131.867183800	1.000584412	0.500035295

Table 6.43 – Triplet, level V S-P, dimension for S Shell=10

Triplet level V S-P

dimension for S Shell = 10

Saturation n_p values: energy ≈ 9, von Neumann entropy ≈ 7, linear entropy ≈ 7.

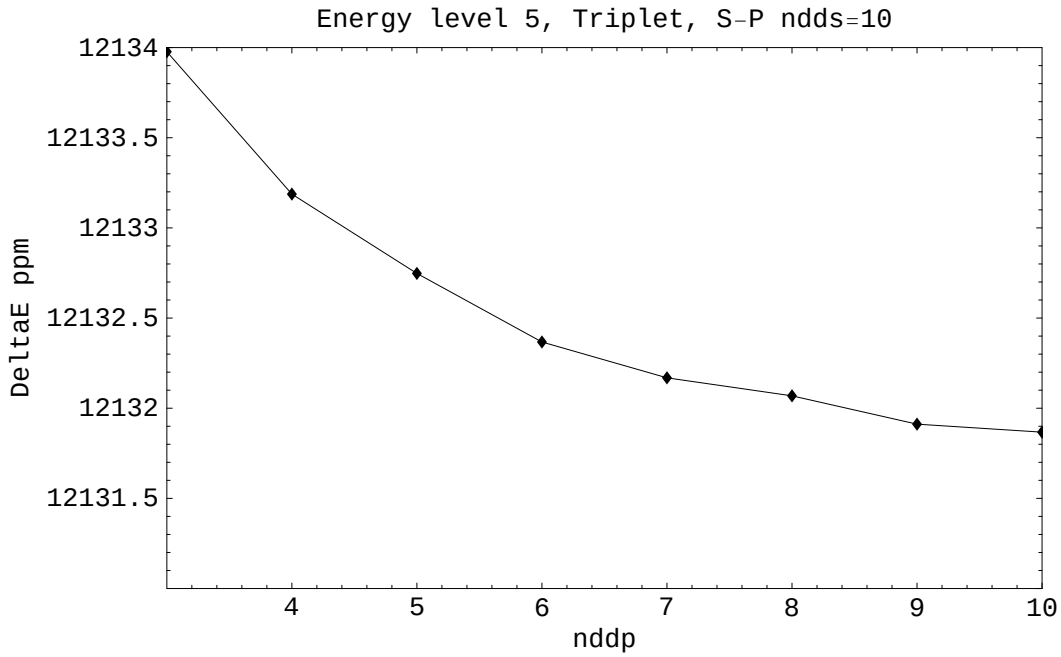

Figure 6.73 – Energy error, level 5, triplet, dimension for S Shell=10 and dimension for P Shell from 2 to 10

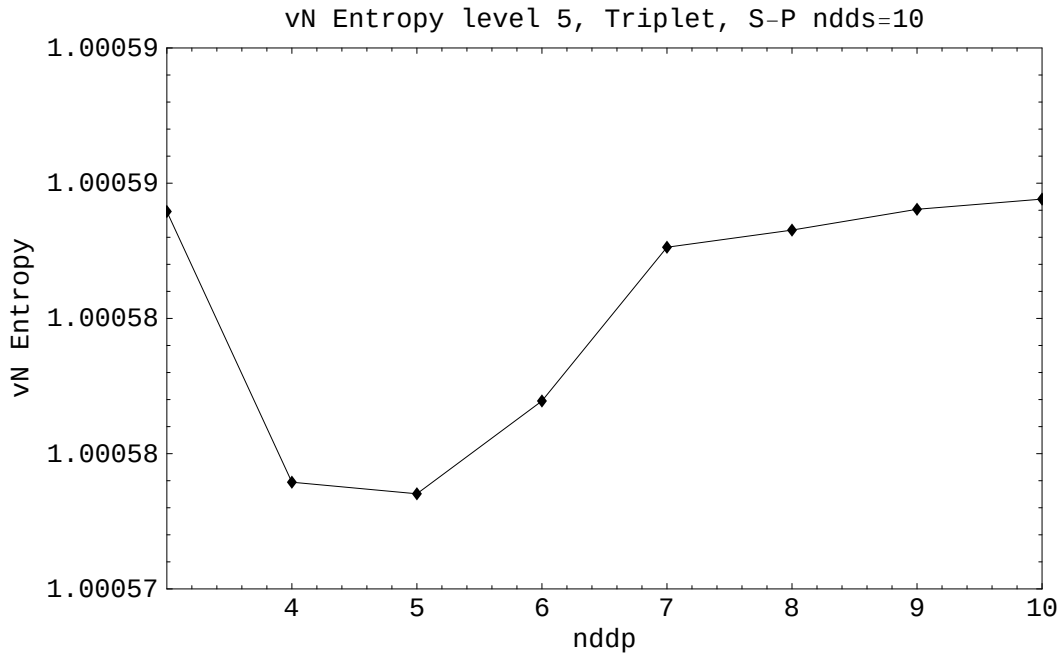

Figure 6.74 – von Neumann entropy, level 5, triplet, dimension for S Shell=10 and dimension for P Shell from 2 to 10

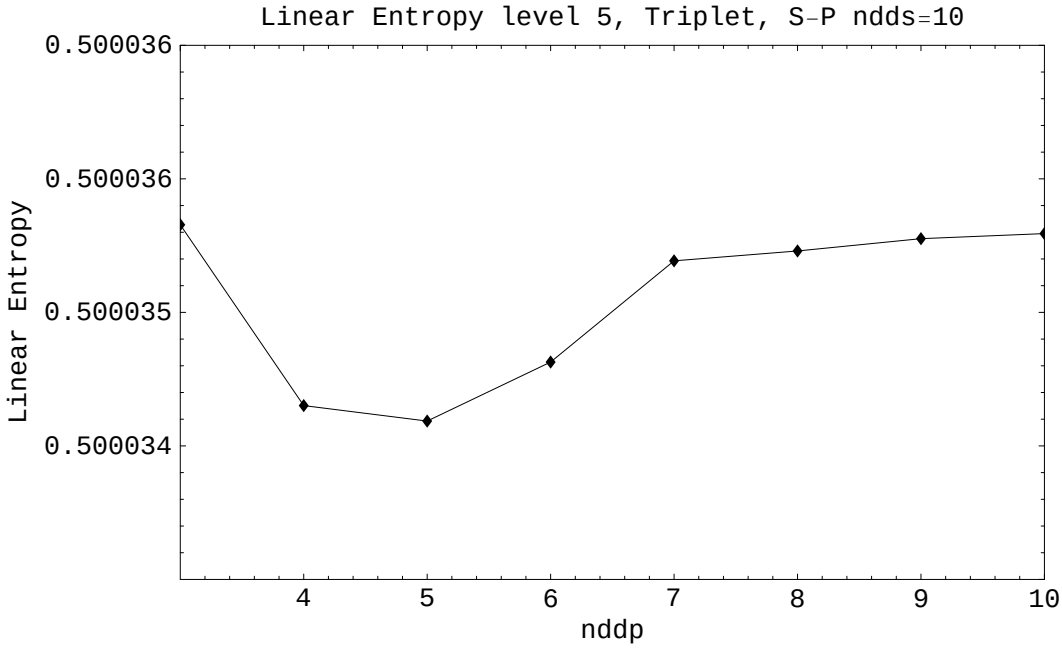

Figure 6.75 – Linear entropy, level 5, triplet, dimension for S Shell=10 and dimension for P Shell from 2 to 10

nddp	energy	von Neumann	linear
2	462.269061039	1.013385214	0.500006251
3	460.930394019	1.000160444	0.500008736
4	460.722953666	1.000157298	0.500008550
5	460.606920576	1.000158111	0.500008591
6	460.465042301	1.000159193	0.500008653
7	460.440574411	1.000160427	0.500008727
8	460.426545631	1.000160577	0.500008735
9	460.365903652	1.000160900	0.500008753
10	460.355347219	1.000161161	0.500008769
11	460.348046482	1.000161156	0.500008768
12	460.342967217	1.000161532	0.500008791
13	460.337579623	1.000161465	0.500008786
14	460.329788819	1.000161550	0.500008791
15	460.325595959	1.000161616	0.500008795

Table 6.44 – Triplet, level V S-P, dimension for S Shell=15

Triplet level V S-P, dimension for S Shell = 15

Saturation n_p values: energy ≈ 9, von Neumann entropy ≈ 7, linear entropy ≈ 7.

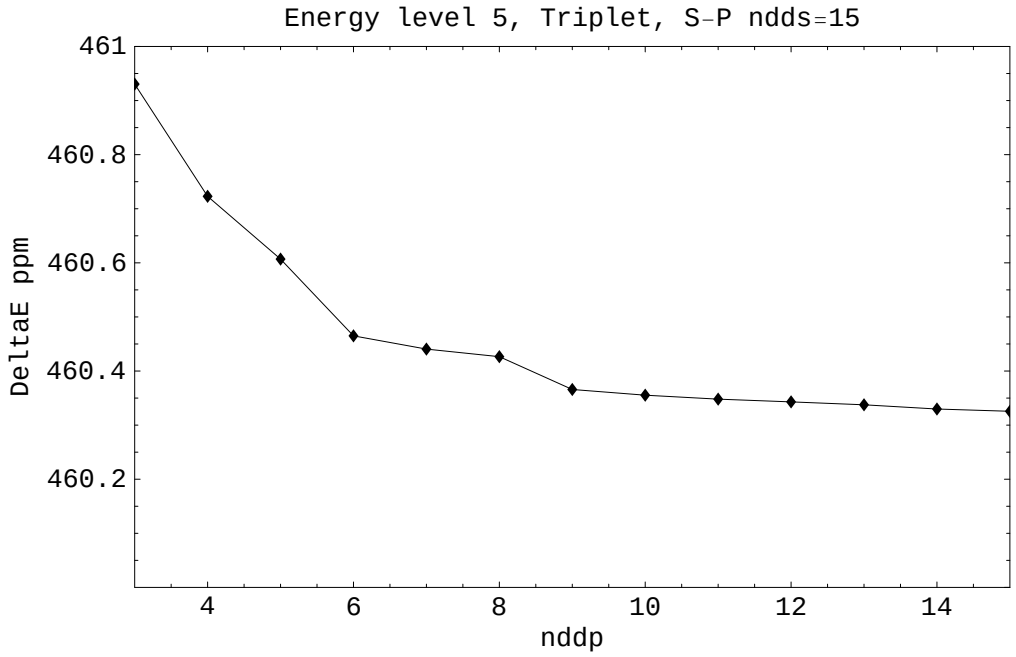

Figure 6.76 – Energy error, level 5, triplet, dimension for S Shell=15 and dimension for P Shell from 2 to 15

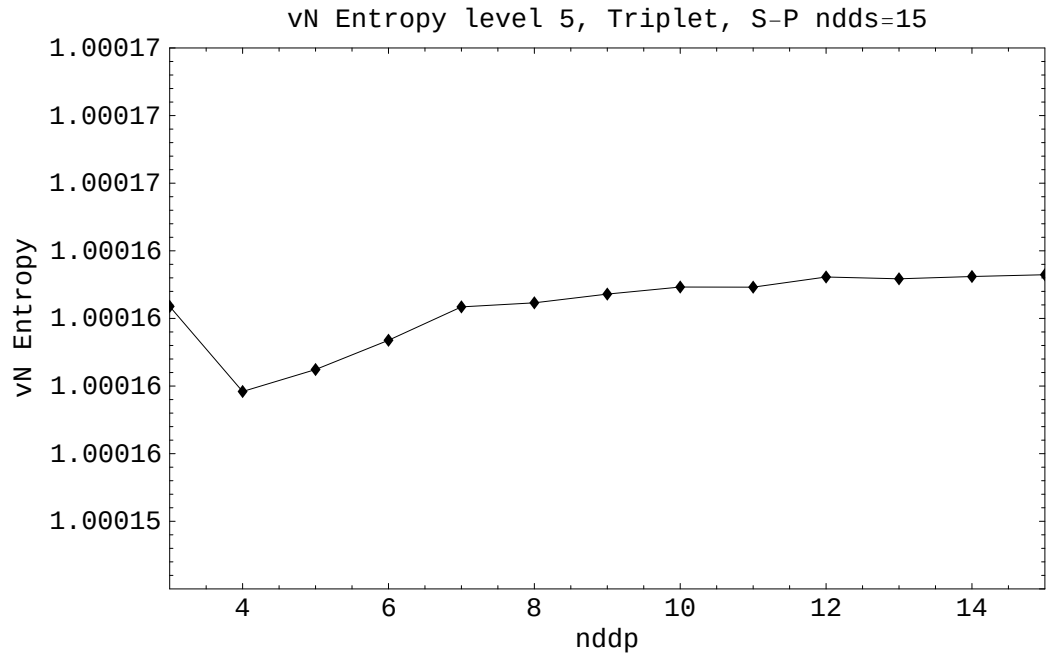

Figure 6.77 – von Neumann entropy, level 5, triplet, dimension for S Shell=15 and dimension for P Shell from 2 to 15

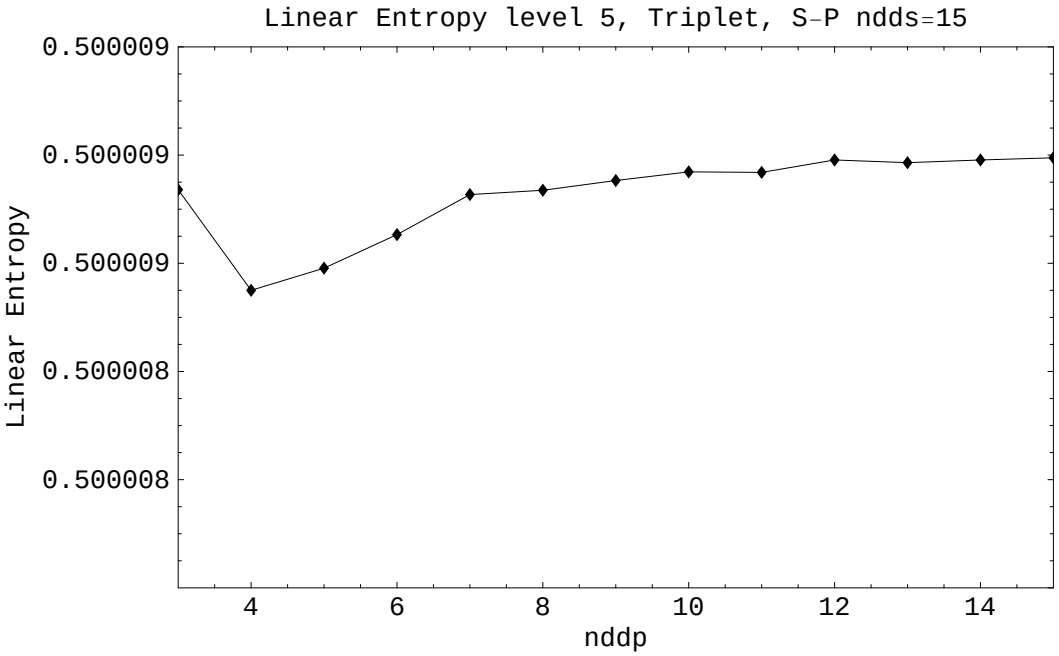

Figure 6.78 – Linear entropy, level 5, triplet, dimension for S Shell=15 and dimension for P Shell from 2 to 15

nddd	energy	von Neumann	linear
2	3.983177845	1.000573719	0.500026812
3	3.262074663	1.000455329	0.500027055
4	2.766340961	1.000458587	0.500027208
5	2.521121331	1.000459480	0.500027251
6	2.405131702	1.000459705	0.500027262
7	2.346603451	1.000470979	0.500027817

Table 6.45 – Triplet, level III S-P-D, dimension for S Shell=15, dimension for P Shell=7

Triplet level III S-P-D

dimension for S Shell = 15, dimension for P Shell = 7

Saturation n_d values: energy > 7, von Neumann entropy > 7, linear entropy > 7.

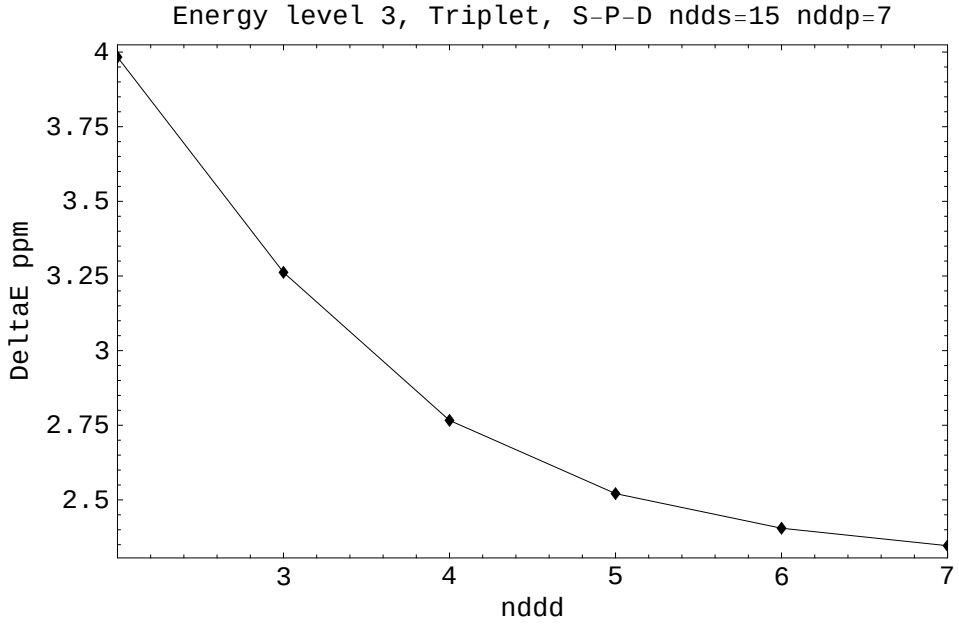

Figure 6.79 – Energy error, level 3, triplet, dimension for S Shell=15 dimension for P Shell=7 and dimension for D Shell from 2 to 7

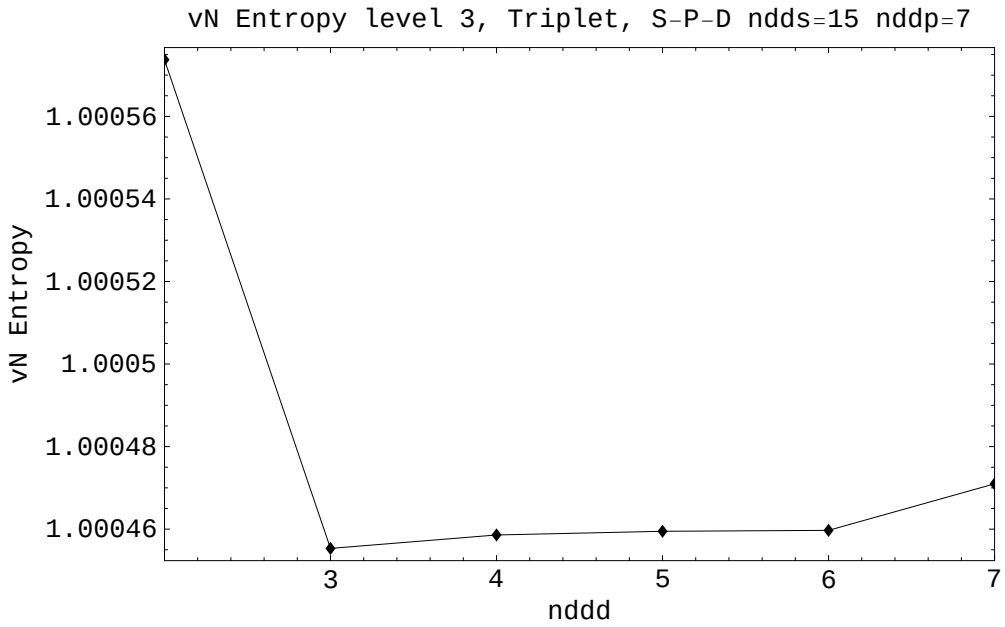

Figure 6.80 – von Neumann entropy, level 3, triplet, dimension for S Shell=15 dimension for P Shell=7 and dimension for D Shell from 2 to 7

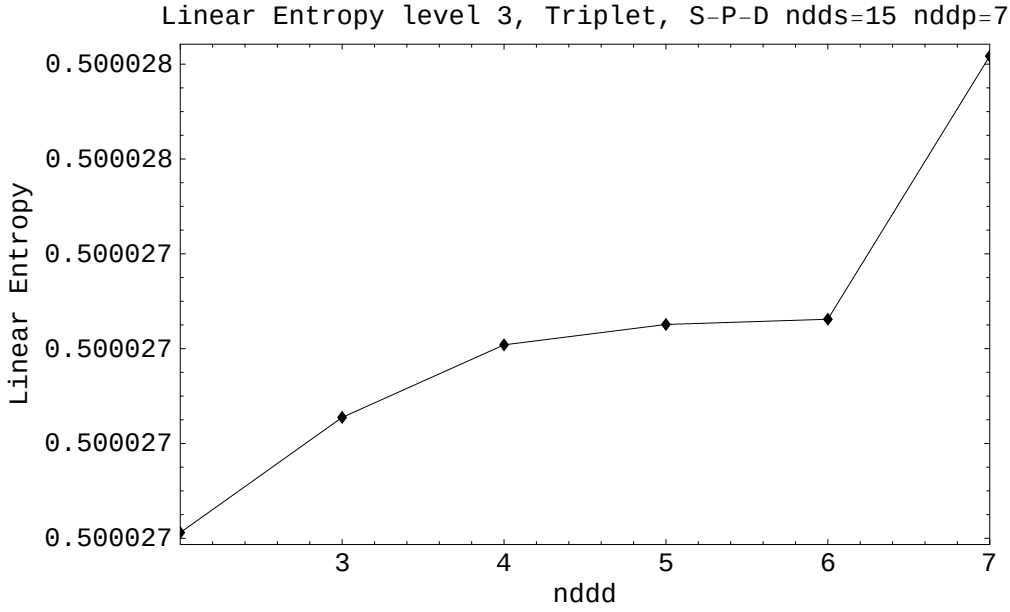

Figure 6.81 – Linear entropy, level 3, triplet, dimension for S Shell=15 dimension for P Shell=7 and dimension for D Shell from 2 to 7

Chapter 7

From the Helium atom to the Hydrogen molecule

7.1 Entanglement and the Slater Type Orbitals-n Gaussians basis

In this final section of the thesis, we will study the entanglement using the STO-nG functions, instead of the STOs used up to now.

STO-nG expansions are approximations of the STO with linear combinations of n Gaussian Type Orbitals (GTO), of the form:

$$r^k \sum_{i=1}^{n} a_i \, exp(-b_i r^2) \tag{7.1}$$

where k is the same as in the STO being approximated, and the coefficients a_i and b_i are found minimizing the error made using the GTOs instead of the STOs (see e.g. (Stewart , 1969)).

These STO-nG expansions are very important, as it is not possible to use STO functions exclusively. Although their use in quantum chemistry is spreading, the available results

are not yet sufficient to be able to use them in the most complex problems.

Then, as we stated in the introduction, we aim to compare the entanglement computations of the preceding chapters to computations performed using the STO-nG, with the well-known techniques of the quantum chemistry. We will evaluate with the greates precision the error in the entanglement computation for several values of n in the STO-nG expansions.

Moreover, we note that the H_2 molecules reduces exactly to the Helium atoms if one reduces to 0 the distance R between the nuclei. We performed some tests, and realized that the H_2 molecule computations is not more difficult than the Helium's, so we will proceed to compute the entanglement in the H_2 molecule.

The computations are performed in a similar manner, the differences will be described.

The outline of the chapter is the following: in section 7.1.1 we compute the H_2^+ molecule, using a single STO. The superposition, coulombian and resonance integrals are computed using the STO first, and then replacing the Gaussian expansions, and their numerical values are compared. Then we compute the single particle operators exploiting the symmetries, use them to compute the energy and entropy and we compare the results obtained with 1 STO to those obtained approximating it with an expansions in n Gaussians, n=1, 2, ...6.

In section 7.2 we describe the one and two body operators for the H_2 molecule, starting again with a single STO and its approximation with up to 6 GTOs.

In section 7.3 we describe the operators for the H_2 molecule, shell S, in the general case of several STOs, each approximated by up to 6 GTOs. It is shown how the superposition, potential and kinetik energy matrix elements are computed exploiting the symmetries.

In section 7.4 we report our results for the H_2 molecule. To check the software, we start in section 7.4.1 comparing the results obtained setting the internuclear distance = 0 in the H_2 programs with those obtained with the Helium program and the same dimension for the S Shell.

Then, in section 7.4.2 we report the computation of the fundamental, I, II and III level of H_2, singlet, obtained with 5 STOs approximated by 6 GTOs.

7.1.1 H_2^+ molecule computation

We will compare the results of the simplest case, using a single STO, with the STO-nG method for some values of n.

Case of a single Slater Type Orbital

The variational method with a single STO in LCAO is well known, we will limit ourselves to some quick considerations to describe our notation.

We start with a single normalized atomic STO-1S orbital:

$$\langle \mathbf{r} \,|,\ 1S\rangle \ = \ \sqrt{\frac{\xi^3}{\pi}} exp\{-\xi \cdot r\} \tag{7.2}$$

where ξ is the variational parameter.

In the case of the H_2^+, molecule we obtain at once the "gerade" molecular orbital (the only ones in which we are presently interested).

$$\langle \mathbf{r} \,|\, \psi_g\rangle \ = \mathcal{N}\left[\sqrt{\tfrac{\xi^3}{\pi}}\, exp\{-\xi \,|\, \mathbf{r}-\mathbf{a} \,|\,\} \ + \ \sqrt{\tfrac{\xi^3}{\pi}}\, exp\{-\xi \,|\, \mathbf{r}+\mathbf{a} \,|\,\}\right] \ =$$

$$= \mathcal{N} \cdot \langle \mathbf{r} \,|\, [|\, 1\rangle \ + \ |\, 2\rangle] \tag{7.3}$$

Imposing the normalization we get:

$$\mathcal{N} = \frac{1}{\sqrt{2(1+S)}} \tag{7.4}$$

with

$$S = [1 + \xi R + \frac{1}{3}(\xi R)^2] \cdot exp\{-\xi R\} \tag{7.5}$$

Superposition integral

$S = [1 + \xi R + \frac{1}{3}\xi^2 R^2] \cdot exp[-\xi R]$ in the expansion in Gaussians we get

$$S_{ij} = [\frac{\pi}{\alpha_i + \alpha_j}]^{3/2} \cdot exp\{-\frac{\alpha_i \alpha_j}{\alpha_i + \alpha_j} R^2\} \tag{7.6}$$

The results for some values of n are reported in the table 7.1.

Coulombian integral

Using the STO-1S we have:

$$J = -\frac{\xi^3}{\pi} \int d\mathbf{r} \frac{e^2}{r_B} exp[-2\xi r_A] = -\xi[-\frac{1}{\xi R} + (1 + \frac{1}{\xi R})exp[-2\xi R]] \tag{7.7}$$

R	STO	n=1	n=2	n=3	n=4	n=5	n=6
0.5	0.88457	0.89825	0.88584	0.88460	0.88459	0.88457	0.88457
1.0	0.71400	0.72521	0.71338	0.71415	0.71399	0.71401	0.71400
1.5	0.57566	0.56905	0.57488	0.57565	0.57566	0.57566	0.57567
2.0	0.46311	0.43465	0.46306	0.46278	0.46314	0.46310	0.46311
2.5	0.37405	0.32635	0.37398	0.37366	0.37403	0.37406	0.37405
3.0	0.29775	0.23489	0.29626	0.29756	0.29766	0.29776	0.29775
3.5	0.23263	0.16047	0.22840	0.23264	0.23251	0.23262	0.23263
4.0	0.17509	0.10030	0.16724	0.17503	0.17503	0.17505	0.17509
4.5	0.13202	0.06090	0.12110	0.13153	0.13204	0.13198	0.13201
5.0	0.09658	0.03381	0.08345	0.09533	0.09661	0.09657	0.09656

Table 7.1 – S integral values

R	STO	n=1	n=2	n=3	n=4	n=5	n=6
0.5	-1.36255	-1.29167	-1.36592	-1.36213	-1.36243	-1.36260	-1.36253
1.0	-0.88326	-0.89112	-0.88266	-0.88332	-0.88324	-0.88328	-0.88326
1.5	-0.63240	-0.64421	-0.63128	-0.63263	-0.63236	-0.63241	-0.63240
2.0	-0.48780	-0.49509	-0.48761	-0.48779	-0.48783	-0.48779	-0.48780
2.5	-0.39507	-0.39890	-0.39536	-0.39499	-0.39509	-0.39507	-0.39507
3.0	-0.33128	-0.33311	-0.33166	-0.33123	-0.33128	-0.33128	-0.33128
3.5	-0.28486	-0.28568	-0.28516	-0.28486	-0.28485	-0.28486	-0.28486
4.0	-0.24966	-0.25000	-0.24985	-0.24969	-0.24966	-0.24966	-0.24966
4.5	-0.22208	-0.22222	-0.22218	-0.22211	-0.22208	-0.22208	-0.22208
5.0	-0.19995	-0.20000	-0.19999	-0.19996	-0.19995	-0.19994	-0.19995

Table 7.2 – J integral values

from the expansion in Gaussians we get:

$$J_{ij} \;=\; -\int b_i(\mathbf{r})\,\frac{1}{|\mathbf{r}-\mathbf{R}'|}\,b_j(\mathbf{r})\,d\mathbf{r} \;=\; -S_{ij}\cdot\frac{1}{|\,\mathbf{R_{ij}}-\mathbf{R}'|}\,erf[\sqrt{\alpha_i+\alpha_j}|\,\mathbf{R_{ij}}-\mathbf{R}'|] \qquad (7.8)$$

Resonance integral

R	STO	n=1	n=2	n=3	n=4	n=5	n=6
0.5	-1.38153	-1.28209	-1.37074	-1.37667	-1.38029	-1.38119	-1.38138
1.0	-0.83857	-0.83722	-0.82827	-0.83728	-0.83789	-0.83845	-0.83849
1.5	-0.53759	-0.54000	-0.53086	-0.53711	-0.53724	-0.53749	-0.53757
2.0	-0.36137	-0.34914	-0.36017	-0.36022	-0.36140	-0.36126	-0.36136
2.5	-0.25140	-0.22596	-0.25303	-0.25032	-0.25139	-0.25139	-0.25138
3.0	-0.17689	-0.14270	-0.17863	-0.17644	-0.17671	-0.17693	-0.17688
3.5	-0.12443	-0.08658	-0.12446	-0.12466	-0.12420	-0.12443	-0.12444
4.0	-0.08567	-0.04855	-0.08316	-0.08621	-0.08557	-0.08561	-0.08568
4.5	-0.05948	-0.02658	-0.05497	-0.05985	-0.05955	-0.05942	-0.05947
5.0	-0.04043	-0.01340	-0.03466	-0.04031	-0.04059	-0.04041	-0.04041

Table 7.3 – K integral values

$$K \;=\; -\int d\mathbf{r}\,\psi_A(r_A)\,\frac{e^2}{r_A}\,\psi_B(r_B) \;=\; -\xi\,[1+\xi\,R]\cdot exp[-\xi\,R] \tag{7.9}$$

H_2^+ *computation*

The computation is very simple. We compute the single particle operators.

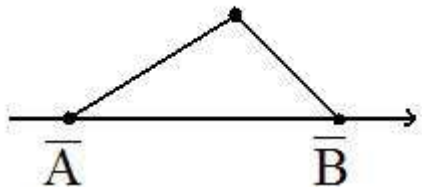

Figure 7.1 – H_2^+ sketch

We need the integrals:

SS = superposition; CC = coulombian integral; aa = resonance integral.

Set

$$r_A = |\mathbf{r} - \mathbf{a}|; \;\; r_B = |\mathbf{r} + \mathbf{a}|; \;\; \mathbf{a} = \frac{\mathbf{R}}{2} \tag{7.10}$$

We take as the first orbital wave function a simple STO-1S

$$\psi_A(\mathbf{r}_A) = \sqrt{\frac{\xi^3}{\pi}} exp[-\xi r_A] \tag{7.11}$$

where ξ is a variational parameter.

All the following expression are given both in terms of STO and of STO-nG, to evaluate the precision that is obtained for several values of n.

The energy expectation value is:

$$\langle \psi_g | H | \psi_g \rangle = \langle \psi_g | T - \frac{1}{|\mathbf{r}-\mathbf{a}|} - \frac{1}{|\mathbf{r}+\mathbf{a}|} + \frac{1}{|\mathbf{R}|} | \psi_g \rangle =$$

$$\frac{1}{2[1+S]} \cdot \{\langle 1\,| + \langle 2\,|\}\{T - \frac{1}{|\,\mathbf{r}-\mathbf{a}\,|} - \frac{1}{|\,\mathbf{r}+\mathbf{a}\,|} + \frac{1}{|\,\mathbf{R}\,|}\}\{|\,1\rangle + |\,2\rangle\} \tag{7.12}$$

We have a total of 16 terms, that reduce to 8 in force of evident symmetries.

$$\langle \psi_g\,|\,H\,|\,\psi_g\rangle = \frac{1}{1+S}\,\{\langle 1\,|\,H\,|\,1\rangle + \langle 1\,|\,H\,|\,2\rangle\} \tag{7.13}$$

Then we need 8 integrals:

$$\langle 1\,|\,T\,|\,1\rangle = [1] = +\frac{1}{2}\,\xi^2 \tag{7.14}$$

$$\langle 1\,|\,T\,|\,2\rangle = [2] = -\frac{1}{2}\,\xi^2 S - \xi K \tag{7.15}$$

$$\langle 1\,|\,\frac{-1}{|\,\mathbf{r}-\mathbf{a}\,|}\,|\,1\rangle = [3] = -\xi \tag{7.16}$$

$$\langle 1\,|\,\frac{-1}{|\,\mathbf{r}-\mathbf{a}\,|}\,|\,2\rangle = [4] = K \tag{7.17}$$

$$\langle 1\,|\,\frac{-1}{|\,\mathbf{r}+\mathbf{a}\,|}\,|\,1\rangle = [5] = J \tag{7.18}$$

$$\langle 1 \,|\, \frac{-1}{|\,\mathbf{r}+\mathbf{a}\,|} \,|\, 2\rangle \;=\; [6] \;=\; K \tag{7.19}$$

$$\langle 1 \,|\, \frac{1}{|\,\mathbf{R}\,|} \,|\, 1\rangle \;=\; [7] \;=\; \frac{1}{|\,\mathbf{R}\,|} \tag{7.20}$$

$$\langle 1 \,|\, \frac{1}{|\,\mathbf{R}\,|} \,|\, 2\rangle \;=\; [8] \;=\; S\frac{1}{|\,\mathbf{R}\,|} \tag{7.21}$$

We recall:

$$\langle \mathbf{r} \,|\, 1\rangle \;=\; \sqrt{\frac{\xi^3}{\pi}}\, exp\{-\xi\,|\,\mathbf{r}-\mathbf{a}\,|\,\}, \quad \langle \mathbf{r} \,|\, 2\rangle \;=\; \sqrt{\frac{\xi^3}{\pi}}\, exp\{-\xi\,|\,\mathbf{r}+\mathbf{a}\,|\,\} \tag{7.22}$$

The integral [1] is immediate, and doesn't need any comment.

$$[2] \;=\; \langle 1 \,|\, T \,|\, 2\rangle \;=\; -\frac{1}{2}\,\xi^2 S \;-\; \xi K,\; where:\; K \;=\; -\xi\,[1 \;+\; \xi\, R]\cdot exp[-\xi\, R] \tag{7.23}$$

Integral [3]

$$[3] \;=\; \langle 1\,|\,\frac{-1}{|\,\mathbf{r}-\mathbf{a}\,|}\,|\,1\rangle \;=\; -\xi \tag{7.24}$$

Integral [4] = K

$$[4] \;=\; \langle 1\,|\,\frac{-1}{|\,\mathbf{r}-\mathbf{a}\,|}\,|\,2\rangle \;=\; \langle \psi_A\,|\,\frac{-1}{r_A}\,|\,\psi_B\rangle \;=\; K \tag{7.25}$$

Beware: K is negative. (fig 7.2).

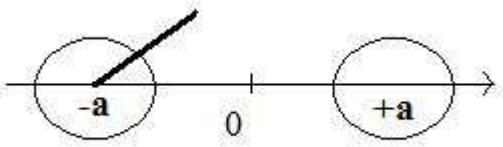

Figure 7.2 – Integral [4]: the circles represent the orbitals ψ_A, ψ_B, the thick line the vector **r-a**

Integral [5] = J

$$[5] \;=\; \langle 1\,|\,\frac{-1}{|\,\mathbf{r}+\mathbf{a}\,|}\,|\,1\rangle \;=\; \langle \psi_A\,|\,\frac{-1}{r_B}\,|\,\psi_A\rangle \;=\; J \tag{7.26}$$

Beware: J is negative.

$$J \;=\; +\xi\cdot\left[-\frac{1}{\xi\,R} \;+\; \left(1\;+\;\frac{1}{\xi\,R}\right) exp[-2\xi\,R]\right] \tag{7.27}$$

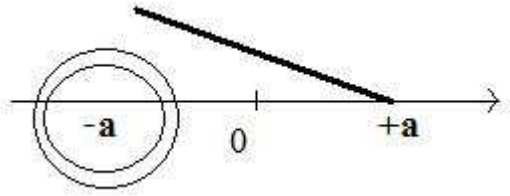

Figure 7.3 – Integral [5]: the circles represent the orbital ψ_A, considered twice, the thick line the vector $\mathbf{r}+\mathbf{a}$

Integral [6]

$$[6] \;=\; \langle 1\,|\,\frac{-1}{|\,\mathbf{r}+\mathbf{a}\,|}\,|\,2\rangle \;=\; \langle \psi_A\,|\,\frac{-1}{r_B}\,|\,\psi_B\rangle \;=$$

$$=\; \frac{\xi^3}{\pi}\int d\mathbf{r}\, exp\{-\xi\,|\,\mathbf{r}-\mathbf{a}\,|\,\}\cdot\frac{-1}{|\,\mathbf{r}+\mathbf{a}\,|}\, exp\{-\xi\,|\,\mathbf{r}+\mathbf{a}\,|\,\} \;=\; K \tag{7.28}$$

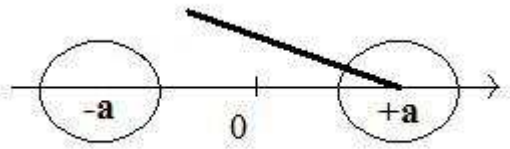

Figure 7.4 – Integral [6]: the circles represent the orbitals ψ_A, ψ_B, the thick line the vector $\mathbf{r}+\mathbf{a}$

Comparison [4] ; [6]

$$[4] \;=\; \langle 1\,|\,\frac{1}{r_A}\,|\,2\rangle;\;\; [6] \;=\; \langle 1\,|\,\frac{1}{r_b}\,|\,2\rangle \tag{7.29}$$

Clearly they are identical.

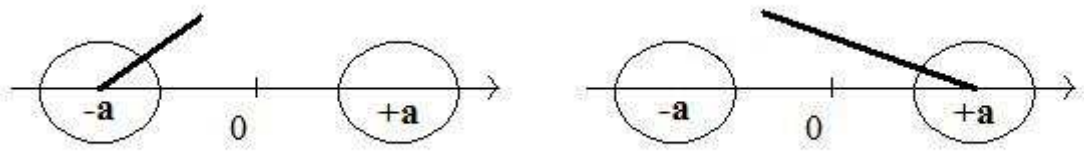

Figure 7.5 – Comparison of integrals [4] and [6]

Check

It is useful to check that when $R \rightarrow 0$ one gets $H_2^+ \rightarrow He^+$

The limits of the integrals [1] ... [6] are:

$[1] = \frac{1}{2}\xi^2$, $[2] = \frac{1}{2}\xi^2$, $[3] = -\xi$

$[4] = -\xi$, $[5] = -\xi$, $[6] = -\xi$

Then we have:

$$E_{H_2^+} = \frac{1}{1+S}\left\{\frac{1}{2}\xi^2(1-S) - \xi(K+1) + J + 2K + \frac{1}{R}(1+S)\right\} \tag{7.30}$$

When $R \rightarrow 0$ we obviously drop the interactions of the nuclei and obtain:

$$E_{H_2^+} \rightarrow E_{Helium^+} = \frac{1}{2}\{\xi^2 - 4\xi\} \tag{7.31}$$

The minimum is attained for $\xi = 2$ and we have $E_{Helium^+} = -\frac{1}{2} \cdot 4$ as it must be.

n	Electronic energy error	Binding energy error
1	1270.12	15951.91
2	699.49	8785.11
3	554.02	6958.46
4	-30.87	-387.68
5	57.55	722.86
6	9.20	115.59

Table 7.4 – Errors 1S-nG at R=2 a.u.

H_2^+ ***1S-nG***

Note: in all the plots we use

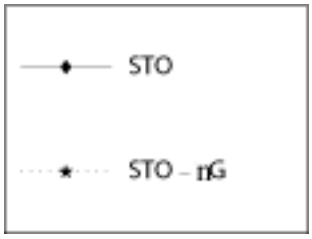

Abscissae and ordinates are in atomic units.

We compare the 1S analytic solution to the 1S-nG, to evaluate how many Gaussians are needed to obtain an assigned error level.

In table 7.4 we report the error in ppm for the value $R = 2\,a.u.$ and several values of the number of gaussians n. Tables 7.5 and 7.6 report the errors for some values of R.

R	n=1	n=2	n=3	n=4	n=5	n=6
0.5	28421.95	-306.05	456.83	120.77	6.28	17.32
1	-2928.52	2165.16	218.65	136.14	16.46	20.82
1.5	-6865.02	2796.26	41.13	135.91	29.80	8.11
2	1270.12	699.49	554.02	-30.87	57.55	9.20
2.5	13231.16	-1246.49	740.08	-4.38	9.34	20.43
3	25128.93	-1681.95	388.49	144.23	-29.89	11.14
3.5	34116.74	-311.13	-207.12	219.63	-3.28	0.00
4	38560.70	2425.92	-597.53	112.79	56.80	-12.70
4.5	38234.15	5151.27	-464.86	-78.64	71.85	13.35
5	34190.76	7244.16	131.30	-214.24	24.06	27.81

Table 7.5 – Electronic energy errors 1S-nG

R	n=1	n=2	n=3	n=4	n=5	n=6
0.5	-64068.52	689.89	-1029.78	-272.23	-14.17	-39.05
1	71525.42	-52881.36	-5339.81	-3324.79	-401.96	-508.47
1.5	-126191.89	51251.49	756.06	2498.19	547.80	0.00
2	15951.91	8785.11	6958.46	-387.68	722.86	115.59
2.5	164444.44	-15492.06	9198.21	-54.45	116.03	253.97
3	350147.44	-23591.49	5412.84	2009.64	-416.50	155.21
3.5	570684.82	-5406.49	-3465.51	3674.94	-54.92	-200.24
4	813286.90	51165.28	-12601.69	2378.75	1197.89	-267.88
4.5	1056805.61	142382.88	-12850.84	-2174.10	1986.33	368.87
5	1280729.17	271354.17	4917.63	-8023.68	901.28	1041.67

Table 7.6 – Binding energy errors 1S-nG

Comparison plots STO - STOnG

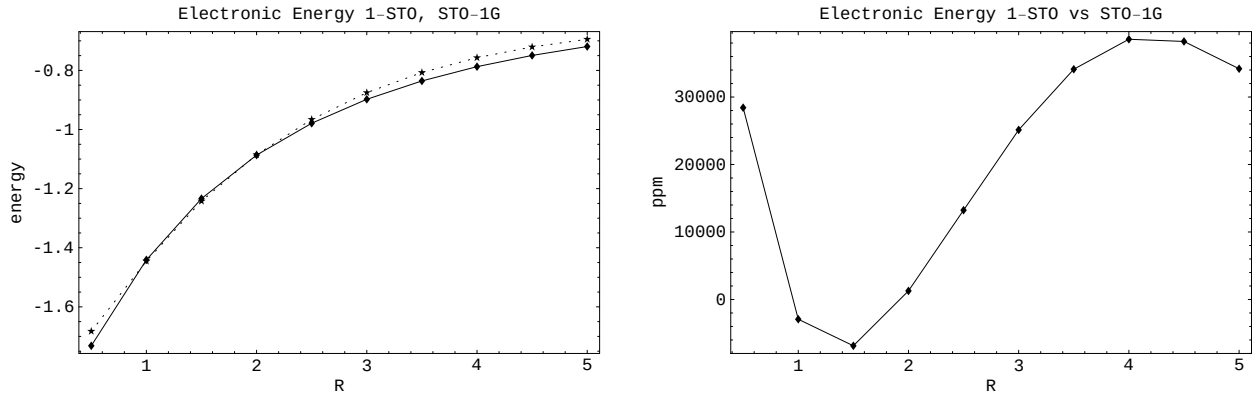

Figure 7.6 – Electronic energy STO / STO-1G and errors in ppm

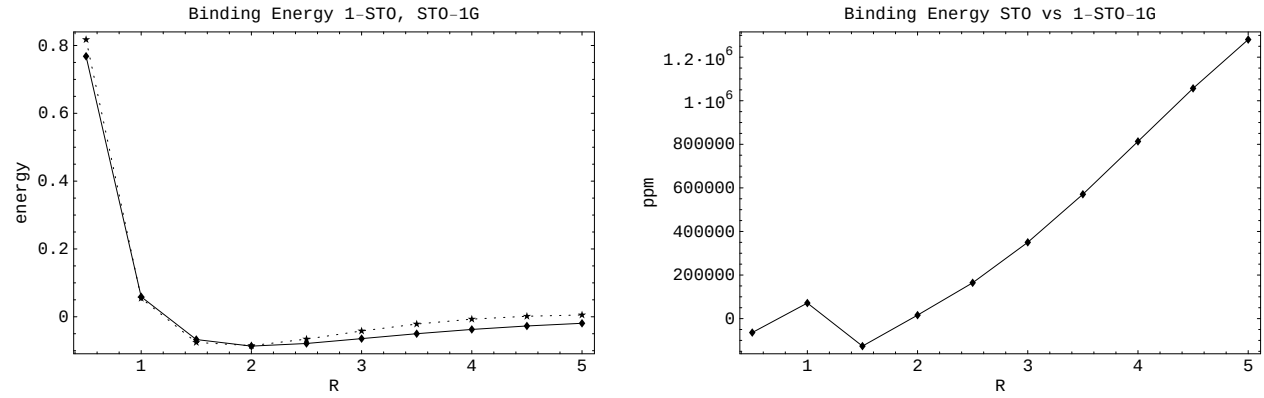

Figure 7.7 – Binding energy STO / STO-1G and errors in ppm

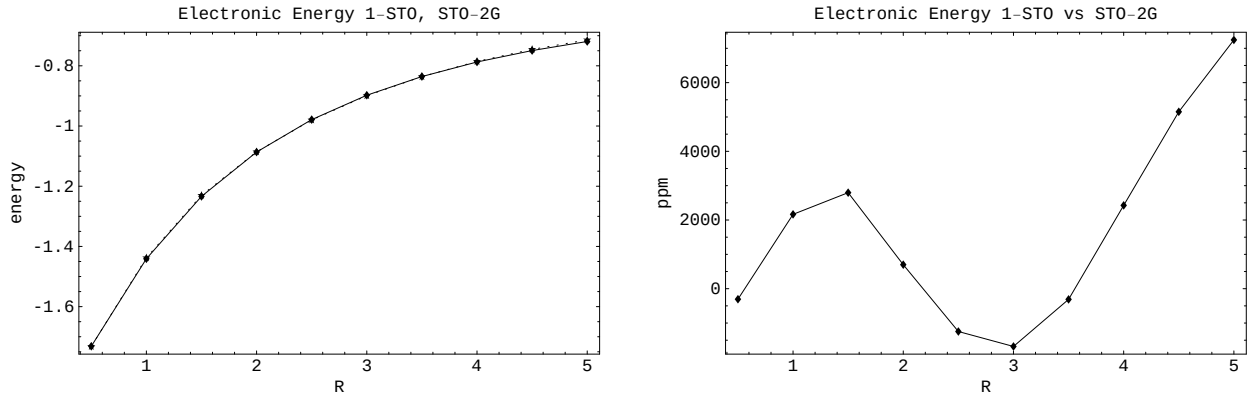

Figure 7.8 – Electronic energy STO / STO-2G and errors in ppm

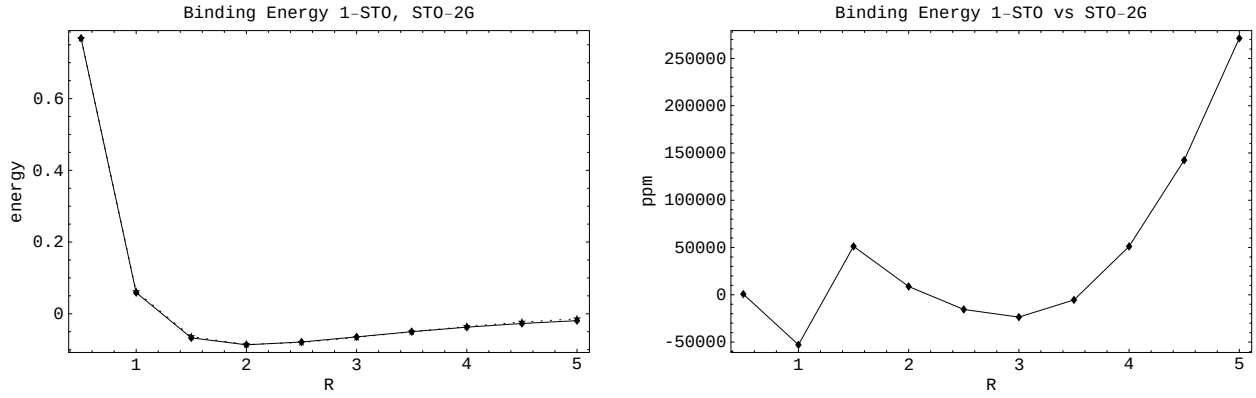

Figure 7.9 – Binding energy STO / STO-2G and errors in ppm

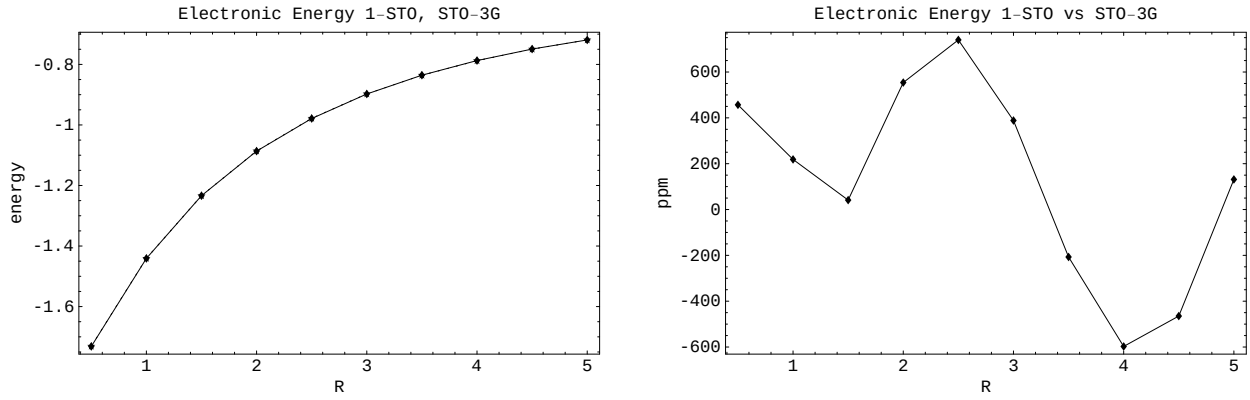

Figure 7.10 – Electronic energy STO / STO-3G and errors in ppm

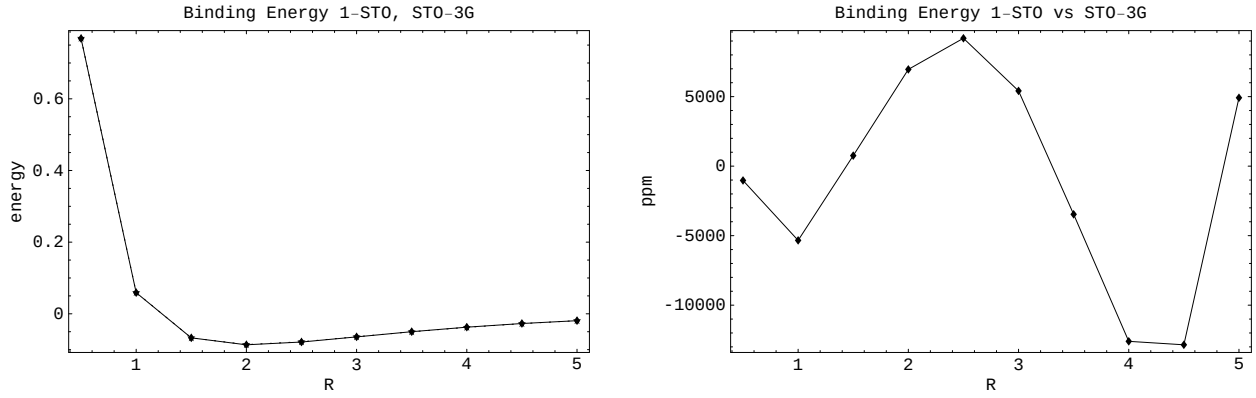

Figure 7.11 – Binding energy STO / STO-3G and errors in ppm

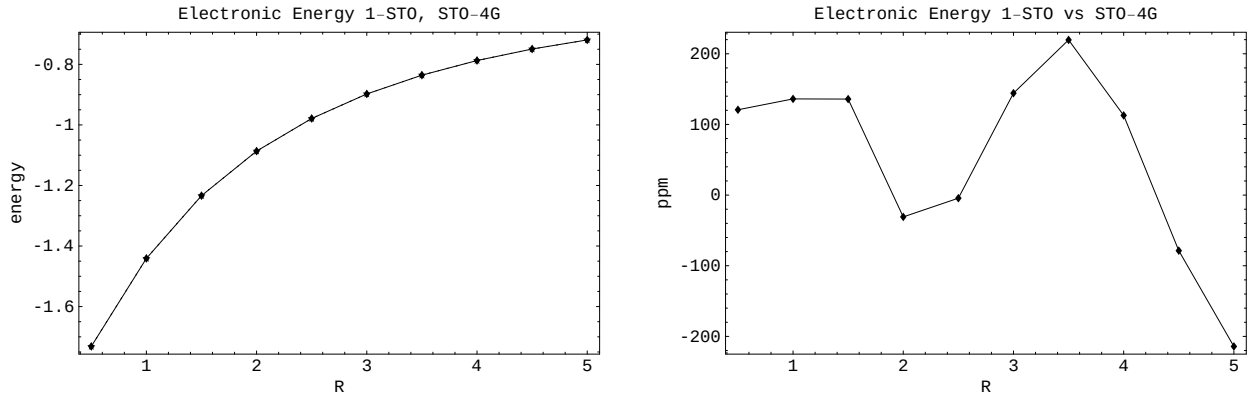

Figure 7.12 – Electronic energy STO / STO-4G and errors in ppm

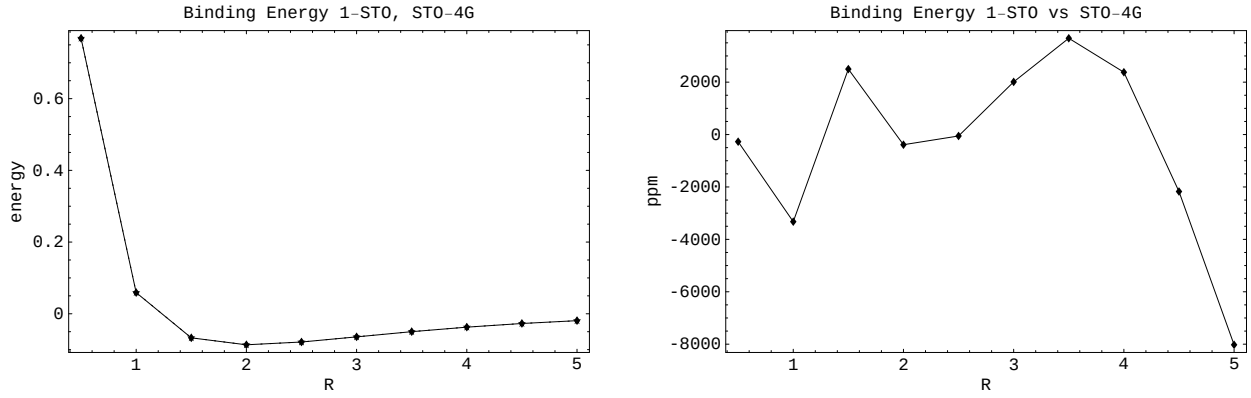

Figure 7.13 – Binding energy STO / STO-4G and errors in ppm

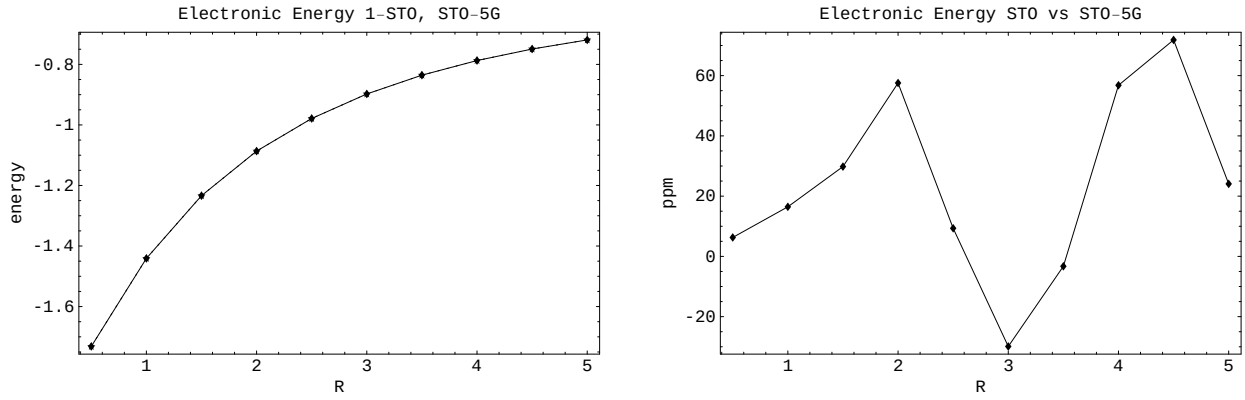

Figure 7.14 – Electronic energy STO / STO-5G and errors in ppm

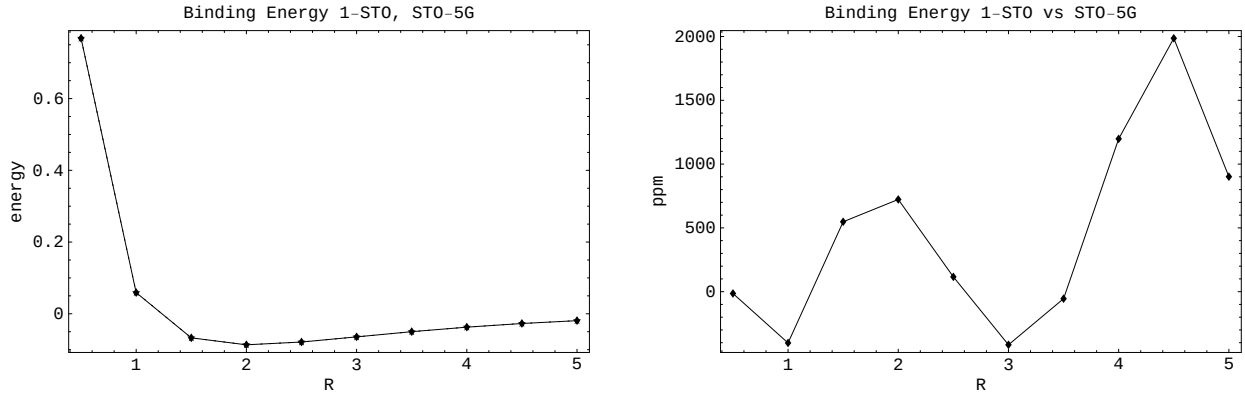

Figure 7.15 – Binding energy STO / STO-5G and errors in ppm

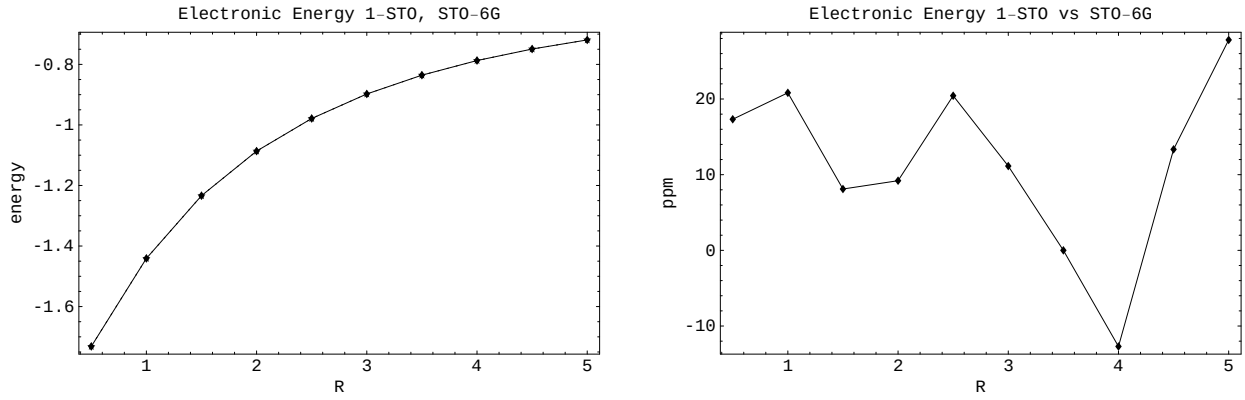

Figure 7.16 – Electronic energy STO / STO-6G and errors in ppm

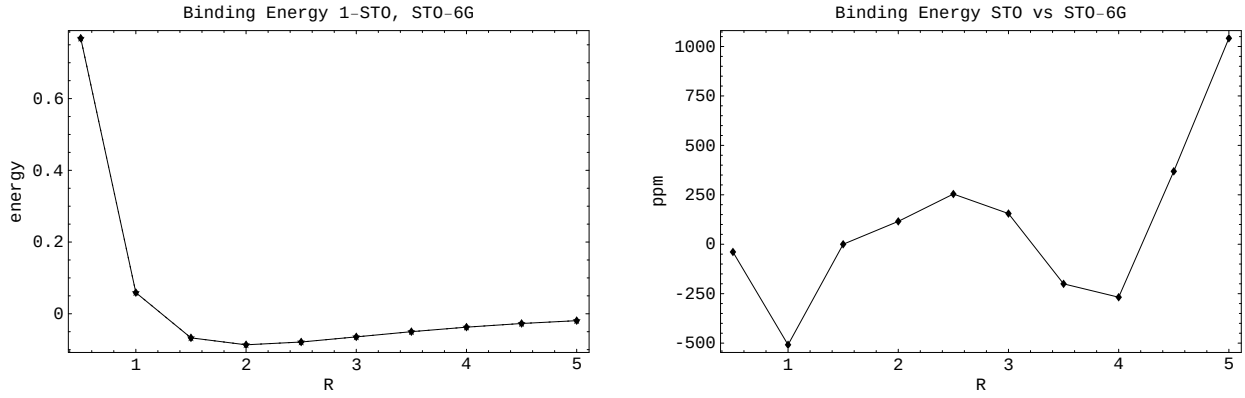

Figure 7.17 – Binding energy STO / STO-6G and errors in ppm

7.2 H_2 molecule with a single Slater Type Orbital

Starting with the simplest case, from the atomic orbital basis we have:

$$a(r_i) \,=\, \sqrt{\frac{\xi^3}{\pi}}\, exp\{-\xi\,|\,\mathbf{r}_i \,-\, \mathbf{a}\,|\,\},\;\; b(r_i) \,=\, \sqrt{\frac{\xi^3}{\pi}}\, exp\{-\xi\,|\,\mathbf{r}_i \,+\, \mathbf{a}\,|\,\} \tag{7.32}$$

$\mathbf{r_A} \,=\, \mathbf{a}$; $\mathbf{r_B} \,=\, -\mathbf{a}$

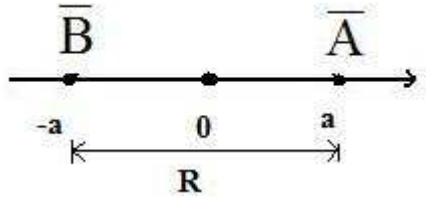

Figure 7.18 – H_2 settings

Using these, we take as test function for the H_2 molecule:

$$|\,\psi\rangle \,=\, \mathcal{N}\,[\,a(r_1)\cdot b(r_2) \,\pm\, b(r_1)\cdot a(r_2)\,] \tag{7.33}$$

We obtain at once the normalization:

$$\mathcal{N} \,=\, \frac{1}{\sqrt{2\,[\,1 \,\pm\, S^2]}} \tag{7.34}$$

Set:

$$\tilde{V}_i \equiv \frac{-1}{|\,\mathbf{r}_i - \mathbf{a}\,|} + \frac{-1}{|\,\mathbf{r}_i + \mathbf{a}\,|} = V_i(r_1) + V_i(r_2) \tag{7.35}$$

7.2.1 One body operators

We have:

$$\langle\psi\,|\,\tilde{V}_1 + \tilde{V}_2\,|\,\psi\rangle = \frac{1}{2\,[\,1 \pm S^2\,]}\cdot$$

$$\cdot\,\{\,a(r_1)\cdot b(r_2) \pm b(r_1)\cdot a(r_2)\,\}\,|\,\tilde{V}_1 + \tilde{V}_2\,|\,\cdot\,\{\,a(r_1)\cdot b(r_2) \pm b(r_1)\cdot a(r_2)\,\} \tag{7.36}$$

We have 8 terms, that can be reduced because of the symmetry for the coulombian interaction:

$$\langle\psi\,|\,\tilde{V}_1 + \tilde{V}_2\,|\,\psi\rangle = \langle\psi\,|\,+\frac{-1}{|\,\mathbf{r}_1 - \mathbf{a}\,|} + \frac{-1}{|\,\mathbf{r}_1 + \mathbf{a}\,|} + \frac{-1}{|\,\mathbf{r}_2 - \mathbf{a}\,|} + \frac{-1}{|\,\mathbf{r}_2 + \mathbf{a}\,|}\,|\,\psi\rangle =$$

$$= \frac{1}{2\,[\,1 \pm S^2\,]}\{\,a(r_1)\cdot b(r_2) \pm b(r_1)\cdot a(r_2)\,\}\cdot\{\left(\frac{-1}{|\,\mathbf{r}_1 - \mathbf{a}\,|} + \frac{-1}{|\,\mathbf{r}_1 + \mathbf{a}\,|}\right) +$$

$$+ \left(\frac{-1}{|\,\mathbf{r}_2 - \mathbf{a}\,|} + \frac{-1}{|\,\mathbf{r}_2 + \mathbf{a}\,|}\right)\}\cdot\{\,a(r_1)\cdot b(r_2) \pm b(r_1)\cdot a(r_2)\,\} = \tag{7.37}$$

= 16 terms which reduce to 8 =

$$= \frac{1}{(\,1 \pm S^2\,)}\{\,a(r_1)\cdot b(r_2) \pm b(r_1)\cdot a(r_2)\,\}\cdot\{\frac{-1}{|\,\mathbf{r}_1 - \mathbf{a}\,|} + \frac{-1}{|\,\mathbf{r}_1 + \mathbf{a}\,|}\}\cdot$$

$$\cdot\,\{\,a(r_1)\cdot b(r_2) \pm b(r_1)\cdot a(r_2)\,\} \tag{7.38}$$

= 4 terms for symmetry =

$$= \frac{2}{1 \pm S^2} \cdot \{\langle a \,|\, V_1 \,|\, a\rangle \pm \langle a \,|\, V_1 \,|\, b\rangle \cdot S + \langle a \,|\, V_2 \,|\, b\rangle \cdot S \pm \langle a \,|\, V_2 \,|\, a\rangle\} \tag{7.39}$$

We need 4 integrals that we already computed, see 7.16, 7.17, 7.18.

$$\langle a \,|\, V_1 \,|\, a\rangle = [\,3\,] = +\xi; \;\; \langle a \,|\, V_1 \,|\, b\rangle = [\,4\,] = +K \tag{7.40}$$

$$\langle a \,|\, V_2 \,|\, b\rangle = [\,4\,] = +K; \;\; \langle a \,|\, V_2 \,|\, a\rangle = [\,5\,] = +J \tag{7.41}$$

Then we have:

$$\langle \psi \,|\, \tilde{V}_1 + \tilde{V}_2 \,|\, \psi\rangle = \frac{2}{1 \pm S^2} \{ -\xi \pm 2K\,S + J\} \tag{7.42}$$

We must now add the kinetic energy:

$\langle \psi \,|\, T_1 + T_2 \,|\, \psi\rangle$ = (for simmetry) =

$$= \frac{2}{2\,(\,1 \pm S^2\,)} \{\, a(r_1) \cdot b(r_2) \pm b(r_1) \cdot a(r_2) \,\} \cdot$$

$$\cdot\,(-\frac{1}{2}\nabla_1^2)\,\{\,a(r_1)\cdot b(r_2)\,\pm\,b(r_1)\cdot a(r_2)\,\}\,= \tag{7.43}$$

$=$ (recalling that $\nabla_1^2 \,=\, \nabla_2^2 \,=\, \nabla^2$) $=$

$$= \frac{2}{(\,1\,\pm\,S^2\,)}\,\{\,\langle a\,|\,-\,\tfrac{1}{2}\nabla^2\,|\,a\rangle\,\pm\langle a\,|\,-\,\tfrac{1}{2}\nabla^2\,|\,b\rangle\,\cdot S\}\,=$$

$$= \frac{2}{(\,1\,\pm\,S^2\,)}\,\{\,[1]\,\pm\,[2]\,\cdot\,S\}\,=\,\frac{2}{(\,1\,\pm\,S\,)}\,\{\frac{1}{2}\,\xi^2\,\pm\,[-\frac{1}{2}\,\xi^2\cdot S\,-\,\xi\cdot K\,]\,S\,\} \tag{7.44}$$

Then the energy of the one body part of the H_2 is:

$$\langle\psi\,|\,E_1\,|\,\psi\rangle\,=\,\frac{2}{1\,\pm\,S^2}\,\{\,-\xi\,\pm\,2K\,S\,+\,J\}+$$

$$+\,\frac{2}{(\,1\,\pm\,S^2\,)}\,\{\frac{1}{2}\,\xi^2\,\pm\,[-\frac{1}{2}\,\xi^2\cdot S\,-\,\xi\cdot K\,]\,S\,\} \tag{7.45}$$

considering the + sign and taking S=1; R=0, we have:

$$\langle\psi\,|\,E_1^0\,|\,\psi\rangle\,=\,\xi^2\,-\,4\,\xi \tag{7.46}$$

We have a minimum for $\xi = 2$ and then $E_1^0 \,=\, -\,4$ as it must be.

We must now add the energy of the two bodies interaction.

7.2.2 Two bodies operators

$$\langle \psi \,|\, \frac{1}{r_{12}} \,|\, \psi \rangle \;=$$

$$= \frac{1}{2\,(\,1 \,\pm\, S^2\,)} \,\{\, a(r_1) \cdot b(r_2) \,\pm\, b(r_1) \cdot a(r_2) \,\} \cdot$$

$$\cdot \frac{1}{r_{12}} \,\{\, a(r_1) \cdot b(r_2) \,\pm\, b(r_1) \cdot a(r_2) \,\} \;= \tag{7.47}$$

= for the symmetries =

$$= \frac{1}{2\,(\,1 \,\pm\, S^2\,)} \,\{ \langle a(r_1) \cdot b(r_2) \,|\, \frac{1}{r_{12}} \,|\, a(r_1) \cdot b(r_2) \rangle \,\pm\, \langle a(r_1) \cdot b(r_2) \,|\, \frac{1}{r_{12}} \,|\, b(r_1) \cdot a(r_2) \rangle \} \tag{7.48}$$

7.3 H_2 molecule in Configurations Interaction S shell only

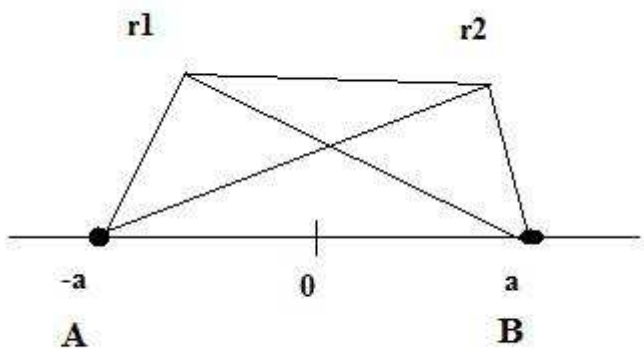

Figure 7.19 – H_2: definitions

Define the following single particle basis functions:

$$\phi_i(\mathbf{r}) = \sum_{ki=1}^{i} uc[\,i,\,1,\,ki\,] \cdot STO\,(\,r,\,ki\,),\ \ \{\,i\,=\,1,\,2,\,...,\,n\,\} \tag{7.49}$$

For the sake of simplicity we will assume that they are real.

Using these, we build **two** sets of single particle orbitals, that are orthonormal within each set but not mutually:

$$a_i(\mathbf{r}) \equiv \phi_i(\mathbf{r} - \mathbf{a});\quad b_i(\mathbf{r}) \equiv \phi_i(\mathbf{r} + \mathbf{a}) \tag{7.50}$$

We stress that we build the single particle orbitals using the $\phi_i(\mathbf{r})$, that are orthonormal by construction, and are centered at the points $\mathbf{A} \equiv \mathbf{a}$ and $\mathbf{B} \equiv -\mathbf{a}$.

Their superposition is given by the integral that we will shortly define; it reduces to δ_{ij} if $\mathbf{a} \equiv \mathbf{0}$, as the $\phi_i(\mathbf{r})$ are orthonormal by construction.

7.3.1 Example: superposition computation

Define:

$$SS\,(i,j) \;=\; \int d\mathbf{r}\, a_i(\mathbf{r}) \cdot b_j(\mathbf{r}) \;=$$

$$= \int d\mathbf{r}\, \phi_i(\,|\,\mathbf{r} \,-\, \mathbf{a}\,|\,) \cdot \phi_j(\,|\,\mathbf{r} \,+\, \mathbf{a}\,|\,) \;=$$

$$= \sum_{ki=1}^{i} \sum_{kj=1}^{j} uc\,[\,i,\,1,\,ki\,] \cdot uc\,[\,j,\,1,\,kj\,] \cdot$$

$$\cdot \int d\mathbf{r}\, STO(\,|\,\mathbf{r} \,-\, \mathbf{a}\,|\,, ki\,) \cdot STO(\,|\,\mathbf{r} \,+\, \mathbf{a}\,|\,, kj\,) \;=$$

$$= \sum_{ki=1}^{i} \sum_{kj=1}^{j} uc\,[\,i,\,1,\,ki\,] \cdot uc\,[\,j,\,1,\,kj\,] \cdot SK(\,ki,\,kj\,) \tag{7.51}$$

It is necessary to distinguish the $SS(i,\,j)$ and the $SK(ki,\,kj)$.

In the program SS(i,j) = ssij(i,j).

The $SK(ki,\,kj)$ depend on ξ and ng and are computed using the gaussian expansion..

Now we must build the Fock space for two particles.

In what follows, we will not write the summations in (i,j) and we will indicate just the kernels of the gaussian expansions for the explicit expressions of the $SK(ki, kj)$ and the potential and kinetic energy.

We will consider separately the case in which both particles use the basis in A, that is either the $a_i(\mathbf{r})$ or $b_i(\mathbf{r})$ orbitals, and the case in which one particle uses the $a_i(\mathbf{r})$ orbitals and the other the $b_i(\mathbf{r})$ orbitals.

The first case is identical with the Fock basis used for Helium (with the only difference that now the atom is H^-), both if only the $a_i(\mathbf{r})$ or only the $b_i(\mathbf{r})$ are used.

We denote I and II these two sets of states.

We are now interested in the case III, when one particle is described by the $a_i(\mathbf{r})$ orbital and the other by the $b_i(\mathbf{r})$. Of course it is required that the total wave function must be symmetrical or antisymmetrical.

Then the Fock space is given by (we will consider only the singlet case):

Symmetrical case (singlet)

In order to avoid too many cases, we will concentrate on the singlet.

The Slater permanents used to build the Fock space can be written: [1]

$$\langle \mathbf{r}_1,\, \mathbf{r}_2 \,|\, i,\, j \rangle \;=\; \mathcal{N}_{ij} \begin{bmatrix} a_i(\mathbf{r}_1) & b_j(\mathbf{r}_1) \\ a_i(\mathbf{r}_2) & b_j(\mathbf{r}_2) \end{bmatrix}_+ \;=$$

$$= \mathcal{N}_{ij} \left[\, a_i(\mathbf{r}_1) \cdot b_j(\mathbf{r}_2) \;+\; b_j(\mathbf{r}_1) \cdot a_i(\mathbf{r}_2) \,\right] \tag{7.52}$$

[1] In the program $\mathcal{N}_{ij} \;=\; anij(i,j)$

Imposing the normalization, the factor $\mathcal{N}_{ij}$ can be computed:

$\langle i,\, j \,|\, i,\, j\rangle \,=$

$= \mathcal{N}_{ij}^2 \int d\mathbf{r}_1 \int d\mathbf{r}_2 \,\{a_i(\mathbf{r}_1)\, b_j(\mathbf{r}_2) \,+\, b_j(\mathbf{r}_1) a_i(\mathbf{r}_2)\}\cdot$

$\cdot\{a_i(\mathbf{r}_1)\, b_j(\mathbf{r}_2) \,+\, b_j(\mathbf{r}_1) a_i(\mathbf{r}_2)\} \,=$

$$= \mathcal{N}_{ij}^2\, 2\,\{1 \,+\, SS(i,j)^2\,\} \,=\, 1 \tag{7.53}$$

then:

$$\mathcal{N}_{ij} \,=\, \frac{1}{\sqrt{2\,(\,1 \,+\, SS(i,j)^2\,)}} \tag{7.54}$$

In the program SS(i, j) = ssij(i, j).

Now we compute [2]

$\langle i,\, j \,|\, k,\, l\rangle \,=$

$= \mathcal{N}_{ij} \cdot \mathcal{N}_{kl} \int d\mathbf{r}_1 \int d\mathbf{r}_2 \,\{a_i(\mathbf{r}_1)\, b_j(\mathbf{r}_2) \,+\, b_j(\mathbf{r}_1) a_i(\mathbf{r}_2)\} \cdot \{a_k(\mathbf{r}_1)\, b_l(\mathbf{r}_2) \,+\, b_l(\mathbf{r}_1) a_k(\mathbf{r}_2)\} \,=$

$$= \,2\,\mathcal{N}_{ij} \cdot \mathcal{N}_{kl}\,\{\delta_{ik} \cdot \delta_{jl} \,+\, SS(i,l) \cdot SS(j,k)\,\} \tag{7.55}$$

Because the $SS(i,j)$ matrix is symmetrical.

The same computation is immediate for the antisymmetrical case and for the cases I+III, II+III, I+II.

[2] In the program $\langle i, j \,|\, k, l\rangle \,=\, sovr(k1, k2)$

Now we come to an important point.

In the simplest case one can use a set of non orthonormal functions, but then one has to solve a generalized eigenvalue problem.

We will orthonormalize the basis functions of the Fock space, greatly simplifying the problem of computing the eigenvalues of the Hamiltonian.

This can be achieved in a relatively simple way.

We note that sometimes in Quantum Chemistry the approximation of setting everywhere

$$SS(i,j) = \delta_{ij} \tag{7.56}$$

is used, that is of neglecting all the superpositions.

As all that we have seen up to this point indicates that the entanglement computation is easier than the energy's because fewer significant digits are required, it is interesting to evaluate how much this approximation is valid for the entanglement.

7.3.2 Potential matrix elements

Define:

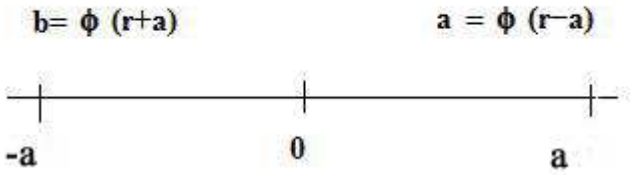

Figure 7.20 – Definitions

We will now compute the matrix elements for the single particle potential. We have:

$$\langle i,\, j \,|\, V \,|\, k,\, l \rangle \;\equiv$$

$$\equiv \mathcal{N}_{ij} \cdot \mathcal{N}_{kl} \int d\mathbf{r}_1 \int d\mathbf{r}_2 \,[a_i(\mathbf{r}_1)\, b_j(\mathbf{r}_2) \;+\; b_j(\mathbf{r}_1) a_i(\mathbf{r}_2)] \cdot$$

$$\cdot \left[\frac{-1}{|\,\mathbf{r_1} - \mathbf{a}\,|} + \frac{-1}{|\,\mathbf{r_1} + \mathbf{a}\,|} + \frac{-1}{|\,\mathbf{r_2} - \mathbf{a}\,|} + \frac{-1}{|\,\mathbf{r_2} + \mathbf{a}\,|} \right] \cdot$$

$$\cdot [a_k(\mathbf{r}_1)\, b_l(\mathbf{r}_2) \;+\; b_l(\mathbf{r}_1) a_k(\mathbf{r}_2)] \tag{7.57}$$

To simplify the formulas, we will not write the factor $\mathcal{N}_{ij} \cdot \mathcal{N}_{kl}$ until the final result.

We have 16 terms, which reduce to 8 for symmetry.

Writing symbolically:

$$\langle i, j \,|\, V \,|\, k, l \rangle \;=\; \langle \tilde{A} \;+\; \tilde{B} \,|\, \alpha \;+\; \beta \;+\; \gamma \;+\; \delta \,|\, \tilde{C} \;+\; \tilde{D} \rangle \tag{7.58}$$

we have:

$$\langle \tilde{A} \,|\, \alpha \,|\, \tilde{C} \rangle \;=\; [\,1\,] \;=\; \int a_i(\mathbf{r}) \frac{-1}{|\,\mathbf{r} - \mathbf{a}\,|}\, a_k(\mathbf{r})\, d\mathbf{r} \cdot \delta_{jl} \;=$$

$$= \int \phi_i(\mathbf{r} - \mathbf{a}) \frac{-1}{|\,\mathbf{r} - \mathbf{a}\,|}\, \phi_k(\mathbf{r} - \mathbf{a})\, d\mathbf{r} \cdot \delta_{jl} \;=$$

$$= \int \phi_i(\rho) \frac{-1}{\rho}\, \phi_k(\rho)\, d\rho \cdot \delta_{jl} \;=\; VV(\,i,\, k\,) \cdot \delta_{jl} \tag{7.59}$$

$$\langle \tilde{B} \,|\, \gamma \,|\, \tilde{D} \rangle \;=\; [\,2\,] \;=\; \int a_i(\mathbf{r}) \frac{-1}{|\,\mathbf{r} - \mathbf{a}\,|}\, a_k(\mathbf{r})\, d\mathbf{r} \cdot \delta_{jl} \;\equiv\; [\,1\,] \tag{7.60}$$

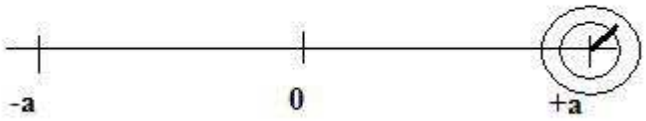

Figure 7.21 – [1]=[2] VV(i,k): the circles represent the orbitals $\phi_i(\mathbf{r}-\mathbf{a})$, $\phi_k(\mathbf{r}-\mathbf{a})$, the thick line the vector **r-a**

$$\langle \tilde{A} \,|\, \delta \,|\, \tilde{C} \rangle \;=\; [\,7\,] \;=\; \int b_j(\mathbf{r}) \, \frac{-1}{|\,\mathbf{r}\,+\,\mathbf{a}\,|} \, b_l(\mathbf{r}) \, d\mathbf{r} \cdot \delta_{ik} \;=$$

$$= \int \phi_j(\mathbf{r}\,+\,\mathbf{a}) \, \frac{-1}{|\,\mathbf{r}\,+\,\mathbf{a}\,|} \, \phi_l(\mathbf{r}\,+\,\mathbf{a}) \, d\mathbf{r} \cdot \delta_{ik} \;=\; VV(\,j,\,l\,) \cdot \delta_{ik} \tag{7.61}$$

$$\langle \tilde{B} \,|\, \beta \,|\, \tilde{D} \rangle \;=\; [\,8\,] \;=\; \int b_j(\mathbf{r}) \, \frac{-1}{|\,\mathbf{r}\,+\,\mathbf{a}\,|} \, b_l(\mathbf{r}) \, d\mathbf{r} \cdot \delta_{ik} \;\equiv\; [\,7\,] \tag{7.62}$$

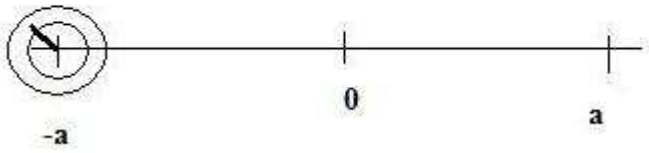

Figure 7.22 – [7]=[8] VV(j,l): the circles represent the orbitals $\phi_j(\mathbf{r}+\mathbf{a})$, $\phi_l(\mathbf{r}+\mathbf{a})$, the thick line the vector **r+a**

The kernel of the gaussian expansion can be written:

$$[1] = [2] = [7] = [8] = VG(m,n) = \mathcal{N}_m \mathcal{N}_n \frac{2\pi}{\alpha_m + \alpha_n} \tag{7.63}$$

$$\langle \tilde{A} \,|\, \beta \,|\, \tilde{C} \rangle = [3] = \int a_i(\mathbf{r}) \frac{-1}{|\,\mathbf{r} + \mathbf{a}\,|} a_k(\mathbf{r})\, d\mathbf{r} \cdot \delta_{jl} =$$

$$= \int \phi_i(\mathbf{r} - \mathbf{a}) \frac{-1}{|\,\mathbf{r} + \mathbf{a}\,|} \phi_k(\mathbf{r} - \mathbf{a})\, d\mathbf{r} \cdot \delta_{jl} = JJ(\,i,\, k\,) \cdot \delta_{jl} \tag{7.64}$$

$$\langle \tilde{B} \,|\, \delta \,|\, \tilde{D} \rangle = [4] = \int a_i(\mathbf{r}) \frac{-1}{|\,\mathbf{r} + \mathbf{a}\,|} a_k(\mathbf{r})\, d\mathbf{r} \cdot \delta_{jl} \equiv [3] \tag{7.65}$$

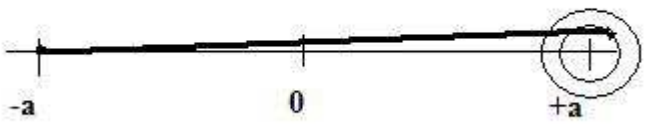

Figure 7.23 – [3]=[4] JJ(i,k): the circles represent the orbitals $\phi_i(\mathbf{r}-\mathbf{a})$, $\phi_k(\mathbf{r}-\mathbf{a})$, the thick line the vector $\mathbf{r}+\mathbf{a}$

$$\langle \tilde{A} \,|\, \gamma \,|\, \tilde{C} \rangle = [5] = \int b_j(\mathbf{r}) \frac{-1}{|\,\mathbf{r} - \mathbf{a}\,|} b_l(\mathbf{r})\, d\mathbf{r} \cdot \delta_{ik} =$$

$$= \int \phi_j(\mathbf{r} + \mathbf{a}) \frac{-1}{|\,\mathbf{r} - \mathbf{a}\,|} \phi_l(\mathbf{r} + \mathbf{a})\, d\mathbf{r} \cdot \delta_{ik} = JJ(\,j,\, l\,) \cdot \delta_{ik} \tag{7.66}$$

$$\langle \tilde{B} \,|\, \alpha \,|\, \tilde{D} \rangle = [6] = \int b_j(\mathbf{r}) \frac{-1}{|\,\mathbf{r} - \mathbf{a}\,|} b_l(\mathbf{r})\, d\mathbf{r} \cdot \delta_{ik} \equiv [5] \tag{7.67}$$

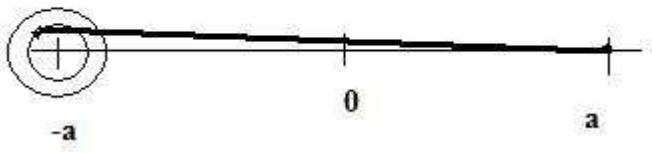

Figure 7.24 – [5]=[6] JJ(j,l): the circles represent the orbitals $\phi_j(\mathbf{r}+\mathbf{a})$, $\phi_l(\mathbf{r}+\mathbf{a})$, the thick line the vector **r-a**

The kernel of the gaussian expansion can be written:

$$[3] \,=\, [4] \,=\, [5] \,=\, [6] \,=\, JG(m,n) \,=$$

$$=\, \mathcal{N}_m \mathcal{N}_n \, \frac{2\pi}{\alpha_m \,+\, \alpha_n} \,\cdot\, F_0[\,(\alpha_m \,+\, \alpha_n) r^2\,] \tag{7.68}$$

$$\langle \tilde{A}\,|\,\gamma\,|\,\tilde{D}\rangle \,=\, [\,13\,] \,=\, \int b_j(\mathbf{r})\, \frac{-1}{|\,\mathbf{r} \,-\, \mathbf{a}\,|}\, a_k(\mathbf{r})\, d\mathbf{r} \cdot\; SS(i,l) \,=$$

$$=\, \int \phi_j(\mathbf{r} \,+\, \mathbf{a})\, \frac{-1}{|\,\mathbf{r} \,-\, \mathbf{a}\,|}\, \phi_k(\mathbf{r} \,-\, \mathbf{a})\, d\mathbf{r} \cdot\; SS(i,l) \,=\, KK2(\,\underline{k},\, j\,) \cdot SS(\,i,\, l\,) \tag{7.69}$$

$$\langle \tilde{B}\,|\,\alpha\,|\,\tilde{C}\rangle \,=\, [\,14\,] \,=\, \int b_j(\mathbf{r})\, \frac{-1}{|\,\mathbf{r} \,-\, \mathbf{a}\,|}\, a_k(\mathbf{r})\, d\mathbf{r} \cdot\; SS(i,l) \,\equiv\, [\,13\,] \tag{7.70}$$

$$\langle \tilde{A}\,|\,\alpha\,|\,\tilde{D}\rangle \,=\, [\,9\,] \,=\, \int a_i(\mathbf{r})\, \frac{-1}{|\,\mathbf{r} \,-\, \mathbf{a}\,|}\, b_l(\mathbf{r})\, d\mathbf{r} \cdot\; SS(j,k) \,=$$

$$=\, \int \phi_i(\mathbf{r} \,-\, \mathbf{a})\, \frac{-1}{|\,\mathbf{r} \,-\, \mathbf{a}\,|}\, \phi_l(\mathbf{r} \,+\, \mathbf{a})\, d\mathbf{r} \cdot\; SS(j,k) \,=\, KK1(\,\underline{i},\, l\,) \cdot SS(\,j,\, k\,) \tag{7.71}$$

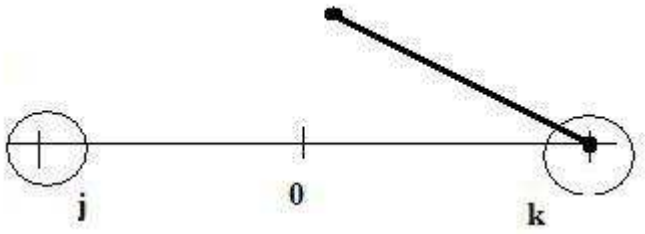

Figure 7.25 – [13]=[14] KK1(k,j: the circles represent the orbitals $\phi_j(\mathbf{r}+\mathbf{a})$, $\phi_k(\mathbf{r}-\mathbf{a})$, the thick line the vector **r-a**

$$\langle \tilde{B} \,|\, \gamma \,|\, \tilde{C} \rangle \;=\; [\,10\,] \;=\; \int a_i(\mathbf{r})\, \frac{-1}{|\,\mathbf{r}\,-\,\mathbf{a}\,|}\, b_l(\mathbf{r})\, d\mathbf{r} \cdot \; SS(j,k) \;\equiv\; [\,9\,] \tag{7.72}$$

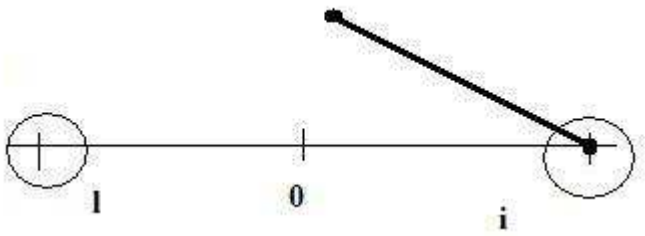

Figure 7.26 – [9]=[10] KK1(i,l): the circles represent the orbitals $\phi_i(\mathbf{r}-\mathbf{a})$, $\phi_l(\mathbf{r}+\mathbf{a})$, the thick line the vector **r-a**

The kernel of the gaussian expansion can be written:

$$[9] \;=\; [10] \;=\; KG1(m,n) \;=$$

$$= \mathcal{N}_m \mathcal{N}_n\, \frac{2\pi}{\alpha_m \,+\, \alpha_n} \;\cdot\; exp[\,-\,\frac{\alpha_m \,\cdot\, \alpha_n}{\alpha_m \,+\, \alpha_n}\, r^2\,] \;\cdot\; F_0[\,-\,\frac{\alpha_n^2}{\alpha_m \,+\, \alpha_n}\, r^2\,] \tag{7.73}$$

$$\langle \tilde{A} \,|\, \delta \,|\, \tilde{D} \rangle \;=\; [\,15\,] \;=\; \int b_j(\mathbf{r})\, \frac{-1}{|\,\mathbf{r}\,+\,\mathbf{a}\,|}\, a_k(\mathbf{r})\, d\mathbf{r} \cdot \; SS(i,l) \;=$$

$$= \int \phi_j(\mathbf{r}+\mathbf{a})\,\frac{-1}{|\,\mathbf{r}+\mathbf{a}\,|}\,\phi_k(\mathbf{r}-\mathbf{a})\,d\mathbf{r}\cdot\ SS(i,l) \;=\; KK2(\,\underline{j},\,k\,)\cdot SS(\,i,\,l\,) \qquad (7.74)$$

$$\langle\tilde{B}\,|\,\beta\,|\,\tilde{C}\rangle \;=\; [\,16\,] \;=\; \int b_j(\mathbf{r})\,\frac{-1}{|\,\mathbf{r}+\mathbf{a}\,|}\,a_k(\mathbf{r})\,d\mathbf{r}\cdot\ SS(i,l) \;\equiv\; [\,15\,] \qquad (7.75)$$

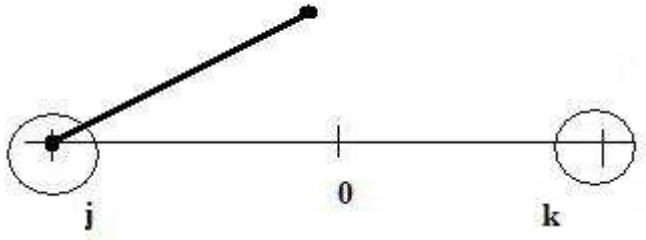

Figure 7.27 – [15]=[16] KK2(j,k): the circles represent the orbitals $\phi_j(\mathbf{r}+\mathbf{a})$, $\phi_k(\mathbf{r}-\mathbf{a})$, the thick line the vector $\mathbf{r}+\mathbf{a}$

$$\langle\tilde{B}\,|\,\delta\,|\,\tilde{C}\rangle \;=\; [\,11\,] \;=\; \int a_i(\mathbf{r})\,\frac{-1}{|\,\mathbf{r}+\mathbf{a}\,|}\,b_l(\mathbf{r})\,d\mathbf{r}\cdot\ SS(j,k) \;=$$

$$= \int \phi_i(\mathbf{r}-\mathbf{a})\,\frac{-1}{|\,\mathbf{r}+\mathbf{a}\,|}\,\phi_l(\mathbf{r}+\mathbf{a})\,d\mathbf{r}\cdot\ SS(j,k) \;=\; KK2(\,\underline{l},\,i\,)\cdot SS(\,j,\,k\,) \qquad (7.76)$$

$$\langle\tilde{A}\,|\,\beta\,|\,\tilde{D}\rangle \;=\; [\,12\,] \;=\; \int a_i(\mathbf{r})\,\frac{-1}{|\,\mathbf{r}+\mathbf{a}\,|}\,b_l(\mathbf{r})\,d\mathbf{r}\cdot\ SS(j,k) \;=$$

$$= \int \phi_i(\mathbf{r}-\mathbf{a})\,\frac{-1}{|\,\mathbf{r}+\mathbf{a}\,|}\,\phi_l(\mathbf{r}+\mathbf{a})\,d\mathbf{r}\cdot\ SS(j,k) \;\equiv\; [\,11\,] \qquad (7.77)$$

The kernel of the gaussian expansion can be written:

$$[11] \;=\; [12] \;=\; KG2(m,n) \;=$$

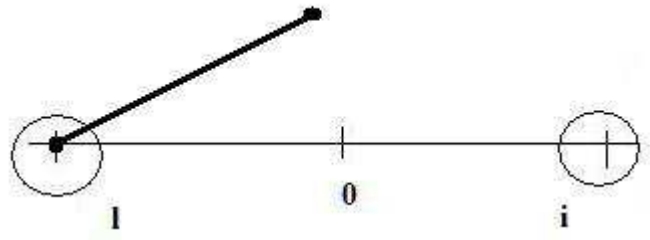

Figure 7.28 – [11]=[12] KK2(l,i): the circles represent the orbitals $\phi_i(\mathbf{r}-\mathbf{a})$, $\phi_l(\mathbf{r}+\mathbf{a})$, the thick line the vector $\mathbf{r}+\mathbf{a}$

$$= \mathcal{N}_m\mathcal{N}_n \frac{2\pi}{\alpha_m + \alpha_n} \cdot exp[-\frac{\alpha_m \cdot \alpha_n}{\alpha_m + \alpha_n} r^2] \cdot F_0[-\frac{\alpha_m^2}{\alpha_m + \alpha_n} r^2] \tag{7.78}$$

Now we must compare the integrals KK1 and KK2 for the same indexes.

We have:

$$\begin{cases} KK1(i,\, j) \,=\, \int \phi_i(\mathbf{r} - \mathbf{a}) \dfrac{-1}{|\mathbf{r} - \mathbf{a}|} \phi_j(\mathbf{r} + \mathbf{a})\, d\mathbf{r} \\ KK2(i,\, j) \,=\, \int \phi_i(\mathbf{r} + \mathbf{a}) \dfrac{-1}{|\mathbf{r} + \mathbf{a}|} \phi_j(\mathbf{r} - \mathbf{a})\, d\mathbf{r} \end{cases} \tag{7.79}$$

Changing variables we have:

$$\begin{cases} KK1(i,\, j) \,=\, \int \phi_i(\rho) \dfrac{-1}{|\rho|} \phi_j(\rho + 2\mathbf{a})\, d\rho \\ KK2(i,\, j) \,=\, \int \phi_i(\rho) \dfrac{-1}{|\rho|} \phi_j(\rho - 2\mathbf{a})\, d\rho \end{cases} \tag{7.80}$$

As in the S shell the ϕ_i have a spherical symmetry, we have

$$KK1(\,i,\, j\,) \,=\, KK2(\,i,\, j) \tag{7.81}$$

Inserting again the normalization factor, the 16 terms, reduced to 8 thanks to the symmetry, can be written

$$\{[1]...[16]\} = \mathcal{N}_{ij} \cdot \mathcal{N}_{kl} \cdot 2 \cdot \{VV(i,\,k) \cdot \delta_{jl} + VV(j,\,l) \cdot \delta_{ik} +$$

$$+ JJ(i,\,k) \cdot \delta_{jl} + JJ(j,\,l) \cdot \delta_{ik} +$$

$$+ [KK1(\underline{i},\,l) + KK1(\underline{l},\,i)] \cdot SS(j,\,k) +$$

$$+ [KK2(\underline{k},\,j) + KK2(\underline{j},\,k)] \cdot SS(i,\,l)\} \tag{7.82}$$

In the program we have:

VV(i, j) = aij3(i, j)

JJ(i, j) = ajjij(i, j)

KK1(i, j) = KK2(i, j) = aaij(i, j)

SS(i, j) = ssij(i, j)

$\mathcal{N}_{ij}$ = anij(i, j)

7.3.3 Case i=j=k=l=1

$$\{\,[\,1\,]\,...\,[\,16\,]\,\} \,=\, \mathcal{N}_{11}\cdot\mathcal{N}_{11}\cdot 2\cdot\{\,2VV(1,1)\,+\,2JJ(1,1)\,+\,4KK(1,1)\}\,=$$

$$=\mathcal{N}_{11}\cdot\mathcal{N}_{11}\cdot 4\cdot\{VV\,+\,JJ\,+\,2\,KK\,\cdot\,SS\} \tag{7.83}$$

that agrees with the computations for a single STO.

Inserting again the normalization factor for the one body electronic energy, we have:

$$E_1 \,=\, \frac{2}{1\,+\,S^2}\,\{\,VV\,+\,JJ\,+\,2\,KK\,\cdot\,SS\,\} \tag{7.84}$$

7.3.4 Kinetic Energy

$\langle i,\,j\,|\,T_1\,+\,T_2\,|\,k,\,l\rangle\,\equiv$

$$\equiv \mathcal{N}_{ij}\cdot\mathcal{N}_{kl}\int d\mathbf{r}_1\int d\mathbf{r}_2\,[a_i(\mathbf{r}_1)\,b_j(\mathbf{r}_2)\,+\,b_j(\mathbf{r}_1)a_i(\mathbf{r}_2)]\cdot$$

$$\cdot\left[-\frac{1}{2}\,\nabla_1^2\,-\,\frac{1}{2}\,\nabla_2^2\right]\,\cdot\,[a_k(\mathbf{r}_1)\,b_l(\mathbf{r}_2)\,+\,b_l(\mathbf{r}_1)a_k(\mathbf{r}_2)]\,= \tag{7.85}$$

We hawe 8 terms which reduce to 4 for symmetry

$$= \mathcal{N}_{ij} \cdot \mathcal{N}_{kl} \{ [1] + ... + [8] \} \tag{7.86}$$

$$[1] = \int d\mathbf{r}_1 \int d\mathbf{r}_2 \, a_i(\mathbf{r}_1) \, b_j(\mathbf{r}_2) \, [-\frac{1}{2} \nabla_1^2] \, a_k(\mathbf{r}_1) b_l(\mathbf{r}_2) \tag{7.87}$$

$$[2] = \int d\mathbf{r}_1 \int d\mathbf{r}_2 \, a_i(\mathbf{r}_1) \, b_j(\mathbf{r}_2) \, [-\frac{1}{2} \nabla_1^2] \, b_l(\mathbf{r}_1) a_k(\mathbf{r}_2) \tag{7.88}$$

$$[3] = \int d\mathbf{r}_1 \int d\mathbf{r}_2 \, b_j(\mathbf{r}_1) \, a_i(\mathbf{r}_2) \, [-\frac{1}{2} \nabla_1^2] \, a_k(\mathbf{r}_1) b_l(\mathbf{r}_2) \tag{7.89}$$

$$[4] = \int d\mathbf{r}_1 \int d\mathbf{r}_2 \, b_j(\mathbf{r}_1) \, a_i(\mathbf{r}_2) \, [-\frac{1}{2} \nabla_1^2] \, b_l(\mathbf{r}_1) a_k(\mathbf{r}_2) \tag{7.90}$$

$$[5] = \int d\mathbf{r}_1 \int d\mathbf{r}_2 \, a_i(\mathbf{r}_1) \, b_j(\mathbf{r}_2) \, [-\frac{1}{2} \nabla_2^2] \, a_k(\mathbf{r}_1) b_l(\mathbf{r}_2) \tag{7.91}$$

$$[6] = \int d\mathbf{r}_1 \int d\mathbf{r}_2 \, a_i(\mathbf{r}_1) \, b_j(\mathbf{r}_2) \, [-\frac{1}{2} \nabla_2^2] \, b_l(\mathbf{r}_1) a_k(\mathbf{r}_2) \tag{7.92}$$

$$[7] = \int d\mathbf{r}_1 \int d\mathbf{r}_2 \, b_j(\mathbf{r}_1) \, a_i(\mathbf{r}_2) \, [-\frac{1}{2} \nabla_2^2] \, a_k(\mathbf{r}_1) b_l(\mathbf{r}_2) \tag{7.93}$$

$$[\,8\,] \;=\; \int d\mathbf{r}_1 \int d\mathbf{r}_2\, b_j(\mathbf{r}_1)\, a_i(\mathbf{r}_2)\, [\,-\frac{1}{2}\,\nabla_2^2\,]\, b_l(\mathbf{r}_1) a_k(\mathbf{r}_2) \tag{7.94}$$

These are pairwise identical

$[\,1\,] = [\,8\,]; \qquad [\,2\,] = [\,7\,];$

$[\,3\,] = [\,6\,]; \qquad [\,4\,] = [\,5\,];$

$$[\,1\,] \;=\; \int d\mathbf{r}_1\, a_i(\mathbf{r}_1)\, [\,-\frac{1}{2}\,\nabla_1^2\,]\, a_k(\mathbf{r}_1)\delta_{jl} \tag{7.95}$$

$$[\,2\,] \;=\; \int d\mathbf{r}_1\, a_i(\mathbf{r}_1)\, [\,-\frac{1}{2}\,\nabla_1^2\,]\, b_l(\mathbf{r}_1) SS(j,k) \tag{7.96}$$

$$[\,3\,] \;=\; \int d\mathbf{r}_1\, b_j(\mathbf{r}_1)\, [\,-\frac{1}{2}\,\nabla_1^2\,]\, a_k(\mathbf{r}_1) SS(i,l) \tag{7.97}$$

$$[\,4\,] \;=\; \int d\mathbf{r}_1\, b_j(\mathbf{r}_1)\, [\,-\frac{1}{2}\,\nabla_1^2\,]\, b_l(\mathbf{r}_1)\delta_{ik} \tag{7.98}$$

Inserting again the normalization factor, we have:

$\langle i,\, j\,|\, T_1 \,+\, T_2\,|\, k,\, l\rangle \;=$

$= \mathcal{N}_{ij} \cdot \mathcal{N}_{kl}\, 2\,\{ \int\, d\mathbf{r}_1\, a_i(\mathbf{r}_1)\, [\,-\frac{1}{2}\,\nabla_1^2\,]\, a_k(\mathbf{r}_1)\delta_{jl} +$

$$+ \int d\mathbf{r}_1\, a_i(\mathbf{r}_1)\,[\,-\frac{1}{2}\,\nabla_1^2\,]\,b_l(\mathbf{r}_1)SS(j,k) +$$

$$+ \int d\mathbf{r}_1\, b_j(\mathbf{r}_1)\,[\,-\frac{1}{2}\,\nabla_1^2\,]\,a_k(\mathbf{r}_1)SS(i,l) +$$

$$+ \int d\mathbf{r}_1\, b_j(\mathbf{r}_1)\,[\,-\frac{1}{2}\,\nabla_1^2\,]\,b_l(\mathbf{r}_1)\delta_{ik}\,\} \tag{7.99}$$

We must compute the four integrals:

$$[\,1\,] \;=\; \int d\mathbf{r}_1\, a_i(\mathbf{r}_1)\,[\,-\frac{1}{2}\,\nabla_1^2\,]\,a_k(\mathbf{r}_1) \tag{7.100}$$

$$[\,2\,] \;=\; \int d\mathbf{r}_1\, a_i(\mathbf{r}_1)\,[\,-\frac{1}{2}\,\nabla_1^2\,]\,b_l(\mathbf{r}_1) \tag{7.101}$$

$$[\,3\,] \;=\; \int d\mathbf{r}_1\, b_j(\mathbf{r}_1)\,[\,-\frac{1}{2}\,\nabla_1^2\,]\,a_k(\mathbf{r}_1) \tag{7.102}$$

$$[\,4\,] \;=\; \int d\mathbf{r}_1\, b_j(\mathbf{r}_1)\,[\,-\frac{1}{2}\,\nabla_1^2\,]\,b_l(\mathbf{r}_1) \tag{7.103}$$

We report just the kernels of the gaussian expansions

$$[\,1\,] \;=\; [\,4\,] \;=\; T_1(m,\,n) \;=$$

$$= \mathcal{N}_m\mathcal{N}_n\,\left[\frac{\pi}{\alpha_m \,+\, \alpha_n}\right]^{3/2} \cdot\, \frac{\alpha_m \,\cdot\, \alpha_n}{\alpha_m \,+\, \alpha_n}\,\cdot 3 \tag{7.104}$$

$$[2] = [3] = T_2(m, n) = \mathcal{N}_m \mathcal{N}_n \left[\frac{\pi}{\alpha_m + \alpha_n}\right]^{3/2} \cdot$$

$$\cdot \frac{\alpha_m \cdot \alpha_n}{\alpha_m + \alpha_n} \cdot exp\left\{\frac{\alpha_m \cdot \alpha_n}{\alpha_m + \alpha_n} \cdot r^2\right\} \cdot \left[3 - 2\frac{\alpha_m \cdot \alpha_n}{\alpha_m + \alpha_n} \cdot r^2\right] \tag{7.105}$$

Then we have:

$$\langle i, j \,|\, T_1 + T_2 \,|\, k, l\rangle = \mathcal{N}_{ij} \cdot \mathcal{N}_{kl} \cdot 2 \cdot \{TT1(i, k) \cdot \delta_{jl} + TT1(j, l) \cdot \delta_{ik} +$$

$$TT2(i, l) \cdot SS(j, k) + TT2(j, k) \cdot SS(i, l)\,\} \tag{7.106}$$

7.4 H_2 molecule: preliminary results

In fig. 7.29 we report some preliminary results of the H_2 computation, using 1 STO approximated by 6 gaussians, compared to standard data from (Sharp , 1971).

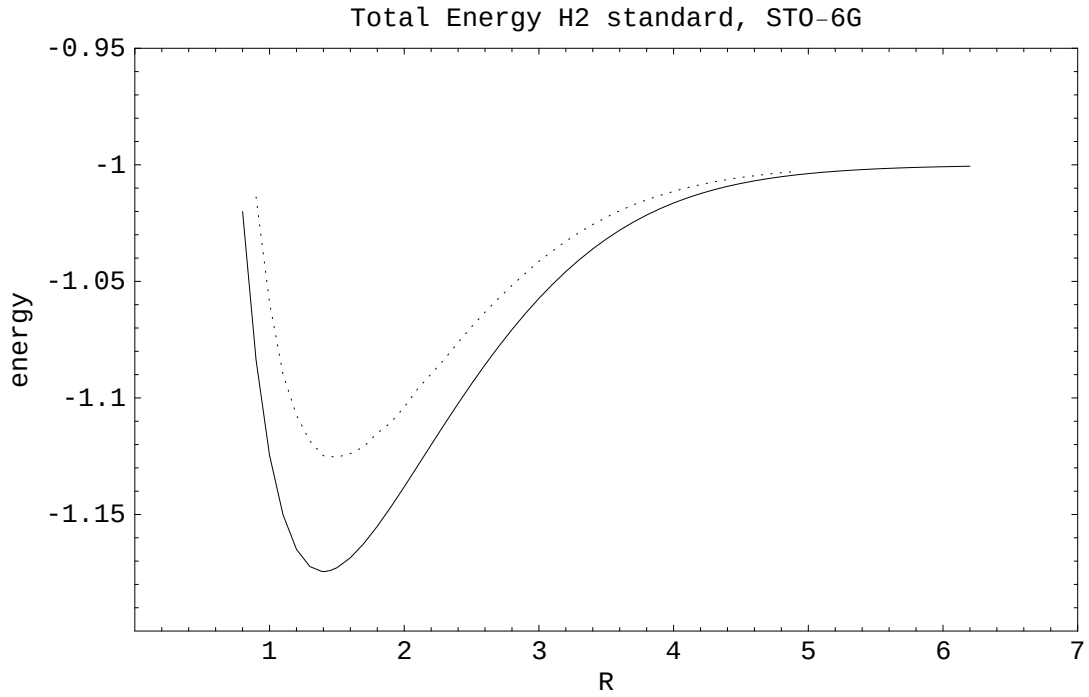

Figure 7.29 – H_2 standard energy (continous line) and energy of 1S-6G

7.4.1 Comparison of H_2 to Helium computations

It is important to compare the results obtained for Helium using a small Hilbert space dimension with those for the H_2 molecule, because we will perform only computations

n	aa1s	Energy	Δ E	EvN	Elin
1	1.687	-2.847656	19309	-	-
2	1.700	-2.860467	14897	0.0344702	0.007189
3	1.900	-2.878305	8754	0.041507	0.008793
4	2.000	-2.878598	8653	0.041210	0.008729
5	2.155	-2.878886	8554	0.041314	0.008741

Table 7.7 – He, Singlet, fundamental level, small n

with small n values at the beginning.

It is of paramount importance to evaluate the speed of convergence for several values of n, and to compare the energy and entropy convergence rates.

From the table inspection, we note energy converges to an approximate value by increaing n for a fixed number of shells and at the same time entropy converges to an approximate value, too.

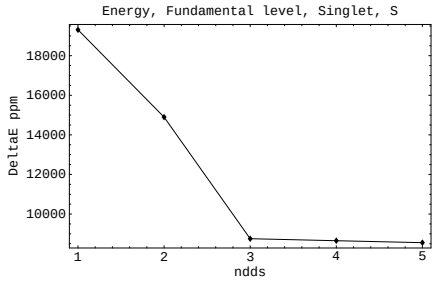

Figure 7.30 – He small n, Energy errors Singlet fundamental level

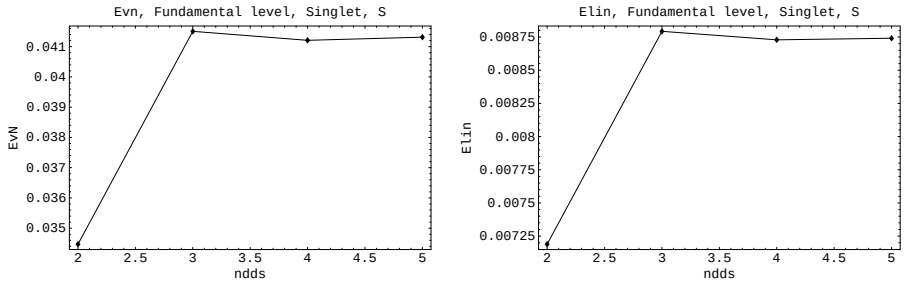

Figure 7.31 – He small n, vN and linear Entropy Singlet fundamental level

In table 7.8, 7.10, 7.12 we compare the results obtained with the Helium computations with those obtained for the H_2 molecule using 1 to 6 gaussian functions and setting the nuclei separation R=0.

	n of gaussian functions						Helium
nnzz	1	2	3	4	5	6	
1	-2.300738	-2.701896	-2.807592	-2.835561	-2.843615	-2.846140	-2.847656
2	-2.506908	-2.770979	-2.826518	-2.848755	-2.856683	-2.859137	-2.860467
3	-2.703910	-2.805933	-2.851666	-2.869493	-2.875258	-2.877178	-2.878305
4	-2.778315	-2.832704	-2.861129	-2.870708	-2.876416	-2.877704	-2.878598
5	-	-2.861246	-2.865119	-2.872408	-2.877225	-2.878190	-2.878886

Table 7.8 – Fundamental level, comparison He vs. H_2 with R=0

n	aa1s	Energy	Δ E	EvN	Elin
3	1.000	-2.068352	36171	0.963958	0.474128
4	1.000	-2.131621	6688	0.981350	0.485558
5	1.021	-2.140920	2355	0.982247	0.486323
6	1.024	-2.143794	1015	0.983651	0.487367
7	1.014	-2.144031	905	0.983769	0.487452

Table 7.9 – He, Singlet, level I, small n

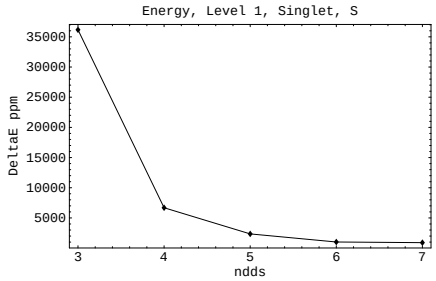

Figure 7.32 – He small n, Energy errors Singlet level I

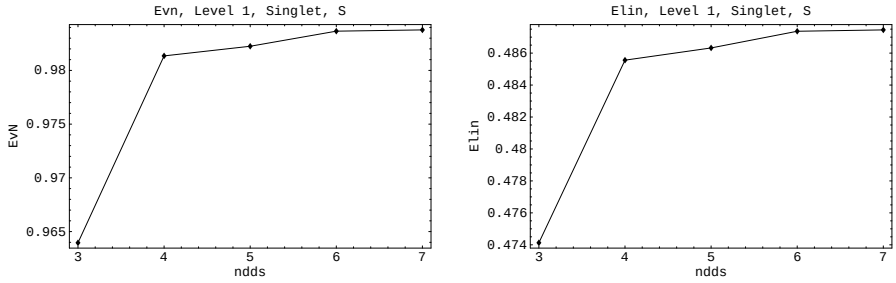

Figure 7.33 – He small n, vN and linear Entropy Singlet level I

	n of gaussian functions						Helium
nnzz	1	2	3	4	5	6	
3	-1.616379	-1.833382	-1.987778	-2.049313	-2.057556	-2.065176	-2.068352
4	-1.811976	-1.988719	-2.048273	-2.114224	-2.119848	-2.128268	-2.131621
5	-	-1.997665	-2.073578	-2.123437	-2.128179	-2.136767	-2.140920

Table 7.10 – Level I, comparison He vs. H_2 with R=0

n	aa1s	Energy	Δ E	EvN	Elin
4	0.800	-1.927450	64922	0.971522	0.479204
5	0.786	-2.024148	18009	0.991662	0.493014
6	0.771	-2.047362	6748	0.993328	0.494585
7	0.76	-2.057126	2011	0.995553	0.496292

Table 7.11 – He, Singlet, level II, small n

	n of gaussian functions						Helium
nnzz	1	2	3	4	5	6	
4	-1.451170	-1.609448	-1.779578	-1.897773	-1.907056	-1.921834	-1.927450
5	sballa	-1.637995	-1.864085	-1.996167	-1.997864	-2.017370	-2.024148

Table 7.12 – Level II, comparison He vs. H_2 with R=0

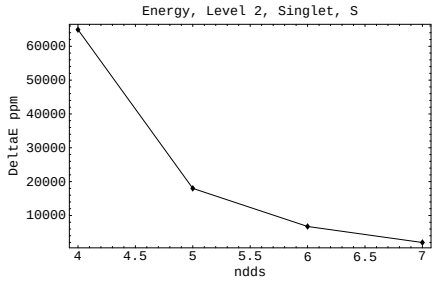

Figure 7.34 – He small n, Energy errors Singlet level II

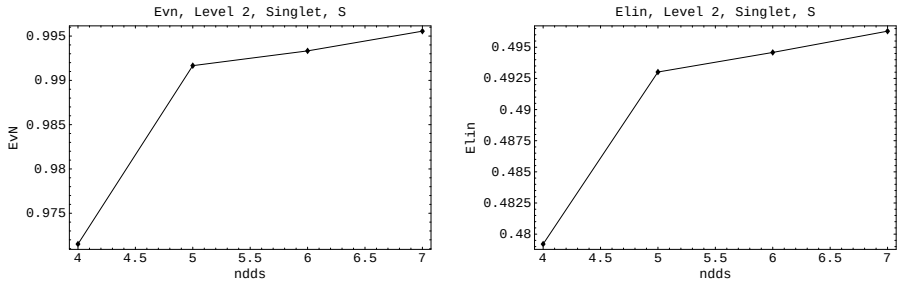

Figure 7.35 – He small n, vN and linear Entropy Singlet level II

Figures 7.36 and 7.37 demonstrate the convergence rate of energy for R=0, fundamental to III level singlet, for several values of the number n of STOs and the number m of gaussians used.

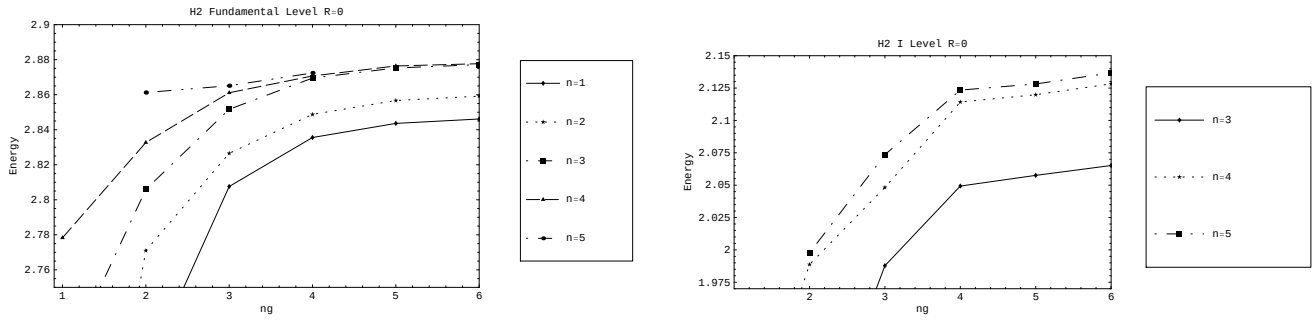

Figure 7.36 – Fundamental and I level nS-mG energy R=0

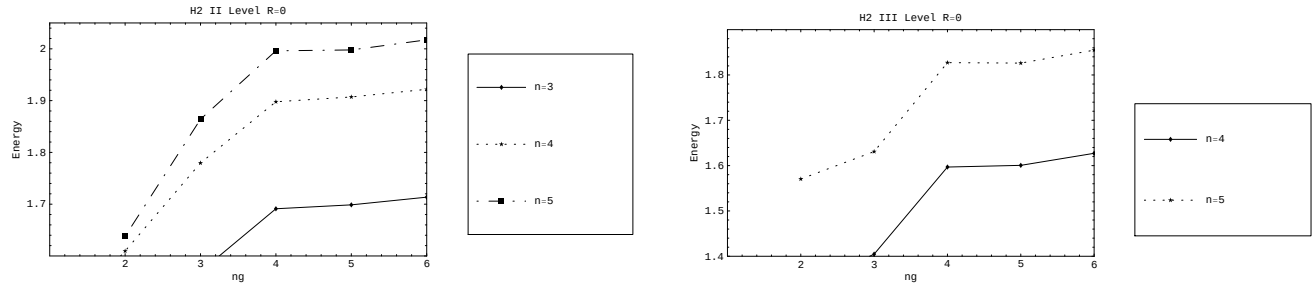

Figure 7.37 – II and III levels nS-mG energy R=0

n	aa1s	Energy	Δ E	EvN	Elin
4	1.100	-2.071159	-47843	1.0000909	0.5000047
5	1.080	-2.173060	-997	1.0000505	0.5000025
6	1.060	-2.174120	-510	1.0000500	0.5000025
7	1.060	-2.174241	-454	1.0000554	0.5000028

Table 7.13 – He, Triplet, level I, small n

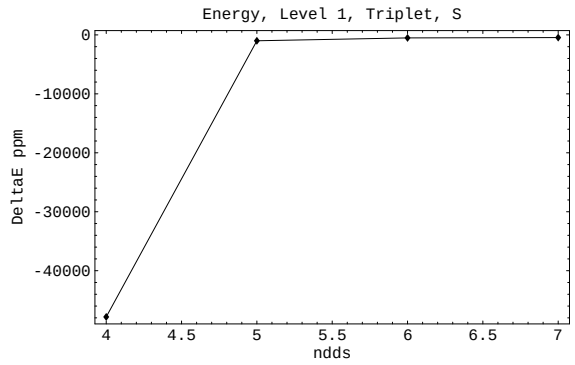

Figure 7.38 – He small n, Energy errors Triplet level I

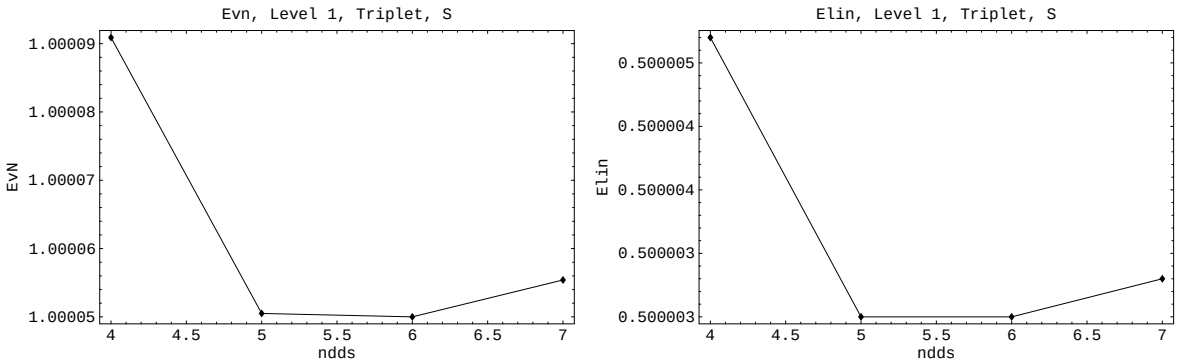

Figure 7.39 – He small n, vN and linear Entropy Triplet level I

n	aa1s	Energy	Δ E	EvN	Elin
4	0.810	-1.971489	-46986	1.000231	0.5000131
5	0.820	-2.041132	-13321	1.000132	0.5000716
6	0.800	-2.059775	-4309	1.000045	0.5000022
7	0.790	-2.066119	-1242	1.000030	0.5000014

Table 7.14 – He, Triplet, level I, small n

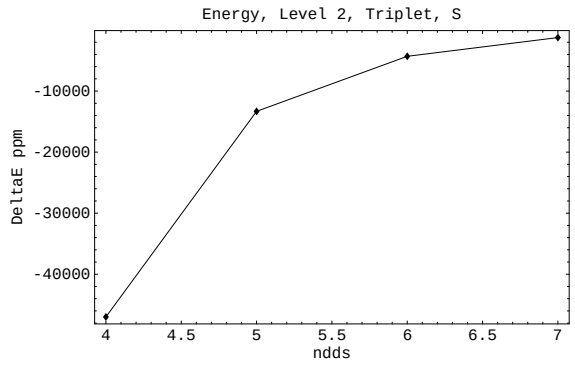

Figure 7.40 – He small n, Energy errors Triplet level II

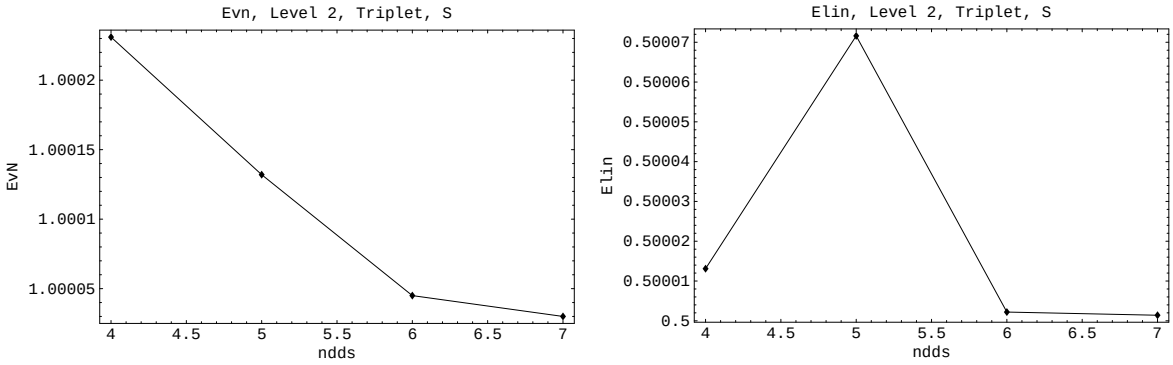

Figure 7.41 – He small n, vN and linear Entropy Triplet level II

n	aa1s	Energy	Δ E	EvN	Elin
5	0.600	-1.906729	-63728	1.0003313	0.5000193
6	0.650	-1.985385	-25105	1.0001759	0.5000097
7	0.650	-2.015153	-10488	1.0000523	0.5000026

Table 7.15 – He, Triplet, level III, small n

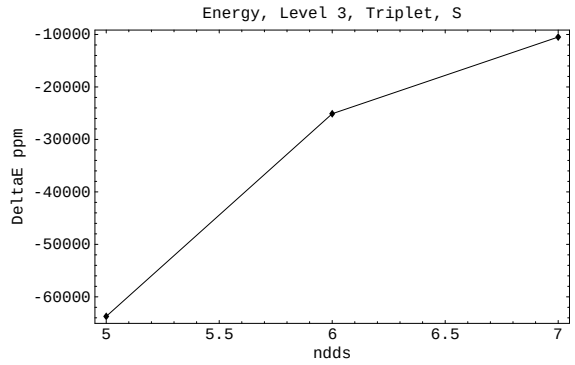

Figure 7.42 – He small n, Energy errors Triplet level III

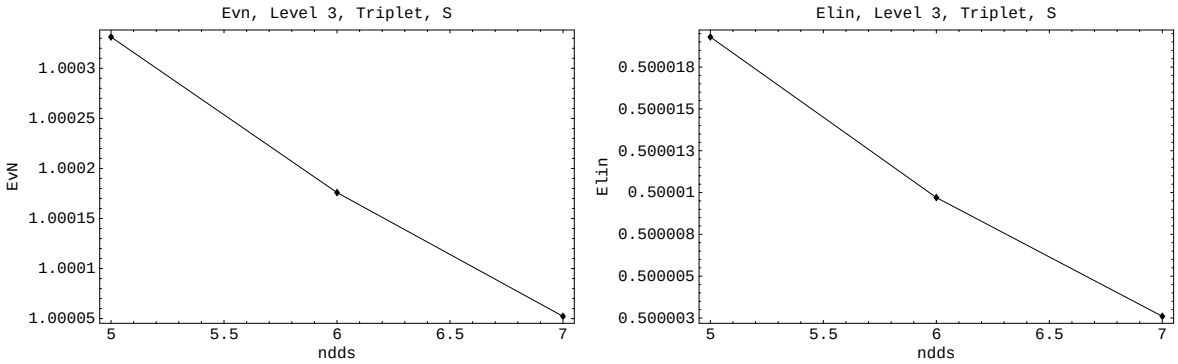

Figure 7.43 – He small n, vN and linear Entropy Triplet level III

7.4.2 Results of 5 Slater Type Orbitals - 6 Gaussians computations

In the following tables and plots we report the results of the H_2 singlet computations for the fundamental level and the I, II and III excited.

R	ξ	energy	evN	elin
1.0	1.283	-1.09738081	0.13046541	0.03144432
1.5	1.140	-1.14377383	0.24967072	0.07374832
2.0	1.053	-1.11135164	0.39039324	0.13529762
2.5	1.010	-1.07240158	0.54317904	0.21365658
3.0	0.993	-1.04218424	0.69021083	0.29833863
4.0	0.990	-1.01116346	0.89317057	0.42737657
5.0	0.997	-1.00221375	0.97182326	0.48056524
6.0	1.000	-1.00016738	0.99341982	0.49544304
7.0	1.000	-0.99975055	0.99855406	0.49899762
8.0	1.000	-0.99967112	0.99970147	0.49979300
9.0	1.000	-0.99965676	0.99994243	0.49996008
10.0	1.000	-0.99965428	0.99998972	0.49999287

Table 7.16 – H_2 fundamental level 5S-6G energy vs.R

Fundamental level

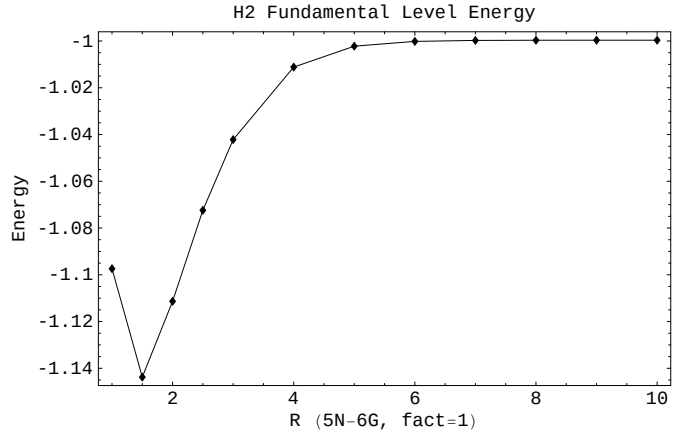

Figure 7.44 – Energy H2, fundamental level, 5S-6G

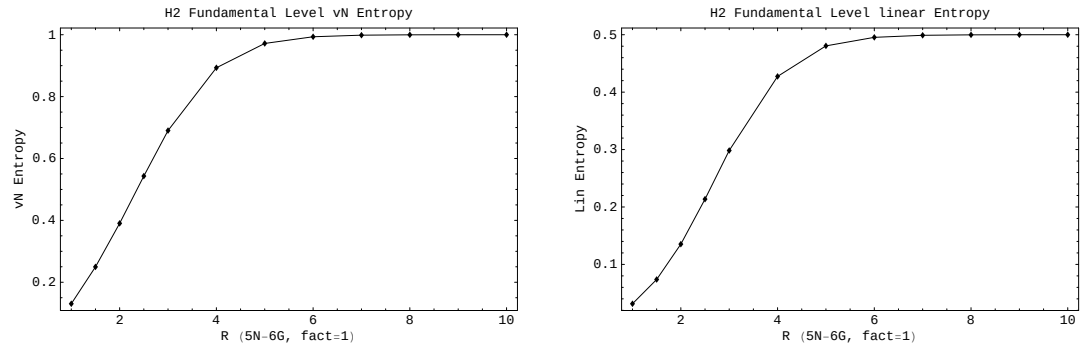

Figure 7.45 – vN and linear entropy H2, fundamental level, 5S-6G

R	ξ	energy	evN	elin
1.0	0.703	-0.53336949	1.02186975	0.48690400
1.5	0.610	-0.64464992	1.06377277	0.49258071
2.0	0.560	-0.65385125	1.12052856	0.50550538
2.5	0.550	-0.64139314	1.17260638	0.52422605
3.0	0.623	-0.63245461	1.08993997	0.50337984
4.0	0.800	-0.63906354	0.83803672	0.38852346
5.0	0.857	-0.64079976	0.81873483	0.37889547
6.0	0.860	-0.63707710	0.85709599	0.40312751
7.0	0.847	-0.63255071	0.90481629	0.43341737
8.0	0.840	-0.62894859	0.94485466	0.45949994
9.0	0.837	-0.62658401	0.97314071	0.47828898
10.0	0.837	-0.62523711	0.98987822	0.48967345

Table 7.17 – H_2 level I, 5S-6G energy vs.R

Level I

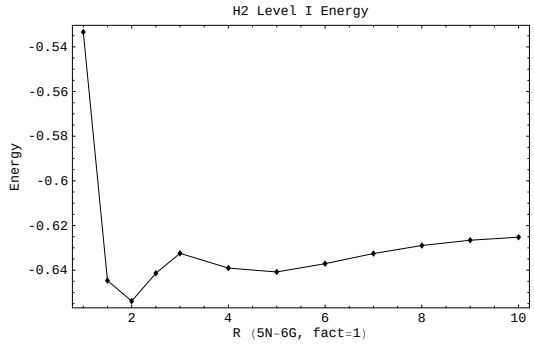

Figure 7.46 – Energy H2, level I, 5S-6G

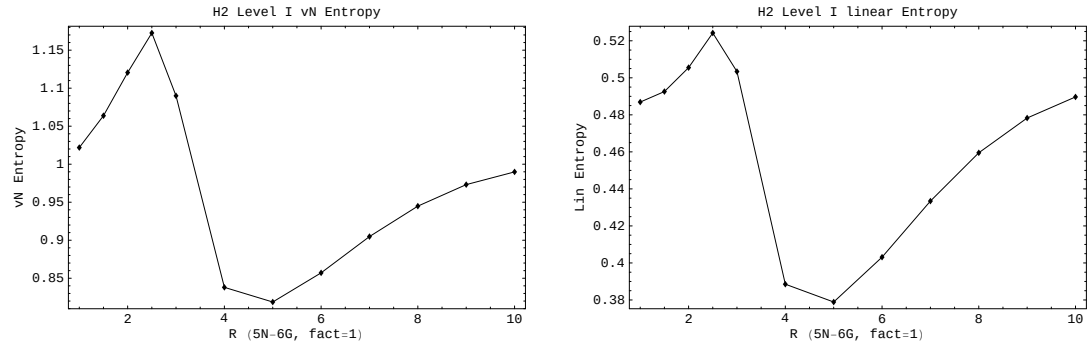

Figure 7.47 – vN and linear entropy H2, level I, 5S-6G

R	ξ	energy	evN	elin
1.0	0.517	-0.43098384	1.08450450	0.50423375
1.5	0.450	-0.54968782	1.10966039	0.50835134
2.0	0.413	-0.56376622	1.13436702	0.51418622
2.5	0.427	-0.55504519	1.13035155	0.51646035
3.0	0.500	-0.55040950	1.05323225	0.49708390
4.0	0.560	-0.55124005	1.00885402	0.48685360
5.0	0.563	-0.55018107	1.02811864	0.49567290
6.0	0.557	-0.54887240	1.05325025	0.50385549
7.0	0.553	-0.54843031	1.07349451	0.50790827
8.0	0.557	-0.54903190	1.07950733	0.50520237
9.0	0.560	-0.55014916	1.07164262	0.49766366
10.0	0.560	-0.55107273	1.06020765	0.49066709

Table 7.18 – H_2 level II, 5S-6G energy vs.R

Level II

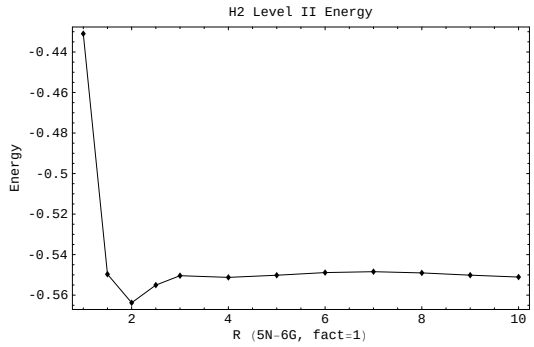

Figure 7.48 – Energy H2, level II, 5S-6G

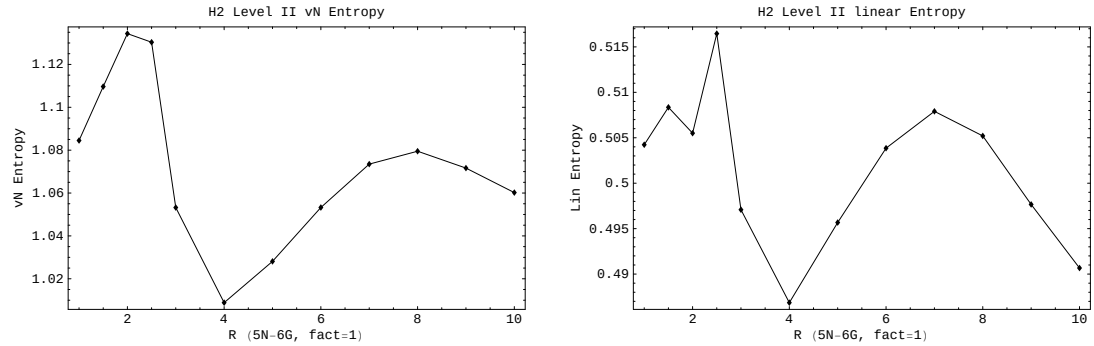

Figure 7.49 – vN and linear entropy H2, level II, 5S-6G

R	ξ	energy	evN	elin
1.0	0.437	-0.34383755	1.10965653	0.50994204
1.5	0.387	-0.48130015	1.14308556	0.51632784
2.0	0.360	-0.51007898	1.16449460	0.52095780
2.5	0.353	-0.51277621	1.16892940	0.52093608
3.0	0.370	-0.51181525	1.14513854	0.49708390
4.0	0.387	-0.50947921	1.18069990	0.51432464
5.0	0.403	-0.50457966	1.22045210	0.52744604
6.0	0.413	-0.50284826	1.21563545	0.52826062
7.0	0.417	-0.50420825	1.20154210	0.51840368
8.0	0.420	-0.50617050	1.17154637	0.50392449
9.0	0.417	-0.50718792	1.16187212	0.49795206
10.0	0.417	-0.50703031	1.16167097	0.50020814

Table 7.19 – H_2 level III, 5S-6G energy vs.R

Level III

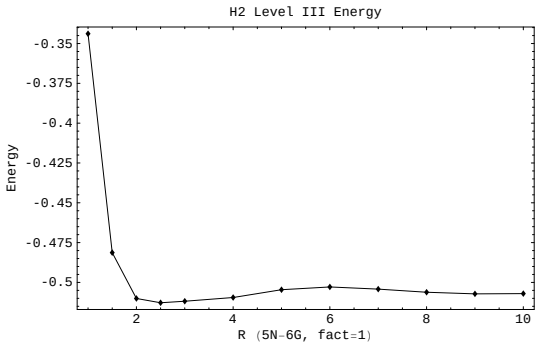

Figure 7.50 – Energy H2, level III, 5S-6G

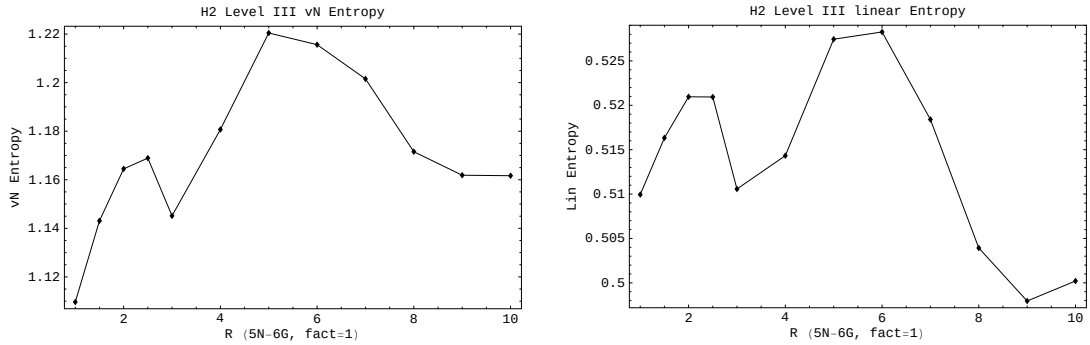

Figure 7.51 – vN and linear entropy H2, level III, 5S-6G

Chapter 8

Conclusions and outlook

The problem of entanglement computation in atoms and molecules is indeed still open, even if the interest in this topic has recently boomed.

For this reason we studied the simplest available case, the Helium problem.

Using an orthonormal basis we have been able to highlight the problems related to the very definition of entanglement for identical particles. The use of an orthonormal basis is not at all a new idea in atomic structure computations, we want to stress the fact that it is a convenient choice to perform entanglement related computations.

An important result is the comparison between states ${}^1S$ and ${}^3S$ of Helium. We verified that they need a different treatment.

When an entanglement measurement is sought, such a simplification is no longer valid.

In the case of Helium, classifying the spin states as singlet and triplet one is able to discriminate in quite a simple manner the different situations, that are only two in this case.

This situation holds if one measures entanglement using both the von Neumann and the linear entropy.

With our method we were able to compute the entanglement for several states of Helium.

We list here some specificities of our work:

1) Previous papers evaluated the entanglement using simplified analytical models, e.g. (Yanez, Plastino et al. , 2010), (Coe, Sudbery et al. , 2008), or with some approximations, like (Osenda, Serra , 2007), (Osenda, Serra , 2008) and (Ferron, Osenda et al. , 2009). Our method considers the exact, complete interactions between the two electrons without simplifying assumptions. Moreover, when computing entanglement we take into account the Pauli exclusion principle and its influence on the entropy values.

2) More appropriately, this work can be considered an extension of (Dehesa, Koga et al. , 2012), whose linear entropy results agree with ours where a comparison is applicable. A difference in the methods employed is that (Dehesa, Koga et al. , 2012) used Montecarlo integrations, implying some statistical errors, while our algebraic method does not.

3) Another difference is that with our method we were able to compute the reduced matrix eigenvectors and hence both the linear and the von Neumann entropies.

4) We extended the number of states for which we computed the entanglement, so that we could propose an empirical law for the dependence of entanglement on the principal quantum numbers.

5) An important characteristic of our method is that it seems to be possible to extend it without much effort in order to compute more interesting cases. Our preliminary computation for the H_2 molecule is, at our knowledge, the first "ab initio" evaluation of the entropy of this system.

First of all, we found that shells S, P and D are sufficient for good entanglement computations, both in the singlet and triplet case. In the second place, one can use lower dimensions for the P and D shells, as we discussed in detail for several specific cases.

Moreover we found that the optimization of the variational parameters can be done separately for each shell, that is one has to perform just 3 optimizations one after the other even in the most complex situation that we considered, that of the S, P and D shells.

For all these reasons the method can be applied to more complex systems like the H_2 molecule.

When more than two electrons are involved, the situation is much more complex, but a large spectroscopic literature is available, at least for simple atoms and molecules, that can be used to extend the present work.

As we have already shown, a natural extension is the study of the Hydrogen molecule, for which many good computations of energies are available.

One of the interesting points in the H_2 molecule is that one can vary the proton distance, and study the entanglement behaviour.

When the distance is 0, the system reduces to the Helium atom.

When the distance is large, we have two possibilities: either two Hydrogen atoms or the system $\{(H^- + p); (p + H^-)\}$ where two electrons are bound to a proton, in the H^- ion.

This ion is the Z=1 component of the Helium isoelectronic series. So a first direction for future work is the computation of entanglement in the atoms of this series, with Z=1,3,4, etc.

During the present work, we performed some computations of the isoelectronic Helium series, and we observed that the computation of H^- is more difficult than the other elements with$Z \geq 3$.

A second direction for future work is the computation of entanglement approximating the STO with gaussians.

As we have shown, using gaussian expansions, we have been able to find again some results obtained for Helium.

Moreover, we have been able to compute the H_2 molecule, although considering the S shell and the "gerade" orbitals only.

The work will continue, completing the study of H_2 considering other shells and the "ungerade" orbitals too.

A third direction is the comparison of our algorithm with the quantum ones that have been proposed to compute atoms and molecules.

As noted in section 5.2.5, it would be very interesting to describe the complexity of the single phases of the computation and to evaluate if and how quantum algorithms could actually enhance the overall efficiency of the computation.

Chapter 9

Appendices

9.1 Description of the main sections of the program for H_2

9.1.1 δ matrix

1

```
do i = 1,50
do j = 1,50
ddd(i,j) = 0._16
end do
end do
do i = 1,50
ddd(i,i) = 1._16
end do
```

9.1.2 UC matrix

```
r = 1.500_16 !  test R value
csi1 = 1.26_16 !  test value, actually it is used to find the minimum
!  Computes the uc[ i, 1, ik] for the wave functions
!  using the generalized Laguerre polynomials
do i = 1,30
do j = 1,10
do kk = 1,20
nnr(i,j,kk) = kk + (j - 1)
nnl(i,j,kk) = j - 1
uc(i,j,kk) = 0._16
coe(i,j,kk) = 0._16
csi(i,j,kk) = csi1
end do
end do
end do
do isw1 = 1,5
isw2 = 1 !  for S states
do i = 1,isw1
csi(isw1,isw2,i) = csi1
end do
56 format(5x,a8,f20.6)
 2
call calcxnew(isw1,isw2)
call arn(isw1,1) !  to check orthonormality 1 = S states
end do
```

9.1.3 One body matrices

```
!  one body matrix computation
nnzz = 3 !  test value
3
do mmz = 1,nnzz
do nnz = 1,nnzz
call clssmn(mmz,nnz,csi1,aaa1,aaa2,ak3,aa5,ab5,aa6,ng)
sskm(mmz,nnz) = aaa1
ajjkm(mmz,nnz) = aaa2
aakm(mmz,nnz) = ak3
amz1(mmz,nnz) = amn1
amz2(mmz,nnz) = amn2
amz3(mmz,nnz) = amn3
end do
end do
```

9.1.4 Matrices of the gaussian expansions used by clssij

```
9
do mu = 1,nnzz
do nu = 1,nnzz
call clssij(mu,nu,csi1,aaa,asz,aaa1,ng)
ssij(mu,nu) = aaa !  sovrapposizione a_i b_i
ajjij(mu,nu) = asz !  JJ
aaij(mu,nu) = aaa1 !  KK
aij1(mu,nu) = abc4 !  T1
aij2(mu,nu) = abc5 !  T2
aij3(mu,nu) = abc6 !  VV
end do
end do
```

9.1.5 Matrix sssz(i,j) i,j=1,...,2*n

```
4
do i = 1,nnzz
do j = 1,nnzz
sssz(i,j) = ddd(i,j)
sssz(i + nnzz,j + nnzz) = ddd(i,j)
sssz(i + nnzz,j) = ssij(i,j)
sssz(i,j + nnzz) = ssij(i,j)
end do
end do
```

The ssij(i,j) is defined by the superposition

$$ssij(i,\, j) \,=\, \int a_i(\mathbf{r}) b_j(\mathbf{r})\, d\mathbf{r} \tag{9.1}$$

It doesn't have a physical meaning, it is just a part of the computation of the Fock space superposition.

We recall that the 2n single particle basis functions of the set $\{a_i(\mathbf{r}),\, b_j(\mathbf{r})\}$, are not orthogonal, so we can define the matrix

$sssz(k,\, l) \,=$

	$a_i(\mathbf{r})$	$b_j(\mathbf{r})$
$a_i(\mathbf{r})$	**1**	ssij
$b_j(\mathbf{r})$	ssij	**1**

(9.2)

$\{\, k,\, l \,=\, 1,\, 2,\, \ldots\, 2n \,\}$

because the $a_i(\mathbf{r})$ e $b_j(\mathbf{r})$ are orthogonal within each set.

Now we compute eigenvalues and eigenvectors of this matrix. In the order they are:

1	1.9126176		
2		1.5870954	
3			1.0011449
4			0.9988550
5		0.4129046	
6	0.0873824		
=	2.0	2.0	2.0

That is they are in pairs ot the form $(1 \pm \alpha)$

Manually writing the equations for small dimensions, it can be seen that the secular equation is a polynomial in $(1 - \lambda)^2$, so that the solutions are of the indicated form, in pairs.

Now we build the ooz matrix to diagonalize the sssz.

9.1.6 Computation of the matrix $\mathcal{N}$

$$\mathcal{N}_{ij} = \frac{1}{\sqrt{2\,(1 + ssij(i,\,j)^2)}} = anij(i,\,j) \tag{9.3}$$

```
5
do i = 1,nnzz
do j = 1,nnzz
abc = 2._16 * (1._16 + ssij(i,j)**2._16)
anij(i,j) = 1._16/sqrt(abc)
end do
```

```
end do
```

9.1.7 Special settings for 1 Slater Type Orbital only

For the orbital 1-STO only we use the special values:

```
!  to test 1-STO
sskk = ssij(1,1) !  matrix ssij(i,j)
cckk = ajjij(1,1) !  matrix ajjij(i,j)
aakk = aaij(1,1) !  matrix aakij(i,j)
azz1 = aij1(1,1) !  matrix aij1(i,j)
azz2 = aij2(1,1) !  matrix aij2(i,j)
azz3 = aij3(1,1) !  matrix aij3(i,j)
```

9.1.8 Matrix sovr(,) $\equiv \langle i, j \,|\, k, l \rangle$ for Fock $\perp$

```
6
k1 = 0
do i1 = 1,nstop
do i2 = i1,nstop
```

```
k1 = k1 + 1
k2 = 0
do j1 = 1,nstop
do j2 = j1,nstop
k2 = k2 + 1
abc = 2._16 * anij(i1,i2) * anij(j1,j2)
ab1 = ddd(i1,j1) * ddd(i2,j2) + ssij(i1,j2) * ssij(i2,j1)
sovr(k1,k2) = abc * ab1
end do
end do
end do
end do
```

9.1.9 Diagonalization of sssz to orthonormalize $\{a_i(\mathbf{r}), b_j(\mathbf{r})\}$

```
7
do ix = 1,2*nstop
do jx = 1,2*nstop
za(ix,jx) = sssz(ix,jx)
end do
end do
nrot = 0
call jacobd(2*nstop,nrot)
call eigsrd(2*nstop)
```

9.1.10 oort, ooz matrices

8

```
do ii = 1,2*nstop
do jj = 1,2*nstop
abc = 0._16
do kk = 1,2*nstop
abc = abc + zv(ii,kk) * zv(jj,kk)
end do
oort(ii,jj) = abc
end do
end do
do ii = 1,2*nstop
do jj = 1,2*nstop
abc = 0._16
do kk = 1,2*nstop
abc = abc + sssz(ii,kk) * zv(kk,jj)
end do
obuf(ii,jj) = abc
end do
end do
do ii = 1,2*nstop
do jj = 1,2*nstop
```

```
abc = 0._16
do kk = 1,2*nstop
abc = abc + zv(kk,ii) * obuf(kk,jj)
end do
oort(ii,jj) = abc
end do
end do
call clxnn
```

A

List of the matrices that we computed up to this point:

1

ddd(i, j) = δ_{ij}

2

matrix UC = uc[i, 1, ik]

3

Computes 6 "standard" matrices

4

Computes

$$sssz = \begin{array}{|c|c|} \hline \mathbf{1} & \text{ssij} \\ \hline \text{ssij} & \mathbf{1} \\ \hline \end{array} \tag{9.4}$$

superposition of the space $\{a_i(\mathbf{r},\, b_j(\mathbf{r})\}$

5

omputes anij(i, j) = $\mathcal{N}_{ij}$

6

computes sovr(k1, k2) = $\langle i,\, j \,|\, k,\, l\rangle$

Finally, we have the superposition in the Fock space:

$$\langle i,\, j \,|\, k,\, l\rangle \;=\; sovr(k1,\, k2) \;=\; 2\,\mathcal{N}_{ij}\,\mathcal{N}_{kl}\,\{\,\delta_{ik}\,\delta_{jl} \;+\; ssij(i,\, l)\,ssij(j,\, k)\,\} \tag{9.5}$$

From this we see that the Fock space we have defined is not orthogonal (if $R \neq 0$), but it is for $R = 0$.

7

za = buffer to diagonalize the sssz matrix of the $\{a_i(\mathbf{r},\, b_j(\mathbf{r})\}$ superposition.

8

computes the oort matrix, to diagonalize the sssz matrix.

9.1.11 Computation of the other matrix needed for the Hamiltonian

Now we write the espressions for the other matrices that we need:

$$\{\,[1]\,...\,[16]\,\} \;=\; +2\,\{\underbrace{\overbrace{VV}^{aij3}(i,\,k)\cdot\delta_{jl}\;+\;\overbrace{VV}^{aij3}(j,\,l)\cdot\delta_{ik}}_{a1}\;+\;\underbrace{\overbrace{JJ}^{ajjij}(i,\,k)\cdot\delta_{jl}\;+\;\overbrace{JJ}^{ajjij}(j,\,l)\cdot\delta_{ik}}_{a2}\;+$$

$$+\,[\underbrace{\overbrace{KK1}^{aaij}(i,\,l)\;+\;\overbrace{KK1}^{aaij}(l,\,i)\,]\cdot ssij(j,\,k)}_{a3}+[\underbrace{\overbrace{KK2}^{aaij}(k,\,j)\;+\;\overbrace{KK2}^{aaij}(j,\,k)\,]\cdot ssij(i,\,l)}_{a4}\,] \quad (9.6)$$

$$\langle i,\,j\,|\,\overbrace{T_1}^{aij1}\;+\;\overbrace{T_2}^{aij2}\,|\,k,\,l\rangle \;=\; \mathcal{N}_{ij}\;\cdot\;\overbrace{\mathcal{N}_{kl}}^{anij}\;\cdot 2\;\cdot\;\{\underbrace{\overbrace{TT1}^{aij1}(i,\,k)\cdot\delta_{jl}\;+\;\overbrace{TT1}^{aij1}(j,\,l)\cdot\delta_{ik}}_{a5}\;+$$

$$+\,\underbrace{\overbrace{TT2}^{aij2}(i,\,l)\cdot ssij(j,\,k)\;+\;\overbrace{TT2}^{aij2}(j,\,k)\cdot ssij(i,\,l)}_{a5}\,\} \quad (9.7)$$

9.1.12 Matrices names

SSIJ = ssij

JJ = ajjij

KK1 = aaij

KK2 = aaij

VV = aij3

TT1 = aij1

TT2 = aij2

$\mathcal{N}_{ij}$ = anij

See **9**

To compute the matrix am0116(k1, k2) we need the usual quadruple loop, see **6**

Quadruple loop **6** computation of am0116(k1, k2) see computation sovr(,)

9.1.13 Energy

```
a1 = 2._16/(1._16 + sskk * sskk)
a5 = (azz1 + azz2 * sskk) * a1
a6 = - azz3 * a1 + cckk * a1
a8 = 2._16 * aakk * sskk * a1
emm(k) = a5 + a6 + a8
emm1(k) = emm(k) + twb + 1._16/rr(k)
```

9.1.14 Subroutine clssij

Important check: for R=0 the H_2 molecule reduces to the Helium atom, then the superposition matrix must reduce to the unity matrix.

From the ssij(i,j) matrix one computes

$$\mathcal{N}_{ij} \;=\; anij(i,\,j) \;=\; \sqrt{2(1 \,+\, ssjj(i,\,j)^2)} \tag{9.8}$$

Finally, we have the Fock space superposition:

$$\langle i,\,j\,|\,k,\,l\rangle \;=\; sovr(k1,\,k2) \;=\; 2\cdot\mathcal{N}_{ij}\cdot\mathcal{N}_{kl}\cdot\{\,\delta_{ik}\,\delta_{jl} \,+\, ssij(i,\,l)\cdot ssij(j,\,k)\} \tag{9.9}$$

This means that such space is non orthogonal, (for $R \neq 0$), but it is for $R = 0$.

We report other useful matrices:

$$\{\,[1]\,...\,[16]\,\} \;=\; +2\cdot\{\,vv(i,\,k)\delta_{jl} \,+\, vv(j,\,l)\delta_{ik} \,+\, JJ(i,\,k)\delta_{jl} \,+\, JJ(j,\,l)\delta_{ik} +$$

$$+\,[\,kk1(i,\,l) \,+\, kk1(l,\,j)\,]\cdot ssij(j,\,k) \,+\, [\,kk2(k,\,j) \,+\, kk2(j,\,k)\,]\cdot ssij(i,\,l)\,\} \tag{9.10}$$

$$\langle i,j\,|\,T_1 \,+\, T_2\,|\,k,l\rangle \;=\; \mathcal{N}_{ij}\cdot\mathcal{N}_{kl}\cdot 2\cdot$$

$$\cdot\{\,tt1(i,\,k)\delta_{jl} \,+\, tt1(j,\,l)\delta_{ik} \,+\, tt2(i,\,l)ssij(j,\,k) \,+\, tt2(j,\,k)ssij(i,\,l)\,\} \tag{9.11}$$

```
subroutine clssij(mmu,nnu,csi1,aaa,asz,aaa1,ng)
aaa = 0._16
asz = 0._16
aaa1 = 0._16
awm1 = 0._16
awm2 = 0._16
awm3 = 0._16
do iu = 1,mu
do ju = 1,nu
a1 = uc(mu,1,iu) !  for NON normalized STOs
a2 = uc(nu,1,ju) !  for NON normalized STOs
b1 = (2._16 * csi1)**dfloat(2*iu + 1)
b2 = gamma(2*iu + 1)
b3 = sqrt(b2/b1)
c1 = (2._16 * csi1)**dfloat(2*ju + 1)
c2 = gamma(2*ju + 1)
c3 = sqrt(c2/c1)
a1 = a1*b3
a2 = a2*c3
mmm = iu
nnn = ju
abc1 = sskm(mmm,nnn)
abc2 = ajjkm(mmm,nnn)
abc3 = aakm(mmm,nnn)
amn1 = amz1(mmm,nnn)
amn2 = amz2(mmm,nnn)
amn3 = amz3(mmm,nnn)
```

```
aaa = aaa + abc1 * a1 * a2 !  S sskm(mmm,nnn,csi1,ng)
asz = asz + abc2 * a1 * a2 !  J ajjkm(mmm,nnn,csi1.ng)
aaa1 = aaa1 + abc3 * a1 * a2 !  K aakm(mmm,nnn,csi1,ng)
awm1 = awm1 + amn1 * a1 * a2 !
awm2 = awm2 + amn2 * a1 * a2 !
awm3 = awm3 + amn3 * a1 * a2 !
end do !  ju
end do !  iu
aaa = aaa !  matrix element of ssij = superposition
asz = - asz !  matrix element of aijij = JJ
aaa1 = aaa1 !  matrix element of aaij = KK
abc4 = awm1 !  kinetic energy 1
abc5 = awm2 !  kinetic energy 2
abc6 = awm3 !  VV
return
end
```

9.1.15 Subroutine clssmn

```
subroutine clssmn(mmz,nnz,csi1,aaa1,aaa2,ak3,aa5,ab5,aa6,nng)
pig = 3.141592654_16
mmm = mmz
nnn = nnz
ng = nng
```

```
go to (101,102,103,104,105),mmm
101 call s1sq(exx1,cs1,ng)
go to 106
102 call s2sq(exx1,cs1,ng)
go to 106
103 call s3sq(exx1,cs1,ng)
go to 106
104 call s4sq(exx1,cs1,ng)
go to 106
105 call s5sq(exx1,cs1,ng)
106 continue
do jj = 1,ng
exx1m(jj) = exx1(jj)
cs1m(jj) = cs1(jj)
end do
go to (111,112,113,114,115),nnn
111 call s1sq(exx1,cs1,ng)
go to 107
112 call s2sq(exx1,cs1,ng)
go to 107
113 call s3sq(exx1,cs1,ng)
go to 107
114 call s4sq(exx1,cs1,ng)
go to 107
115 call s5sq(exx1,cs1,ng)
107 continue
```

```
do jj = 1,ng
exx1n(jj) = exx1(jj)
cs1n(jj) = cs1(jj)
end do
do l = 1,ng
eim(l) = exx1m(l)*(csi1*csi1)
cim(l) = cs1m(l) * (2._16 * eim(l)/pig) ** 0.75_16
end do !  loop l
do l = 1,ng
ein(l) = exx1n(l)*(csi1*csi1)
cin(l) = cs1n(l) * (2._16 * ein(l)/pig) ** 0.75_16
end do !  loop l
ss = 0._16
ssj = 0._16
szk = 0._16
amn1 = 0._16
amn2 = 0._16
amn3 = 0._16
do ni = 1,ng
do nj = 1,ng
!------------------------------------------ superposition
bbb = pig/(eim(ni) + ein(nj))
aaa = sqrt(bbb*bbb*bbb)
ctot = cim(ni) * cin(nj) * aaa
etot = eim(ni) * ein(nj)/(eim(ni) + ein(nj))
ss = ss + ctot * exp( - etot * r*r )
```

```
!------------------------------------------- J
aaz = sqrt(eim(ni) + ein(nj)) * r !  erf argument
call errf(aaz,erf,100)
aaw = cim(ni) * cin(nj) * aaa
ssj = ssj + (aaw/r) * erf !  integral J
!------------------------------------------- K
aa = eim(ni) * ein(nj)/(eim(ni) + ein(nj))
az = exp( - aa * r * r)
b = ( (eim(ni) - ein(nj)) * r/2._16 ) /(eim(ni) + ein(nj))
b = b + r/2._16
w = (eim(ni) + ein(nj)) * b * b
z = sqrt(w)
call errf(z,erf,100)
fff = (sqrt(pig) / (2._16 * z)) * erf
akkij = 2._16 * az * pig * fff/(eim(ni) + ein(nj))
szk = szk + cim(ni) * cin(nj) * akkij
!------------------------------------------- TK1
abce = 3._16 * eim(ni) * ein(nj)/(eim(ni) + ein(nj))
amn1 = amn1 + cim(ni) * cin(nj) * aaa * abce
!------------------------------------------- TK2
abce = eim(ni) * ein(nj)/(eim(ni) + ein(nj))
abcf = exp( - abce * r * r)
abcg = 3._16 - 2._16 * abce * r * r
agg = aaa * abce * abcf * abcg
amn2 = amn2 + cim(ni) * cin(nj) * agg
!------------------------------------------- VV
```

```
abcd = 2._16 * pig/(eim(ni) + ein(nj))
amn3 = amn3 + cim(ni) * cin(nj) * abcd
end do !  loop nj
end do !  loop ni
aaa1 = ss !  superposition
aaa2 = ssj !  J
ak3 = - szk !  K
return
end
```

Subroutines s1sq, s2sq etc. return the gaussian coefficients for the expansions of the STOs, see (Stewart , 1969)

9.1.16 Subroutine diag1 - entropy computation

```
subroutine diag1(nstop)
do ix = 1,2*nstop
do jx = 1,2*nstop
za(ix,jx) = sssz(ix,jx)
end do
end do
nrot = 0
call jacobd(2*nstop,nrot) !  computes the sssz matrix eigenvalues
call eigsrd(2*nstop) !  and sorts them
do i = 1,2*nstop
do j = 1,2*nstop
```

```
ali(i,j) = 0._16
end do
end do
do i = 1,2*nstop
ali(i,i) = 1._16 / sqrt(zd(i)) = [1/√λ_i]
end do
do ii = 1,2*nstop
do jj = 1,2*nstop
abc = 0._16
do kk = 1,2*nstop
abc = abc + ali(ii,kk) * zv(jj,kk)
end do
oort(ii,jj) = abc
end do
end do
oort = [1/√λ_i] · zv^⊤
do i = 1,2*nstop
do j = 1,2*nstop
ali(i,j) = 0._16
end do
end do
do i = 1,2*nstop
ali(i,i) = sqrt(zd(i))
end do
do ii = 1,2*nstop
do jj = 1,2*nstop
abc = 0._16
```

```
do kk = 1,2*nstop
abc = abc + zv(ii,kk) * ali(jj,kk)
end do
ooinv(ii,jj) = abc
end do
end do
```

$ooinv = zv \cdot [\sqrt{\lambda_i}]$

```
do ii = 1,2*nstop
do jj = 1,2*nstop
abc = 0._16
do kk = 1,2*nstop
abc = abc + ooinv(ii,kk) * oort(kk,jj)
end do
obuf(ii,jj) = abc
end do
end do
do ii = 1,nstop
do jj = 1,nstop
do ihh = 1,2*nstop
do kk = 1,2*nstop
aa = ooinv(ii,ihh) * ooinv(jj + nstop,kk)
bb = ooinv(ii,kk) * ooinv(jj + nstop,ihh)
ww(ii,jj,ihh,kk) = aa + bb
end do
end do
end do
end do
```

```
ndz = nstop*(nstop+1)/2 !  Fock space dimension
do irep = 1,3
nnt = ndz - irep + 1
do ihf = 1,2*nstop
do ihfp = 1,2*nstop
ault = 0._16
ndz = nstop*(nstop+1)/2
do n = 1, ndz
do np = 1, ndz
do nk = 1,n
do nkp = 1,np
ifz = ind1(nk)
jfz = ind2(nk)
ifp = ind1(nkp)
jfp = ind2(nkp)
nnt = ndz - irep + 1
aff1 = ttza(n,nnt) * ttza(np,nnt)
aff2 = uf(n,1,nk) * uf(np,1,nkp)
aff3 = anij(ifz,jfz) * anij(ifp,jfp) !  N_ij = anij(i,j)
do ikf = 1,2*nstop
aff4 = ww(ifz,jfz,ihf,ikf) * ww(ifp,jfp,ihfp,ikf)
ault = ault + aff1*aff2*aff3*aff4
end do !  loop k
end do !  loop nkp
end do !  loop nk
end do !  loop np
```

```
end do !  loop n
rhorid(ihf,ihfp) = ault
end do !  ihp
end do !  ih
ttrr = 0._16
do i = 1,2*nstop
ttrr = ttrr + rhorid(i,i) !  rhorid trace
end do
do ii = 1,2*nstop
do jj = 1,2*nstop
rrr(ii,jj) = rhorid(ii,jj)
end do
end do
trr = 0._16
do i = 1,2*nstop
trr = trr + rrr(i,i)
end do
do ix = 1,2*nstop
do jx = 1,2*nstop
za(ix,jx) = rrr(ix,jx)
end do
end do
nrot = 0
call jacobd(2*nstop,nrot)
call eigsrd(2*nstop)
!  density matrix eigenvalues in zd
abc = 0._16
```

```
do jx = 1,2*nstop
abz = log10(zd(jx) + 0.000000000001_16 )/log10(2._16)
abc = abc - zd(jx) * abz
end do
!  abc = von Neumann entropy
do ii = 1,2*nstop
do jj = 1,2*nstop
aaa = 0._16
do kk = 1,2*nstop
aaa = aaa + rrr(ii,kk) * rrr(kk,jj)
end do
rrq(ii,jj) = aaa
end do
end do
trrq = 0._16
do i = 1,2*nstop
trrq = trrq + rrq(i,i)
end do
!  trrq = squared rho trace
end do !  irep
1000 continue
return
end
```

n = 1,2,3,4,5

$$a_i(\mathbf{r}) \;=\; \phi_i(\mathbf{r} - \mathbf{a});\;\; b_i(\mathbf{r}) \;=\; \phi_i(\mathbf{r} + \mathbf{a}) \tag{9.12}$$

$$\phi_i(\mathbf{r}) \;=\; \sum_{ik=1}^{i} uc[i,\, 1,\, ik] \;\cdot\; STO(r,\, ik,\, \xi) \tag{9.13}$$

$$STO(r,\, ik,\, \xi) \;=\; r^{ik-1} \;\cdot\; exp\{-\xi r\} \tag{9.14}$$

We set:

$$c_k(\mathbf{r}) \;=\; a_i(\mathbf{r}) \;\; \{\, i, k = 1, 2, ..., n\} \tag{9.15}$$

$$c_k(\mathbf{r}) \;=\; b_i(\mathbf{r}) \;\; \{\, i = 1, 2, ..., n;\;\; k = n+1, n+2, ..., 2n\} \tag{9.16}$$

Example: n=1

$$ssij(1,\, 1) \;=\; S \tag{9.17}$$

$$sssz \;=\; \begin{bmatrix} 1 & S \\ S & 1 \end{bmatrix} \tag{9.18}$$

$$\lambda_{1,2} \,=\, 1 \,\pm\, S \tag{9.19}$$

$$\begin{cases} \psi_1^{\perp}(\mathbf{r}) \,=\, \dfrac{1}{\sqrt{2(1\,+\,S)}}\{\, a(\mathbf{r}) \,+\, b(\mathbf{r})\,\} \\[2ex] \psi_2^{\perp}(\mathbf{r}) \,=\, \dfrac{1}{\sqrt{2(1\,-\,S)}}\{\, a(\mathbf{r}) \,-\, b(\mathbf{r})\,\} \end{cases} \tag{9.20}$$

$$\begin{cases} a(\mathbf{r}) \,=\, \sqrt{\dfrac{1\,+\,S}{2}}\,\psi_1^{\perp}(\mathbf{r}) \,+\, \sqrt{\dfrac{1\,-\,S}{2}}\,\psi_2^{\perp}(\mathbf{r}) \\[2ex] b(\mathbf{r}) \,=\, \sqrt{\dfrac{1\,+\,S}{2}}\,\psi_1^{\perp}(\mathbf{r}) \,-\, \sqrt{\dfrac{1\,-\,S}{2}}\,\psi_2^{\perp}(\mathbf{r}) \end{cases} \tag{9.21}$$

$$\begin{bmatrix} \psi_1^{\perp} \\ \psi_2^{\perp} \end{bmatrix} \,=\, \begin{bmatrix} \dfrac{1}{\sqrt{2}} & 0 \\ 0 & \dfrac{1}{\sqrt{2}} \end{bmatrix} \begin{bmatrix} \dfrac{1}{\sqrt{2}} & \dfrac{1}{\sqrt{2}} \\ \dfrac{1}{\sqrt{2}} & -\dfrac{1}{\sqrt{2}} \end{bmatrix} \begin{bmatrix} a(\mathbf{r}) \\ b(\mathbf{r}) \end{bmatrix} \tag{9.22}$$

$$\lambda_{1,2} \,=\, 1 \,\pm\, S \tag{9.23}$$

$$anij \,=\, \mathcal{N}_{ij} \,=\, \frac{1}{\sqrt{2\,(1\,+\,ssij^2)}} \tag{9.24}$$

9.1.17 Two-body interaction

Recall the states definition:

$$|\, i,\, j\rangle \;=\; \mathcal{N}_{ij}\,[\, a_i(\mathbf{r}_1)b_j(\mathbf{r}_2) \;+\; b_j(\mathbf{r}_1)a_i(\mathbf{r}_2)\,] \tag{9.25}$$

The two bodies interaction reads:

$$\langle i,\, j\,|\,\frac{1}{r_{12}}\,|\,k,\, l\rangle \;=\; \mathcal{N}_{ij}\cdot\mathcal{N}_{kl}\;\cdot\;\int d\mathbf{r}_1\, d\mathbf{r}_2\,\cdot$$

$$\cdot\,[\, a_i(\mathbf{r}_1)b_j(\mathbf{r}_2) \;+\; b_j(\mathbf{r}_1)a_i(\mathbf{r}_2)\,]\cdot\frac{1}{r_{12}}\cdot\,[\, a_k(\mathbf{r}_1)b_l(\mathbf{r}_2) \;+\; b_l(\mathbf{r}_1)a_k(\mathbf{r}_2)\,] \tag{9.26}$$

We have 4 terms, that reduce to 2 for the usual simmetries:

$$a_i(\mathbf{r}) \;=\; \phi_i(\mathbf{r}\;-\;\mathbf{a});\;\; b_i(\mathbf{r}) \;=\; \phi_i(\mathbf{r}\;+\;\mathbf{a}) \tag{9.27}$$

$$\langle i,\, j\,|\,\frac{1}{r_{12}}\,|\,k,\, l\rangle \;=\; \mathcal{N}_{ij}\cdot\mathcal{N}_{kl}\;\cdot\;2\int d\mathbf{r}_1\, d\mathbf{r}_2\,\cdot$$

$$\cdot\,\{\,\phi_i(\mathbf{r}_1\;-\;\mathbf{a})\phi_j(\mathbf{r}_2\;+\;\mathbf{a})\frac{1}{|\mathbf{r_1}\;-\;\mathbf{r_2}|}\phi_k(\mathbf{r}_1\;-\;\mathbf{a})\phi_l(\mathbf{r}_2\;+\;\mathbf{a}) +$$

$$+\,\phi_i(\mathbf{r}_1\;-\;\mathbf{a})\phi_j(\mathbf{r}_2\;+\;\mathbf{a})\frac{1}{|\mathbf{r_1}\;-\;\mathbf{r_2}|}\phi_l(\mathbf{r}_1\;+\;\mathbf{a})\phi_k(\mathbf{r}_2\;-\;\mathbf{a})\,\} \tag{9.28}$$

Recalling the expansions:

$$\phi_i(\mathbf{r}) \;\equiv\; \sum_{ik=1}^{i} uc[\, i,\, 1,\, ik]\;\cdot\; STO(\mathbf{r},\, ik) \tag{9.29}$$

we have:

A	**B**	**C**	**D**
r_1	r_1	r_2	r_2
$+\mathbf{a}$	$+\mathbf{a}$	$-\mathbf{a}$	$-\mathbf{a}$
ik	kk	jk	lk
$\alpha(ik)$	$\beta(kk)$	$\gamma(jk)$	$\delta(lk)$

Table 9.1 – Direct integral

$$\langle i,\, j\,|\,\frac{1}{r_{12}}\,|\,k,\, l\rangle \;=\; \mathcal{N}_{ij}\cdot\mathcal{N}_{kl}\;\cdot\;2\,\sum_{ik=1}^{i}\,\sum_{jk=1}^{j}\,\sum_{kk=1}^{k}\,\sum_{lk=1}^{l}\,\int d\mathbf{r}_1\,d\mathbf{r}_2\,\cdot$$

$$\cdot\,uc[i,\,1,\,ik]\,uc[j,\,1,\,jk]\,uc[k,\,1,\,kk]\,uc[l,\,1,\,lk]\,\cdot$$

$$\cdot\,\{\,STO(\mathbf{r}_1\,-\,\mathbf{a},\,ik)\,\cdot\,STO(\mathbf{r}_2\,+\,\mathbf{a},\,jk)\frac{1}{|\mathbf{r_1}\,-\,\mathbf{r_2}|}STO(\mathbf{r}_1\,-\,\mathbf{a},\,kk)\,\cdot\,STO(\mathbf{r}_2\,+\,\mathbf{a},\,lk)+$$

$$+\,STO(\mathbf{r}_1\,-\,\mathbf{a},\,ik)\,\cdot\,STO(\mathbf{r}_2\,+\,\mathbf{a},\,jk)\frac{1}{|\mathbf{r_1}\,-\,\mathbf{r_2}|}STO(\mathbf{r}_1\,+\,\mathbf{a},\,lk)\,\cdot\,STO(\mathbf{r}_2\,-\,\mathbf{a},\,kk)\,\}\;=$$

$$=\;DIRECT\,+\,EXCHANGE \tag{9.30}$$

Ignoring the coefficients and the sum, we have:

Direct integral

$$DD\;=\;\int d\mathbf{r}_1\,d\mathbf{r}_2\,\cdot\,STO(\mathbf{r}_1\,-\,\mathbf{a},\,ik)\,\cdot\,STO(\mathbf{r}_2\,+\,\mathbf{a},\,jk)\,\cdot\,|\,V\,|\,\cdot$$

$$\cdot\,STO(\mathbf{r}_1\,-\,\mathbf{a},\,kk)\,\cdot\,STO(\mathbf{r}_2\,+\,\mathbf{a},\,lk)\;=$$

$$=\;\int d\mathbf{r}_1\,d\mathbf{r}_2\,\cdot\,STO(\mathbf{r}_1\,-\,\mathbf{a},\,ik)\,\cdot\,STO(\mathbf{r}_1\,-\,\mathbf{a},\,kk)\,\cdot\,|\,V\,|\,\cdot$$

$$\cdot\,STO(\mathbf{r}_2\,+\,\mathbf{a},\,jk)\,\cdot\,STO(\mathbf{r}_2\,+\,\mathbf{a},\,lk) \tag{9.31}$$

and the table 9.1

A	**B**	**C**	**D**
r_1	r_1	r_2	r_2
$+\mathbf{a}$	$-\mathbf{a}$	$-\mathbf{a}$	$+\mathbf{a}$
ik	lk	jk	kk
$\alpha(ik)$	$\beta(lk)$	$\gamma(jk)$	$\delta(kk)$

Table 9.2 – Exchange integral

Exchange integral

$$SC = \int d\mathbf{r}_1\, d\mathbf{r}_2 \cdot STO(\mathbf{r}_1 - \mathbf{a},\, ik) \cdot STO(\mathbf{r}_2 + \mathbf{a},\, jk) \cdot |\, V \,| \cdot$$

$$\cdot STO(\mathbf{r}_1 + \mathbf{a},\, lk) \cdot STO(\mathbf{r}_2 - \mathbf{a},\, kk) =$$

$$= \int d\mathbf{r}_1\, d\mathbf{r}_2 \cdot STO(\mathbf{r}_1 - \mathbf{a},\, ik) \cdot STO(\mathbf{r}_1 + \mathbf{a},\, lk) \cdot |\, V \,| \cdot$$

$$\cdot STO(\mathbf{r}_2 + \mathbf{a},\, jk) \cdot STO(\mathbf{r}_2 - \mathbf{a},\, kk) \tag{9.32}$$

and table 9.2

$$ak1 = k1 = exp\{-\frac{\alpha\beta}{\alpha + \beta} |\, \overline{AB} \,|^2\} \tag{9.33}$$

$$pp = P = \frac{\alpha\mathbf{A} + \beta\mathbf{B}}{\alpha + \beta} \tag{9.34}$$

$$aabb = |\, \overline{AB} \,|^2 = |\, \mathbf{B} - \mathbf{A} \,|^2 \tag{9.35}$$

$$ak2 = k2 = exp\{-\frac{\gamma\delta}{\gamma + \delta} |\, \overline{CD} \,|^2\} \tag{9.36}$$

$$qq = Q = \frac{\gamma\mathbf{C} + \delta\mathbf{D}}{\gamma + \delta} \tag{9.37}$$

$$ccdd = |\,\overline{CD}\,|^2 = |\,\mathbf{D} - \mathbf{C}\,|^2 \tag{9.38}$$

$$aa1 = \frac{2 \cdot ak1 \cdot ak2 \cdot \pi^{5/2}}{(\alpha + \beta)(\gamma + \delta)\sqrt{(\alpha + \beta)(\gamma + \delta)}} \tag{9.39}$$

$$ppqq = |\,\mathbf{P} - \mathbf{Q}\,|^2 \tag{9.40}$$

$$aa5 = \frac{(\alpha + \beta)(\gamma + \delta)}{\alpha + \beta + \gamma + \delta} \cdot |\,\mathbf{P} - \mathbf{Q}\,|^2 \tag{9.41}$$

call efff(aa5, aa6, 80) ! efff = $\sqrt{\pi/2}$ erf(z)/z

$$aaa = aa1 \cdot aa6 \tag{9.42}$$

Gaussians' centers

A B C D

r_1:

$$\begin{cases} \mathbf{r}_A = \mathbf{r}_1 - \mathbf{A} \\ \mathbf{r}_B = \mathbf{r}_1 - \mathbf{B} \end{cases} \tag{9.43}$$

r_2:

$$\begin{cases} \mathbf{r}_C \;=\; \mathbf{r}_2 \;-\; \mathbf{C} \\ \mathbf{r}_B \;=\; \mathbf{r}_2 \;-\; \mathbf{D} \end{cases} \tag{9.44}$$

We have the product of 4 gaussians.

$$exp\{-\alpha r_A^2\} \cdot exp\{-\beta r_B^2\} \;=\; K_1\, exp\{-\xi_1 r_P^2\} \tag{9.45}$$

$$exp\{-\gamma r_C^2\} \cdot exp\{-\delta r_D^2\} \;=\; K_2\, exp\{-\xi_2 r_Q^2\} \tag{9.46}$$

$$\xi_1 \;=\; \alpha \;+\; \beta;\;\; \xi_2 \;=\; \gamma \;+\; \delta \tag{9.47}$$

$$k1 \;=\; exp\,\{-\,\frac{\alpha\beta}{\alpha \;+\; \beta}\,|\,\overline{AB}\,|^2\} \tag{9.48}$$

$$k2 \;=\; exp\,\{-\,\frac{\gamma\delta}{\gamma \;+\; \delta}\,|\,\overline{CD}\,|^2\} \tag{9.49}$$

$$\begin{array}{cccc} G_A(\alpha,\, A) & G_B(\beta,\, B) & G_C(\gamma,\, C) & G_D(\delta,\, D) \\ r_1 & r_1 & r_2 & r_2 \end{array} \tag{9.50}$$

$$\mathbf{P} \;=\; \frac{\alpha\mathbf{A} \;+\; \beta\mathbf{B}}{\alpha \;+\; \beta} \tag{9.51}$$

$$\mathbf{Q} \;=\; \frac{\gamma\mathbf{C} \;+\; \delta\mathbf{D}}{\gamma \;+\; \delta} \tag{9.52}$$

$$\mathbf{r}_P = \mathbf{r}_1 - \mathbf{P}; \;\; \mathbf{r}_Q = \mathbf{r}_2 - \mathbf{Q}; \tag{9.53}$$

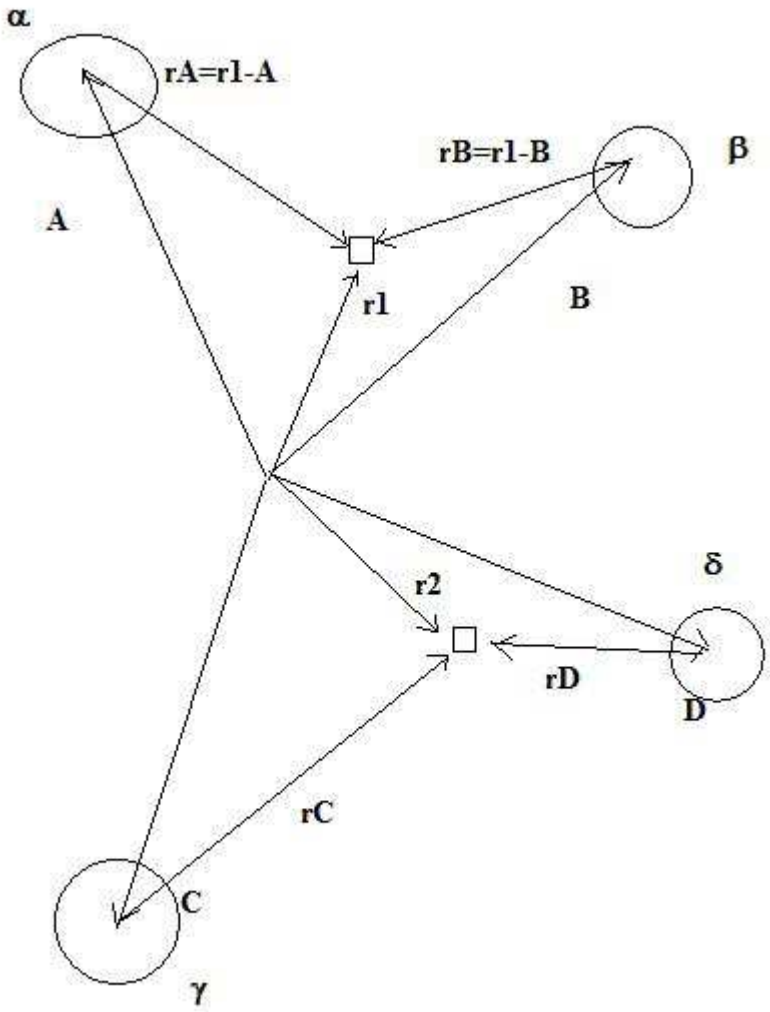

Figure 9.1 – Sketch of the gaussians centers

$$\frac{1}{r_{12}} = \frac{1}{\pi} \int_0^\infty exp\{-r_{12}^2 \cdot \rho\} \frac{1}{\sqrt{\rho}} \, d\rho \tag{9.54}$$

We get for the electronic repulsion integral:

A	**B**	**C**	**D**
r_1	r_1	r_2	r_2
$+\mathbf{a}$	$+\mathbf{a}$	**- a**	**- a**
ik	kk	jk	lk
$\alpha(ik)$	$\beta(kk)$	$\gamma(jk)$	$\delta(lk)$

Table 9.3 – Direct integral summary

$$R = \frac{\mathcal{N}_A \mathcal{N}_B \mathcal{N}_C \mathcal{N}_D}{\sqrt{\pi}} \cdot K_1 \cdot K_2 \cdot \int_0^\infty d\rho \, \frac{1}{\sqrt{\rho}} U_x^R \, U_y^R \, U_z^R \tag{9.55}$$

$$U_h^R = \int dh_1 \int dh_2 \, h_A^{k_h} \, h_B^{l_h} \, h_C^{m_h} \, h_D^{n_h} \cdot$$

$$\cdot exp\,[-\rho(h_2 - h_1)^2\,]\, exp\,[-\epsilon_1(h_1 - P_h)^2\,]\, exp\,[-\epsilon_2(h_2 - Q_h)^2\,] \tag{9.56}$$

Subroutine twdir, direct integral

subroutine twdir(abc,ik,jk,kk,lk,ng)

$$\int d\mathbf{r}_1 \, d\mathbf{r}_2 \cdot STO(\mathbf{r}_1 - \mathbf{a},\, ik) \cdot STO(\mathbf{r}_1 - \mathbf{a},\, kk) \cdot |\, V \,| \cdot$$

$$\cdot STO(\mathbf{r}_2 + \mathbf{a},\, jk) \cdot STO(\mathbf{r}_2 + \mathbf{a},\, lk) \tag{9.57}$$

```
!  switch n.  1
go to (111,112,113,114,115),ik
111 call s1sq(exx1,cs1,ng)
```

```
go to 107
112 call s2sq(exx1,cs1,ng)
go to 107
113 call s3sq(exx1,cs1,ng)
go to 107
114 call s4sq(exx1,cs1,ng)
go to 107
115 call s5sq(exx1,cs1,ng)
107 continue
do jj = 1,ng
exx1m(jj) = exx1(jj)
cs1m(jj) = cs1(jj)
end do
!  switch n.  3
go to (311,312,313,314,315),jk
311 call s1sq(exx1,cs1,ng)
go to 307
312 call s2sq(exx1,cs1,ng)
go to 307
313 call s3sq(exx1,cs1,ng)
go to 307
314 call s4sq(exx1,cs1,ng)
go to 307
315 call s5sq(exx1,cs1,ng)
307 continue
do jj = 1,ng
```

```
exx1o(jj) = exx1(jj)
cs1o(jj) = cs1(jj)
end do
!  switch n.  2
go to (211,212,213,214,215),kk
211 call s1sq(exx1,cs1,ng)
go to 207
212 call s2sq(exx1,cs1,ng)
go to 207
213 call s3sq(exx1,cs1,ng)
go to 207
214 call s4sq(exx1,cs1,ng)
go to 207
215 call s5sq(exx1,cs1,ng)
207 continue
do jj = 1,ng
exx1n(jj) = exx1(jj)
cs1n(jj) = cs1(jj)
end do
!  switch n.  4
go to (411,412,413,414,415),lk
411 call s1sq(exx1,cs1,ng)
go to 407
412 call s2sq(exx1,cs1,ng)
go to 407
413 call s3sq(exx1,cs1,ng)
```

```
go to 407
414 call s4sq(exx1,cs1,ng)
go to 407
415 call s5sq(exx1,cs1,ng)
407 continue
do jj = 1,ng
exx1p(jj) = exx1(jj)
cs1p(jj) = cs1(jj)
end do
do l = 1,ii !  ii = number of gaussian functions
ei1(l) = exx1m(l)*(csz1*csz1)
ci1(l) = cs1m(l) * (2._16 * ei1(l)/pig) ** 0.75_16
ei2(l) = exx1n(l)*(csz2*csz2)
ci2(l) = cs1n(l) * (2._16 * ei2(l)/pig) ** 0.75_16
ei3(l) = exx1o(l)*(csz3*csz3)
ci3(l) = cs1o(l) * (2._16 * ei3(l)/pig) ** 0.75_16
ei4(l) = exx1p(l)*(csz4*csz4)
ci4(l) = cs1p(l) * (2._16 * ei4(l)/pig) ** 0.75_16
end do
alpha = ei1(i1)
beta = ei2(i2)
gamm = ei3(i3)
delta = ei4(i4)
abc = 0._16
do i1 = 1,ii
do i2 = 1,ii
```

```
do i3 = 1,ii
do i4 = 1,ii
aa = r/2._16
zz1 = aa
zz2 = aa
zz3 = - aa
zz4 = - aa
pp = (alpha*zz1 + beta *zz2)/(alpha + beta )
qq = (gamm *zz3 + delta*zz4)/(gamm + delta)
eps1 = alpha + beta
eps2 = gamm + delta
ee1 = alpha * beta /(alpha + beta)
ee2 = gamm * delta/(gamm + delta)
aabb = (zz2 - zz1)*(zz2 - zz1)
ccdd = (zz4 - zz3)*(zz4 - zz3)
ak1 = exp(1._16)**( - ee1 * aabb)
ak2 = exp(1._16)**( - ee2 * ccdd)
aa1 = 2._16 * ak1 * ak2 * pig**2.5_16
aa1 = aa1/( eps1 * eps2 * sqrt(eps1 + eps2))
ppqq = (pp - qq)*(pp - qq)
aa5 = (eps1 * eps2/(eps1 + eps2)) * ppqq
37 format(3x,a41,f20.15)
call efff(aa5,aa6,80) !
aaa = aa1 * aa6
aa2 = ci1(i1) * ci2(i2) * ci3(i3) * ci4(i4)
abc = abc + aa2 * aaa
```

A	**B**	**C**	**D**
r_1	r_1	r_2	r_2
$+\mathbf{a}$	$-\mathbf{a}$	$-\mathbf{a}$	$+\mathbf{a}$
ik	lk	jk	kk
$\alpha(ik)$	$\beta(lk)$	$\gamma(jk)$	$\delta(kk)$

Table 9.4 – Exchange integral summary

```
end do
end do
end do
end do
return
end
```

Subroutine twscc, exchange integral

subroutine twscc(abd,ik,jk,kk,lk,ng)

We must compute

$$\int d\mathbf{r}_1\, d\mathbf{r}_2 \cdot STO(\mathbf{r}_1 - \mathbf{a},\, ik) \cdot STO(\mathbf{r}_1 + \mathbf{a},\, lk) \cdot |\, V \,| \cdot$$

$$\cdot STO(\mathbf{r}_2 + \mathbf{a},\, jk) \cdot STO(\mathbf{r}_2 - \mathbf{a},\, kk) \tag{9.58}$$

```
ii = ng
!  switch n.  1
go to (111,112,113,114,115),ik
111 call s1sq(exx1,cs1,ng)
go to 107
112 call s2sq(exx1,cs1,ng)
go to 107
113 call s3sq(exx1,cs1,ng)
go to 107
114 call s4sq(exx1,cs1,ng)
go to 107
115 call s5sq(exx1,cs1,ng)
107 continue
do jj = 1,ng
exx1m(jj) = exx1(jj)
cs1m(jj) = cs1(jj)
end do
!  switch n.  2
go to (211,212,213,214,215),lk
211 call s1sq(exx1,cs1,ng)
go to 207
212 call s2sq(exx1,cs1,ng)
go to 207
213 call s3sq(exx1,cs1,ng)
go to 207
214 call s4sq(exx1,cs1,ng)
```

```
go to 207
215 call s5sq(exx1,cs1,ng)
207 continue
do jj = 1,ng
exx1n(jj) = exx1(jj)
cs1n(jj) = cs1(jj)
end do
!  switch n.  3
go to (311,312,313,314,315),jk
311 call s1sq(exx1,cs1,ng)
go to 307
312 call s2sq(exx1,cs1,ng)
go to 307
313 call s3sq(exx1,cs1,ng)
go to 307
314 call s4sq(exx1,cs1,ng)
go to 307
315 call s5sq(exx1,cs1,ng)
307 continue
do jj = 1,ng
exx1o(jj) = exx1(jj)
cs1o(jj) = cs1(jj)
end do
!  switch n.  4
go to (411,412,413,414,415),kk
411 call s1sq(exx1,cs1,ng)
```

```
go to 407
412 call s2sq(exx1,cs1,ng)
go to 407
413 call s3sq(exx1,cs1,ng)
go to 407
414 call s4sq(exx1,cs1,ng)
go to 407
415 call s5sq(exx1,cs1,ng)
407 continue
do jj = 1,ng
exx1p(jj) = exx1(jj)
cs1p(jj) = cs1(jj)
end do
do l = 1,ii !  ii = number of gaussian functions
ei1(l) = exx1m(l)*(csz1*csz1)
ci1(l) = cs1m(l) * (2._16 * ei1(l)/pig) ** 0.75_16
ei2(l) = exx1n(l)*(csz2*csz2)
ci2(l) = cs1n(l) * (2._16 * ei2(l)/pig) ** 0.75_16
ei3(l) = exx1o(l)*(csz3*csz3)
ci3(l) = cs1o(l) * (2._16 * ei3(l)/pig) ** 0.75_16
ei4(l) = exx1p(l)*(csz4*csz4)
ci4(l) = cs1p(l) * (2._16 * ei4(l)/pig) ** 0.75_16
end do
alpha = ei1(i1)
beta = ei2(i2)
gamm = ei3(i3)
```

```
delta = ei4(i4)
abc = 0._16
do i1 = 1,ii
do i2 = 1,ii
do i3 = 1,ii
do i4 = 1,ii
aa = r/2._16
zz1 = aa
zz2 = - aa
zz3 = - aa
zz4 = aa
pp = (alpha*zz1 + beta *zz2)/(alpha + beta )
qq = (gamm *zz3 + delta*zz4)/(gamm + delta)
eps1 = alpha + beta
eps2 = gamm + delta
ee1 = alpha * beta /(alpha + beta)
ee2 = gamm * delta/(gamm + delta)
aabb = (zz2 - zz1)*(zz2 - zz1)
ccdd = (zz4 - zz3)*(zz4 - zz3)
ak1 = exp(1._16)**( - ee1 * aabb)
ak2 = exp(1._16)**( - ee2 * ccdd)
aa1 = 2._16 * ak1 * ak2 * pig**2.5_16
aa1 = aa1/( eps1 * eps2 * sqrt(eps1 + eps2))
ppqq = (pp - qq)*(pp - qq)
aa5 = (eps1 * eps2/(eps1 + eps2)) * ppqq
37 format(3x,a41,f20.15)
```

```
call efff(aa5,aa6,80) !
aaa = aa1 * aa6
aa2 = ci1(i1) * ci2(i2) * ci3(i3) * ci4(i4)
abd = abd + aa2 * aaa
end do
end do
end do
end do
return
end
```

l	m	n	ω	k
0	0	0	0	1.
0	0	1	1	2.
0	0	2	2	4.
0	1	2	3	9.
0	1	3	4	15.
0	2	0	2	6.
0	2	1	3	10.
0	2	2	4	16.
0	2	3	5	25.
1	0	0	1	4.
1	0	1	2	6.
1	0	2	3	10.

Table 9.5 – Schema for triples for some values of l, m, n - singlet case

l	m	n	ω	k
0	0	0	0	1.
0	0	1	1	2.
0	0	2	2	4.
0	1	2	3	9.
0	1	3	4	15.
0	2	0	2	6.
0	2	1	3	10.
0	2	2	4	16.
0	2	3	5	25.
1	0	0	1	4.
1	0	1	2	6.
1	0	2	3	10.

Table 9.6 – Schema for triples for some values of l, m, n - triplet case

9.2 Pekeris coefficients

The triples (l,m,n) are obtained with the schema of table 9.5 for the singlet and of table 9.6 for the triplet.

Here we report the a_{ik} and b_{ik} of order 13 for the singlet and triplet.

Singlet

$$a_{1,1}-a_{7,7}\begin{bmatrix} 5-16z & -4+4z & -6+28z & 1 & 2-4z & -8z & 2-4z \\ -4+4z & 15-24z & 2-4z & -12+8z & -10+36z & 0 & 0 \\ -6+28z & 2-4z & 26-112z & 0 & -12+16z & -12+88z & -14+44z \\ 1 & -12+8z & 0 & 31-32z & 4-8z & 0 & 0 \\ 2-4z & -10+36z & -12+16z & 4-8z & 54-144z & 4-8z & 2-4z \\ -8z & 0 & -12+88z & 0 & 4-8z & 34-224z & 8-16z \\ 2-4z & 0 & -14+44z & 0 & 2-4z & 8-16z & 25-104z \end{bmatrix} \tag{9.59}$$

$$a_{1,8}-a_{13,13}\begin{bmatrix} 0 & 0 & 0 & 0 & 0 & 0 \\ 3 & 4-8z & -8z & 2-4z & 0 & 0 \\ 0 & 2 & 4-8z & 2-4z & -24z & 8-24z \\ -24+12z & -14+44z & 0 & 0 & 0 & 0 \\ 0 & -32+32z & -20+104z & -18+52z & 0 & 0 \\ 0 & 0 & -16+24z & 0 & -18+180z & -22+60z \\ 0 & 0 & 0 & -8+12z & 0 & -28+120z \end{bmatrix} \tag{9.60}$$

$$a_{8,1}-a_{13,7}=(a_{1,8}-a_{13,13})^T \tag{9.61}$$

$$a_{8,8} - a_{13,13} \begin{bmatrix} 53+40z & 6-12z & 0 & 0 & 0 & 0 \\ 6-12z & 94-176z & 8-16z & 4-8z & 0 & 0 \\ 0 & 8-16z & 70-272z & 8-16z & 6-12z & 2-4z \\ 0 & 4-8z & 8-16z & 43-128z & 0 & 4-8z \\ 0 & 0 & 6-12z & 0 & 46-392z & 12-24z \\ 0 & 0 & 2-4z & 4-8z & 12-24z & 94-392z \end{bmatrix} \tag{9.62}$$

$$b_{1,1} - b_{7,7} \begin{bmatrix} 16 & -4 & -28 & 0. & 4 & 8 & 4 \\ -4 & 48 & -8 & -16 & -60 & 8 & 0 \\ -28 & -8 & 144 & 4 & -16 & -104 & -72 \\ 0. & -16 & 4 & 96 & -20 & 0 & 0 \\ 4 & -60 & -16 & -20 & 336 & -32 & -4 \\ 8 & 8 & -104 & 0 & -32 & 320 & 24 \\ 4 & 0 & -72 & 0 & -4 & 24 & 208 \end{bmatrix} \tag{9.63}$$

$$b_{1,8} - b_{7,13} \begin{bmatrix} 0 & 0 & 0 & 0 & 0 & 0 \\ 0 & 12 & 16 & 4 & 0 & 0 \\ 0 & 0 & 8 & 8 & 24 & 40 \\ -36 & -96 & 16 & 0 & 0 & 0 \\ 12 & -64 & -216 & -112 & 24 & 0 \\ 0 & 8 & -16 & 0 & -228 & -132 \\ 0 & 4 & 0 & -20 & 0 & -240 \end{bmatrix} \tag{9.64}$$

$$b_{8,1} - b_{13,7} = (b_{1,8} - b_{7,13})^T \tag{9.65}$$

$$b_{8,8} - b_{13,13} \begin{bmatrix} 160 & -36 & 0 & 0 & 0 & 0 \\ -36 & 592 & -72 & -12 & 0 & 0 \\ 0 & -72 & 720 & 24 & -72 & 0 \\ 0 & -12 & 24 & 384 & 0 & -24 \\ 0 & 0 & -72 & 0 & 584 & 48 \\ 0 & 0 & 0 & -24 & 48 & 920 \end{bmatrix} \tag{9.66}$$

Triplet

$$a_{1,1}-a_{7,7}\begin{bmatrix} 9-48z & -6+8z & -6+44z & 1 & 2-4z & -12z & 4-12z \\ -6+8z & 23-64z & 2-4z & -16+16z & -10+52z & 0 & 0 \\ -6+44z & 2-4z & 17-112z & 0 & -8+12z & -9+90z & -11+30z \\ 1 & -16+16z & 0 & 43-80z & 4-8z & 0 & 0 \\ 2-4z & -10+52z & -8+12z & 4-8z & 35-136z & 3-6z & 1-2z \\ -12z & 0 & -9+90z & 0 & 3-6z & 23-196z & 6-12z \\ 4-12z & 0 & -11+30z & 0 & 1-2z & 6-12z & 47-196z \end{bmatrix} \tag{9.67}$$

$$a_{1,8}-a_{7,13}\begin{bmatrix} 0 & 0 & 0 & 0 & 0 & 0 \\ 3 & 4-8z & -12z & 0 & 4-4z & 0 \\ 0 & 1 & 3-6z & -24z & 1-2z & 6-12z \\ -30-24z & -14+60z & 0 & 0 & 0 & 0 \\ 0 & -20+24z & -15+102z & 0 & -13+34z & 0 \\ 0 & 0 & -10+16z & -12+152z & 0 & -15+38z \\ 0 & 0 & 0 & 0 & -10+16z & -21+114z \end{bmatrix} \tag{9.68}$$

$$a_{8,1}-a_{13,7}=(a_{1,8}-a_{7,13})^T \tag{9.69}$$

$$a_{8,8} - a_{13,13} \begin{bmatrix} 69-96z & 6-12z & 0 & 0 & 0 & 0 \\ 6-12z & 59-160z & 6-12z & 0 & 2-4z & 0 \\ 0 & 6-12z & 45-228z & 4-8z & 6-12z & 1-2z \\ 0 & 0 & 4-8z & 29-304z & 0 & 8-16z \\ 0 & 2-4z & 6-12z & 0 & 58-196z & 3-6z \\ 0 & 0 & 1-2z & 8-16z & 3-6z & 53-280z \end{bmatrix} \tag{9.70}$$

$$b_{1,1} - b_{7,7} \begin{bmatrix} 64 & -8 & -52 & 0. & 4 & 12 & 20 \\ -8 & 160 & -16 & -32 & -108 & 12 & 0 \\ -52 & -16 & 160 & 4 & -8 & -114 & -66 \\ 0. & -32 & 4 & 288 & -36 & 0 & 0 \\ 4 & -108 & -8 & -36 & 360 & -36 & 0 \\ 12 & 12 & -114 & 0 & -36 & 292 & 24 \\ 20 & 0 & -66 & 0 & 0 & 24 & 460 \end{bmatrix} \tag{9.71}$$

$$b_{1,8} - b_{7,13} \begin{bmatrix} 0 & 0 & 0 & 0 & 0 & 0 \\ 0 & 12 & 24 & 0 & 0 & 0 \\ 0 & 0 & 6 & 24 & 6 & 24 \\ -72 & -168 & 24 & 0 & 0 & 0 \\ 12 & -40 & -234 & 24 & -90 & 0 \\ 0 & 6 & -4 & -200 & 0 & -104 \\ 0 & 2 & 0 & 0 & -28 & -252 \end{bmatrix} \tag{9.72}$$

$$b_{8,1} - b_{13,7} = (b_{1,8} - b_{7,13})^T \tag{9.73}$$

$$b_{8,8} - b_{13,13} \begin{bmatrix} 448 & -60 & 0 & 0 & 0 & 0 \\ -60 & 608 & -78 & 0 & -2 & 0 \\ 0 & -78 & 636 & -64 & 24 & 2 \\ 0 & 0 & -64 & 464 & 0 & 40 \\ 0 & -2 & 24 & 0 & 692 & -30 \\ 0 & 0 & 2 & 40 & -30 & 728 \end{bmatrix} \tag{9.74}$$

For easy of reference, we report here the first 10 Laguerre polynomials and some graphs of the autofunctions of the basis.

n

0 1

1 $1 - x$

2 $1 - 2x + \frac{x^2}{2}$

3 $1 - 3x + \frac{3x^2}{2} - \frac{x^3}{6}$

4 $1 - 4x + 3x^2 - \frac{2x^3}{3} + \frac{x^4}{24}$

5 $1 - 5x + 5x^2 - \frac{5x^3}{3} + \frac{5x^4}{24} - \frac{x^5}{120}$

6 $1 - 6x + \frac{15x^2}{2} - \frac{10x^3}{3} + \frac{5x^4}{8} - \frac{x^5}{20} + \frac{x^6}{720}$

7 $1 - 7x + \frac{21x^2}{2} - \frac{35x^3}{6} + \frac{35x^4}{24} - \frac{7x^5}{40} + \frac{7x^6}{720} - \frac{x^7}{5040}$

8 $1 - 8x + 14x^2 - \frac{28x^3}{3} + \frac{35x^4}{12} - \frac{7x^5}{15} + \frac{7x^6}{180} - \frac{x^7}{630} + \frac{x^8}{40320}$

9 $1 - 9x + 18x^2 - 14x^3 + \frac{21x^4}{4} - \frac{21x^5}{20} + \frac{7x^6}{60} - \frac{x^7}{140} + \frac{x^8}{4480} - \frac{x^9}{362880}$

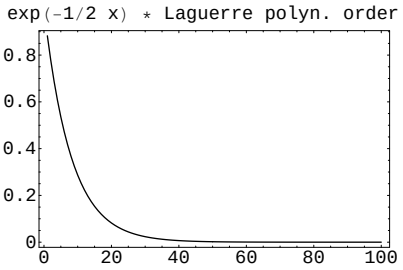

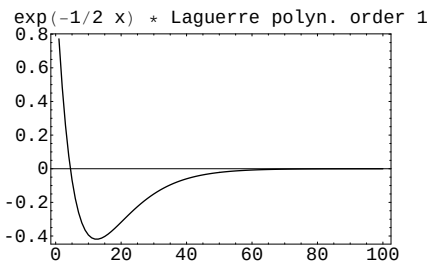

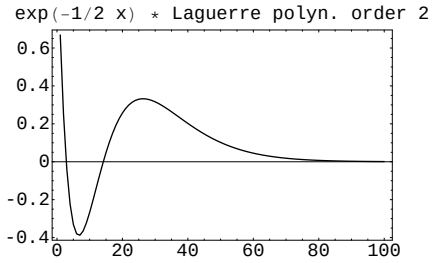
exp(-1/2 x) * Laguerre polyn. order 2
0.6
0.4
0.2
0
-0.2
-0.4
0
20
40
60
80
100

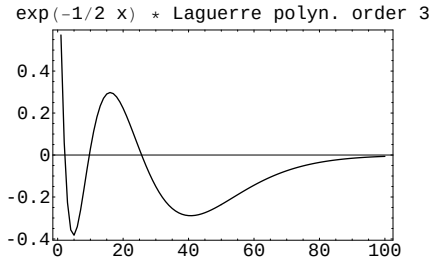
exp(-1/2 x) * Laguerre polyn. order 3
0.4
0.2
0
-0.2
-0.4
0
20
40
60
80
100

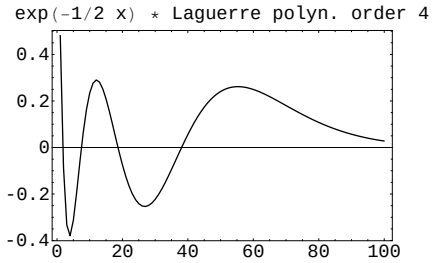
exp(-1/2 x) * Laguerre polyn. order 4
0.4
0.2
0
-0.2
-0.4
0
20
40
60
80
100

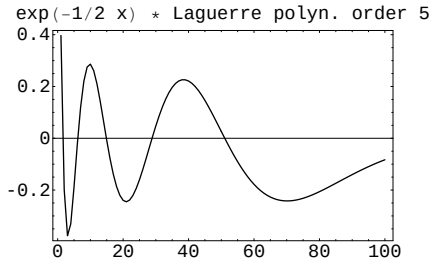
exp(-1/2 x) * Laguerre polyn. order 5
0.4
0.2
0
-0.2
0
20
40
60
80
100

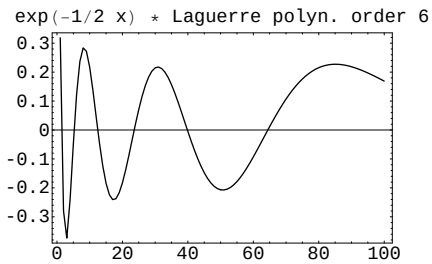
exp(-1/2 x) * Laguerre polyn. order 6
0.3
0.2
0.1
0
-0.1
-0.2
-0.3
0
20
40
60
80
100

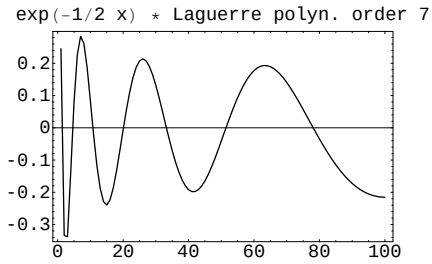
exp(-1/2 x) * Laguerre polyn. order 7
0.2
0.1
0
-0.1
-0.2
-0.3
0
20
40
60
80
100

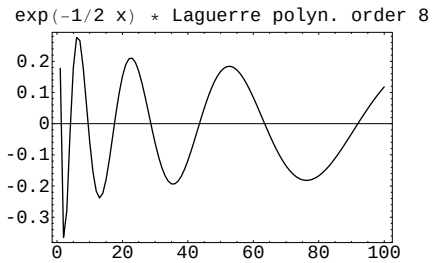
exp(-1/2 x) * Laguerre polyn. order 8
0.2
0.1
0
-0.1
-0.2
-0.3
0
20
40
60
80
100

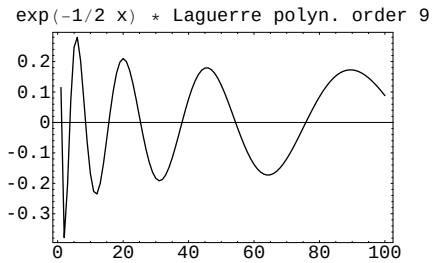
exp(-1/2 x) * Laguerre polyn. order 9
0.2
0.1
0
-0.1
-0.2
-0.3
0
20
40
60
80
100

9.3 Orthonormalization in the Fock space: program details (clxnn)

Referring to section 5.7.1.3, recall the definitions:

sovr(i, j) = initial superposition

axx(i, j) = unknown matrix to be recursively computed

We impose that the $|\, i\rangle$ must be normalized:

$$\langle i \,|\, i\rangle \;=\; 1 \tag{9.75}$$

But in general

$$sovr(i,\, j) \;=\; \langle i,\, j\rangle \neq \delta_{ij} \tag{9.76}$$

```
kmax = 15 !(presently)
do k = 2, kmax
do j = 1,k-1
do ih = 1,k-1
abc = 0._16
do i = 1,ih
abc = abc + axx(ih,i) * sovr(i,j)
```

```
end do !  loop i
alf(ih,j) = abc
end do !  loop ih
end do !  loop j
do ih = 1,k-1
abc = 0._16
do i = 1,ih
abc = abc + axx(ih,i) * sovr(i,k)
end do !  loop i
vvk(ih,1) = - abc
end do !  loop ih
call gauss(alf,k-1,50,vvk,1,50)
do i= 1, k-1
axx(k,i) = vvk(i,1)
end do
axx(k,k) = 1
an1 = 0._16
nn1 = k
nn2 = k
do kz = 1,nn1
do lz = 1,nn2
a1 = axx(k,kz) * axx(k,lz)
an1 = an1 + a1 * sovr(kz,lz)
end do
end do
an1 = sqrt(an1)
do kz = 1,nn1
```

```
axx(k,kz) = axx(k,kz)/an1
end do
end do
```

Here gauss() is a standard routine to find solutions of linear equations with the Gauss-Jordan method.

9.4 Useful expressions: Gaunt formulas

$\int_0^{\pi} sin\,\theta\, d\theta \int_0^{2\pi} d\phi\, Y^*_{l'm'}(\theta,\phi)\, Y_{LM}(\theta,\phi)\, Y_{lm}(\theta,\phi) =$

$= \int Y^*_{l'm'}(\theta,\phi)\, Y_{LM}(\theta,\phi)\, Y_{lm}(\theta,\phi) d\Omega \equiv$

$\equiv \langle l'm' \,|\, Y_{LM} \,|\, lm \rangle = (-1)^{m'} \sqrt{\frac{(2l'+1)(2L+1)(2l+1)}{4\pi}} \times$

$$\times \begin{pmatrix} l' & L & l \\ -m' & M & m \end{pmatrix} \begin{pmatrix} l' & L & l \\ 0 & 0 & 0 \end{pmatrix} \tag{9.77}$$

$-m' + M + m = 0$

$l' + L + l$ *even*

$$\begin{aligned} l' + L - l &\geq 0 \\ l' - L + l &\geq 0 \\ -l' + L + l &\geq 0 \end{aligned} \tag{9.78}$$

$$Y_{LM}(\theta,\,\phi) = (-1)^{l'-l-M} \sqrt{2L+1} \sum_{mm'} \begin{pmatrix} l & l' & L \\ m & m' & M \end{pmatrix} \times$$

$$\times Y_{lm}(\theta,\,\phi)\, Y_{l'm'}(\theta,\,\phi) \tag{9.79}$$

$Y_{lm}(\theta,\,\phi)\, Y_{l'm'}(\theta,\,\phi) = \sum_{LM} \sqrt{\frac{(2l+1)\,(2l'+1)\,(2L+1)}{4\pi}} \times$

$$\times \begin{pmatrix} l & l' & L \\ m & m' & M \end{pmatrix} \begin{pmatrix} l & l' & L \\ 0 & 0 & 0 \end{pmatrix} Y^*_{LM}(\theta,\, \phi) \tag{9.80}$$

$Y^*_{lm}(\theta,\, \phi)\, Y_{l'm'}(\theta,\, \phi) = \sum_{LM} (-1)^{m'} \sqrt{\frac{(2l+1)\,(2l'+1)\,(2L+1)}{4\pi}} \times$

$$\times \begin{pmatrix} l & l' & L \\ m & -m' & M \end{pmatrix} \begin{pmatrix} l & l' & L \\ 0 & 0 & 0 \end{pmatrix} Y_{LM}(\theta,\, \phi) \tag{9.81}$$

ndds	aa1s	energy	Δ E(ppm)	vN entr	lin entr
5	2.1553	-2.878885258	8554.22	0.041314400	0.008741626
6	2.3579	-2.878969795	8525.11	0.041330427	0.008741803
7	2.5237	-2.878997343	8515.62	0.041332628	0.008741389
8	2.6974	-2.879012160	8510.52	0.041336318	0.008741842
9	2.8868	-2.879018943	8508.18	0.041337172	0.008741818
10	3.0684	-2.879022692	8506.89	0.041337828	0.008741866
11	3.2474	-2.879024823	8506.16	0.041338194	0.008741892
12	3.4105	-2.879026110	8505.72	0.041338479	0.008741928
13	3.6211	-2.879026917	8505.44	0.041338463	0.008741902
14	3.7789	-2.879027448	8505.26	0.041338603	0.008741924
15	3.9368	-2.879027803	8505.13	0.041338679	0.008741935
16	4.0947	-2.879028048	8505.05	0.041338720	0.008741940
17	4.2918	-2.879028222	8504.99	0.041338707	0.008741933
18	4.4640	-2.879028347	8504.95	0.041338731	0.008741937
19	4.6312	-2.879028439	8504.91	0.041338735	0.008741936
20	4.8065	-2.879028507	8504.89	0.041338734	0.008741935

Table 9.7 – Fundamental level S shell only

9.5 Detailed results of computations

In this section we report the results of computations of levels fundamental to VI, shells S, S-P and S-P-D of singlet; levels I to VI, shells S, S-P of triplets, computed using several Hilbert space dimensions.

The aim is to show the dependence of energy and of the entropies on these parameters.

9.5.1 Singlet states - S shell only

Fundamental level

In the table 9.7 we report our results for the S shell only, fundamental state, starting with $n_s = 5$.

We note that the asymptotical values of the energy and of the von Neumann and linear

entropies are obtained very quickly, increasing the radial quantum number n.

In particular, values of n_s of the order of 10 suffice to obtain a value of the energy within $\approx 1\,ppm$ of the asymptotical values for the S shell.

The linear entropy varies only in its fifth digit for $5 \leq n_s \leq 20$ and the von Neumann entropy in its fourth digit for $5 \leq n_s \leq 10$.

This indicates that the von Neumann entropy computation is slightly more complex than the linear entropy computation.

We recall that we are not interested in the energy computation, that is reported here just as a comparation item. Of course, it must always be computed, as one must find its minimum to determine the correct value of the parameter (aa1s).

It is noteworthy that for this shell, and also for others, a single varational parameter for each shell has been sufficient.

In the first versions of the programs we had the possibility of varying the STO parameter also within the shells.

After a large number of computations, we concluded that a small increase of the radial quantum number n can compensate for the use of these extra degrees of freedom.

So we decided to avoid them, greatly simplifying the variational problem, that, in the S shell case, is limited to a single variational parameter.

Of course there are no variational theorems available for entropies.

In the figures 9.2, 9.3 e 9.4 we reported ΔE, evN, elin vs the parameter aa1s for $n_s = 7$ and $n_s = 15$.

We note that, as expected, a greater value for n_s implies a lower sensitivity for the aa1s parameter.

We note also that, in general, the minimum in the energy plot, that corresponds to the

"true" value of energy, falls in regions of the von Neumann and linear entropies that are almost flat.

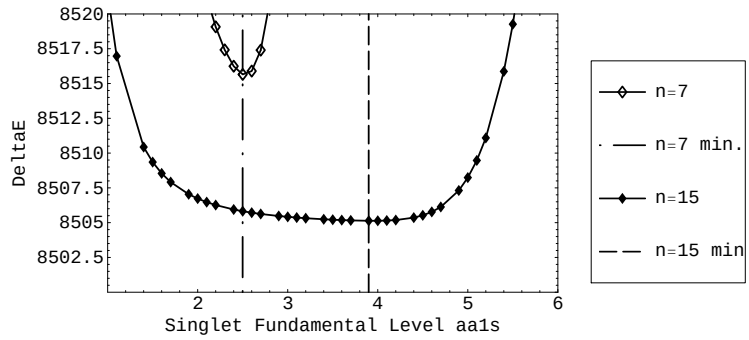

Figure 9.2 – Singlet Fundam. level, S only ,Energy error for n=7 and n=15

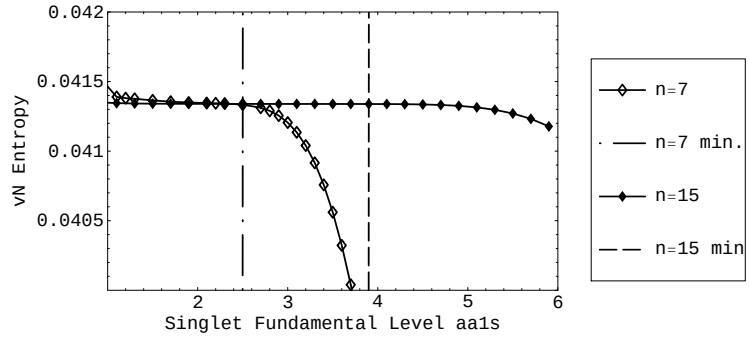

Figure 9.3 – Singlet Fundam. level, S only, von Neumann entropy for n=7 and n=15

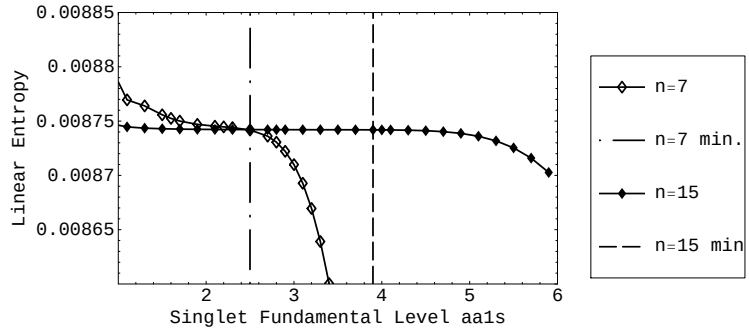

Figure 9.4 – Singlet Fundam. level, S only, Linear entropy for n=7 and n=15

ndds	aa1s	energy	Δ E(ppm)	vN entr	lin entr
5	1.0218	-2.140920080	2355.09	0.982247976	0.486323422
6	1.0242	-2.143794459	1015.66	0.983651299	0.487367848
7	1.0136	-2.144031778	905.07	0.983769064	0.487452071
8	1.0427	-2.144162784	844.03	0.983872476	0.487523056
9	1.0731	-2.144173674	838.95	0.983889978	0.487529911
10	1.1301	-2.144185289	833.54	0.983900083	0.487536886
11	1.1999	-2.144189950	831.37	0.983903989	0.487539348
12	1.2501	-2.144192457	830.20	0.983905883	0.487540828
13	1.3186	-2.144194267	829.36	0.983907335	0.487541828
14	1.3734	-2.144195144	828.95	0.983908128	0.487542344
15	1.4357	-2.144195823	828.63	0.983908699	0.487542741
16	1.4945	-2.144196216	828.45	0.983909064	0.487542975
17	1.5544	-2.144196504	828.31	0.983909312	0.487543145
18	1.6139	-2.144196695	828.23	0.983909484	0.487543257
19	1.6755	-2.144196834	828.16	0.983909607	0.487543341
20	1.7297	-2.144196933	828.11	0.983909696	0.487543401

Table 9.8 – Level I, S shell only

Level I

In the table 9.8 we report our results for the S shell only, I excited state, starting with $n_s = 5$.

Also in this case the asymptotic values are achieved very quickly.

We note that, from this level, we get von Neumann entropy values near 1, and linear entropy values near 0.5, as expected.

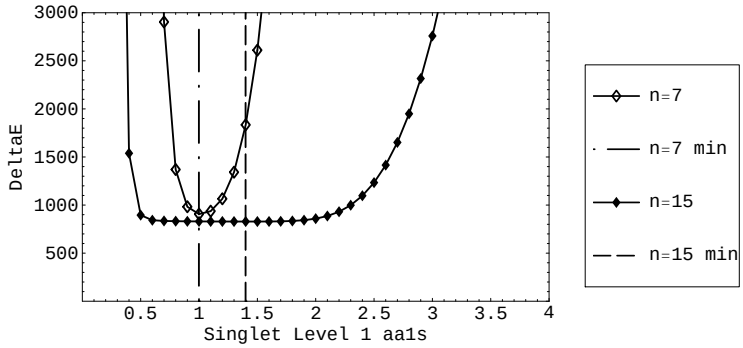

Figure 9.5 – Singlet level I, S only, Energy error for n=7 and n=15

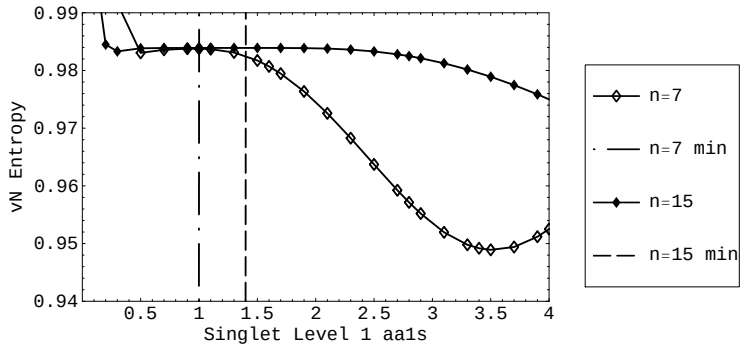

Figure 9.6 – Singlet level I, S only, von Neumann entropy for n=7 and n=15

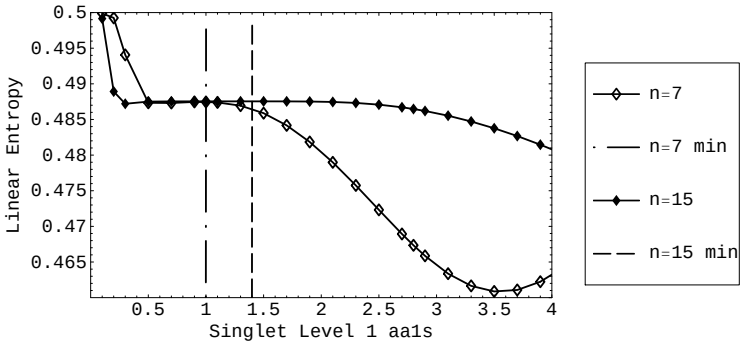

Figure 9.7 – Singlet level I, S only, Linear entropy forn=7 and n=15

ndds	aa1s	energy	Δ E(ppm)	vN entr	lin entr
5	0.7861	-2.024148520	18009.98	0.991662720	0.493014343
6	0.7706	-2.047362403	6748.06	0.993328234	0.494585451
7	0.7628	-2.057126101	2011.33	0.995553707	0.496292723
8	0.7515	-2.059504122	857.66	0.995921683	0.496617396
9	0.7504	-2.060495486	376.71	0.996227022	0.496862704
10	0.7459	-2.060682014	286.22	0.996278223	0.496902107
11	0.7525	-2.060768408	244.31	0.996315230	0.496931460
12	0.7549	-2.060780326	238.52	0.996322731	0.496935261
13	0.7726	-2.060788280	234.67	0.996327848	0.496938881
14	0.7974	-2.060789933	233.86	0.996329675	0.496939691
15	0.8278	-2.060791381	233.16	0.996330559	0.496940432
16	0.8660	-2.060792198	232.76	0.996331148	0.496940833
17	0.8951	-2.060792689	232.53	0.996331449	0.496941089
18	0.9333	-2.060793093	232.33	0.996331728	0.496941292
19	0.9626	-2.060793312	232.22	0.996331900	0.496941411
20	1.0019	-2.060793505	232.13	0.996332035	0.496941509

Table 9.9 – Level II, S shell only

Level II

In the table 9.9 we report our results for the S shell only, I excited state, starting with $n_s = 5$.

Also in this case the asymptotic values are achieved very quickly, but with variabilities that are slightly greater than in the preceding cases (fifth significant digit for energy, fourth for the von Neumann entropy and fifth for the linear).

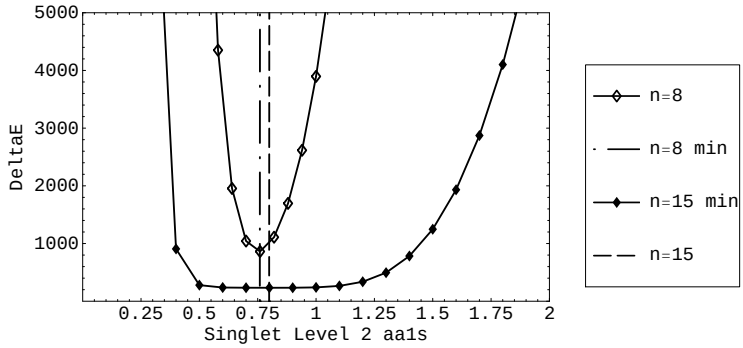

Figure 9.8 – Singlet level II, S only, Energy error for n=8 and n=15

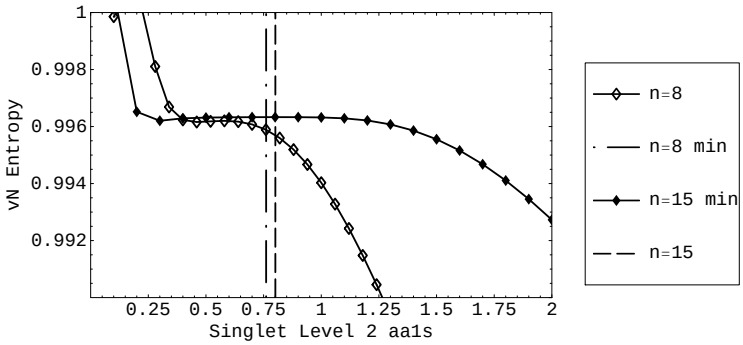

Figure 9.9 – Singlet level II, S only, von Neumann entropy for n=8 and n=15

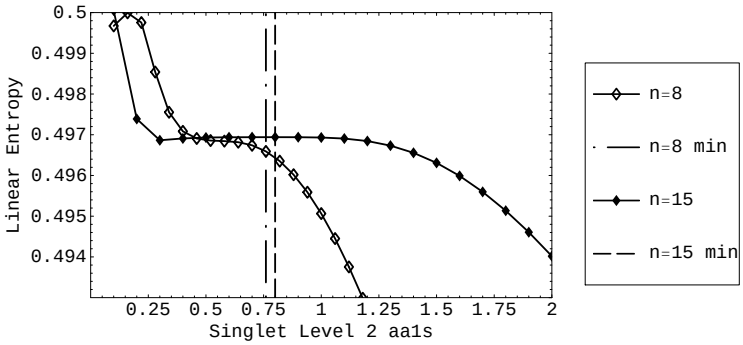

Figure 9.10 – Singlet level II, S only, Linear entropy for n=8 and n=15

ndds	aa1s	energy	Δ E(ppm)	vN entr	lin entr
5	0.6061	-1.863523588	83627.18	0.979589433	0.485268083
6	0.6339	-1.971356819	30601.05	0.993800794	0.494604834
7	0.6255	-2.005480133	13821.19	0.994780185	0.495717987
8	0.6187	-2.022668984	5368.71	0.997326940	0.497669306
9	0.6084	-2.028734554	2386.01	0.997793228	0.498114785
10	0.6032	-2.031728327	913.85	0.998330154	0.498551589
11	0.5978	-2.032709260	431.48	0.998458964	0.498665720
12	0.5973	-2.033175865	202.03	0.998566145	0.498756067
13	0.5957	-2.033304518	138.77	0.998592364	0.498776938
14	0.5989	-2.033366861	108.11	0.998610696	0.498792563
15	0.5997	-2.033380810	101.25	0.998615537	0.498795558
16	0.6068	-2.033388527	97.46	0.998618580	0.498798031
17	0.6124	-2.033390112	96.68	0.998619696	0.498798544
18	0.6262	-2.033391261	96.11	0.998620311	0.498799031
19	0.6456	-2.033391675	95.91	0.998620664	0.498799221
20	0.6638	-2.033392002	95.75	0.998620824	0.498799381

Table 9.10 – Level III, S shell only

Level III

In the table 9.10 we report our results for the S shell only, III excited state, starting with $n_s = 5$.

Now the changes in the entropy from dimension for S Shell=10 to dimension for S Shell=20 regard the fourth decimal digit.

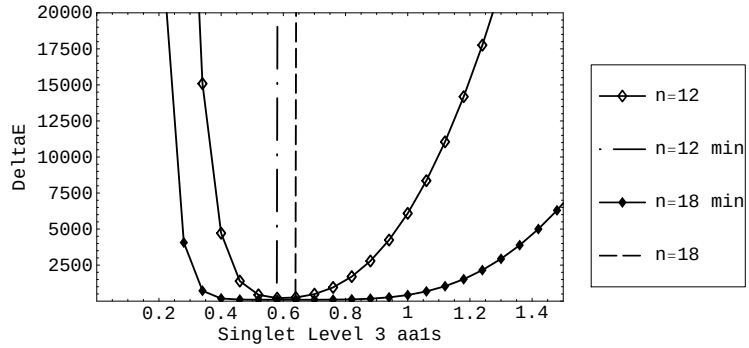

Figure 9.11 – Singlet level III, S only, Energy error for n=12 and n=18

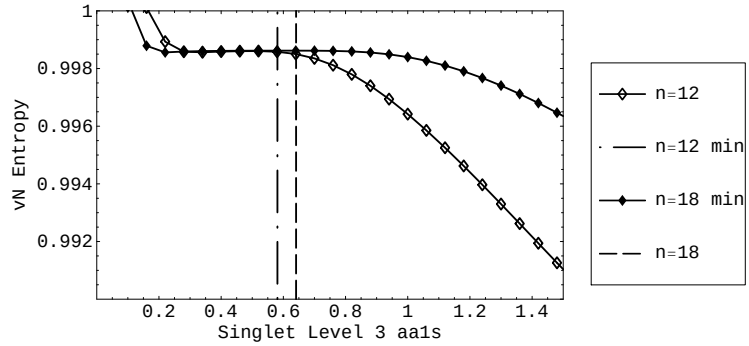

Figure 9.12 – Singlet level III, S only, von Neumann entropy for n=12 and n=18

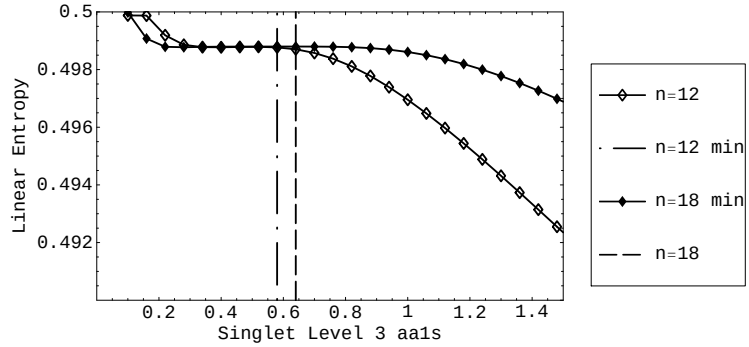

Figure 9.13 – Singlet level III, S only, Linear entropy for n=12 and n=18

ndds	aa1s	energy	Δ E(ppm)	vN entr	lin entr
5	0.4442	-1.610326948	203272.61	0.996318952	0.496992753
6	0.5059	-1.824953333	97083.79	0.981950571	0.486977635
7	0.5352	-1.938536716	40887.14	0.994800204	0.495364914
8	0.5318	-1.978864285	20934.62	0.995241802	0.496085578
9	0.5266	-2.001473878	9748.27	0.997767539	0.498000460
10	0.5168	-2.011074730	4998.14	0.998157877	0.498413099
11	0.5106	-2.016543611	2292.35	0.998831046	0.498957687
12	0.5040	-2.018876908	1137.92	0.999008185	0.499124746
13	0.5007	-2.020151922	507.10	0.999199442	0.499286513
14	0.4977	-2.020653611	258.88	0.999257922	0.499338357
15	0.4980	-2.020915818	129.15	0.999306142	0.499380450
16	0.4975	-2.021006601	84.23	0.999321402	0.499392876
17	0.4997	-2.021053565	61.00	0.999332062	0.499402378
18	0.5006	-2.021067603	54.05	0.999335549	0.499404774
19	0.5048	-2.021075239	50.27	0.999337674	0.499406658
20	0.5072	-2.021077265	49.27	0.999338540	0.499407114

Table 9.11 – Level IV, S shell only

Level IV

In the table 9.11 we report our results for the S shell only, IV excited state, starting with da $n_s = 5$.

Now the changes in the entropy from n=10 to n=20 regard the third decimal digit.

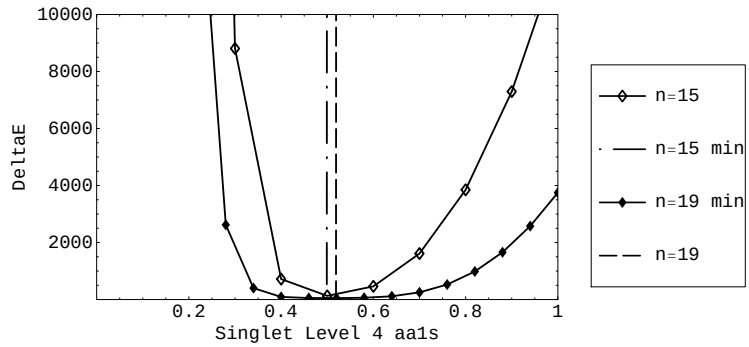

Figure 9.14 – Singlet level IV, S only, Energy error for n=15 and n=19

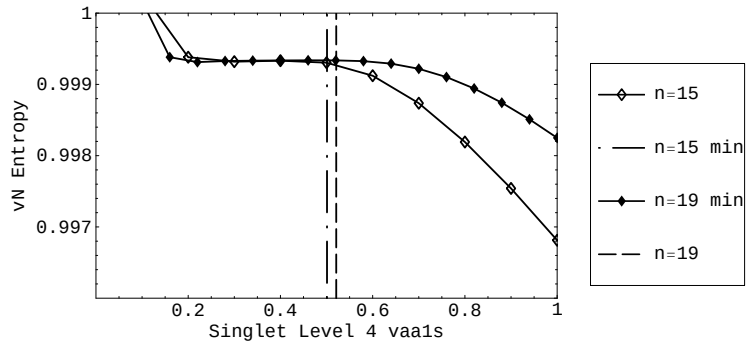

Figure 9.15 – Singlet level IV, S only, von Neumann entropy for n=15 and n=19

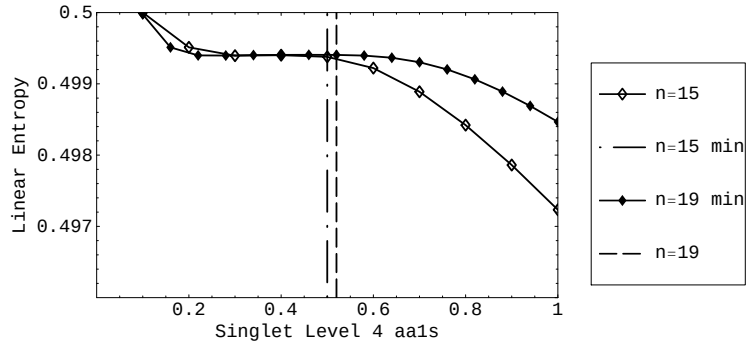

Figure 9.16 – Singlet level IV, S only, Linear entropy for n=15 and n=19

ndds	aa1s	energy	Δ E(ppm)	vN entr	lin entr
5	0.6576	-0.719812470	642695.50	0.083919929	0.018064581
6	0.3765	-1.588385334	211548.48	0.997060101	0.497495940
7	0.4351	-1.800581960	106217.14	0.983392313	0.488019168
8	0.4653	-1.916479755	48687.15	0.995406351	0.495835404
9	0.4653	-1.960238369	26966.01	0.995516644	0.496304939
10	0.4624	-1.986242501	14057.94	0.997987074	0.498163487
11	0.4540	-1.998420023	8013.19	0.998269750	0.498505835
12	0.4472	-2.006033298	4234.07	0.998971433	0.499065935
13	0.4399	-2.009812093	2358.33	0.999139998	0.499236289
14	0.4351	-2.012139339	1203.12	0.999389895	0.499446104
15	0.4309	-2.013260960	646.36	0.999470985	0.499521921
16	0.4290	-2.013919508	319.47	0.999555737	0.499595767
17	0.4275	-2.014213665	173.45	0.999586869	0.499623410
18	0.4277	-2.014378729	91.52	0.999612370	0.499646294
19	0.4278	-2.014445387	58.43	0.999621934	0.499654215
20	0.4297	-2.014482001	40.26	0.999628689	0.499660431

Table 9.12 – Level V, S shell only

Level V

In the table 9.12 we report our results for the S shell only, V excited state, starting with $n_s = 5$.

Now the changes in the entropy from n=10 to n=20 regard the third decimal digit.

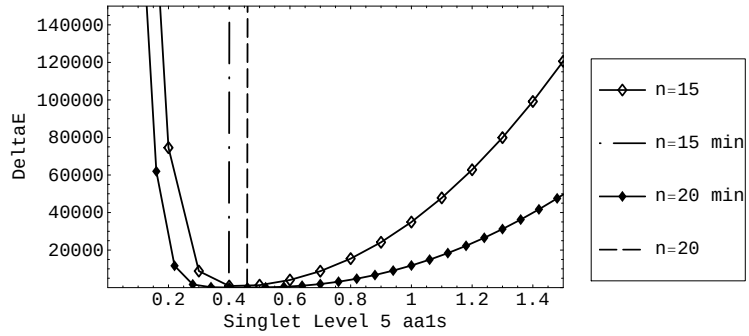

Figure 9.17 – Singlet level V, S only, Energy error for n=15 and n=20

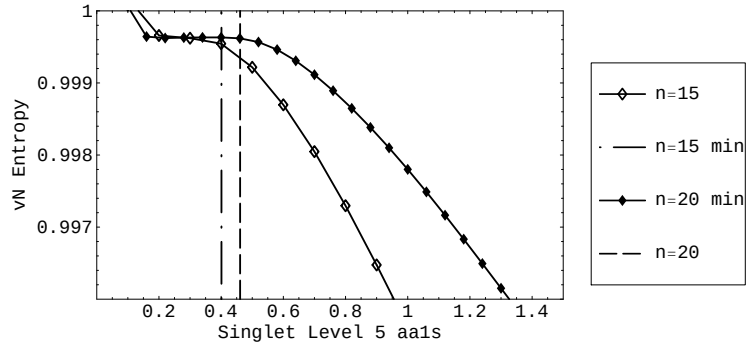

Figure 9.18 – Singlet level V, S only, von Neumann entropy for n=15 and n=20

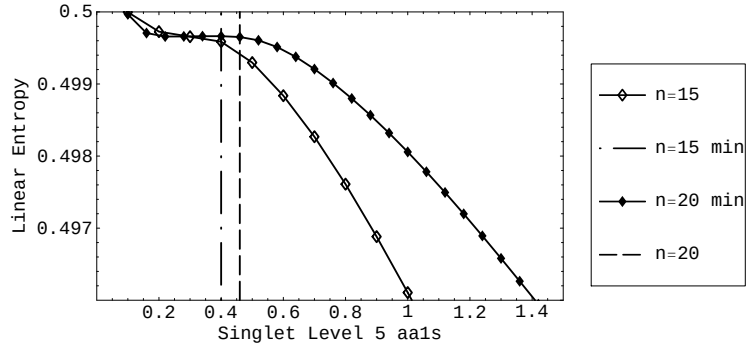

Figure 9.19 – Singlet level V, S only, Linear entropy for n=15 and n=20

ndds	aa1s	energy	Δ E(ppm)	entr vN	e lin
5	0.6205	-0.569991855	716510.22	0.968067950	0.471797062
6	0.5621	-0.719478775	642161.77	0.088610675	0.019105710
7	0.3271	-1.574340456	216989.82	0.997493189	0.497792473
8	0.3825	-1.784162982	112632.99	0.984370635	0.488726531
9	0.4124	-1.900912492	54566.74	0.995788091	0.496131844
10	0.4153	-1.946634357	31826.62	0.995734631	0.496481091
11	0.4142	-1.974768133	17834.07	0.998141172	0.498280309
12	0.4075	-1.988694982	10907.45	0.998325391	0.498551769
13	0.4015	-1.997878848	6339.78	0.999043803	0.499119777
14	0.3943	-2.002848271	3868.20	0.999176288	0.499267078
15	0.3886	-2.006172242	2215.00	0.999447569	0.499491975
16	0.3834	-2.007992271	1309.79	0.999529751	0.499572975
17	0.3800	-2.009176097	721.01	0.999642060	0.499670003
18	0.3770	-2.009798555	411.42	0.999684337	0.499709324
19	0.3757	-2.010184455	219.49	0.999728139	0.499748437
20	0.3750	-2.010373825	125.31	0.999746151	0.499764460

Table 9.13 – Level VI, S shell only

Level VI

In the table 9.13 we report our results for the S shell only, VI excited state, starting with $n_s = 5$.

Now the changes in the entropy from n=10 to n=20 regard the third decimal digit.

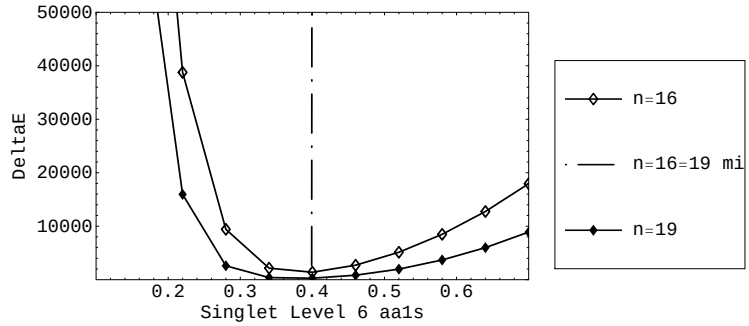

Figure 9.20 – Singlet level VI, S only, Energy error for n=16 and n=19

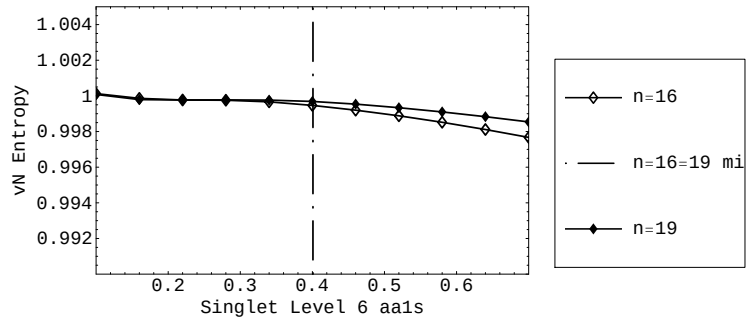

Figure 9.21 – Singlet level VI, S only, von Neumann entropy for n=16 and n=19

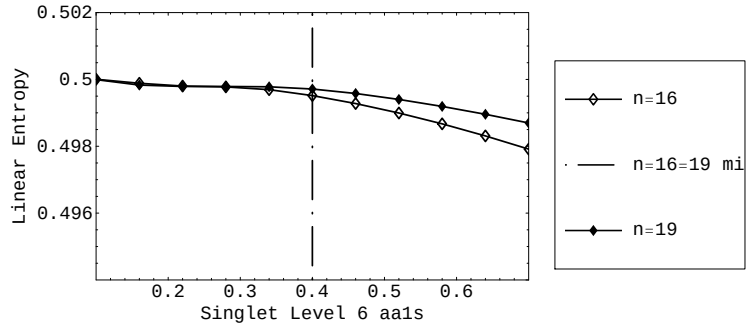

Figure 9.22 – Singlet level VI, S only, Linear entropy for n=16 and n=19

n	aa1s	aa1p	Δ E(ppm)	lin ent r	vN entr
5	2.155	3.800	1159.10	0.016158	0.077721
6	2.358	4.000	1128.57	0.016162	0.077758
7	2.524	4.300	1117.61	0.016162	0.077763
8	2.607	4.600	1111.97	0.016163	0.077770
9	2.887	4.900	1109.05	0.016163	0.077770
10	3.068	5.200	1107.49	0.016163	0.077773
11	3.247	5.400	1106.59	0.016163	0.077773
12	3.411	5.700	1106.03	0.016163	0.077774
13	3.621	6.000	1105.68	0.016163	0.077774
14	3.779	6.100	1105.44	0.016163	0.077774
15	3.937	6.400	1105.28	0.016163	0.077774

Table 9.14 – Fundamental Level, S-P shell only

9.5.2 Singlet states - S-P shells only

In all the computation, we have used ns = np.

Fundamental level

In the table 9.14 we report our results for the S-P shells only, fundamental state, starting with $n_p = 5$.

The von Neumann entropy changes passing from dimension for S Shell=10 to dimension for S Shell=15 involve the fifht significant digit, those of the linear entropy the sixth.

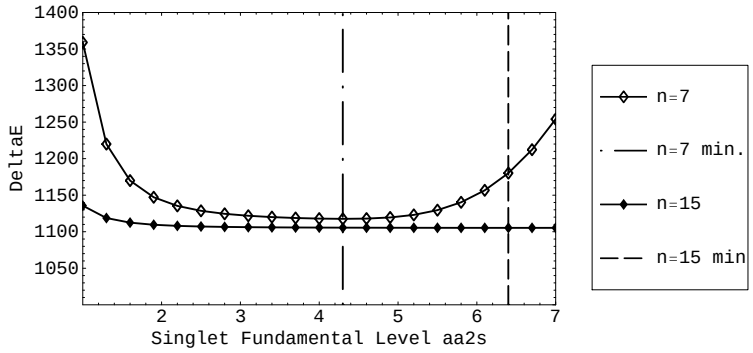

Figure 9.23 – Energy error for n=7 and n=15, fundamental level, S-P

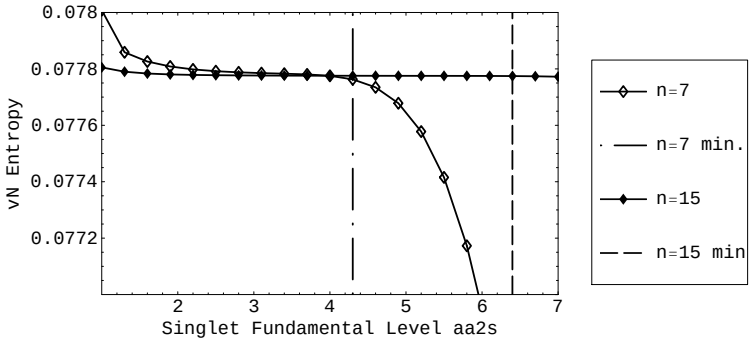

Figure 9.24 – von Neumann entropy for n=7 and n=15, fundamental level, S-P

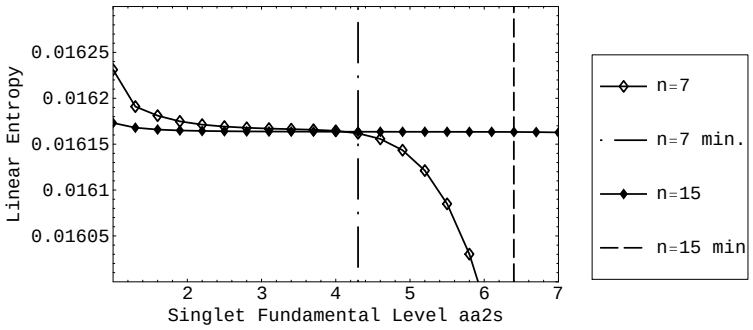

Figure 9.25 – Linear entropy forn=7 and n=15, fundamental level, S-P

n	aa1s	aa1p	Δ E(ppm)	lin entr	vN entr
5	1.0218	1.900	1565.29	0.487567	0.989644
6	1.0242	2.000	281.62	0.488480	0.990607
7	1.0136	2.100	173.29	0.488552	0.990674
8	1.0427	2.200	113.40	0.488618	0.990767
9	1.0731	2.300	108.18	0.488624	0.990783
10	1.1301	2.423	102.46	0.488631	0.990795
11	1.1999	2.524	100.30	0.488633	0.990800
12	1.2501	2.626	99.04	0.488635	0.990801
13	1.319	2.700	98.18	0.488636	0.990803
14	1.373	2.800	97.74	0.488636	0.990804
15	1.436	2.900	97.40	0.488637	0.990804

Table 9.15 – Level I, S-P shell only

Level I

In the table 9.15 we report our results for the S-P shells only, level I, starting with $n_p = 5$.

The von Neumann entropy changes passing from dimension for S Shell=10 to dimension for S Shell=15 involve the fifht significant digit, those of the linear entropy the sixth.

We have an enhancement of about an order of magnitude in the energy precision for dimension for S Shell=dimension for P Shell=15, comparing these figures to the results obtained using the S shell only. The changes of the von Neumann entropy are reduced to 1/100, those of the linear entropy to 1/1000.

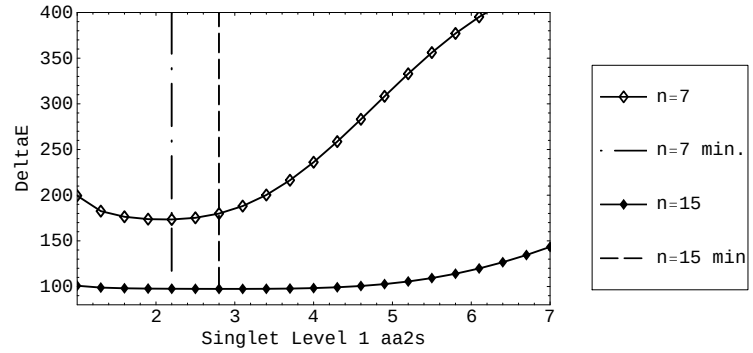

Figure 9.26 – Singlet Energy error for n=7 and n=15, level I, S-P

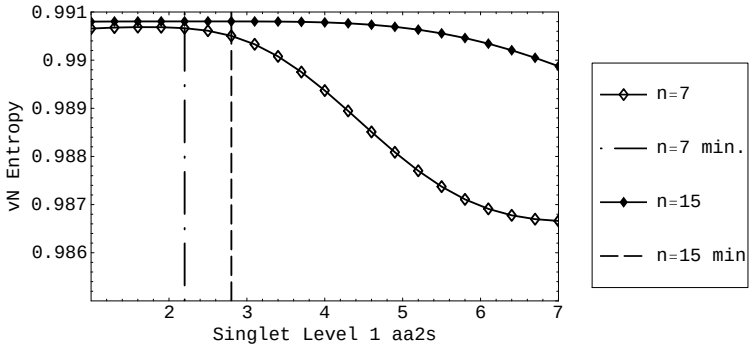

Figure 9.27 – Singlet von Neumann entropy for n=7 and n=15, level I, S-P

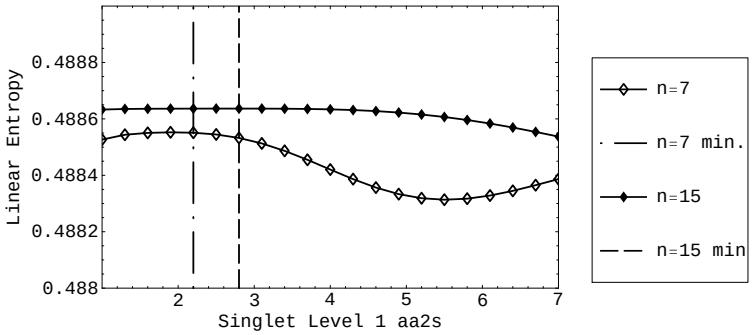

Figure 9.28 – Singlet Linear entropy forn=7 and n=15, level I, S-P

n	aa1s	aa1p	Δ E(ppm)	lin entr	vN entr
5	0.786	2.400	17533.91	0.493807	0.996401
6	0.771	2.600	6390.81	0.495178	0.996773
7	0.763	1.600	1768.84	0.496663	0.998075
8	0.751	1.600	635.38	0.496943	0.998196
9	0.750	1.600	168.89	0.497159	0.998381
10	0.746	1.700	80.87	0.497191	0.998396
11	0.752	1.700	40.07	0.497218	0.998425
12	0.755	1.700	34.46	0.497221	0.998430
13	0.773	1.800	30.57	0.497224	0.998435
14	0.797	1.800	29.78	0.497225	0.998437
15	0.828	1.900	29.04	0.497225	0.998437

Table 9.16 – Level II, S-P shell only

Level II

In the table 9.16 we report our results for the S-P shells only, level II, starting with $n_p = 5$.

The von Neumann and linear entropy changes passing from dimension for S Shell=10 to dimension for S Shell=15 involve the fourth significant digit.

We have an enhancement of about an order of magnitude in the energy precision for ns=np=15, comparing these figures to the results obtained using the S shell only. The changes of the von Neumann and linear entropy are reduced to 1/1000.

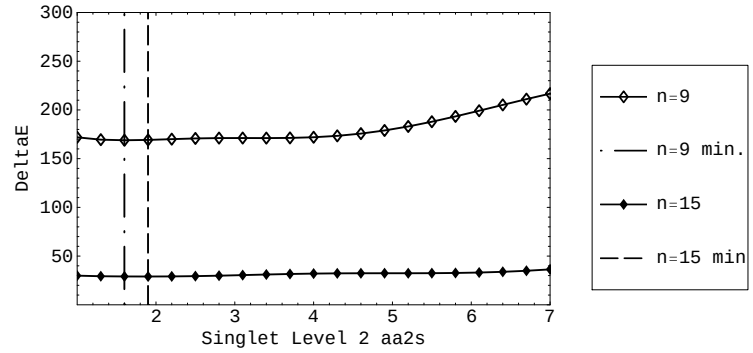

Figure 9.29 – Singlet Energy error for n=9 and n=15, level II, S-P

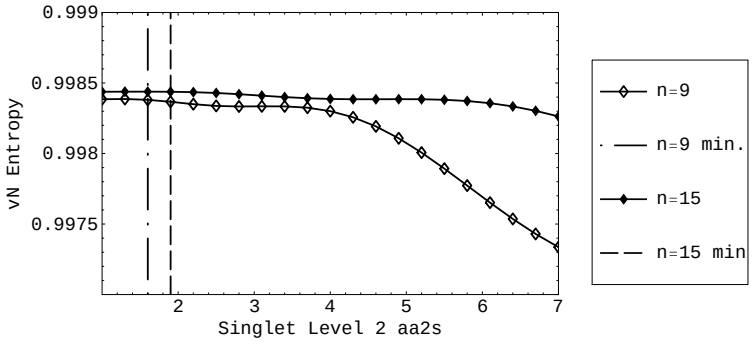

Figure 9.30 – Singlet von Neumann entropy for n=9 and n=15, level II, S-P

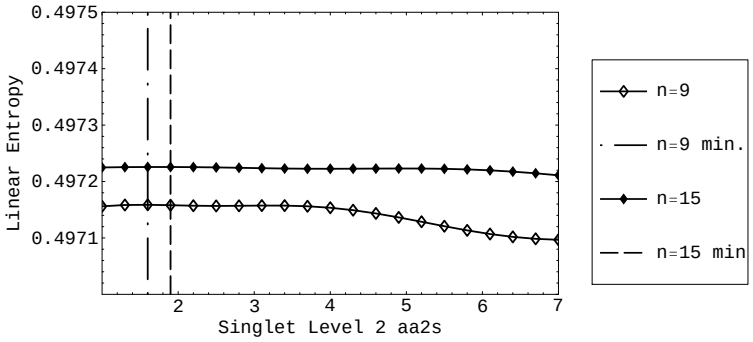

Figure 9.31 – Singlet Linear entropy forn=9 and n=15, level II, S-P

n	aa1s	aa1p	Δ E(ppm)	lin entr	vN entr
5	0.606	2.700	82274.70	0.487653	0.991266
6	0.634	1.700	30184.41	0.495256	0.998041
7	0.625	1.700	13517.44	0.496223	0.997738
8	0.619	1.800	5206.28	0.497926	0.999088
9	0.608	1.900	2255.69	0.498315	0.999170
10	0.603	1.900	813.28	0.498701	0.999443
11	0.598	2.000	339.16	0.498799	0.999469
12	0.597	2.100	115.43	0.498878	0.999524
13	0.596	2.200	53.79	0.498896	0.999530
14	0.599	1.500	23.97	0.498909	0.999542
15	0.600	1.500	17.35	0.498912	0.999544
16	0.607	1.500	13.60	0.498914	0.999547

Table 9.17 – Level III, S-P shell only

Level III

In the table 9.17 we report our results for the S-P shells only, level III, starting with $n_p = 5$.

The von Neumann and linear entropy changes passing from dimension for S Shell=10 to dimension for S Shell=15 involve the fourth significant digit.

We have an enhancement of about 5 times in the energy precision for ns=np=15, comparing these figures to the results obtained using the S shell only. The changes of the von Neumann and linear entropy are reduced to 1/1000.

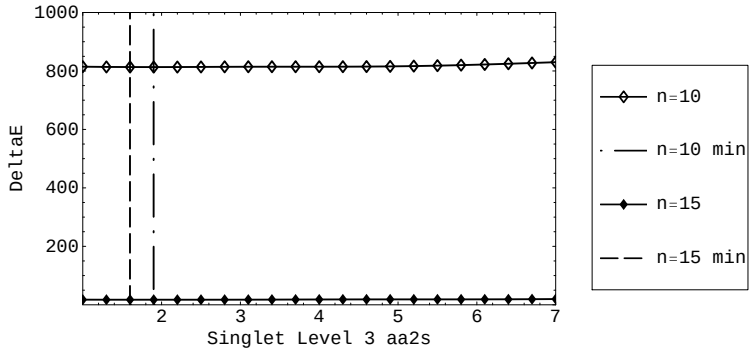

Figure 9.32 – Singlet Energy error for n=10 and n=15, level III, S-P

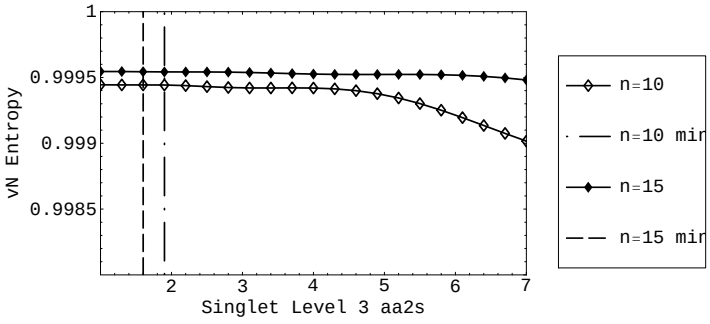

Figure 9.33 – Singlet von Neumann entropy for n=10 and n=15, level III, S-P

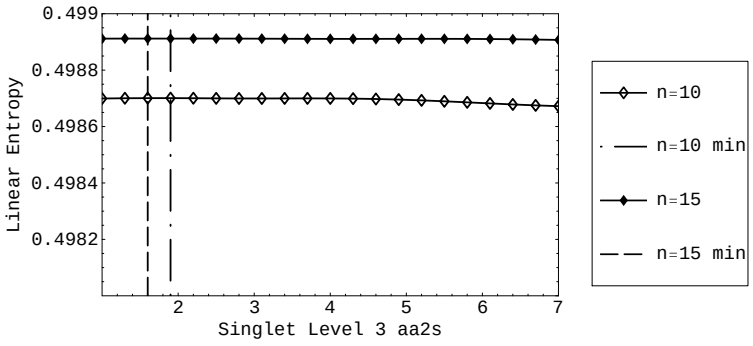

Figure 9.34 – Singlet Linear entropy forn=10 and n=15, level III, S-P

n	aa1s	aa1p	Δ E(ppm)	lin entr	vN entr
5	0.444	2.100	200042.36	0.500696	1.028408
6	0.506	1.900	95795.63	0.489176	0.993279
7	0.535	1.900	40496.73	0.495947	0.998793
8	0.532	1.800	20643.35	0.496561	0.998062
9	0.527	2.000	9604.56	0.498227	0.999362
10	0.517	2.100	4885.21	0.498590	0.999353
11	0.511	2.100	2218.17	0.499072	0.999679
12	0.504	2.200	1076.13	0.499218	0.999702
13	0.501	2.400	456.37	0.499361	0.999789
14	0.498	2.500	212.07	0.499405	0.999798
15	0.498	2.500	85.05	0.499443	0.999820
16	0.497	1.900	41.10	0.499453	0.999823
17	0.500	1.800	18.40	0.499462	0.999829
18	0.501	1.800	11.60	0.499464	0.999830
19	0.505	1.800	7.95	0.499465	0.999831
20	sballa				

Table 9.18 – Level IV, S-P shell only

Level IV

In the table 9.18 we report our results for the S-P shells only, fundamental state, starting with $n_p = 5$.

The von Neumann and linear entropy changes passing from dimension for S Shell=10 to dimension for S Shell=15 involve the fourth significant digit.

We have an enhancement of about 1.5 times in the energy precision for ns=np=15, comparing these figures to the results obtained using the S shell only. The changes of the von Neumann and linear entropy are reduced to 1/10000.

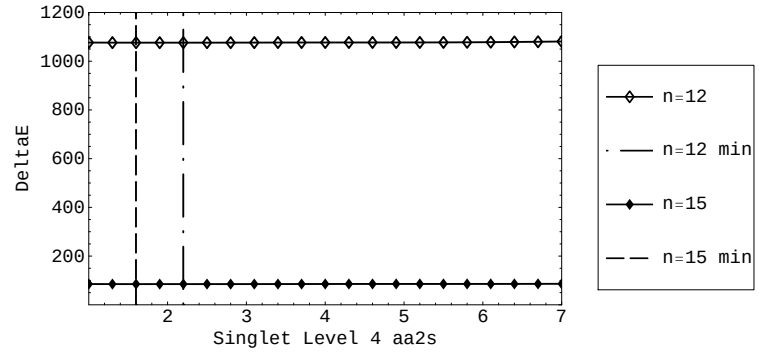

Figure 9.35 – Singlet Energy error for n=12 and n=15, level IV, S-P

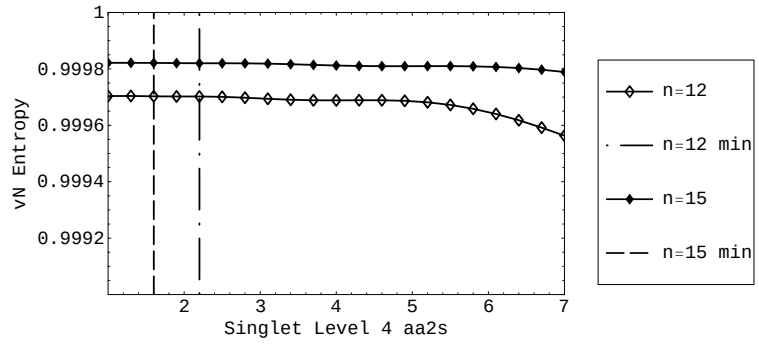

Figure 9.36 – Singlet von Neumann entropy for n=12 and n=15, level IV, S-P

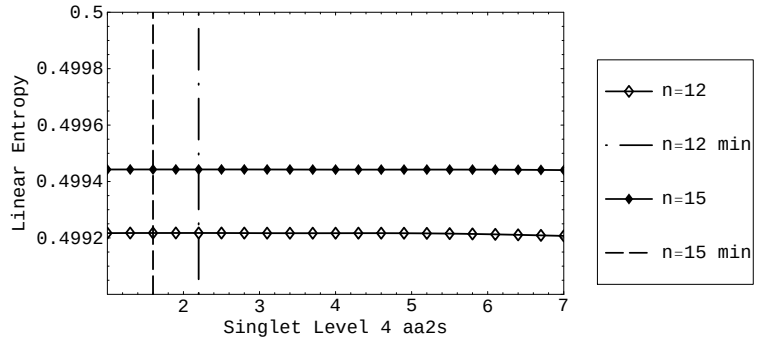

Figure 9.37 – Singlet Linear entropy forn=12 and n=15, level IV, S-P

n	aa1s	aa1p	Δ E(ppm)	lin entr	vN entr
7	0.435	2.100	104975.81	0.490104	0.994417
8	0.465	2.100	58312.76	0.496364	0.999243
9	0.465	2.000	26683.62	0.496778	0.998266
10	0.462	2.200	13920.27	0.498374	0.999505
11	0.454	2.300	7904.01	0.498668	0.999411
12	0.447	2.300	4166.53	0.499172	0.999755
13	0.440	2.400	2303.48	0.499321	0.999756
14	0.425	2.600	1163.26	0.499506	0.999865
15	0.431	2.700	612.23	0.499573	0.999873
16	0.429	2.500	290.37	0.499638	0.999908
17	0.427	2.400	146.46	0.499663	0.999911
18	0.428	2.100	66.00	0.499682	0.999922
19	0.428	2.000	33.56	0.499689	0.999924
20	sballa				

Table 9.19 – Level V, S-P shell only

Level V

In the table 9.19 we report our results for the S-P shells only, level V, starting with $n_p = 5$.

The von Neumann and linear entropy changes passing from dimension for S Shell=10 to dimension for S Shell=15 involve the fourth significant digit.

We have only a slight enhancement in the energy precision for ns=np=15, comparing these figures to the results obtained using the S shell only. The changes of the von Neumann and linear entropy are reduced to 1/10000 and 1/100000 respectivley.

For this reason we used values of n_p up to 19.

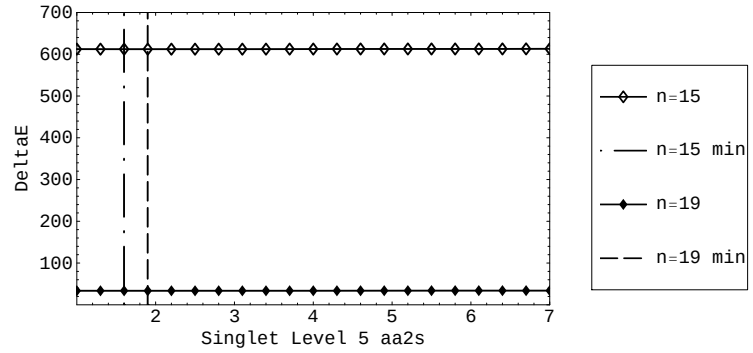

Figure 9.38 – Singlet Energy error for n=15 and n=19, level V, S-P

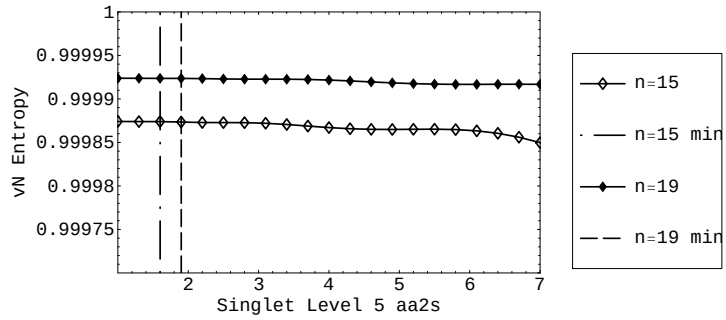

Figure 9.39 – Singlet von Neumann entropy for n=15 and n=19, level V, S-P

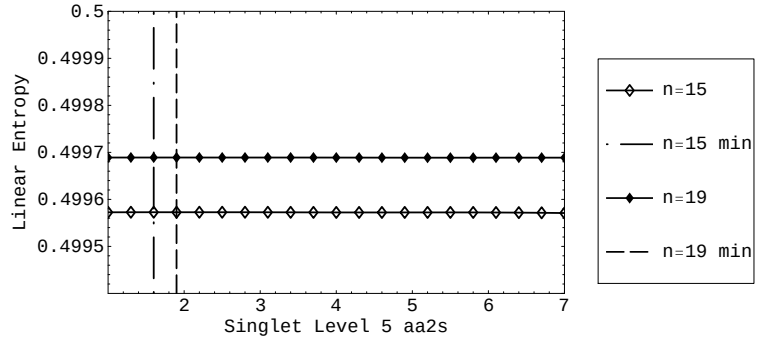

Figure 9.40 – Singlet Linear entropy forn=15 and n=19, level V, S-P

n	aa1s	aa1p	Δ E(ppm)	lin entr	vN entr
10	0.415	2.200	31550.84	0.496927	0.998406
11	0.414	2.400	17701.48	0.498476	0.999603
12	0.407	2.400	10800.51	0.498717	0.999449
13	0.401	1.700	6274.89	0.499217	0.999798
14	0.394	1.700	3815.08	0.499347	0.999773
15	0.389	1.700	2178.04	0.499548	0.999894
16	0.383	1.800	1279.03	0.499619	0.999893
17	0.380	1.800	697.02	0.499705	0.999938
18	0.377	1.700	390.51	0.499740	0.999941
19	0.376	1.600	201.24	0.499775	0.999957

Table 9.20 – Level VI, S-P shell only

Level VI

In the table 9.20 we report our results for the S-P shells only, level VI, starting with $n_p = 5$.

The von Neumann and linear entropy changes passing from dimension for S Shell=10 to dimension for S Shell=15 involve the third significant digit.

We have only a 8% enhancement in the energy precision, of 1/10000 in the von Neumann entropy and of 1/100000 in the linear entropy even for ns=np=19.

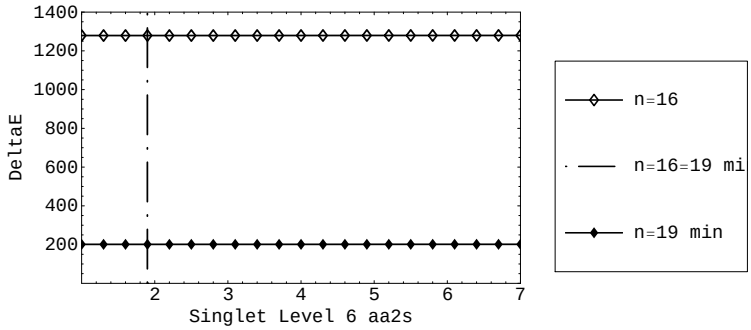

Figure 9.41 – Singlet Energy error for n=16 and n=19, level VI, S-P

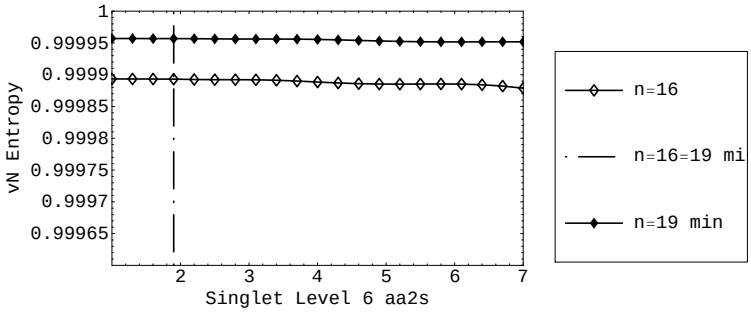

Figure 9.42 – Singlet von Neumann entropy for n=16 and n=19, level VI, S-P

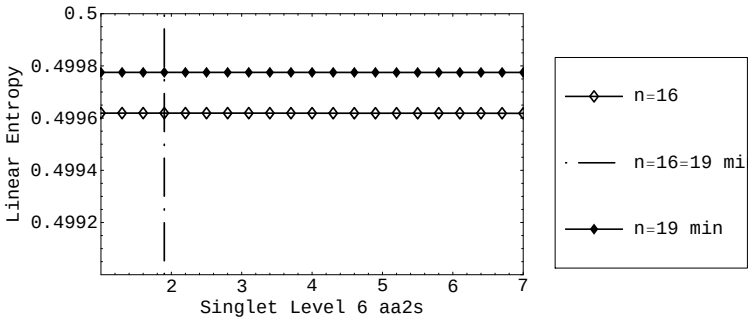

Figure 9.43 – Singlet Linear entropy forn=16 and n=19, level VI, S-P

n	aa1s	aa1p	aa1d	Δ E(ppm)	lin entr	vN entr
5	2.16	3.80	5.20	387.79	0.016053	0.078444
6	2.36	4.00	5.60	355.81	0.016056	0.078479
7	2.52	4.40	5.90	343.97	0.016056	0.078485
8	2.52	4.40	6.20	337.82	0.016057	0.078493
9	2.52	4.40	6.60	334.61	0.016056	0.078492
10	2.52	4.40	7.00	332.86	0.016056	0.078494

Table 9.21 – Fundamental Level, S-P-D shell

9.5.3 Singlet states - S-P-D shells

Fundamental level

In all the computation, if not stated otherwise, ns = np = nd.

In the table 9.21 we report our results for the S-P-D shells, fundamental state, starting with $n_d = 5$.

We get an error reduction of the energy of about 14% passing from $n_s = n_p = n_d = 5$ to $n_s = n_p = n_d = 10$. The von Neumann entropy changes involve the fifth significant digit, those of the linear entropy the sixth.

Comparing these figures with the results obtained considering the S shell only and $n_s = 15$, we find an ehancement of about 20 times; comparing with the results considering the S and P shells and $n_d = 10$ the enhancement is about 3 times.

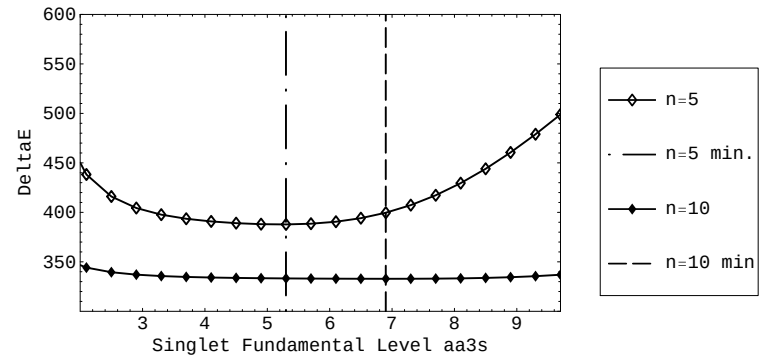

Figure 9.44 – Singlet Energy error for n=5 and n=10, fundamental level, S-P-D

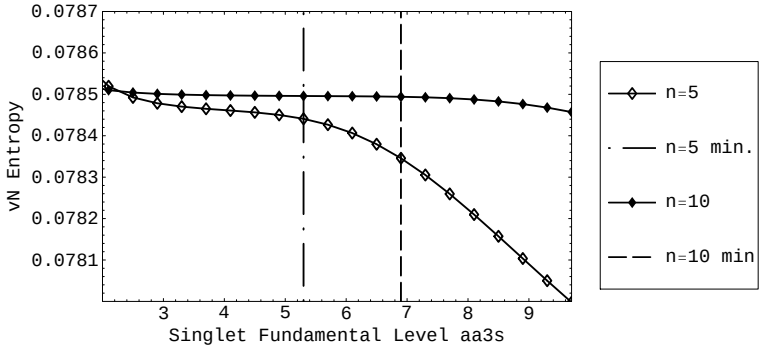

Figure 9.45 – Singlet von Neumann entropy for n=5 and n=10, fundamental level, S-P-D

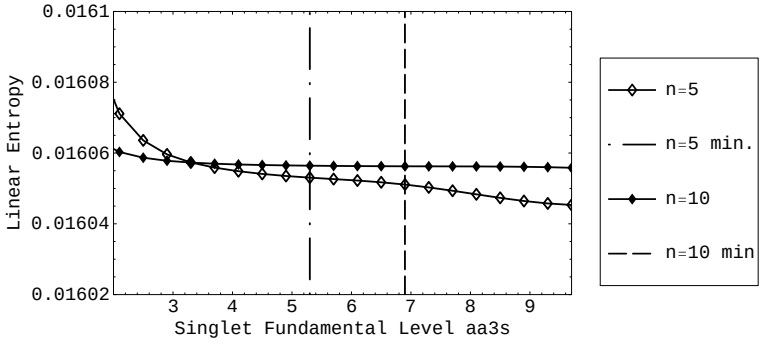

Figure 9.46 – Singlet Linear entropy forn=5 and n=10, fundamental level, S-P-D

n	aa1s	aa1p	aa1d	Δ E(ppm)	lin entr	vN entr
5	1.02	1.90	3.10	1491.10	0.487653	0.989965
6	1.02	2.00	3.30	212.96	0.488554	0.990906
7	1.01	2.10	3.40	104.61	0.488626	0.990972
8	1.01	2.10	3.50	44.70	0.488692	0.991066
9	1.01	2.10	3.70	39.38	0.488698	0.991083
10	1.01	2.10	3.80	33.58	0.488705	0.991095
11	1.01	2.10	3.90	31.40	0.488707	0.991099

Table 9.22 – Level I, S-P-D shell

Level I

In the table 9.22 we report our results for the S-P-D shells, level I, starting with $n_d = 5$.

Passing from $n_s = n_p = n_d = 5$ to $n_s = n_p = n_d = 10$ we have an enhancement in the energy precision of about 40 times. The von Neumann entropy changes involve the second significant digit, those of the linear entropy the third.

Comparing these figures with the results obtained considering the S shell only and $n_s = 15$ we find an ehancement of about 20 times; comparing with the results considering the S and P shells and $n_d = 10$, the enhancement is about 3 times.

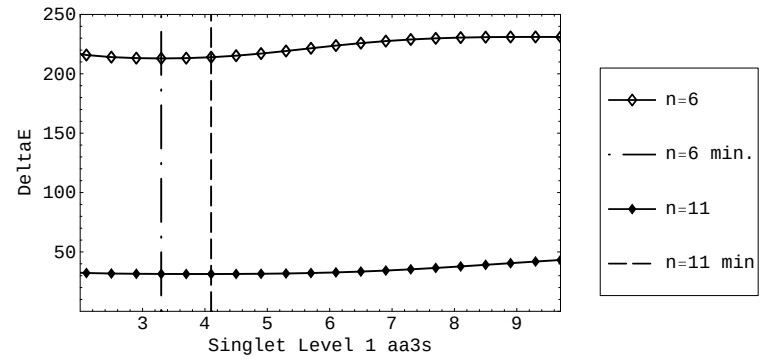

Figure 9.47 – Singlet Energy error for n=6 and n=11, level I, S-P-D

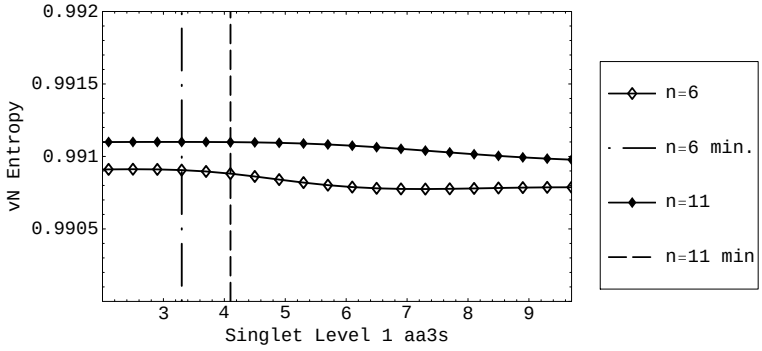

Figure 9.48 – Singlet von Neumann entropy for n=6 and n=11, level I, S-P-D

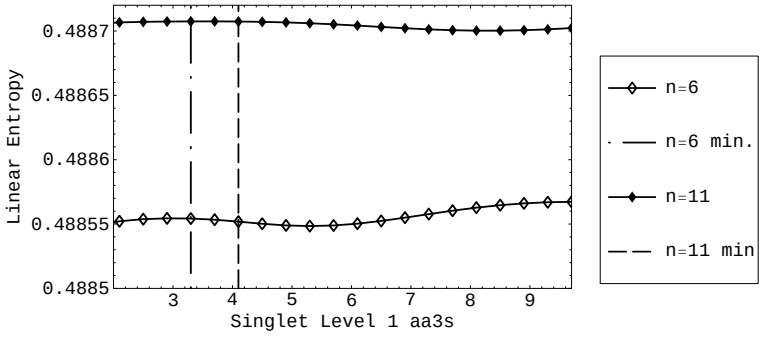

Figure 9.49 – Singlet Linear entropy forn=6 and n=11, level I, S-P-D

n	aa1s	aa1p	aa1d	Δ E(ppm)	lin entr	vN entr
5			3.20	17489.99	0.493860	0.996584
6			3.50	6355.23	0.495220	0.996920
7			3.80	1745.24	0.496687	0.998176
8			4.00	613.55	0.496964	0.998287
9			4.20	148.67	0.497178	0.998466
10			4.50	60.92	0.497210	0.998480
11			4.70	20.27	0.497236	0.998508
12			4.90	14.69	0.497239	0.998513

Table 9.23 – Level II, S-P-D shell

Level II

In the table 9.23 we report our results for the S-P-D shells, level II, starting with $n_d = 5$.

Passing from $n_s = n_p = n_d = 5$ to $n_s = n_p = n_d = 10$ we have an enhancement in the energy precision of about 30 times. The von Neumann and linear entropy changes involve the third significant digit.

Comparing these figures with the results obtained considering the S shell only and $n_s = 15$ we find an ehancement of about 4 times; comparing these figures to the results obtained using S and P shells and $n_s = n_p = 15$, it is necessary to take a minimum of $n_d = 11$ a to get a better result.

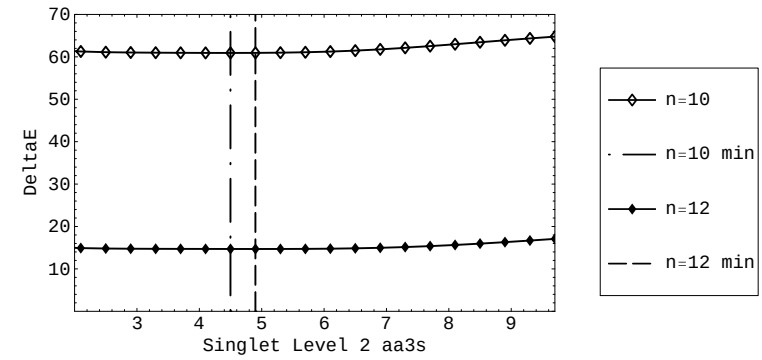

Figure 9.50 – Singlet Energy error for n=10 and n=12, level II, S-P-D

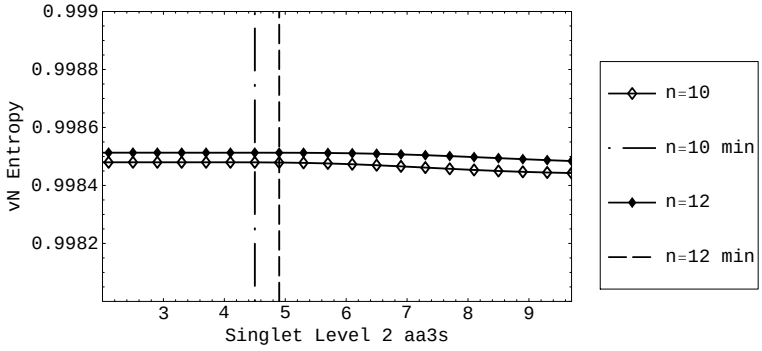

Figure 9.51 – Singlet von Neumann entropy for n=10 and n=12, level II, S-P-D

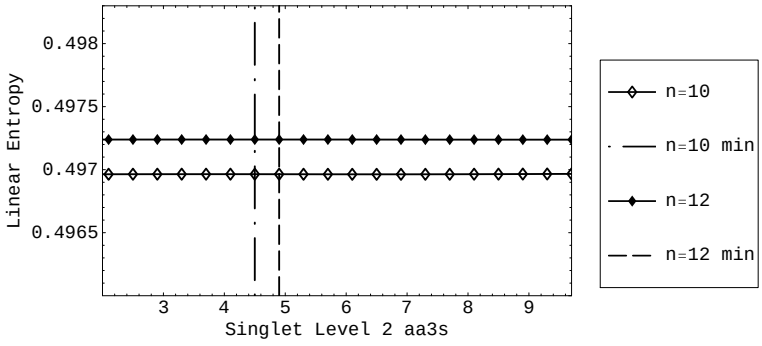

Figure 9.52 – Singlet Linear entropy forn=10 and n=12, level II, S-P-D

n	aa1s	aa1p	aa1d	Δ E(ppm)	lin entr	vN entr
5	0.61	2.70	3.70	82145.40	0.487812	0.991716
6	0.63	1.70	3.50	30145.50	0.495298	0.998193
7	0.63	1.70	3.90	13486.80	0.496259	0.997861
8	0.63	1.70	4.30	5190.66	0.497943	0.999155
9	0.63	1.70	4.40	2242.78	0.498329	0.999224
10	0.63	1.70	4.60	803.56	0.498711	0.999485
11	0.63	1.70	5.00	330.09	0.498807	0.999507
12	0.63	1.70	5.20	107.00	0.498886	0.999560
13	0.63	1.70	5.40	45.49	0.498903	0.999565
14	0.63	1.70	5.40	(15)	0.498917	0.999577

Table 9.24 – Level III, S-P-D shell

Level III

In the table 9.24 we report our results for the S-P-D shells, level III, starting with $n_d = 5$.

Passing from $n_s = n_p = n_d = 5$ to $n_s = n_p = n_d = 10$ we have an enhancement in the energy precision of about 10 times. The von Neumann and linear entropy changes involve the third significant digit.

Comparing these figures to the results obtained using S shells and $n_s = 15$, the errors are of the same order of magnitude, using $n_d = 12$. A minimum of $n_d = 14$ is required to obtain a result similar to the computations using the S and P shell and $n_s = n_p = 15$.

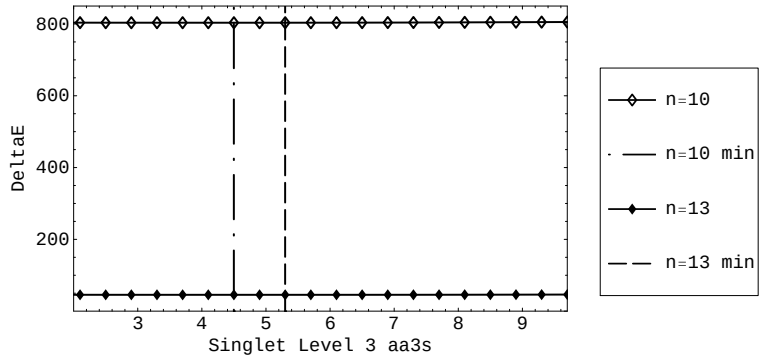

Figure 9.53 – Singlet Energy error for n=10 and n=13, level III, S-P-D

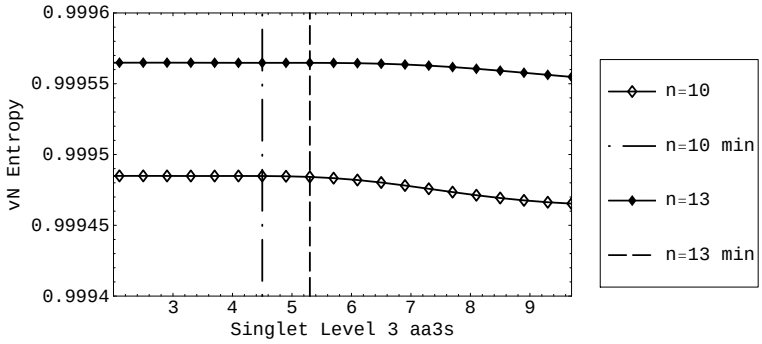

Figure 9.54 – Singlet von Neumann entropy for n=10 and n=13, level III, S-P-D

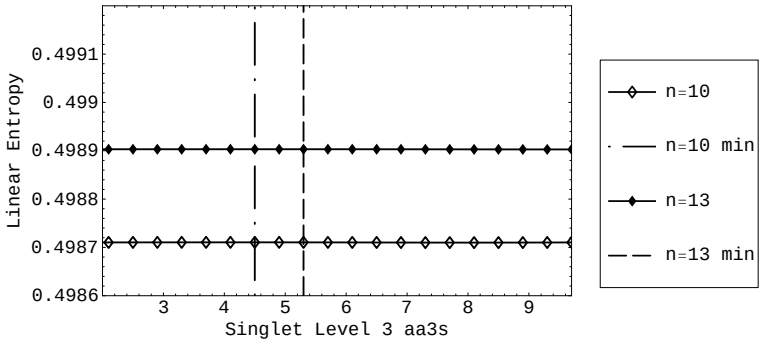

Figure 9.55 – Singlet Linear entropy forn=10 and n=13, level III, S-P-D

n	aa1d	Δ E(ppm)	lin entr	vN entr
6	4.0	95672.66	0.489319	0.993696
7	3.8	40460.19	0.495983	0.998927
8	4.2	20613.88	0.496595	0.998179
9	4.6	9589.10	0.498242	0.999420
10	4.8	4873.78	0.498601	0.999399
11	5.0	2210.92	0.499077	0.999710
12	5.2	1070.0	0.499244	0.999728
13	5.6	451.4	0.499365	0.999810
14	6.0	207.5	0.499409	0.999817
15	6.5	80.7	0.499447	0.999838
16	6.5	36.9	0.499457	0.999841
17	5.0	15.1	0.499465	0.999838

Table 9.25 – Level IV, S-P-D shell

Level IV

In the table 9.25 we report our results for the S-P-D shells, level IV, starting with $n_d = 6$.

Passing from $n_s = n_p = n_d = 6$ to $n_s = n_p = n_d = 11$ we have an enhancement in the energy precision of about 40 times. The von Neumann entropy changes involve the third significant digit, those of the linear entropy the second.

The error using $n_s = n_p = n_d = 15$ is of the same order of magnitude of the computations made using only the S and $n_s = 15$, or S and P shells and $n_s = n_p = 15$.

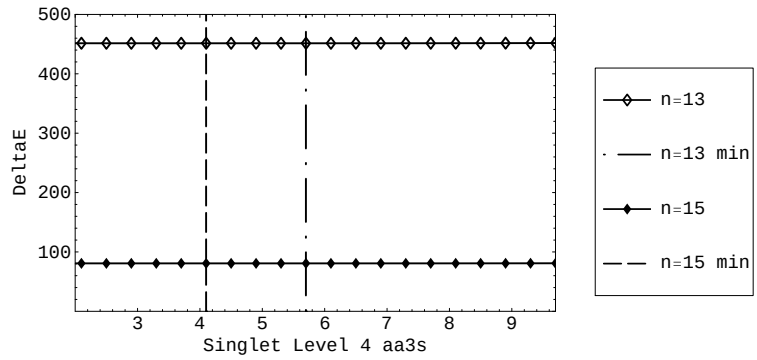

Figure 9.56 – Singlet Energy error for n=13 and n=15, level IV, S-P-D

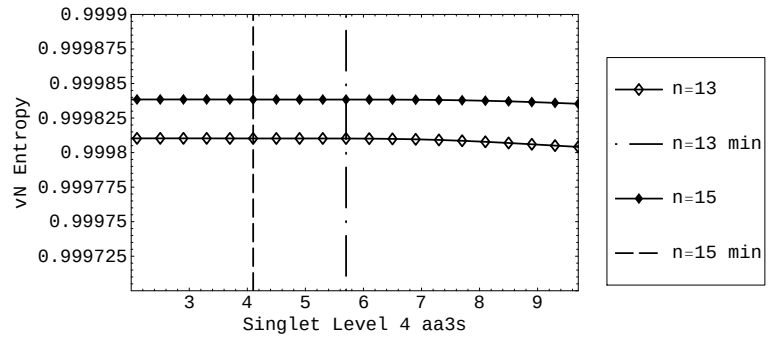

Figure 9.57 – Singlet von Neumann entropy for n=13 and n=15, level IV, S-P-D

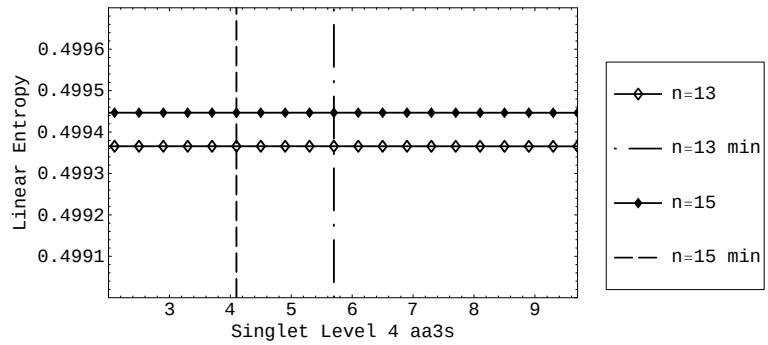

Figure 9.58 – Singlet Linear entropy forn=13 and n=15, level IV, S-P-D

n	aa1d	Δ E(ppm)	lin entr	vN entr
8	4.0	48278.7	0.496405	0.999371
9	4.5	26656	0.496816	0.998379
10	5.0	13907	0.498392	0.999562
11	5.0	7893	0.498679	0.999455
12	5.5	4160	0.499180	0.999784
13	5.5	2298.3	0.499326	0.999778
14	6.0	1190	0.499540	0.999893
15	6.0	608.8	0.499576	0.999887
16	6.5	287.5	0.499641	0.999920
17	6.5	143.9	0.499665	0.999923

Table 9.26 – Level V, S-P-D shell

Level V

In the table 9.26 we report our results for the S-P-D shells, level V, starting with $n_d = 8$.

Passing from $n_s = n_p = n_d = 8$ to $n_s = n_p = n_d = 13$ we have an enhancement in the energy precision of about 20 times. The von Neumann and linear entropy changes involve the third significant digit.

The error using $n_s = n_p = n_d = 15$ is of the same order of magnitude of the computations made using only the S or S and P shells. The same situation holds also increasing n up to 17, so that it seems that taking into account the D shell is not useful for this level.

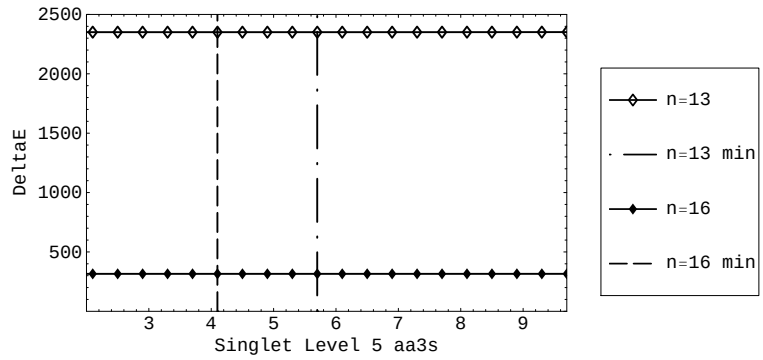

Figure 9.59 – Singlet Energy error for n=13 and n=16, level V, S-P-D

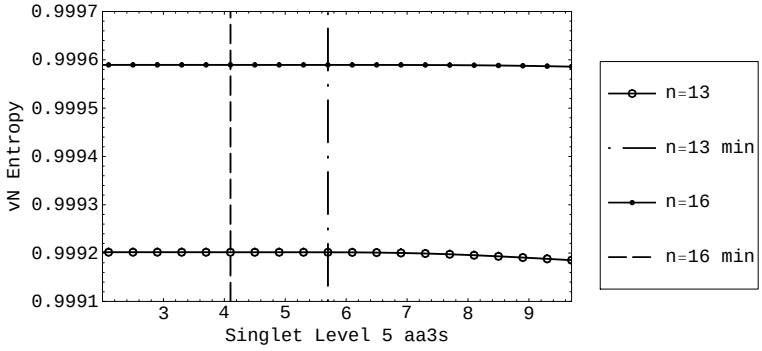

Figure 9.60 – Singlet von Neumann entropy for n=13 and n=16, level V, S-P-D

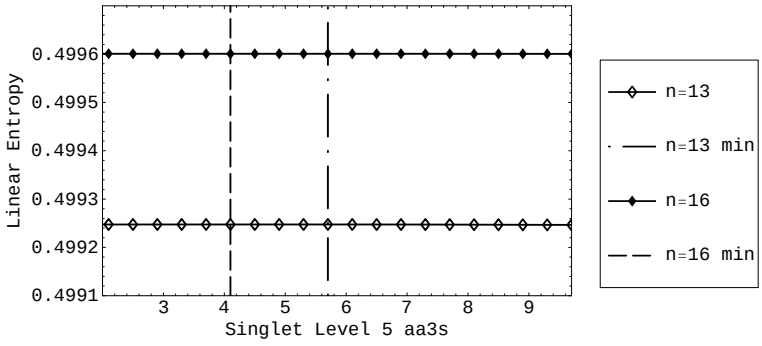

Figure 9.61 – Singlet Linear entropy forn=13 and n=16, level V, S-P-D

n	aa1d	Δ E(ppm)	lin entr	vN entr
10	5.0	31523	0.496964	0.998516
11	5.0	17689	0.498491	0.999656
12	5.0	10790	0.498773	0.999494
13	6.0	6269	0.499226	0.999826
14	6.0	3810	0.499354	0.999795
15	6.5	2174	0.499550	0.999909
16	6.5	1276.1	0.499623	0.999906
17	7.0	694.7	0.499708	0.999948
18	7.5	389	0.499743	0.999945
19	7.5	348	0.499777	0.999961

Table 9.27 – Level VI, S-P-D shell

Level VI

Remark: dimension for S Shell=18, dimension for P Shell=18, dimension for D Shell=3; dimension for S Shell=19, dimension for P Shell=19, dimension for D Shell=3

In the table 9.27 we report our results for the S-P-D shells, level VI, starting with $n_d = 10$.

Passing from $n_s = n_p = n_d = 10$ to $n_s = n_p = n_d = 15$ we have an enhancement in the energy precision of about 15 times. The von Neumann and linear entropy changes involve the third significant digit.

The error using $n_s = n_p = n_d = 15$ is of the same order of magnitude of the computations made using only the S or S and P shells. The same situation holds also increasing n up to 17, so that it seems that taking into account the D shell is not useful for this level.

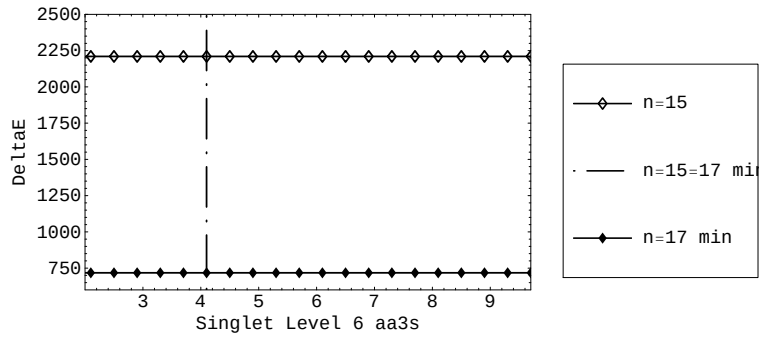

Figure 9.62 – Singlet Energy error for n=15 and n=17, level VI, S-P-D

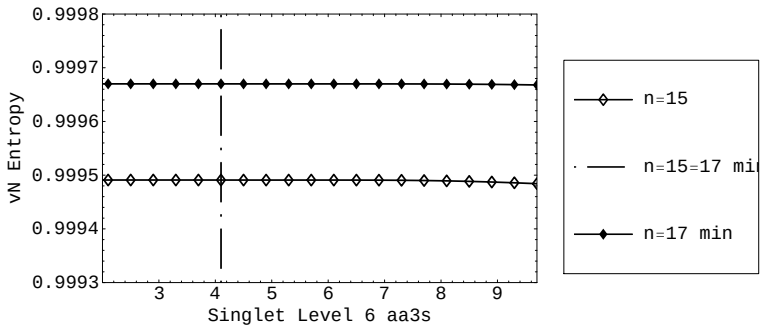

Figure 9.63 – Singlet von Neumann entropy for n=15 and n=17, level VI, S-P-D

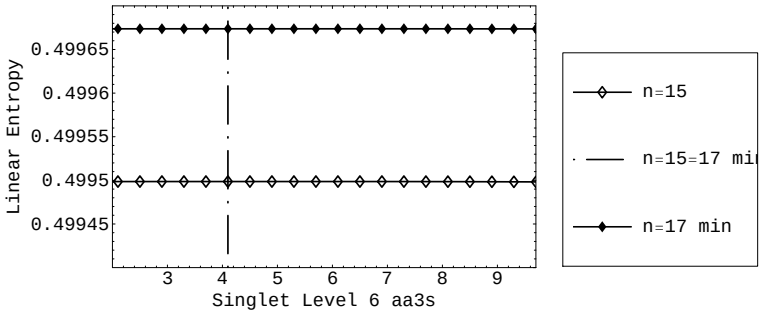

Figure 9.64 – Singlet Linear entropy forn=15 and n=17, level VI, S-P-D

ndds	aa1s	Δ E(ppm)	lin.entr.1	lin.entr.2	vN entr
5	1.080	-997.31	0.500002522	0.000005045	1.000050548
6	1.060	-510.799	0.500002492	0.000004985	1.000050047
7	1.060	-454.018	0.500002782	0.000005565	1.000055428
8	1.060	-445.203	0.500002933	0.000005865	1.000058219
9	1.080	-443.899	0.500002988	0.000005976	1.000059264
10	1.100	-443.692	0.500002995	0.000005990	1.000059423
11	1.180	-443.538	0.500003003	0.000006006	1.000059612
12	1.220	-443.495	0.500003008	0.000006016	1.000059726
13	1.300	-443.459	0.500003011	0.000006022	1.000059794

Table 9.28 – ${}^3S$ Level I, S shell

9.5.4 Triplet states - S shell only

Level I

In the table 9.28 we report our results for the S shell only of triplet, level I, starting with $n_s = 5$.

We report the first and second linear entropies, that are related by the formula $E_{lin2} = (E_{lin1} - 0.5) \times 2$.

We note that, in contrast with what holds for the singlet states, both the entropies are greater than their referral values 1 and 0.5 and that the energy differences are negative.

Passing from $n_s = 5$ to $n_s = 10$ we have an enhancement in the energy precision of about 2 times. The von Neumann and linear entropy changes involve the second significant digit.

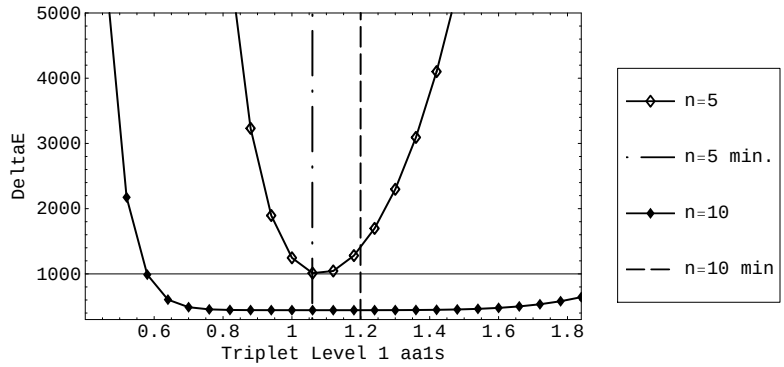

Figure 9.65 – Triplet Energy error for n=5 and n=10, level I, S

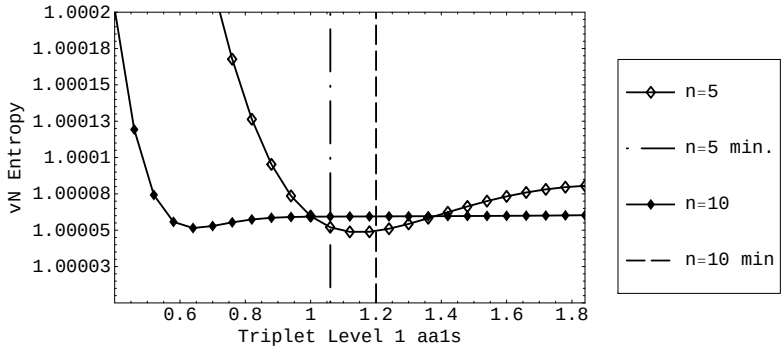

Figure 9.66 – Triplet von Neumann entropy for n=5 and n=10, level I, S

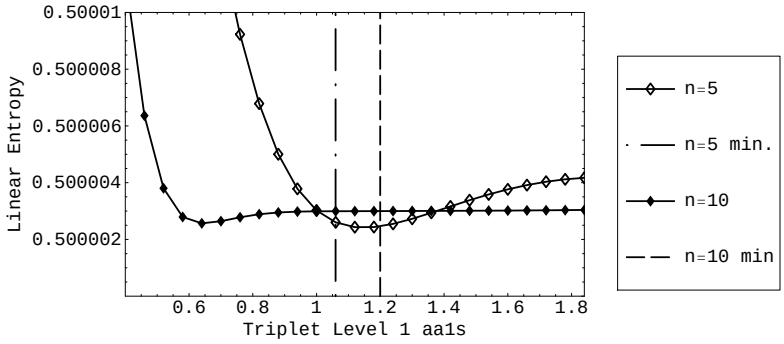

Figure 9.67 – Triplet Linear entropy forn=5 and n=10, level I, S

ndds	aa1s	Δ E(ppm)	lin.entr.1	lin.entr.2	vN entr
4	0.810	-46986.191	0.500013135	0.000026271	1.000231957
5	0.820	-13321.130	0.50007164	0.00014327	1.000132769
6	0.800	-4309.404	0.500002218	0.000004436	1.000044905
7	0.790	-1242.234	0.500001419	0.000002838	1.000029730
8	0.780	-421.065	0.500001193	0.000002385	1.000025258
9	0.780	-173.879	0.500001214	0.000002428	1.000025662
10	0.780	-115.707	0.500001279	0.000002558	1.000026927
11	0.780	-100.633	0.500001302	0.000002603	1.000027372
12	0.780	-97.218	0.500001317	0.000002634	1.000027683
13	0.780	-96.481	0.500001320	0.000002639	1.000027734
14	0.790	-96.266	0.500001321	0.000002642	1.000027773

Table 9.29 – ^3S Level II, S shell

Level II

In the table 9.29 we report our results for the S shell only of triplet, level II, starting with $n_s = 4$.

Passing from $n_s = 5$ to $n_s = 10$ we have an enhancement in the energy precision of about 100 times. The von Neumann and linear entropy changes involve the first significant digit.

The dependence of the entropies on n stabilizes starting with n=8.

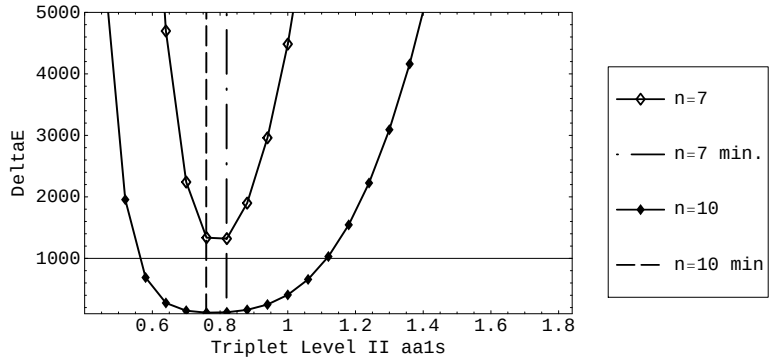

Figure 9.68 – Triplet Energy error for n=7 and n=10, level II, S

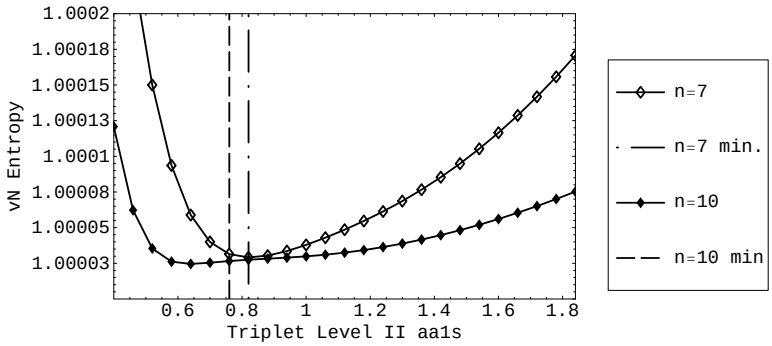

Figure 9.69 – Triplet von Neumann entropy for n=7 and n=10, level II, S

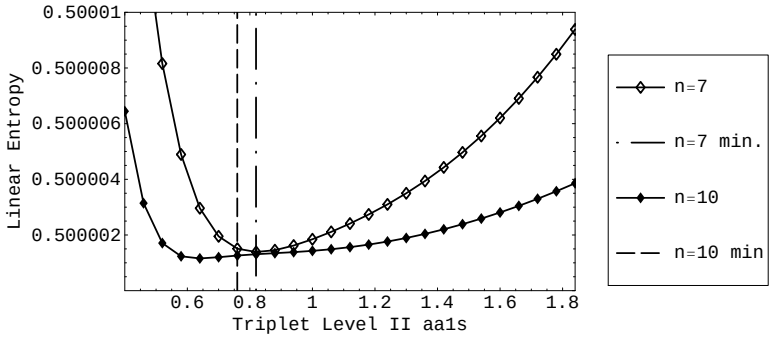

Figure 9.70 – Triplet Linear entropy forn=7 and n=10, level II, S

ndds	aa1s	Δ E(ppm)	lin.entr.1	lin.entr.2	vN entr
6	0.650	-25105.814	0.500009714	0.000019428	1.000175957
7	0.650	-10488.830	0.500002606	0.000005213	1.000052268
8	0.640	-4051.515	0.500001360	0.000002720	1.000028628
9	0.630	-1618.851	0.500000703	0.000001412	1.000015551
10	0.620	-600.939	0.500000570	0.000001141	1.000012717
11	0.620	-238.847	0.500000540	0.000001081	1.000012063
12	0.615	-101.888	0.500000533	0.000001066	1.000011902
13	0.615	-57.631	0.500000551	0.000001102	1.000012271
14	0.615	-42.686	0.500000555	0.000001110	1.000012359
15	0.620	-38.099	0.500000562	0.000001125	1.000012511
16	0.620	-36.720	0.500000563	0.000001126	1.000012523
17	0.620	-36.283	0.500000564	0.000001128	1.000012547

Table 9.30 – ^3S Level III, S shell

Level III

In the table 9.30 we report our results for the S shell only of triplet, level III, starting with $n_s = 6$.

Passing from $n_s = 6$ to $n_s = 11$ we have an enhancement in the energy precision of about 100 times. The von Neumann and linear entropy changes involve the first significant digit.

The dependence of the entropies on n stabilizes starting with n=10.

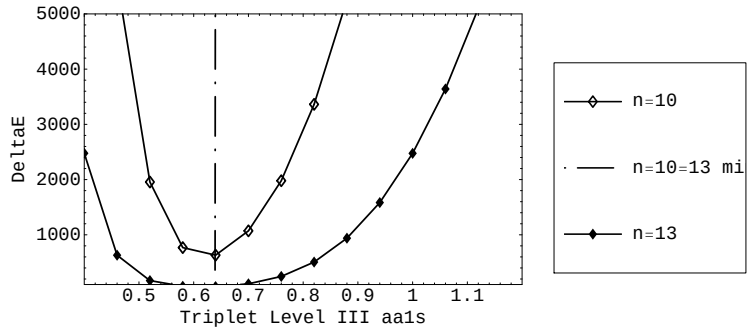

Figure 9.71 – Triplet Energy error for n=10 and n=13, level III, S

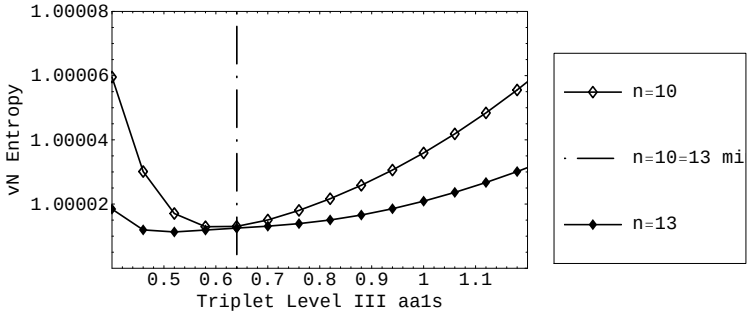

Figure 9.72 – Triplet von Neumann entropy for n=10 and n=13, level III, S

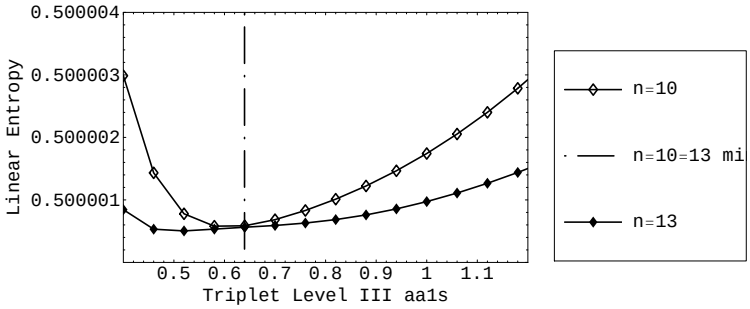

Figure 9.73 – Triplet Linear entropy forn=10 and n=13, level III, S

ndds	aa1s	Δ E(ppm)	lin.entr.1	lin.entr.2	vN entr
6	0.530	-82023.067	0.500020217	0.000040433	1.000344433
7	0.550	-35275.899	0.500011264	0.000022529	1.000201759
8	0.545	-17203.226	0.500003314	0.000006628	1.000065365
9	0.535	-8040.148	0.500001752	0.000003505	1.000036262
10	0.530	-3876.736	0.500000699	0.000001397	1.000015433
11	0.520	-1761.535	0.500000473	0.000000946	1.000010710
12	0.515	-804.878	0.500000331	0.000000662	1.000007651
13	0.515	-349.062	0.500000291	0.000000583	1.000006774
14	0.510	-155.789	0.500000280	0.000000560	1.000006518
15	0.510	-71.438	0.500000275	0.000000549	1.000006393
16	0.510	-38.408	0.500000281	0.000000561	1.000006524
17	0.515	-25.173	0.500000281	0.000000561	1.000006539
18	0.515	-20.238	0.500000284	0.000000568	1.000006601

Table 9.31 – ^3S Level IV, S shell

Level IV

In the table 9.31 we report our results for the S shell only of triplet, level IV, starting with $n_s = 6$.

Passing from $n_s = 6$ to $n_s = 11$ we have an enhancement in the energy precision of about 50 times. The von Neumann and linear entropy changes involve the first significant digit.

The dependence of the entropies on n stabilizes starting with n=13.

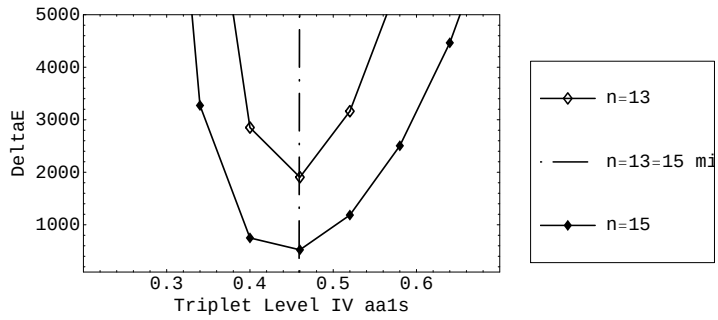

Figure 9.74 – Triplet Energy error for n=13 and n=15, level IV, S

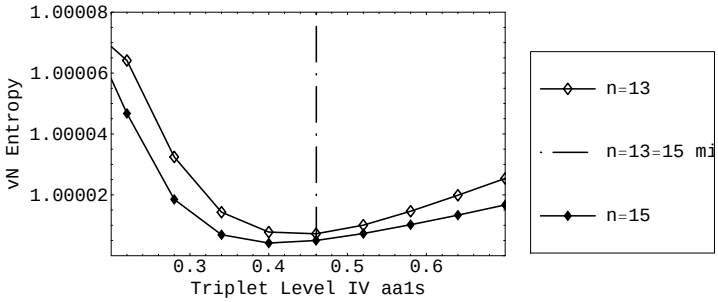

Figure 9.75 – Triplet von Neumann entropy for n=13 and n=15, level IV, S

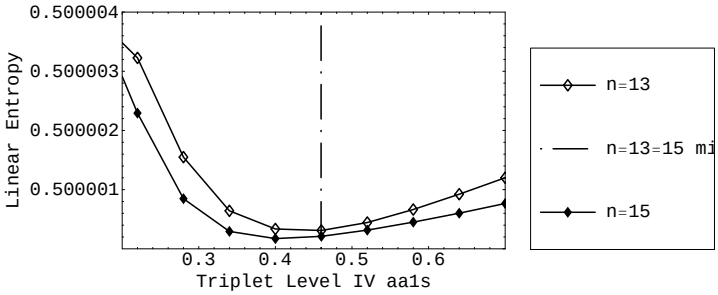

Figure 9.76 – Triplet Linear entropy forn=13 and n=15, level IV, S

ndds	aa1s	Δ E(ppm)	lin.entr.1	lin.entr.2	vN entr
6	0.395	-190243.7	0.500001346	0.000002692	1.000028235
7	0.455	-91816.456	0.500021683	0.000043367	1.000367265
8	0.475	-43164.944	0.500012330	0.000024659	1.000219333
9	0.475	-23138.142	0.500003809	**0.000007618?**	1.000074401
10	0.470	-12176.99	0.500002086	0.000004171	1.000042638
11	0.470	-6713.209	0.500000787	0.000001573	1.000017251
12	0.455	-3516.72	0.500000532	0.000001064	1.000011963
13	0.450	-1836.333	0.500000301	0.000000601	1.000007009
14	0.445	-940.359	0.500000232	0.000000464	1.000005482
15	0.440	-472.007	0.500000188	0.000000376	1.000004495
16	0.440	-227.817	0.500000169	0.000000338	1.000004066
17	0.435	-111.314	0.500000163	0.000000326	1.000003923
18	0.435	-54.743	0.500000158	0.000000317	1.000003817
19	0.440	-29.400	0.500000162	0.000000324	1.000003897
20	0.440	-17.995	0.500000161	0.000000321	1.000003864

Table 9.32 – ^3S Level V, S shell

Level V

In the table 9.32 we report our results for the S shell only of triplet, level V, starting with $n_s = 6$.

Passing from $n_s = 6$ to $n_s = 11$ we have an enhancement in the energy precision of about 30 times. The von Neumann and linear entropy changes involve the first significant digit.

The dependence of the entropies on n stabilizes starting with n=15.

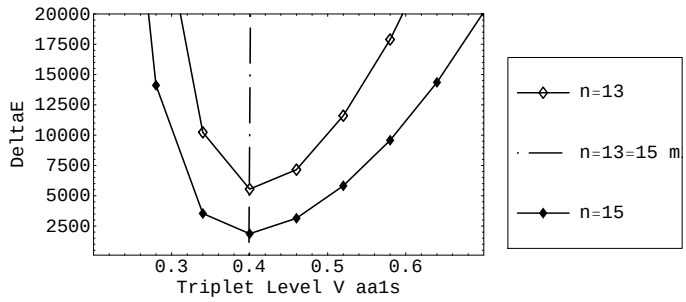

Figure 9.77 – Triplet Energy error for n=13 and n=15, level V, S

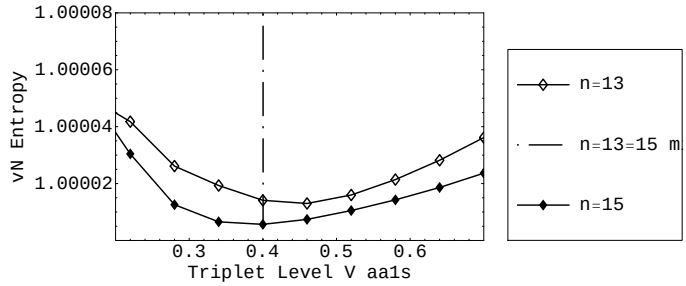

Figure 9.78 – Triplet von Neumann entropy for n=13 and n=15, level V, S

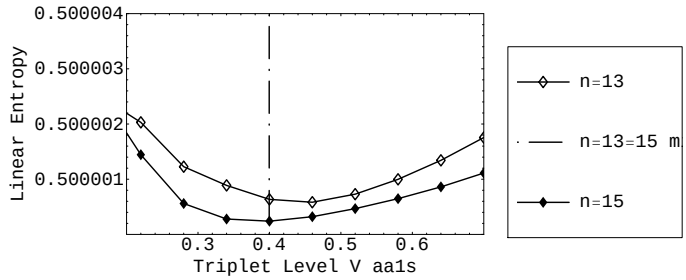

Figure 9.79 – Triplet Linear entropy forn=13 and n=15, level V, S

ndds	aa1s	Δ E(ppm)	lin.entr.1	lin.entr.2	vN entr
10	0.420	-28026.560	0.500004228	0.000008457	1.000081983
11	0.420	-15897.326	0.500002347	0.000004694	1.000047584
12	0.410	-9478.708	0.500000938	0.000001876	1.000020334
13	0.405	-5517.729	0.500000621	0.000001243	1.000013843
14	0.400	-3253.610	0.500000318	0.000000636	1.000007405
15	0.395	-1853.745	0.500000237	0.000000475	1.000005619
16	0.390	-1050.184	0.500000165	0.000000330	1.000003984
17	0.385	-572.067	0.500000134	0.000000267	1.000003266
18	0.385	-308.483	0.500000119	0.000000237	1.000002911
19	0.385	-161.240	0.500000107	0.000000215	1.000002650
20	0.385	-84.505	0.500000105	0.000000211	1.000002600

Table 9.33 – ^3S Level VI, S shell

Level VI

In the table 9.33 we report our results for the S shell only of triplet, level VI, starting with $n_s = 10$.

Passing from $n_s = 10$ to $n_s = 15$ we have an enhancement in the energy precision of about 15 times. The von Neumann and linear entropy changes involve the first significant digit.

The dependence of the entropies on n stabilizes starting with n=16.

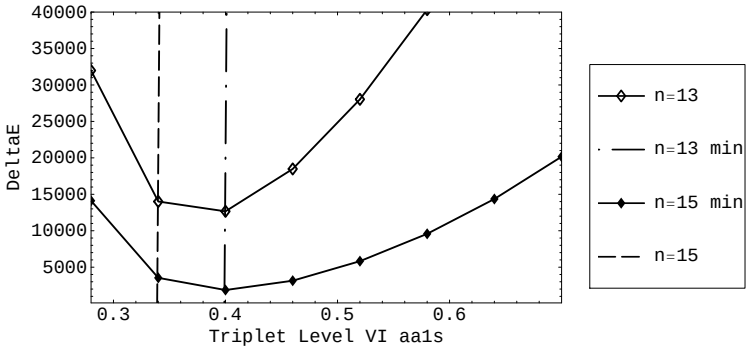

Figure 9.80 – Triplet Energy error for n=13 and n=15, level VI, S

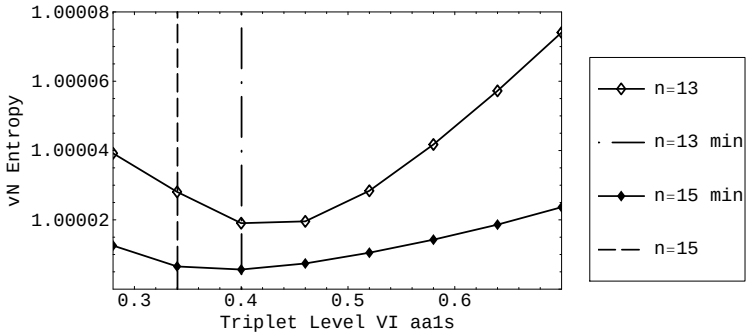

Figure 9.81 – Triplet von Neumann entropy for n=13 and n=15, level VI, S

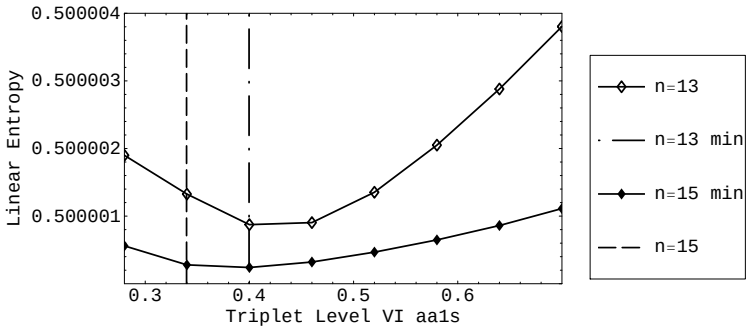

Figure 9.82 – Triplet Linear entropy forn=13 and n=15, level VI, S

ndds	aa1p	Δ E(ppm)	lin.entr.1	lin.entr.2	vN entr
5	1.700	-572.214	0.500376828	0.000753656	1.004853436
6	1.800	-92.824	0.500371684	0.000743368	1.004793766
7	1.800	-36.886	0.500370939	0.000741878	1.004786999
8	1.900	-28.096	0.500370918	0.000741836	1.004787760
9	2.000	-26.867	0.500370901	0.000741803	1.004788009
10	2.100	-26.658	0.500370901	0.000741803	1.004788091

Table 9.34 – ^3S Level I, S-P shell

9.5.5 Triplet states - S-P shells

We used dimension for P Shell=dimension for S Shell in all the computations

Level I

In the table 9.34 we report our results for the S-P shells of triplet, level I, starting with $n_s = 5$.

Passing from $n_s = 5$ to $n_s = 10$ we have an enhancement in the energy precision of about 20 times. The von Neumann entropy changes involve the second significant digit, those of the linear entropy the third.

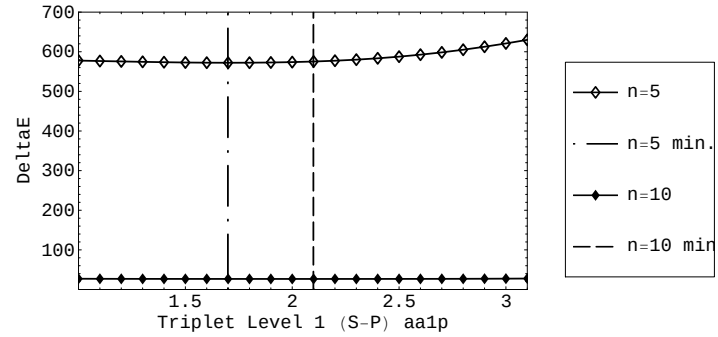

Figure 9.83 – Triplet Energy error for n=5 and n=10, level I, S-P

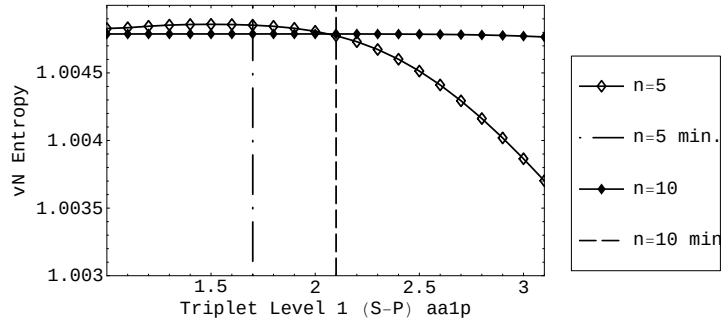

Figure 9.84 – Triplet von Neumann entropy for n=5 and n=10, level I, S-P

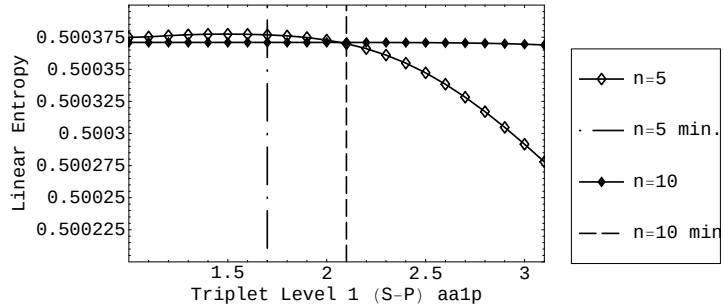

Figure 9.85 – Triplet Linear entropy forn=5 and n=10, level I, S-P

ndds	aa1p	Δ E(ppm)	lin.entr.1	lin.entr.2	vN entr
7	1.200	-1141.230	0.500081373	0.000162745	1.001232509
8	1.200	-327.356	0.500074985	0.000149969	1.001143783
9	1.300	-82.485	0.500073268	0.000146535	1.001120117
10	1.300	-25.145	0.500072634	0.000145267	1.001111757
11	1.300	-10.226	0.500072513	0.000145026	1.001110214
12	1.400	-6.894	0.500072457	0.000144914	1.001109546

Table 9.35 – ^3S Level II, S-P shell

Level II

In the table 9.35 we report our results for the S-P shells of triplet, level II, starting with $n_s = 7$.

Passing from $n_s = 7$ to $n_s = 12$ we have an enhancement in the energy precision of about 200 times. The von Neumann entropy changes involve the second significant digit, those of the linear entropy the first.

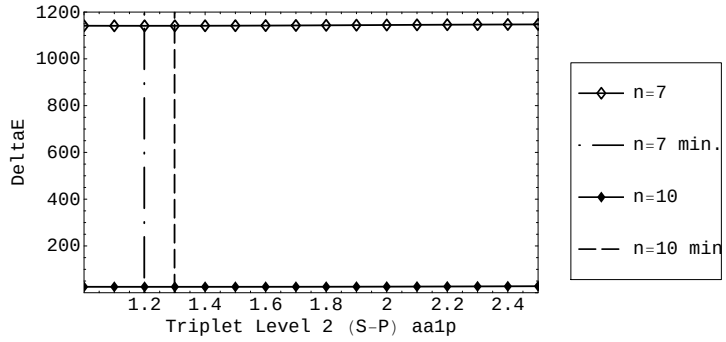

Figure 9.86 – Triplet Energy error for n=7 and n=10, level II, S-P

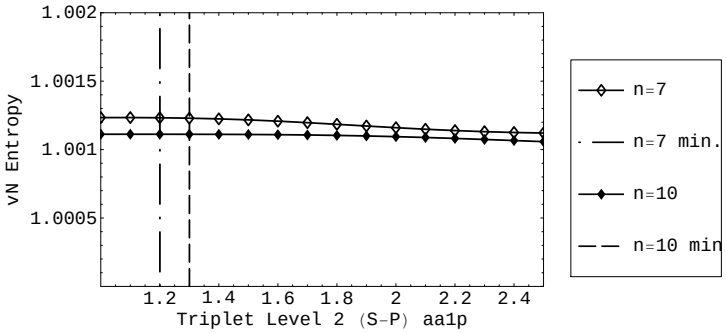

Figure 9.87 – Triplet von Neumann entropy for n=7 and n=10, level II, S-P

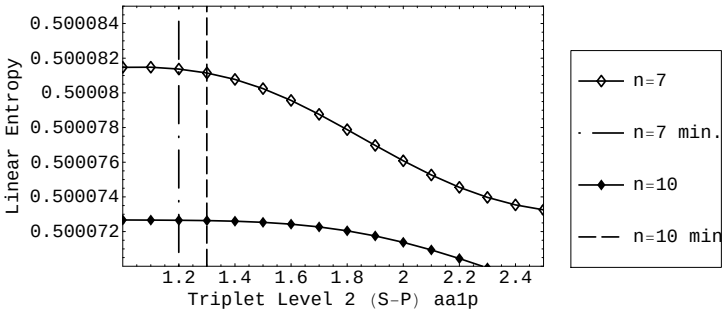

Figure 9.88 – Triplet Linear entropy forn=7 and n=10, level II, S-P

ndds	aa1p	Δ E(ppm)	lin.entr.1	lin.entr.2	vN entr
9	1.000	-1573.404	0.500034846	0.000069691	1.000571016
10	1.000	-562.615	0.500029748	0.000059496	1.000493940
11	1.000	-203.097	0.500027641	0.000055282	1.000461900
12	1.000	-67.339	0.500026763	0.000053526	1.000448475
13	1.000	-23.555	0.500026413	0.000052814	1.000443155
14	1.100	-8.736	0.500026300	0.000052600	1.000441551
15	1.100	-4.213	0.500026262	0.000052525	1.000441020
16	1.100	-2.844	0.500026252	0.000052503	1.000440861

Table 9.36 – ^3S Level III, S-P shell

Level III

In the table 9.36 we report our results for the S-P shells of triplet, level III, starting with $n_s = 9$.

Passing from $n_s = 9$ to $n_s = 14$ we have an enhancement in the energy precision of about 200 times. The von Neumann and linear entropy changes involve the first significant digit.

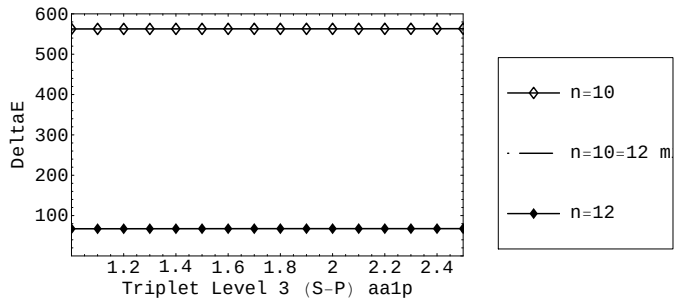

Figure 9.89 – Triplet Energy error for n=10 and n=12, level III, S-P

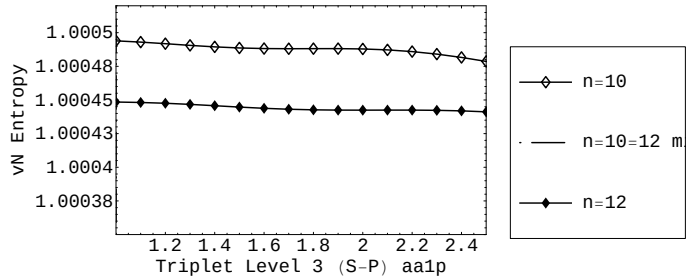

Figure 9.90 – Triplet von Neumann entropy for n=10 and n=12, level III, S-P

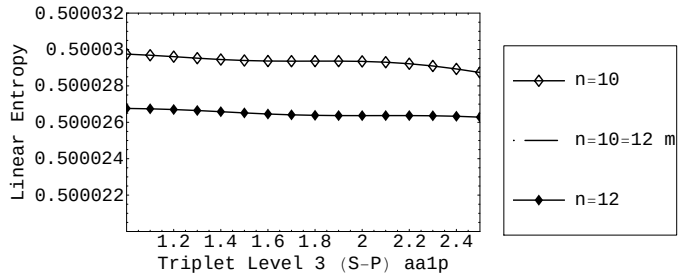

Figure 9.91 – Triplet Linear entropy forn=10 and n=12, level III, S-P

ndds	aa1p	Δ E(ppm)	lin.entr.1	lin.entr.2	vN entr
10	1.200	-3841.291	0.500026520	0.000053040	1.000446034
11	1.200	-1736.025	0.500019589	0.000039178	1.000337719
12	1.300	-783.783	0.500015949	0.000031899	1.000279373
13	1.300	-330.326	0.500014284	0.000028568	1.000252377
14	1.300	-138.483	0.500013166	0.000026332	1.000234220
15	1.200	-54.682	0.500012765	0.000025530	1.000227647
16	1.100	-21.940	0.500012560	0.000025119	1.000224336
17	0.900	-8.773	0.500012517	0.000025034	1.000223639
18	0.900	-3.904	0.500012474	0.000024948	1.000222956

Table 9.37 – ^3S Level IV, S-P shell

Level IV

In the table 9.37 we report our results for the S-P shells of triplet, level IV, starting with $n_s = 10$.

Passing from $n_s = 10$ to $n_s = 15$ we have an enhancement in the energy precision of about 60 times. The von Neumann and linear entropy changes involve the first significant digit.

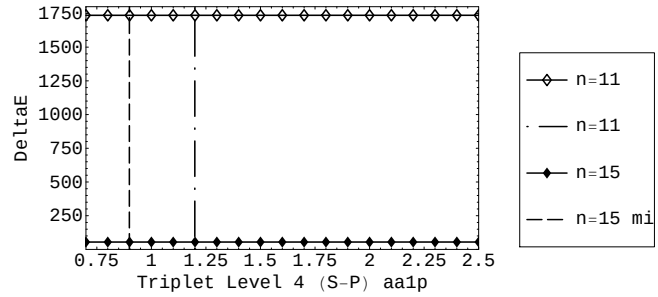

Figure 9.92 – Triplet Energy error for n=11 and n=15, level IV, S-P

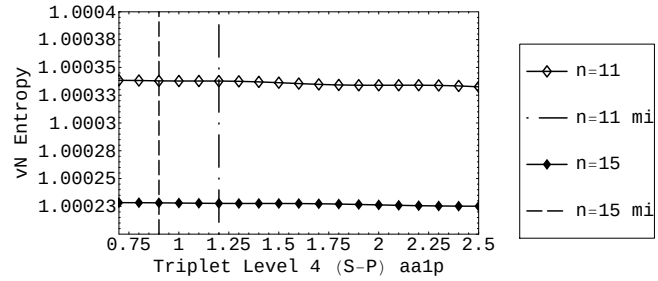

Figure 9.93 – Triplet von Neumann entropy for n=11 and n=15, level IV, S-P

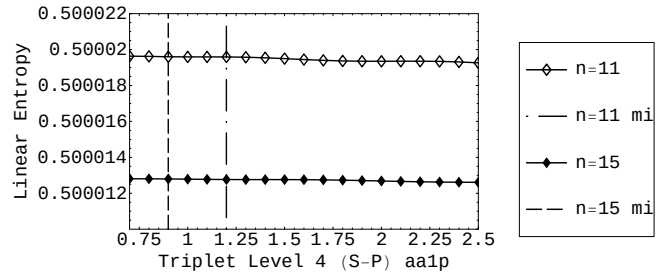

Figure 9.94 – Triplet Linear entropy forn=11 and n=15, level IV, S-P

ndds	aa1p	Δ E(ppm)	lin.entr.1	lin.entr.2	vN entr
6	1.900	-189513.879	0.500497036	0.000994072	1.006208767
7	1.300	-91460.688	0.500290997	0.000581993	1.003951434
8	1.300	-43044.779	0.500097340	0.000194680	1.001491520
9	1.300	-23057.634	0.500060259	0.000120517	1.000952161
10	1.300	-12131.867	0.500035295	0.000070589	1.000584412
11	1.300	-6678.656	0.500025540	0.000051080	1.000431590
12	1.300	-3494.095	0.500017353	0.000034706	1.000302848
13	1.000	-1845.707	0.500013169	0.000026338	1.000234523
14	1.000	-926.47	0.500010553	0.000021105	1.000191190
15	1.000	-460.3	0.500008795	0.000017590	1.000161616
16	1.000	-217.3	0.500007986	0.000015972	1.000147809
17	1.000	-101.590	0.500007352	0.000014705	1.000137010
18	0.800	-45.336	0.500007121	0.000014242	1.000133020
19	0.800	-20.151	0.500007007	0.000014014	1.000131083
20	0.800	-8.829	0.500006942	0.000013883	1.000129951

Table 9.38 – ^3S Level V, S-P shell

Level V

In the table 9.38 we report our results for the S-P shells of triplet, level V, starting with $n_s = 6$.

Passing from $n_s = 6$ to $n_s = 11$ we have an enhancement in the energy precision of about 30 times. The von Neumann and linear entropy changes involve the first significant digit.

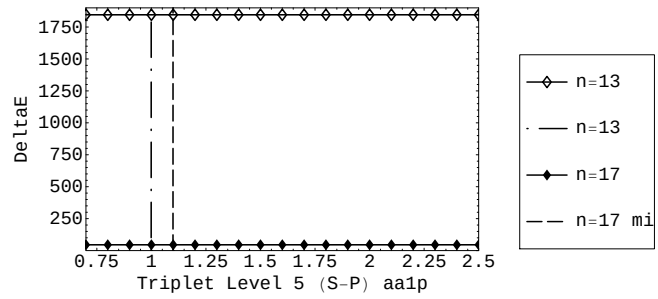

Figure 9.95 – Triplet Energy error for n=13 and n=17, level V, S-P

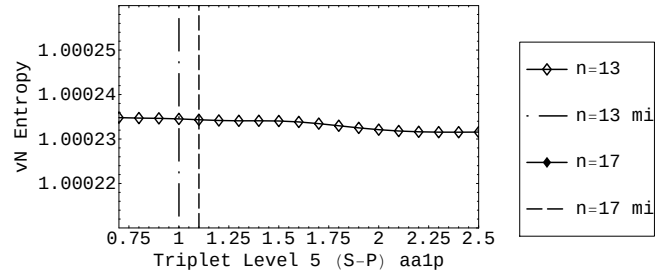

Figure 9.96 – Triplet von Neumann entropy for n=13 and n=17, level V, S-P

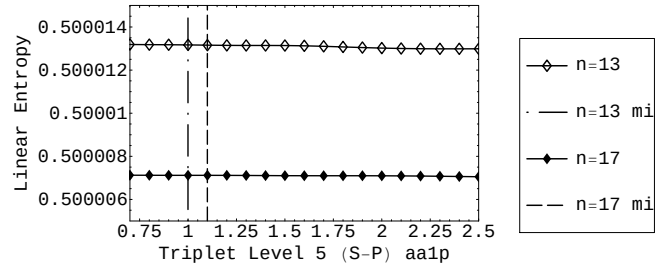

Figure 9.97 – Triplet Linear entropy forn=13 and n=17, level V, S-P

ndds	aa1p	Δ E(ppm)	lin.entr.1	lin.entr.2	vN entr
11	1.000	-15854.349	0.500033758	0.000067516	1.000562701
12	1.000	-9447.677	0.500022971	0.000045941	1.000392883
13	1.000	-5496.577	0.500016276	0.000032551	1.000286205
14	1.000	-3237.132	0.500012219	0.000024438	1.000219187
15	1.000	-1841.285	0.500009469	0.000018938	1.000173231
16	1.000	-1040.203	0.500007450	0.000014899	1.000138745
17	0.800	-563.915	0.500006159	0.000012349	1.000116358
18	0.900	-301.315	0.500005381	0.000010762	1.000102703
19	0.900	-154.709	0.500004920	0.000009840	1.000094528
20	0.700	-78.4	0.500004592	0.000009185	1.000088710

Table 9.39 – ^3S Level VI, S-P shell

Level VI

In the table 9.39 we report our results for the S-P shells of triplet, level VI, starting with $n_s = 11$.

Passing from $n_s = 11$ to $n_s = 16$ we have an enhancement in the energy precision of about 15 times. The von Neumann and linear entropy changes involve the first significant digit.

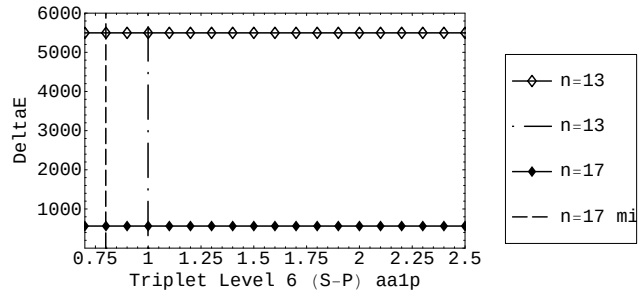

Figure 9.98 – Triplet Energy error for n=13 and n=17, level VI, S-P

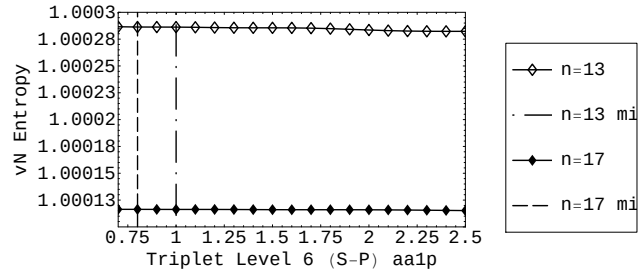

Figure 9.99 – Triplet von Neumann entropy for n=13 and n=17, level VI, S-P

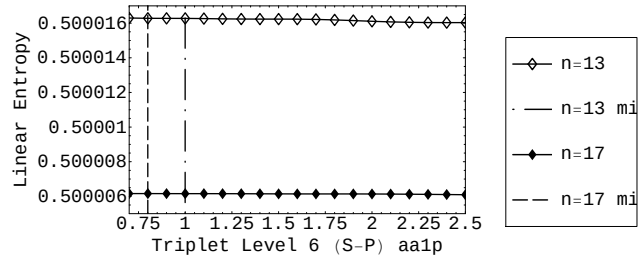

Figure 9.100 – Triplet Linear entropy forn=13 and n=17, level VI, S-P

9.6 Some results for the Helium isoelectronic series

We tried our programs to compute some other elements of the Helium isoelectronic series. We found that this extensions do not present difficulties, and decided to postpone this study to the Hydrogen molecule treatment, that is indeed more interesting.

As an example, we report here the von Neumann and linear entropy plots for Z=3 (Li^+) singlets, computed for the S shell only.

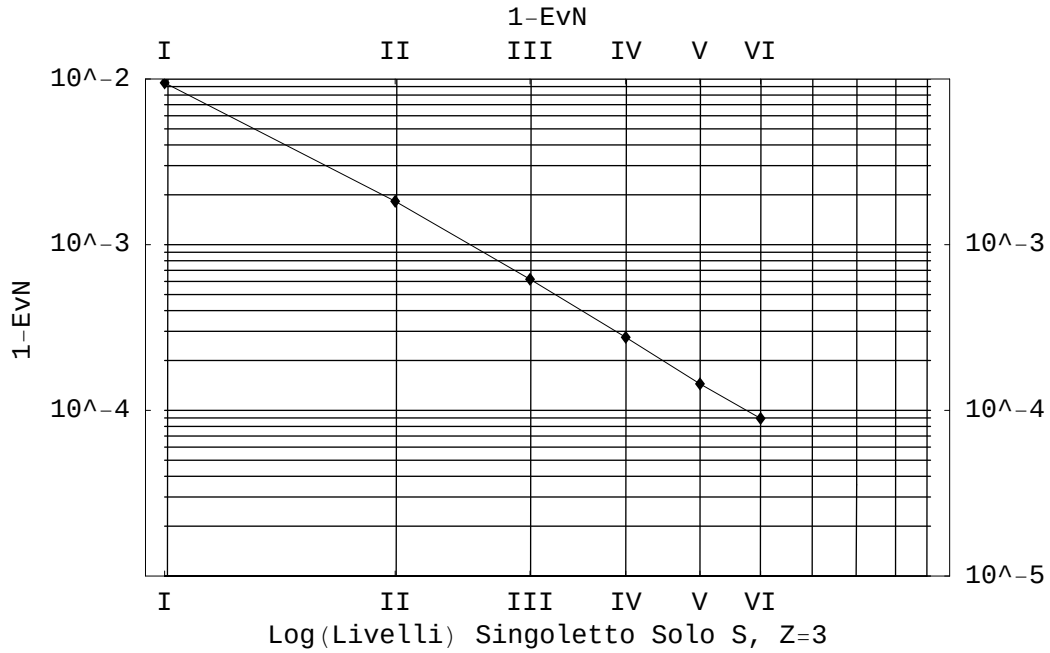

Figure 9.101 – 1 - EvN vs levels, singlet S, Z=3

Moreover, table 9.40 contains the computation of energy and entropies for the fundamental level, singlet, shell S only. The energy is compared to the value -7.279913412 found in (Koga , 1996).

As a further example, a run with n=10 and considering the S and P shells gave: ΔEnergy = 553, von Neumann Entropy = 0.03562975, Linear entropy = 0.00652547.

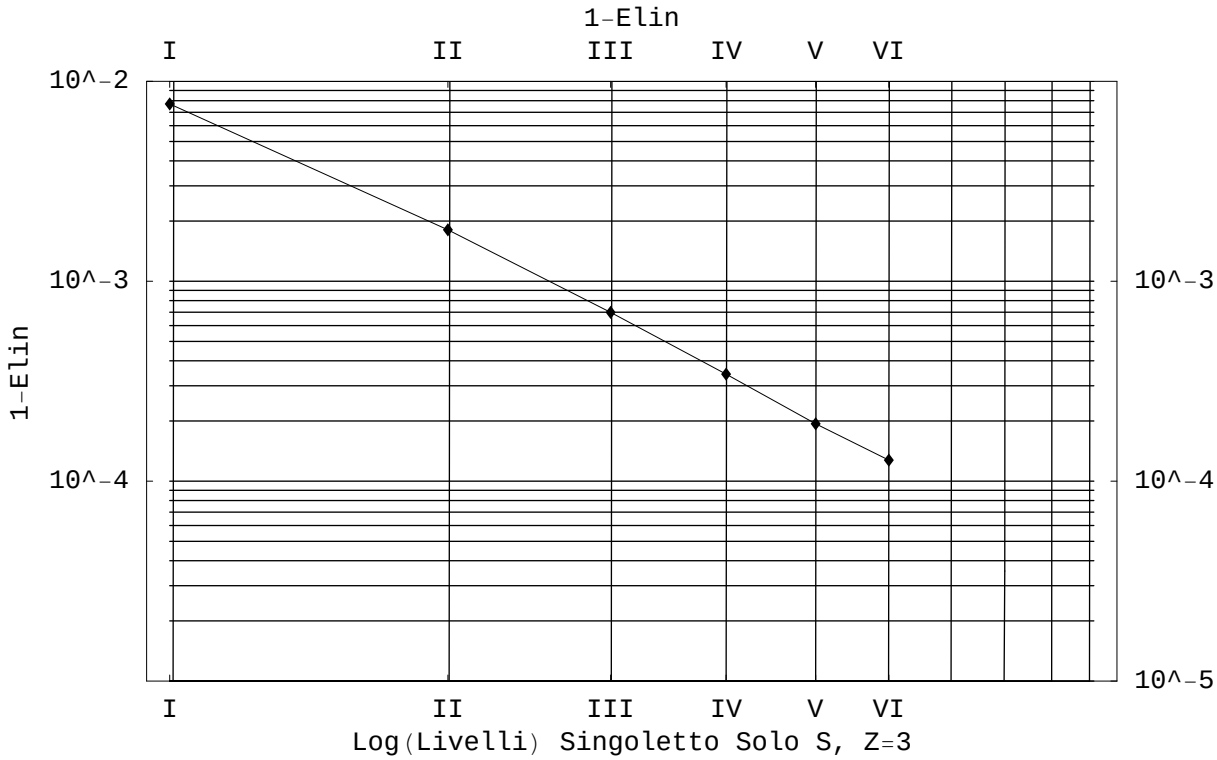

Figure 9.102 – 1 - Elin vs levels, singlet S, Z=3

ndds	aa1s	ΔEnergy	elin	evN
5	3.700	3789	0.002995833	0.016476391
6	3.700	3775	0.002999688	0.016498473
7	4.200	3771	0.002998959	0.016496971
8	4.200	3769	0.002999324	0.016499281
9	4.700	3768	0.002999199	0.016499169
10	5.200	3767	0.002999120	0.016498996
11	5.200	3767	0.002999214	0.016499523
12	5.700	3767	0.002999184	0.016499449
13	5.700	3767	0.002999209	0.016499592
14	6.200	3767	0.002999196	0.016499557
15	5.700	3767	0.002999210	0.016499622
16	6.700	3767	0.002999198	0.016499583
17	6.200	3767	0.002999203	0.016499611
18	5.700	3767	0.002999204	0.016499614
19	8.200	3767	0.002999182	0.016499517
20	5.200	3767	0.002999204	0.016499612

Table 9.40 – ^1S Level I, S shell, Z=3

9.7 A comparison to (Osenda, Serra , 2007) results

The aim of this section is to check if the results of (Osenda, Serra , 2007), that were obtained with a simplified Hamiltonian, are consistent with the same computations made with the complete Hamiltonian that we used.

In order to compare our results with those of (Osenda, Serra , 2007), we run our programs varying the coupling strength of the electrons. The results are plotted in fig. 9.103 left for shells S only and S-P. The figure should be compared to 9.103 right, taken from the quoted work.

The behaviour is quite similar.

We plotted also the behaviour of the two first eigenvalues, in fig. 9.104 left, where we used the S shell only. It should be compared to the analogous figure in 9.104 right taken from the original work. Again the behaviour is very similar.

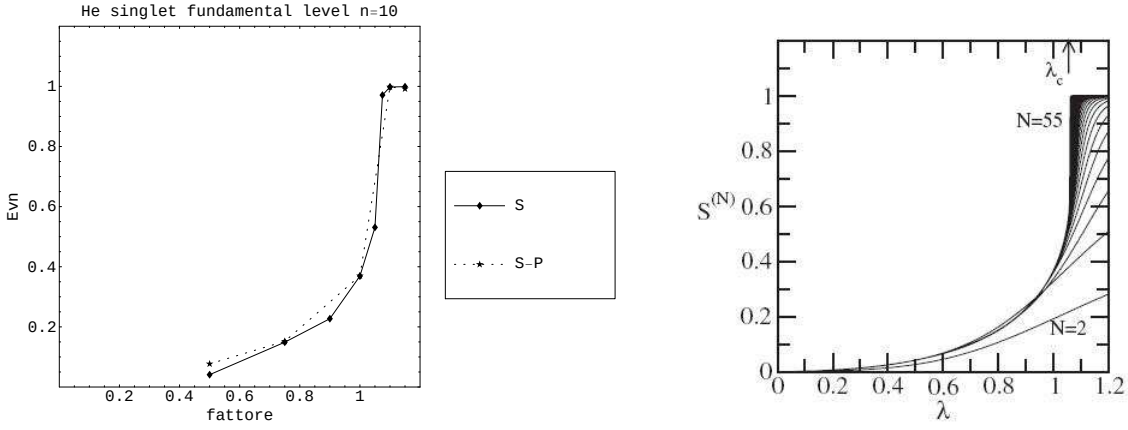

Figure 9.103 – von Neumann entropy singlet fundamental level, S and S-P, varying the coupling strength, our computation and the plot from (Osenda, Serra , 2007)

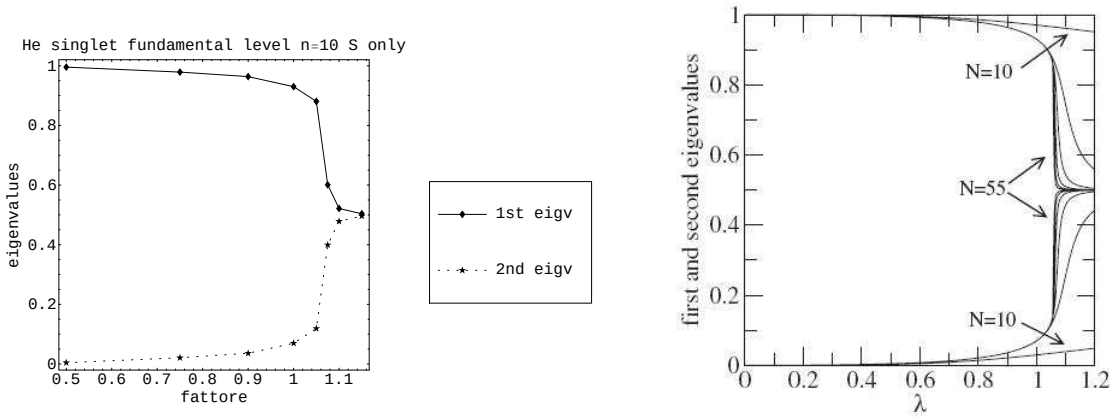

Figure 9.104 – The two first eigenvalues singlet fundamental level, S shell, varying the coupling strength, our data and the plot from (Osenda, Serra , 2007)

References

J. Adolphs, F. Muḧ, M. El-Amine Madjet, M. Schmidt am Busch, T. Renger (2010); *Structure-Based Calculations of Optical Spectra of Photosystem I Suggest an Asymmetric Light-Harvesting Process* Journal of the American Chemical Society, 132, p.3331.

D. Akoury, K. Kreidi, T. Jahnke, Th. Weber, A. Staudte, M. Schöffler, N. Neumann, J. Titze, L. Ph. H. Schmidt, A. Czasch, O. Jagutzki, R. A. Costa Fraga, R. E. Grisenti, R. Dez Muino, N. A. Cherepkov, S. K. Semenov, P. Ranitovic, C. L. Cocke, T. Osipov, H. Adaniya, J. C. Thompson, M. H. Prior, A. Belkacem, A. L. Landers, H. Schmidt-Böcking, R. Dörner(2007); *The Simplest Double Slit: Interference and Entanglement in Double Photoionization of* H_2 Science, 318, p.949.

R. Alicki, W. Miklaszewski (2012); *A resonance mechanism of efficient energy transfer mediated by Fenna- Matthews-Olson complex* Journal of Chemical Physics, 136, p.134103.

L. Amico, R. Fazio, A. Osterloh, and V. Vedral (2008); *Entanglement in many-body systems* Reviews of Modern Physics, 80, p.517.

C. Amovilli, N. H. March (2003); *Exact density matrix for a two-electron model atom and approximate proposals for realistic teo-electron systems* Phisical Review A, 67, p. 22509

C. Amovilli, N. H. March (2004); *Quantum information: Jaynes and Shannon entropies in a two-electron entangled artificial atom* Physical Review A, 69, p. 54302

R. Atre, C. S. Mohapatra, P. K. Panigrahi (2004); *Information entropy and correlation of the Hooke atom* ArXiv:quant.ph/0411016v1

H. Bachau, P. Lambropoulos, X. Tang (1991); *Discretization techniques applied to the study of two-photon ionization in systems with two active electrons* Physical Review A, 44, p.4516

G. Barcza, O. Legeza, K. H. Marti, M. Reiher (2011); *Quantum-information analysis of electronic states of different molecular structures* Physical Review A, 83, p.012508

M. P. Barnett (2003); *Chemistry and computer algebra: past, present, future* in J. R. Sendra, ed. Proceedings of the 2003 International Symposium on Symbolic and Algebraic Computation, ACM Press: New York, 1-2, 2003.

M. P. Barnett, J. F. Capitani, J. von zur Gathen and J. Gerhard (2004); *Symbolic calculation in chemistry: selected examples* International Journal of Quantum Chemustry, 100, p.80.

U. Becker, B. Langer (2009); *Correlation and coherence phenomena studied by photoelectron spectroscopy* Nuclear Instruments and Methods in Physics Research A, 601, p.78.

G. Benenti, G. Casati, G. Strini (2007); *Principles of quantum computation and information, vol. I-II* World Scientific

G. Benenti, G. Strini (2007); *A bird's eye view of quantum computers* arXiv:quant-ph/0703105

G. Benenti, G. Strini (2008); *Quantum simulation of the single-particle Schröedinger equation*, American Journal of Physics, 76, p.657.

R. Blatt, D. Wineland (2008); *Entangled states of trapped atomic ions* Nature, 453, p. 1008

I. Bloch (2008); *Quantum coherence and entanglement with ultracold atoms in optical lattices* Nature, 453, p. 1016

K. Boguslawski, P. Tecmer, O. legeza, M. Reiher (2012); *Entanglement measures for Single- and Multi-reference correlation effects* arXiv:1208.6586v1

R. P. Brent (2002); *Algorithms for minimization without derivatives* Dover Publications.

I. Buluta, S. Ashhab, F. Nori (2011); *Natural and artificial atoms for quantum computation* Reports on Progress in Physics, 74, p. 104401

A. Bürgers, D. Wintgen, J.-M. Rost (1995); *Highly doubly excited S states of the helium atom* Journal of Physics B, 28, p.3163.

F.L. Carter (1987); *Molecular electronic devices* Dekker Inc.

N. Christensson, H. F. Kauffmann, T. Pullerits, Tomas Mancal (2012); *Origin of Long-Lived Coherences in Light-Harvesting Complexes* Journal of Physical Chemistry B, 116, p. 7449.

J. P. Coe, A. Sudbery, I. D'amico (2008); *Entanglement and density-functional theory: testing approximations on Hooke's atom* Physical Review B, 77, p. 205122

E. Cornier, P. Lambropoulos (1995); *Extrapolation method for the evaluation of above threshold ionization cross sections for one- and two-electron systems* Journal of Physics B, 28, p.5043.

H.T. Dashti, A.F. Siahpirani, L. Wang, M. Kloc, A.H. Assadi (2010); *Parallel Evolutionary Computation in Very Large Scale Eigenvalue Problems* arXiv:1008.5391

J. S. Dehesa, T. Koga, R. J. Yanez, A. R. Plastino, and R. O. Esquivel (2012); *Quantum entanglement in helium* Journal of Physics B 45, p. 015504

G. W. F. Drake (1999); *High precision theory of atomic helium* Physica Scripta T83, p.83.

Daniel Dundas, K. T. Taylor, J. S. Parker, E. S. Smyth (1999); *Double-ionization dynamics of laser-driven helium* Journal of Physics B, 32, p. L231.

G. S. Engel, T.R. Calhoun, E. L. Read1 T-K. Ahn, T. Manal, Y-C. Cheng, R. E. Blankenship, G. R. Fleming (2007); *Evidence for wavelike energy transfer through quantum coherence in photosynthetic systems* Nature, 446, p.782

P. Facchi, G. Florio, S. Pascazio (2006) *Probability-density-function characterization of multipartite entanglement* Physical Review A, 74, p. 042331

A. Ferron, O. Osenda, P. Serra (2009) *Entanglement in resonances of two-electron quantum dots* Physical Review A, 79, p. 032509

R. P. Feynman (1982); *Simulating physics with computers*, International Journal of Theoretical Physics, 21, p.467.

P. Fulde (2002); *Electron correlations in molecules and solids*, Springer, Third Edition.

B. Gremaud, D. Delande (1997); *Photo-ionization of the helium atom close to the double-ionization threshold: Towards the Ericson regime*, Europhycs Letters, 40, p.363.

G. Ghirardi, L. Marinatto (2004); *General criterion for the entanglement of two indistinguishable particles*, Physical Review A, 70, p.012109.

L. Hilico, N. Billy, B. Gremaud, D. Delande (2000); *Ab initio calculation of the $J = 0$ and $J = 1$ states of the H_2^+ , D_2^+ and HD^+ molecular ions*, European Physical Journal D, 12, p. 449.

R. Horodecki, P. Horodecki, M. Horodecki, and K. Horodecki (2009); *Quantum entanglement* Reviews of Modern Physics, 81, 865 (2009).

T. Koga (1996); *Optimal Kinoshita wave functions with half-integer powers* Journal of Chemical Physics 104, p.6308.

A. Kono and S. Hattori, (1985); *Variational calculations for excited states in He I: Improved estimation of the ionization energy from accurate energies for the n^3 S, n^1 D, n^3 D series* Physical Review A 31, p.1199.

A. Kono and S. Hattori, (1986); *Energy levels for S, P, and D states in He through precision variational calculations* Physical Review A 34, p.1727.

A. Kono and S. Hattori, (1988); *Erratum: Energy levels for S, P, and D states in He through precision variational calculations* Physical Review A 34, p.2241.

C. Koutschan, D. Zeilberger (2010); *The 1958 Pekeris-Accad-Weizac ground-breaking collaboration that computed ground states of two-electron atoms (and its 2010 redux)* ArXiv:quant.ph/1006.0200v1.

P-F. Loos (2010) *Hooke's law correlation in two-electron systems* ArXiv:quant.ph/1002.3396v2

J. Madronero, P. Schlagheck, L. Hilico, B. Gremaud, D. Delande, A. Buchleitner (2005); *Decay rates of planar helium* Europhysics Letters, 70, p. 183.

J. Madronero, B. Piraux (2010); *The dynamics of the ionization of atoms exposed to strong low-frequency fields* Journal of Physics, conference series, 212, p. 012027.

D. Manzano, A. R. Plastino, J. S. Dehesa, and T. Koga (2011); *Quantum entanglement in two-electron atomic models* Journal of Physics A, 43, p. 275301.

N. H. March, A. Cabo, F. Claro, G. G. N. Angilella (2008) *Proposed definitions of the correlation energy density from a Hartree-Fock starting point: the two-electron Moshinsky model atom as an exactly solvable model* ArXiv:cond-mat.other/0803.2594v1 (2008)

A. Micheli, G.K. Brennen, P. Zoller (2006); *A toolbox for latticespin models with polar molecules* Nature Physics 2, p.341

F. Mintert, A. R.R. Carvalho, M. Kus, A. Buchleitner (2005); *Measures and dynamics of entangled states* Physics Reports 415, p.207

M. Mohseni, P. Rebentrost, S. Lloyd, A. Aspuru-Guzik (2008); *Environment-assisted quantum walks in photosynthetic energy transfer* Journal of Chemical Physics, 129, p.174106

G.E. Moore (1965); *Cramming more components onto integrated circuits* Electronics, 38, N. 8

M. Moshinsky (1968) *How good is the Hartree-Fock approximation?* The American Journal of Physics, 36, p. 52

A. Nagy (2006); *Fisher information in a two-electron entangled artificial atom* Chemical Physics Letters, 425, p.154

L. A. A. Nikolopoulos, P. Lambropoulos (2001); *Multichannel theory of two-photon single and double ionization of helium* Journal of Physics B, 34, p.545.

C. Olbrich, T. L. C. Jansen, J. Liebers, M. Aghtar, J. Strümpfer, K. Schulten, J. Knoester, U. Kleinekathöfer (2011); *From Atomistic Modeling to Excitation Transfer and Two-Dimensional Spectra of the FMO Light-Harvesting Complex* Journal of Physical Chemistry B, 115, p.8609

O. Osenda, P. Serra (2007) *Scaling of the von Neumann entropy in a two-electron system near the ionization threshold* Physical Review A, 75, p. 042331

O. Osenda, P. Serra (2008) *Excited state entanglement on a two-electron system near the ionization threshold* Journal of Physics B, 41, p. 065502

C. L. Pekeris (1958) *Ground state of two-electron atoms* Pysical Review, vol. 111, p. 1649

C. L. Pekeris (1959) 1^1S *and* 2^3S *States of Helium* Physical Reviews 115, p.1216.

A. Pereverzev, E. R. Bittner, I. Burghardt (2009) *Energy and charge-transfer dynamics using projected modes* Journal of Chemical Physics 131, p. 034104.

M. B. Plenio, S. Virmani(2007) *An introduction to entanglement measures* Quantum Information and Computation, 7, p. 1.

W.H. Press, S.A Teukolsky, W.T. Vetterling, B.P. Flannery (2001); *Fortan numerical recipes* Cambridge University Press.

R. P̈ttner, B. Gremaud, D. Delande, M. Domke, M. Martins, A. S. Schlachter, G. Kaindl (2001); *Statistical Properties of Inter-Series Mixing in Helium: From Integrability to Chaos* Physical Reviews Letters, 86, p. 3747

T. Renger, V. May (1998); *Ultrafast Exciton Motion in Photosynthetic Antenna Systems: The FMO-Complex* Journal of Physical Chemistry, 102, p.4381.

Y. Saad (2011); *Numerical methods for large eigenvalue problems* SIAM Philadelphia 2011.

M. Saffman, T.G. Walker, K. Molmer (2010); *Quantum information with Rydberg atoms* Reviews of Modern Physics 82, p.2313

M. Sarovar, A. Ishizaki, G. R. Fleming, and K. B. Whaley (2010); *Quantum entanglement in photosynthetic light harvesting complexes* Nature Physics, 6, 462 (2010).

M. Sarovar, K. B. Whaley (2012); *Design principles and fundamental trade-offs in biomimetic light harvesting* arXiv:bio-ph/1210.2111.

J. Schliemann, J. I. Cirac, M. Kus, M. Lewenstein, D. Loss (2001); *Quantum correlations in two-fermion systems* Physical Review A, 64, p.022302.

J. Schliemann, D. Loss, A. H. MacDonald (2001); *Double-occupancy errors, adiabaticity, and entanglement of spin qubits in quantum dots* Physical Review B, 63, p.085311.

T. Scholak, F. de Melo, T. Wellens, F. Mintert, A. Buchleitner (2011); *Efficient and coherent excitation transfer across disordered molecular networks* Physical Review E, 83, p. 021912

T. Scholak, F. Mintert, T. Wellens, A. Buchleitner (2010); *Quantum Efficiency in Complex Systems: Part I. Biomolecular Systems* (Semiconductors and Semimetals vol 83) ed E R Weber, M Thorwart and U Würfel (Amsterdam: Elsevier)

T. Scholak, T. Wellens, A. Buchleitner (2011); *Optimal networks for excitonic energy transport* Journal of Physics B, p. 184012

N. Schuch, F. Verstraete (2010); *Computational Complexity of interacting electrons and fundamental limitations of Density Functional Theory* arXiv:quant-ph/0712.0483.

A. Scrinzi, B. Piraux (1997); *Ionization and double excitation of helium by short intense laser pulses* Physical Review A, 56, p.R13.

A. Scrinzi, B. Piraux (1998); *TwoElectron Atoms in Short Intense Laser Pulses* arXiv:atom-ph/9803010.

J. T. Seeley, M. J. Richards, P. J. Love (2012); *The Bravyi-Kitaev transformation for quantum computation of electronic structure* arXiv:1208.5986v1.

T. E. Sharp (1971); *Potential-energy curves for molecular Hydrogen and its ions* Atomic Data, 2, p.119.

R. F. Stewart (1969); *Small Gaussian Expansions of Atomic Orbitals* Journal of Chemical Physics, 50, p. 2485.

M. C. Tichy, F. Mintert and A. Buchleitner (2011); *Essential entanglement for atomic and molecular physics*, Journal of Physics B, 44, p.192001.

M. Tiersch, S. Popescu, H. J. Briegel, (2012); *A critical view on transport and entanglement in models of photosynthesis* Phil. Trans. R. Soc. A 370, 3771

F. Tisseur, J. Dongarra (1999); *A Parallel Divide and Conquer Algorithm for the Symmetric Eigenvalue Problem on Distributed Memory Architectures* SIAM Journal on Scientific Computing, 20, p. 2223

V. Vedral, M. B. Plenio, M. A. Rippin, P. L. Knight(1997); *Quantifying Entanglement* Physical Review Letters, 78, p. 2275

M. Walschaers, R. Mulet, A. Buchleitner (2012); *Centro-symmetric Hamiltonians foster quantum transport* ArXiv:quant.ph/1207.4072

K. B. Whaley, M. Sarovar, A Ishizaki (2010); *Quantum entanglement phenomena in photosynthetic light harvesting complexes* ArXiv:quant.ph/1012.4059

S. R. White (1992); *Density Matrix Formulation for Quantum Renormalization Groups* Physical Reviews Letters, 69, p. 2863

J.D. Whitfield, P.J. Loved, Alan Aspuru-Guzik (2012); *Computational Complexity in Electronic Structure* arXiv:physics.chem-ph/1208.3334

D. Wintgen, D. Delande (1993); *Double photoexcitation of* $^1P^0$ *states in helium* Journal of Physics B, 26, p. L399.

R. J. Yanez, A. R. Plastino, J. S. Dehesa (2010) *Quantum entanglement in a soluble two-electron model atom* European Physics Journal D, 56, p. 141

M-H Yung, J. D. Whitfield, S. Boixo, D. G. Tempel, A. Aspuru-Guzik (2012); *Introduction to quantum algorithms for Physics and Chemistry*, arXiv:1203.1331v1.

T. Zech, R. Mulet, T. Wellens, A. Buchleitner (2012); *Hidden symmetries enhance quantum transport in Light Harvesting systems*, arXiv:1205.5519.